Membrane Currents and Pacemaking in Corticotrophs and hiPSC-Derived Dopaminergic Neurons

Matthew Robert Stephen Euston

Submitted for the Degree of Doctor of Philosophy

Heriot-Watt University

School of Engineering & Physical Sciences

November 2017

ABSTRACT

Many neural networks are required to function at particular frequencies. These processes are often driven by rhythmic, intrinsically generated electrical activity that is produced by cells described as pacemaker neurons. Two disease-relevant *in-vitro* models were investigated that display poorly understood pacemaker activity; AtT20 anterior pituitary corticotrophs and human induced pluripotent stem cell (hiPSC)-derived dopaminergic (DA) neurons. Using electrophysiology and Ca^{2+} imaging, gaps in our understanding of pacemaking in these cell types were investigated. For AtT20s, it was revealed that hormone secretion in this cell type is uncoupled from its electrical activity. Novel roles were found for T-type voltage-gated calcium channels (VGCCs) in pacemaking and for L-type VGCCs in maintaining intracellular Ca^{2+} concentrations. hiPSC-derived DA neurons were found to produce apparently spontaneous electrical activity in culture that was dependent upon L-type VGCCs. This pacemaking was not found to be intrinsic, instead being driven by and developing in parallel with synaptic input in culture. These DA neurons immunostained for the L-type VGCC subtype $Ca_V1.3$, which is involved in the death of DA neurons in Parkinson's disease. Using a novel cell death assay these neurons were found to be selectively susceptible to the DA toxin 6-hydroxydopamine but displayed a resistance to glutamate-induced excitotoxicity. Data here provides valuable information on the similarities and differences between these *in-vitro* models and their *in-vivo* counterparts. This allowed for an in-depth assessment of their suitability as models for their respective diseases, hopefully leading to the targeted, efficient design of studies that use these cell types.

Acknowledgements

First I would like to thank my supervisor, Dr Euan Brown. Your knowledge, expertise and jovial nature have helped me more times than I can count.

Special thanks to those who have aided my research either through your advice, training, the lending of reagents or your witty banter.

And to the spearing crew, for pulling me through.

ACADEMIC REGISTRY

Research Thesis Submission

Name*:*	Matthew Robert Stephen Euston		
School:	Engineering & Physical Sciences		
Version: *(i.e. First, Resubmission, Final)*	Final	Degree Sought:	PhD

Declaration

In accordance with the appropriate regulations I hereby submit my thesis and I declare that:

1) The thesis embodies the results of my own work and has been composed by myself
2) Where appropriate, I have made acknowledgement of the work of others and have made reference to work carried out in collaboration with other persons
3) The thesis is the correct version of the thesis for submission and is the same version as any electronic versions submitted*.
4) My thesis for the award referred to, deposited in the Heriot-Watt University Library, should be made available for loan or photocopying and be available via the Institutional Repository, subject to such conditions as the Librarian may require
5) I understand that as a student of the University I am required to abide by the Regulations of the University and to conform to its discipline.
6) I confirm that the thesis has been verified against plagiarism via an approved plagiarism detection application e.g. Turnitin.

* *Please note that it is the responsibility of the candidate to ensure that the correct version of the thesis is submitted.*

Signature of Candidate*:*		Date:	

Submission

Submitted By *(name in capitals):*	
Signature of Individual Submitting:	
Date Submitted:	

For Completion in the Student Service Centre (SSC)

Received in the SSC by *(name in capitals):*			
Method of Submission *(Handed in to SSC; posted through internal/external mail):*			
E-thesis Submitted (**mandatory for final theses)**			
Signature:		Date:	

TABLE OF CONTENTS

LIST OF FIGURES

Chapter 1 – Introduction

Chapter 2 - The Mechanism of Pacemaking in AtT20 Anterior Pituitary Corticotrophs

Chapter 3 - The Development of Pacemaking in hiPSC-Derived Dopaminergic Neurons

Chapter 4 - $Ca_V1.3$ Expression and Selective Vulnerability in hiPSC-Derived Dopaminergic Neurons

Chapter 5

Supplementary

List of Tables

Glossary

6-OHDA - Hydroxydopamine

ACTH - Adrenocorticotropic hormone

AMPA - α-amino-3-hydroxy-5-methyl-4-isoxazolepropionic acid

AVP - Arginine vasopressin

cAMP – Cyclic adenosine monophosphate

CNQX - 6-cyano-7-nitroquinoxaline-2,3-dione

CRH - Corticotropin releasing hormone

DA – Dopaminergic

D-AP5 - (2R)-amino-5-phosphonovaleric acid

dV/dt – Rate of change of the membrane potential

ESPSC - Excitatory spontaneous postsynaptic current

GABA - γ-aminobutyric acid

GPe - External globus pallidum

GPi - Internal globus pallidum

HCN – Hyperpolarisation-activated cyclic nucleotide channel

hiPSC - Human induced pluripotent stem cell

HNE - Hydroxynonenal

hNPC - Human neural progenitor cell

Kv- Voltage-gated potassium channel

MPTP - 1-methyl-4-phenyl-1,2,3,6-tetrahydropyridine

MSN - Medium spiny neuron

Nav - Voltage-gated sodium channel

NMDA - N-methyl-D-aspartate

PD - Parkinson's disease

PPN - Pedunculopontine nucleus

ROS - Reactive oxygen species

S.E.M. – Standard error of the mean

SHH – Sonic hedgehog

SNc - Substantia nigra pars compacta

STED – Stimulated emission depletion

STN - Subthalamic nucleus

TEA –Tetraethylammonium

TH – Tyrosine hydroxylase

TTX - Tetrodotoxin

VGCC - Voltage-gated calcium channel

Chapter 1

Introduction

Many neural networks are required to function at particular frequencies. These processes are often driven by rhythmic, intrinsically generated electrical activity that is produced by cells described as pacemaker neurons. This activity is known to drive processes such as motor control, release of hormones/neurotransmitters and synaptic plasticity (Pike et al., 1999). This pacemaking is also implicated in diseases such as epileptic seizures and Parkinson's disease (PD) (Brozoski et al., 1979; Ludwig et al., 2003). Understanding the biophysical mechanisms of how pacemaking is generated, maintained and impaired is therefore critical to the understanding of such diseases.

The research in this thesis focusses on two disease-relevant *in-vitro* models that exhibit poorly understood pacemaker activity. **AtT20 D16v-F2** is a mouse tumour cell line derived from corticotrophs in the anterior pituitary. Corticotrophs are involved in the regulation of the stress hormone cortisol *in-vivo*. Dysregulation of corticotroph activity can lead to Cushing's disease (Bornstein et al., 2008). The role of voltage-gated calcium channel (VGCC) subtypes in AtT20 pacemaking is relatively underexplored. **Human induced pluripotent stem cell (hiPSC) derived dopaminergic (DA) neurons** have recently come to the foreground as a human model for Parkinson's disease (PD). *In-vivo*, DA neurons tonically release the neurotransmitter dopamine to control fine motor processes. Their death is associated with the main motor symptoms of PD (Burns et al., 1983). Cultured DA neurons from rats have been shown to fire rhythmically in culture (Grace & Onn, 1989) though the electrical properties of hiPSC-derived DA neurons are relatively underexplored. Given that the majority of research into PD has been performed on animal models, these neurons provide an opportunity to learn more about human forms of the disease.

This introduction will give a review of the literature so as to allow the reader to understand the background and aims of the following research. Later chapters will focus on my research into understanding the role of VGCC subtypes in pacemaking in AtT20s and how pacemaking develops in hiPSC-derived DA neurons. It is possible to define pacemaking as being either endogenously or exogenously generated. The data obtained from these chapters allows for a comparison between the mechanisms of pacemaking in these models and their *in-vivo* counterparts to be performed in greater depth than has previously been documented in the literature. This allows for the answering of one simple question in the discussion: Are these cell types suitable for modelling the role of excitability in their respective *in-vivo* diseases?

1.1 Pacemaker Activity in the Nervous System

1.1.1 Excitable Cells, their Roles & their Discovery

It has long been known that the brain is a critical organ for the centralised control of the body. In the 4th century BC the Greek philosopher Hippocrates believed the brain to be the seat of intelligence, a notion that has been proven correct by anatomical lesion studies. In 1550 the first link between the visual system and the brain was established by the discovery that the optic nerve originates in the brain (reviewed in Shampo & Kyle, 1981). In 1855 Bartolomeo Panizzas' treatise "Observations of the Optic Nerve" presented evidence for the occipital lobe being critical to the visual system (Colombo et al., 2002). In 1760 it was shown that compression of the cerebellum can produce sleep and that a puncture of the spinal cord between the second and third vertebrae causes immediate cessation of breathing (Lorry, 1760). Lesion studies in frogs soon localised this respiratory centre to the medulla oblongata within the hindbrain (Fye, 1995). This idea of separate brain regions for separate functions was backed up by Jean Pierre Flourens in 1822. His layer by layer lesioning of brain regions in pigeons showed the role of the brain in cognition, motor control and autonomic processes (reviewed in Dennis, 1948).

This ability of the brain to control processes peripheral to itself gives rise to several important questions:

1. How are signals reaching different parts of the body?
2. How are these signals propagated?
3. Do signals originate from external or internal sources?

Early theories centred on the idea that the tissue as a whole was the source of the signal (Harris & Almerigi, 2009) though with the invention of silver nitrate staining (Golgi, 1873) and pioneering work by Jan Evangelista Purkyně and Santiago Ramón y Cajal it was discovered that the nervous system is composed of discrete individual cells known as neurons (reviewed in López-Muñoz et al., 2006). Before this, in 1852, it had been definitively shown that motor nerves originated in the anterior horn of the spinal cord. This proved for the first time that neuronal processes directly interact with tissues throughout the body to send and receive signals (in JAMA, 1968).

The nature of the signal was a more complicated question to answer, with incremental advances in its understanding having occurred since the 1700's. Luigi Galvani's observations on frogs were the first to suggest the existence of electrical potentials in animals. He discovered that when two different metals came into contact with a frog's leg the muscle would twitch (Bresadola, 1998). This was later confirmed to be an electrical signal passing through the muscle and was theorised to be caused by "electric molecules" on either side of the muscle fibre membrane (Pearce, 2001). In 1928, experiments by Edgar Adrian on the optic nerve of frogs led to the conclusion of an all-or-nothing response of electrical firing. This was later termed an 'action potential' (Hodgkin et al., 1979). The carriers of the action potential in neurons were identified and described in detail by Alan Hodgkin and Andrew Huxley in 1952. By performing voltage clamp experiments they were able to deduce that the selective flow of sodium and potassium ions across the membrane were responsible for the initiation and propagation of the squid giant axon action potential (Hodgkin & Huxley, 1952). Throughout the 1980's work primarily by William Catterall identified and functionally reconstituted the voltage-gated sodium channel, the first known membrane protein responsible for the selective permeability of ions across the membrane (Hartshorne & Catterall, 1981, 1985). Later, channels were discovered for the other constituent ions. This, coupled with the invention of the patch clamp technique allowing the recording of single channel currents (Neher & Sakmann, 1976), has led to the characterisation of the action potential and to a modern definition of an excitable cell: that which can be electrically excited in response to a stimulus, resulting in the generation of action potentials.

1.1.2 Spontaneous Excitability in the Nervous System

There is a great deal of evidence to suggest that much of the electrical activity within the nervous system is generated by external stimuli, with action potential firing often being driven by synaptic input from other neurons (Magee, 2000). However, not all activity in the nervous system occurs in response to an identifiable external stimulus. Firing has been identified that is driven solely by intrinsic factors. This is known as 'spontaneous excitability.' Activity of this nature has been seen in a vast number of neuronal cell types during embryonic development and is believed to be a property shared by all developing neural networks (Donovan, 1999). Spontaneous, periodic

activity has been identified in the developing networks of the spinal cord, hippocampus and neocortex in the absence of synaptic connections (Yuste et al., 1995; Chub & O'Donovan, 1998; Feller, 1999). Increasing the rate of spontaneous firing in maturing cortical neurons by raising intracellular Ca^{2+} may halt their migration and promote dendrite formation (Bando et al., 2016). Depression of spontaneous excitability is associated with a lower number of synaptic connections but increased synaptic strength to those already formed (Burrone et al., 2002). It is therefore apparent that spontaneous activity is required for the formation and modulation of synaptic networks during development and possibly has an important role to play in synaptic plasticity. Spontaneous firing has also been detected in the adult nervous system in cells such as cerebellar Purkinje, retinal dopaminergic, amacrine and reticular thalamic neurons (Avanzini et al., 1989; Häusser & Clark, 1997; Feigenspan et al., 1998). Changes in neuronal spontaneity have also been linked to disease states such as spinal muscular atrophy and epilepsy (Benardete et al., 2002; Jablonka et al., 2007).

Given how energetically demanding the firing of action potentials is, spontaneous activity must serve an important purpose. Several possible roles have been suggested (Häusser & Clark, 1997). Firstly, changes in firing rate could provide a mechanism of plasticity independent of synaptic input. Secondly, it could cause cells to become more sensitive to excitatory input. Thirdly, if the activity is regular in nature, it could act as a pacemaking controller for other systems. Evidence for it fulfilling all of these roles has been identified: intrinsic excitability has been shown to be mediated by changes in the levels of particular of proteins such as CaMKII, providing a mechanism for non-synaptic plasticity (Nelson et al., 2005). Neurons that normally receive a large number of inputs, such as reticular thalamic neurons, have been seen to show spontaneous activity in the absence of synaptic connections, suggesting that spontaneous activity increases their sensitivity to synaptic input (Steriade et al., 1987). Pacemaker neurons have been identified in numerous autonomic processes and will be discussed in detail in the next section.

1.1.3 Pacemaker Neurons

Systems in the nervous system that are required to perform at set frequencies often have associated sets of neurons that act as controllers to ensure their correct functioning.

These neurons, termed pacemaker neurons, fire spontaneous action potentials at regular intervals to entrain the system to the rate of pacemaking (Ramirez et al., 2004).

Neurons possessing pacemaker properties have been identified in the neocortex, basal ganglia, thalamus, hypothalamus, ventral tegmentum area, hippocampus, substantia nigra and amygdala among others. These areas of the brain have been associated with the sleep/wake cycle, motivation, addiction, memory consolidation, cognition, fear and motor control (Ramirez et al., 2004).

Pacemakers of this sort have benefits over other mechanisms of synchronised control. First, functional states can be quickly modulated by changes in excitability at the cellular level, such as the observed changes in firing patterns during sleep-wake transition (Henn et al., 1984). Second, groups of cells can be synchronised to fire in an ensemble, as is the case for cardiac pacemaker cells in the sinoatrial node (Rekling et al., 1996).

Pacemaking is tightly controlled either by the firing of single action potentials at a particular frequency (tonic firing) or by firing in rhythmic bursts or plateaus followed by periods of quiescence (**Figure 1.1**). An interplay of different voltage-sensitive ionic conductances allows pacemaker cells to produce rhythmic changes in membrane potential, on-top of which action potentials are generated. This allows for the retention of a set firing rate independent of synaptic input (Schweitzer et al., 2003). In contrast, non-pacemaking neurons gradually change their firing pattern to correspond to their synaptic input (Ramirez et al., 2004). The mechanisms that control pacemaking can roughly be broken down into two categories: intrinsic and agonist-induced.

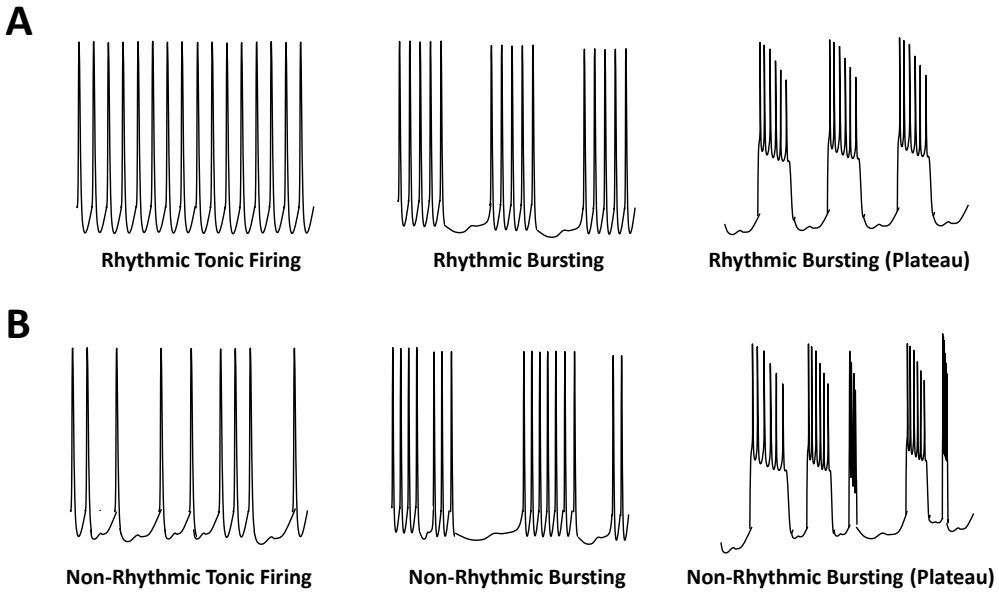

Figure 1.1 - Rhythmic vs Non-rhythmic activity. (A) 3 rhythmic firing patterns that can be present in pacemaker cell types. (B) This is contrasted against the arrhythmic activity of non-pacemaker cell types. Rhythmic and arrhythmic activity isn't always so clear cut, with cells being rhythmic at times and arrhythmic at others depending on their intracellular dynamics and synaptic input. Pacemakers are therefore defined by their ability to produce rhythmic activity in synaptic isolation.

1.1.3.1 Intrinsic drivers of excitability

The innate properties of the action potential typically act to prevent spontaneous or repetitive action potential firing. The squid giant axon for example, when stimulated, produces a single action potential at the other end of the fibre (Curtis & Cole, 1942). This acts to prevent the loss of signal integrity and spontaneous firing, resulting in high fidelity, 1:1 propagation of action potentials. It is obvious why this high-fidelity signalling has developed, as unwanted activation of critical systems could have potentially disastrous effects. This lack of spontaneous firing is due to there being a refractory period between action potentials (**Figure 1.2**).

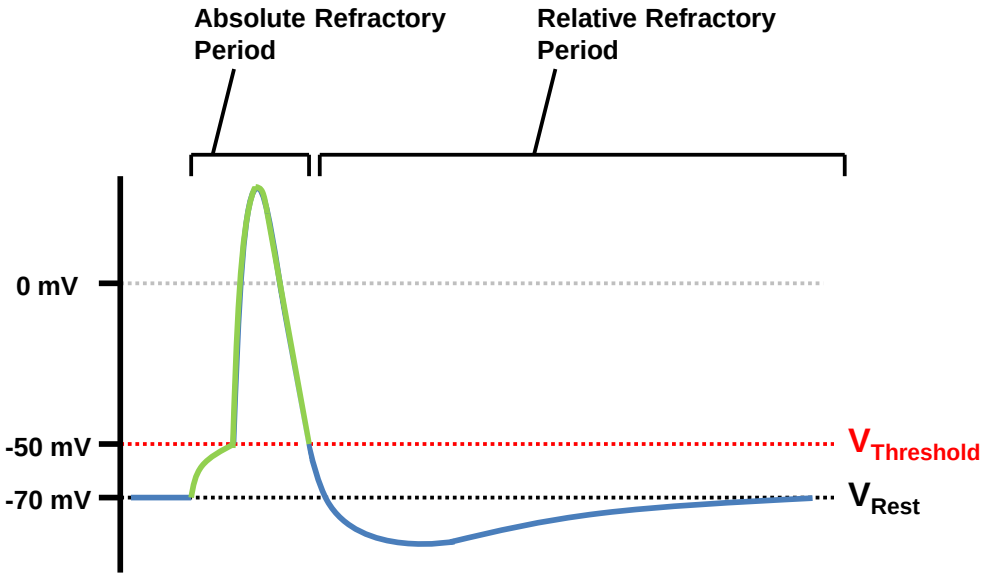

Figure 1.2 - Action potential properties in excitable cells. Diagram of a typical action potential where a change in resting membrane potential (V_{Rest}) up to threshold ($V_{Threshold}$) produces an all-or-nothing response followed by hyperpolarisation and repolarisation. The absolute (green) and relative (blue) refractory periods are highlighted. Diagram by M. Euston, with information from Lodish et al., 2000.

This can be broken down into two constituent parts: The absolute refractory period (where no stimulus no matter how strong can cause a repeat firing) which is dependent upon Na^+ channel inactivation and the relative refractory period (where a strong enough stimulus can still induce firing) which is the result of slow inactivation of K^+ channels after the membrane hyperpolarisation (Lodish et al., 2000). In ureter smooth muscle, for example, the refractory period is over 10 seconds long (Burdyga & Wray, 2005). How then does repetitive or burst firing occur in pacemaker cell types despite these limitations?

The answer appears to lie in the unique combination of ion channels expressed within spontaneously active neurons. A range of voltage gated ion channels have been seen in the cell bodies and dendrites of various pacemaker cell types, ranging from voltage-gated ion channels such as L-type VGCCs, voltage-gated sodium (Na_V) and voltage-gated potassium ($K_{V)}$ channels, Ca^{2+} activated SK, BK and Cl^- channels, hyperpolarization-activated cyclic nucleotide–gated (HCN) channels and rectifiers such as the Ca^{2+}-ATPase pump and the K^+ inwardly rectifying channels. The balance of these different channel conductances appears to be critically important, as the modelling of eight different voltage-sensitive currents with varying conductances can produce excitatory states ranging from single action potentials to rhythmic burst firing in neurons (Prinz et al., 2003). VGCCs appear to be of particular importance, with internal changes in the cytoplasmic Ca^{2+} concentration being present in numerous pacemaker systems including thalamic neurons and DA neurons of the substantia nigra (Coulon et al., 2009; Ferrari et al., 2012).

The line between pacemaking and non-pacemaking neurons can be difficult to distinguish, with the same neurons displaying pacemaker activity at certain times and non-pacemaker activity at others. Respiratory neurons show variation between cells with arrhythmic bursting, tonic firing and rhythmic bursting seen within the same population (Peña et al., 2004). Electrically coupled pacemaker neurons in lobsters have different reactions to the same electrical stimulus (Marder & Eisen, 1984). This heterogeneity can be partially explained by the fact that neurons of the same phenotype may not express the same combinations of ion channels (Amaya et al., 2000).

Differences in ion channel expression can result in several changes in excitability. The refractory period in neurons varies between cell types and is believed to be dependent upon the expression of Ca^{2+} and K^+ channels. Alteration of these conductances has been

observed to reduce or elongate the time between action potential firing in ureter smooth muscle cells by affecting the relative refractory period (Burdyga & Wray, 2005).

Action potentials also require the reaching of a threshold potential in order for firing to occur (Hodgkin & Huxley, 1952). This threshold can vary between cell types and can even vary between regions of a cell with dendrites typically showing lower thresholds than cell bodies (Kole & Stuart, 2008). Increases in external [K^+] can shift the threshold for firing, suggesting that ionic concentration gradients and therefore ion channel expression are critical in setting the potential at which cells fire (Chen & Gettes, 1976). The rate of change of membrane potential (dV/dt) is also of critical importance. Due to the capacitive properties of neuronal cell membranes any changes in potential do not occur instantaneously, instead occurring in a ramp-like fashion that takes into account the charging time of the membrane (Martin, 1976). Modelling studies in cortical neurons show that changes in dV/dt have drastic effects on action potential firing, controlling whether or not they occur as well as their amplitude and duration (Naundorf et al., 2006). dV/dt is dependent upon both the capacitive properties (which are dependent upon cell size) and the resistive properties of the membrane, which are dependent upon ion channel expression (Kandel et al., 1997). This provides a mechanism whereby small differences in ion channel expression can have much larger influences on cell excitability, explaining the diversity seen within and between pacemaker cell types.

The importance of dV/dt is related to the gating properties of voltage-gated ion channels, with particular emphasis on Na_V channels (**Figure 1.2**). Na_V channels can exist in one of 3 conformations. When at resting membrane potentials Na_V channels are typically closed. Upon reaching the required potential threshold for channel opening, these channels rapidly open to allow Na^+ conductance. These channels cannot return directly to a closed state however. First they are required to cycle through an inactivation state before recovering to the closed state. When the rate of membrane potential change to threshold is slow (low dV/dt), these channels can inactivate without fully reaching an open state (Armstrong, 2006). Computer modelling has shown that this inactivation can directly affect the firing threshold and prevent action potential firing (Platkiewicz & Brette, 2011) (**Figure 1.3**).

Pacemaker activity can therefore be intrinsically driven in these cell types by careful balancing of the various ion channel conductances that control their action potential properties. This results in underlying fast changes in membrane potential and changes in

properties such as the refractory period and firing threshold that allow for the repetitive or burst firing of action potentials

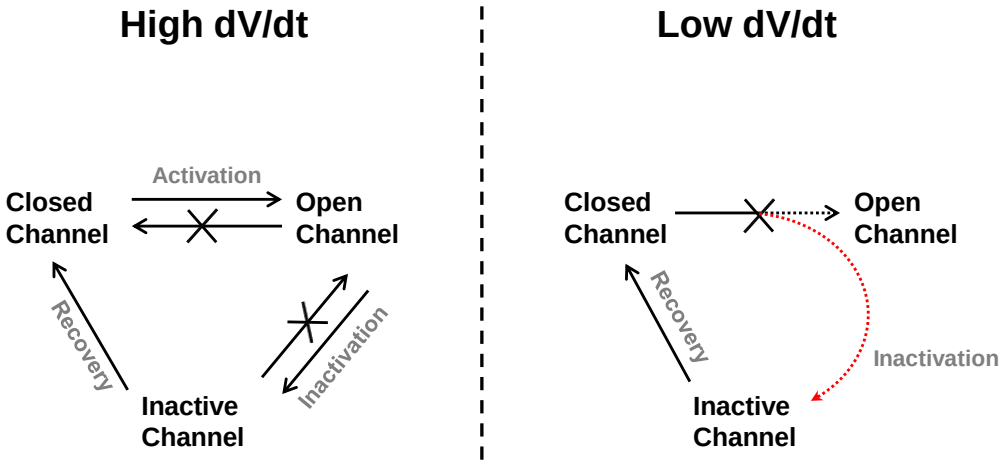

Figure 1.3 - Na_V channel activation and inactivation. Diagrams showing the activation properties of Na_V channels in response to fast (high dV/dt) and slow (low dV/dt) changes in membrane potential up to threshold. Diagram by M. Euston, with information from Armstrong, 2006.

1.1.3.2 Agonist-Induced Excitability

Heterogeneity is not only explained by ion channel expression however, as internal mechanisms such as phosphorylation, intracellular Ca^{2+} dynamics and receptor activation can alter ion channel conductances (Pape et al., 2004). Pacemaker currents can be altered by cAMP synthesis in response to G-protein coupled receptor activation (Frère & Lüthi, 2004). Activation-dependent firing is seen in pacemakers in the hypothalamic arcuate nucleus in response to orexigens and in pancreatic islets in response to glucose (Atwater et al., 1978; van den Top et al., 2004).

Although pacemaker cells are characterised by their ability to fire without input, synaptic inputs are often able to alter their activity patterns. Changing the frequency of regularly spaced synaptic inputs in computer-based models of *Aplysia* pacemaker neurons results in frequency-dependent changes in excitability (Perkel et al., 1964). This proposed effect of neurotransmitter-dependent changes in activity has been experimentally confirmed. For example, inhibition of DA transmission in lobster pyloric neurons causes irregular and infrequent burst firing (Johnson et al., 2003).

It is clear then that pacemaking in the nervous system is a complicated process, with intrinsic drivers of excitability being regulated by activity-dependent processes such as intracellular signalling and synaptic activity.

Two disease relevant examples of pacemakers in the nervous system are anterior pituitary corticotrophs and DA neurons of the substantia nigra pars compacta (SNc). As neuroendocrine cells the principle role of corticotrophs is to release adrenocorticotropic hormone (ACTH). Disturbance of ACTH release can lead to Cushing's disease (Bornstein et al., 2008). DA neurons are involved in the control of fine motor control and their intrinsic excitability is believed to lie behind their specific cell death in PD (Surmeier & Schumaker, 2013). Both cell types have *in-vitro* models that present an opportunity to study how pacemaking develops as these cell types mature into electrically active cells. The following review sections will focus on the literature surrounding these models, focusing on their roles *in-vivo* and what is and isn't known about their excitability.

1.2 Pacemaking in Anterior Pituitary Corticotrophs

1.2.1 The Role of Corticotrophs *In-Vivo*

The anterior pituitary is a gland, located in the midbrain, whose function is the release of hormones to regulate homeostatic processes such as stress, development and reproduction. A subpopulation of cells within this region, when identified using electron microscopy, have been found to contain numerous large (~0.5 μM in diameter), dense core vesicles that contain ACTH (Kurosumi et al., 1966). ACTH is a key regulator of stress responses through its induction of cortisol secretion from the adrenal cortex, as well as indirect roles in the release of adrenaline and noradrenaline. This hormonal response chain is termed the hypothalamic–pituitary–adrenal (HPA)-axis (Fulkerson & Pamela, 1982; Valenta et al., 1986). ACTH causes a time-dependent increase in plasma cortisol levels following exposure to a stressor (Fulkerson & Pamela, 1982). Optogenetic release of ACTH in zebrafish promotes avoidance behaviour, indicating its importance in immediate responses to stress (De Marco et al., 2016). ACTH is also critical for long term responses to stress and the control of circadian rhythms such as those involved in sleep and alertness. Corticotrophs display pacemaker activity *in-vivo*

and the release of ACTH is linked to action potential firing (Guérineau et al., 1991; Lee & Tse, 1997). This provides a link between pacemaking and diseases of ACTH secretion, such as Cushing's disease.

1.2.1.1 Cushing's Disease: A Case Study of HPA-Axis Function

Cushing's disease is a form of ACTH-dependent Cushing's syndrome that is caused by pituitary corticotroph tumours. Over-production of ACTH in these tumours leads to excessive release of cortisol and subsequent dysfunction of cortisol-related processes (Nelson et al., 1960). It is also associated with reduced regularity, orderliness and synchrony of hormone release, indicating that abnormal pacemaking may be involved (van den Berg et al., 1997).

Cushing's disease and increased cortisol levels are associated with weight gain and obesity (Greening et al., 2006). Intravenous injection of cortisol in rats causes sustained increases in the appetite promoter Neuropeptide Y in the hypothalamus and, paradoxically, increases in the appetite suppressant leptin (Zakrzewska et al., 1999). Weight gain in Cushing's therefore appears to be caused by complex changes in levels of proteins with contradictory effects, resulting in an overall trend towards weight gain.

Stunted growth and osteoporosis have been seen in Cushing's disease patients (Raff et al., 2014). Elevating cortisol levels in rats causes an increase in the number of osteoblasts and osteoclasts seen undergoing apoptosis (Weinstein et al., 1998). ACTH can also interact with osteoblasts through the MC2R receptor to directly regulate bone mass. *In-vitro*, ACTH stimulates osteoblast proliferation while inhibiting proliferation at high concentrations (Isales et al., 2010). ACTH aids in the regulation of bone density through direct, concentration-dependent effects on osteoblast proliferation and indirectly by promoting apoptosis through the release of cortisol.

A study looking at the psychiatric condition of patients with Cushing's disease found high levels of association with depression, decreased concentration, decreased libido and insomnia. The severity of the disability, although found to be reduced, was still present in patients with high cortisol but low ACTH levels, indicating that effects of ACTH independent of cortisol are involved in many of the symptoms (Starkman & Schteingart, 1981). The predominant theory for the mechanism of ACTH induction of psychiatric illnesses centres on increased net glucocorticoid signalling in affected brain regions. Indeed, regions such as the neocortex and hippocampus that are associated with

memory formation have been seen to express high numbers of glucocorticoid receptors (Hansson et al., 2000).

Diabetes and insulin resistance are seen in a proportion of patients (Raff et al., 2014). Patients infused with high doses of cortisol showed increased gluconeogenesis in the pancreas (Khani & Tayek, 2001). Cortisol also promotes glucagon and catecholamine action, contributing to insulin resistance and increased blood glucose levels (Gerich et al., 1980).

1.2.1.2 Mechanisms of ACTH Secretion

Secretion of adrenal hormones is caused by ACTH binding to melanocyte type-2 receptor, a G-protein coupled receptor on cells of the zona fasciculata and zona reticularis in the adrenal cortex (Cone & Mountjoy, 1993). This causes induction of cAMP synthesis (Gallo-Payet & Payet, 2003) and the translocation of cholesterol to the inner cell membrane by the action of steroidogenic acute regulatory protein, the proposed rate-limiting step in steroid hormone synthesis (Lin et al., 1995). Increased expression of the mitochondrial genes cytochrome P450, cytochrome oxidase and ATPase have been detected following ACTH binding (Hanukoglu et al., 1990). Upregulation of these genes increases energy-producing capacity and in turn steroid hormone production. This provides a mechanism for long-term changes in hormone release through the regulation of gene expression (Raikhinstein & Hanukoglu, 1993).

ACTH secretion is regulated through interaction with other brain regions, most notably the posterior pituitary, the suprachiasmatic nucleus (SCN) and the hypothalamus. Corticotropin releasing hormone (CRH), a 41 amino acid peptide released from periventricular neurons in the hypothalamus, is the primary stimulator of ACTH release by interaction with the CRH-R1 receptor on corticotroph cells. Upon binding to its receptor it stimulates synthesis of ACTH from its precursor, pro-opiomelanocortin, through the activation of cAMP pathways (Kageyama & Suda, 2009). Different isoforms of this receptor have been found which could explain why only a proportion of ACTH-containing vesicles go through exocytosis at any one time, giving a mechanism for pulsatile release (Pisarchik & Slominski, 2001). Arginine vasopressin (AVP), either released from the posterior pituitary or synthesised by corticotrophs, also stimulates ACTH secretion (Aguilera & Rabadan-Diehl, 2000). It acts through the V1b receptor to

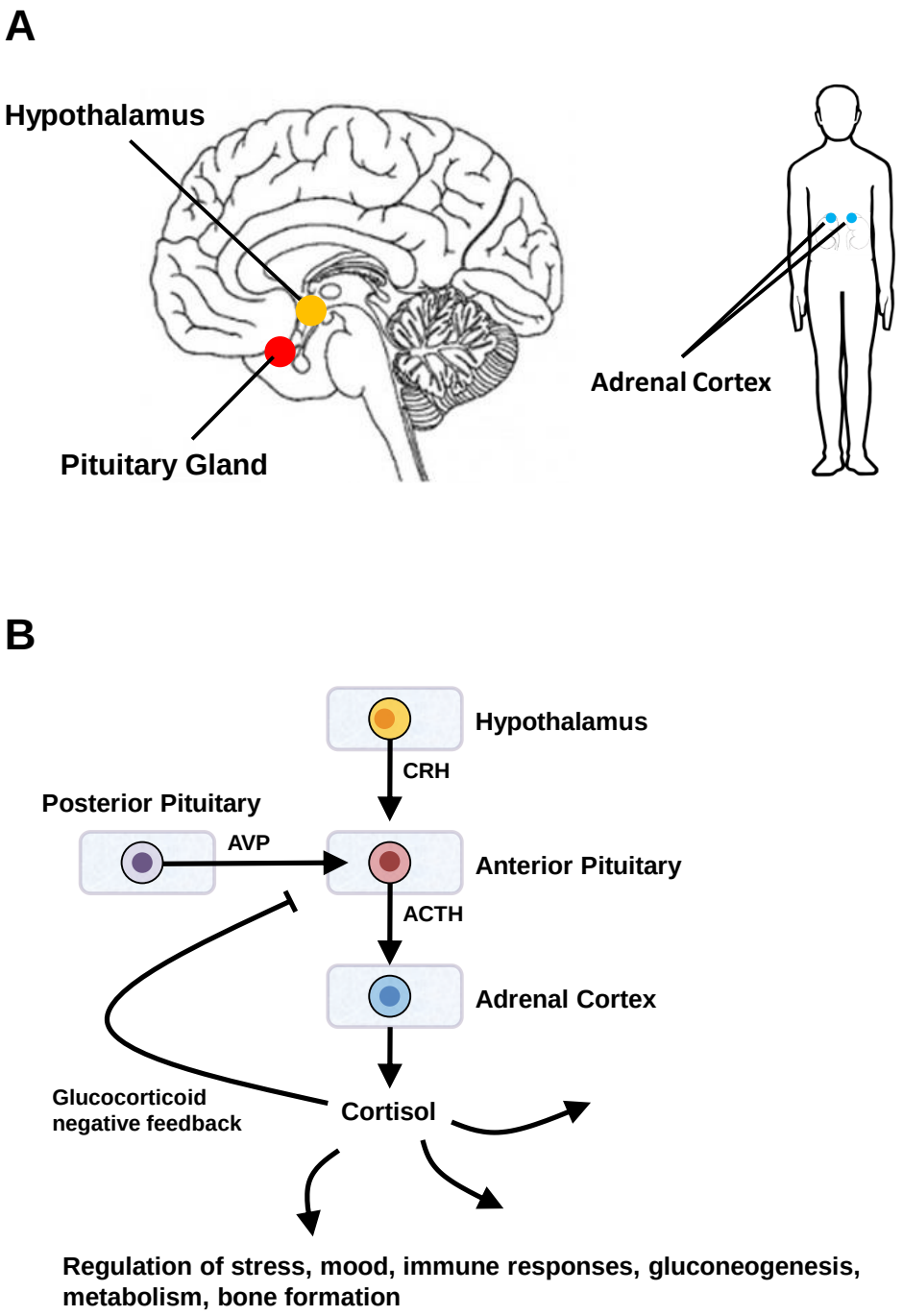

Figure 1.4 - The principle components of the HPA-axis. (A) The regions involved in the HPA-axis. Hypothalamic stimulation of the anterior pituitary, located at the base of the hypothalamus, causes stimulation of the adrenal glands located at the top of the kidneys. (B) Release of CRH from the hypothalamus or AVP from the posterior pituitary stimulates ACTH secretion from corticotrophs within the anterior pituitary. This leads to release of cortisol from the adrenal cortex. Cortisol, aside from its physiological effects, acts as part of a negative feedback loop by binding to receptors on corticotrophs to inhibit its own release. In Cushing's disease, excessive ACTH secretion results in excessive release of cortisol (Diagram by M. Euston).

increase the responsiveness of cells to CRH (Spiga et al., 2009) and has been found to rescue the stress response in CRH-R1 knockout mice (Turnbull et al., 1999).

Various other receptors have been implicated in ACTH release from corticotrophs. Lesioning of the suprachiasmatic nucleus causes the release of ACTH to become less rhythmic, an effect that can be replicated by blockade of serotonin receptors (Spinedi & Negro-Vilar, 1983; Sage et al., 2001). Lastly, glucocorticoid receptors on corticotrophs provide evidence for a cortisol-dependent feedback loop (Yokote et al., 1991). Corticotrophs show reduced secretion of ACTH in high concentrations of cortisol, perhaps through the attenuation of Ca^{2+}-dependent voltage-gated potassium currents (Duncan et al., 2016).

It is clear then that secretion of ACTH is involved in a large number of physiological processes, either directly or indirectly through the release of cortisol, and is controlled by several pacemaker systems or feedback loops. The components of the HPA-axis are outlined in **Figure 1.4**. Due to the finding that ACTH secretion is coupled to membrane depolarisation (Lee & Tse, 1997), a vast body of research has been performed on the mechanisms of corticotroph pacemaking to determine the role of electrical activity in diseases of ACTH secretion.

1.2.2 Corticotroph Pacemaking *In-Vivo*

ACTH release from corticotrophs is highly dependent upon changes in membrane potential, with secretion being associated with membrane depolarisation and an increased intracellular Ca^{2+} concentration (Lee & Tse, 1997). Their firing activity consists of two modalities: low frequency tonic firing or plateau-like bursts of action potentials. Activity is rhythmic in nature, acting as a pacemaker for ACTH release (Zemkova et al., 2016). This pacemaker is controlled by two complementary systems: intrinsic and agonist-induced excitability (**Figure 1.5**).

1.2.2.1 Intrinsic Excitability in Corticotrophs

Various voltage-gated currents have been implicated in the regulation of intrinsic excitability in corticotrophs. Inactive corticotrophs have a more depolarised resting membrane potential compared to active cells, an effect likely caused by the membrane potential being depolarised past the threshold for firing (Zemkova et al., 2016). This

indicates that maintenance of this potential is important in progressing corticotrophs to an excitable state. Patch clamp recording and channel knockout experiments have reported that inwardly-rectifying potassium channels and TREK-1, a potassium channel activated by polyunsaturated fats and lysophospholipids, all maintain this hyperpolarised resting membrane potential (Kuryshev et al., 1995; Liang et al., 2011). RT-PCR has revealed the presence of HCN channels (Kretschmannova et al., 2012). These channels are commonly found in pacemaking cells and act at hyperpolarised potentials to drive membrane repolarisation (Zolles et al., 2006).

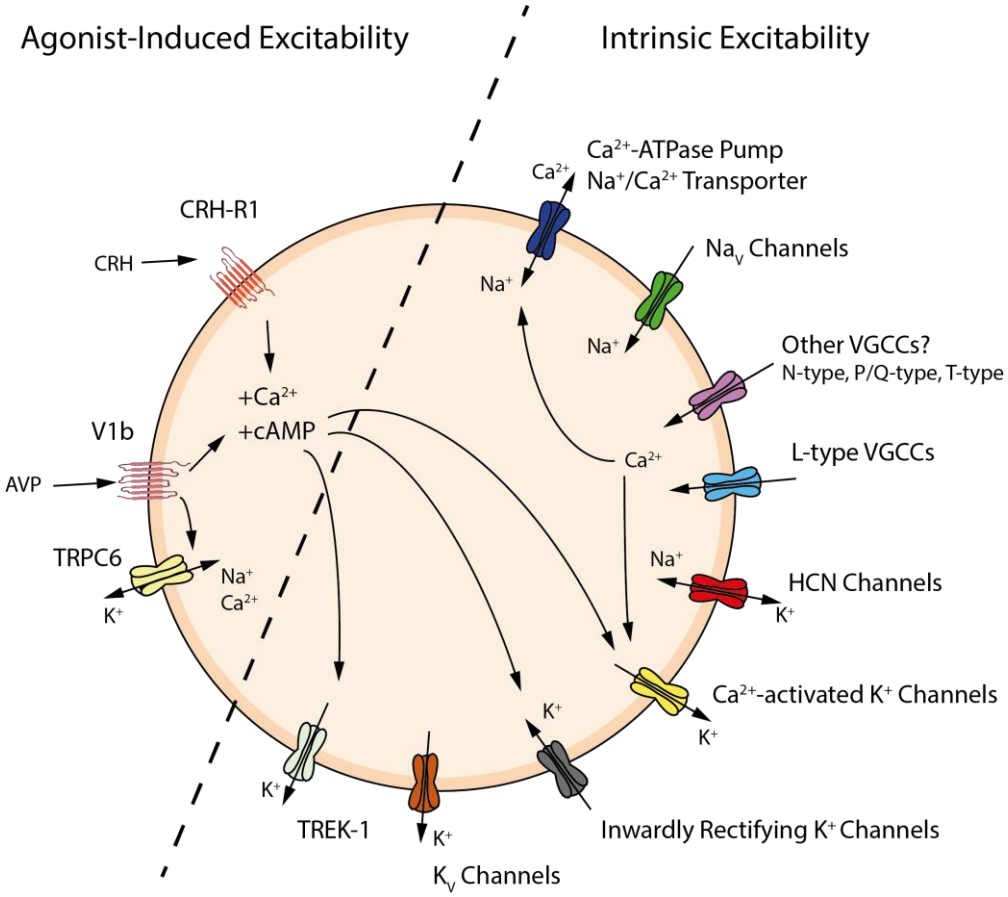

Figure 1.5 - Excitability in corticotrophs *in-vivo*. Pacemaking is controlled by intrinsic and agonist-induced factors. The resting membrane potential is maintained by K^+ channels such as K_V, BK, SK and TREK-1. Action potentials are generated by Na_V channels with underlying Ca^{2+} waves produced by L-type VGCCs. Inwardly rectifying K^+ channels, Ca^{2+}-ATPase pumps and Na^+/Ca^{2+} transporters maintain ionic concentrations following an action potential. HCN channels act as pacemaker channels to help return the cell to its resting potential following an action potential, aided by K^+ channels. CRH and AVP, act on receptors to induce increases in Ca^{2+} concentration and cAMP synthesis. This causes changes in the activity of TREK-1, BK/SK and inwardly rectifying K^+ channels. V1b activation also affects TRPC6 channels via an as-of-yet unknown mechanism (Diagram by M Euston).

Block of Na_V channels or L-type VGCCs abolishes pacemaking. Block of L-type channels reveals single Na^+-dependent action potential firing upon current injection, while block of Na_V channels alone reveals underlying, subthreshold Ca^{2+}-dependent changes in membrane potential (Zemkova et al., 2016). It would seem then that both of these channels are involved in pacemaking, with VGCCs producing a fast, rhythmic dV/dt that brings the membrane potential past a threshold that induces firing of Na^+ dependent action potentials. Modelling of ion channel properties in corticotrophs has shown that the relative balance of these different ion channel conductances can explain the spiking patterns seen *in-vivo*, as well as a possible role for BK channels. When Na^+ conductances are low, changes in BK conductance decide whether a fire tonically or burst fire. For inactive cells however, changes in BK conductance do not cause them to become active (Fletcher et al., 2017). A further modelling study suggested that raising or lowering K^+ and Ca^{2+} conductances was able to shift the threshold for firing and cause faster, more exaggerated shifts in dV/dt. This resulted in rhythmic spiking within the model and explains the effects seen in the previous study (LeBeau et al., 1997). The Ca^{2+} dependence of BK channels also implicates VGCCs in the regulation of spike duration and could help explain how rhythmic firing is generated. A Ca^{2+} transient during depolarisation could promote the activation of BK channels in a concentration-dependent manner, providing a feedback mechanism to limit spike duration to within a set range. BK channels are present in corticotrophs (Duncan et al., 2015) and VGCCs have been seen to regulate BK channel activity in other pacemaker systems (Marcantoni et al., 2010). Experimental evidence for their involvement in intrinsic excitability is sparse, however there is evidence for BK channels affecting spike frequency in subsets of mouse corticotroph knockouts (Liang, 2012).

1.2.2.2 Agonist-Induced Excitability in Corticotrophs

The main hormonal regulators of ACTH secretion, CRH and AVP, have been reported to induce firing in corticotrophs (Kuryshev et al., 1995; Lee et al., 2015). Both agonists can switch non-active cells to a burst firing modality and increase the firing rate of active cells.

CRH, upon binding to CRH-R1, causes an initial membrane depolarisation followed by an increase in the intracellular [Ca^{2+}] and cAMP concentrations caused by activation of the PKA signalling pathway (Lee & Tse, 1997). This in turn has been proposed to

modulate certain ionic currents within the cell.For example, inwardly rectifying K^+ channel currents were reduced by the addition of CRH, an effect that was mimicked by the addition of extracellular cAMP (Kuryshev et al., 1997). A similar reduction has been seen in TREK-1 currents, which are partially responsible for maintaining a depolarised resting membrane potential (Lee et al., 2015). CRH-induced burst firing is reduced in BK knockout mice, an effect that is also suspected to be cAMP-dependent (Liang, 2012). L-type VGCCs are critical for pacemaking in AtT20 pituitary tumour cells and produce predictions in line with experimental data when incorporated into models of CRH-dependent corticotroph excitability, however there is as of yet no experimental evidence for their role *in-vivo* (Luini et al., 1985; Duncan et al., 2016). The relative degree to which each of these channels are involved in CRH-induced excitability is unknown at this stage and remains a complex matter.

AVP acts on the G-coupled V1b receptor to cause opening of L-type VGCCs via an IP3-dependent release of Ca^{2+} from stores in the endoplasmic reticulum. This causes a membrane hyperpolarisation followed by a sustained depolarisation that increases tonic firing and bursting activity. This effect is blocked by the Ca^{2+}-dependent potassium channel blocker apamin and is likely due to block of TREK-1 channel currents (Lee et al., 2015). AVP was also shown to stimulate the non-specific cation channel TRPC6 though its role in excitability has not been determined (Mani et al., 1985).

Firing frequencies in corticotrophs are therefore maintained by intrinsic ion channel conductances which are modulated by agonist-induced changes in excitability. There is some overlap in the channels involved but it remains uncertain whether intrinsic and agonist-induced excitability in corticotrophs act via the same or different mechanisms.

1.2.3 AtT20: A Spontaneously Excitable Mouse Anterior Pituitary Corticotroph Tumour Cell Line

For many years, *in-vitro* models have been used to study corticotroph function as they allow the mechanisms of pacemaking and secretion to be studied in more controlled conditions that are independent of extrinsic input. AtT20 is a cell line cloned from a mouse anterior pituitary corticotroph adenoma (Woods et al., 1992). They readily secrete ACTH and, similar to corticotrophs *in-vivo*, show spontaneous electrical activity either as regular tonic firing or in plateau-like bursts with a frequency of ~1.4 Hz at a

resting potential of -55 mV without any synaptic input (Adler et al., 1983). CRH has been seen to facilitate the secretion of ACTH but, unlike their *in-vivo* counterparts, effects on excitability are not always seen (Surprenant, 1982; Guérineau et al., 1991). These properties, along with their simple culture conditions, have made them ideal for various studies into the mechanisms of secretion and spontaneous activity in corticotrophs and their associated diseases.

Pacemaking in AtT20's was found to be Na^+ and Ca^{2+} dependent, with the removal of either ion from the external medium leading to cessation of firing. Block of Na_V channels with TTX revealed underlying Ca^{2+} waves that were suspected to be generating pacemaking**.** Depolarising pulses evoked a Ca^{2+} current during an action potential followed by the subsequent repolarisation of the membrane. Block of L-type VGCCs prevents rhythmic bursting, causes a membrane depolarisation and eliminates Ca^{2+} oscillations, though holding the membrane potential to resting levels under current clamp allows rhythmic firing to continue (Adler et al., 1983). Single channel recordings revealed the presence of Ca^{2+}-dependent K^+ channels which drive repolarisation in response to the Ca^{2+} influx during the action potential (Adler et al., 1983).

Various other channels with as yet unknown functions in pacemaking have been identified. A Ca^{2+}-dependent Cl^- current and two inwardly rectifying potassium currents, one voltage-sensitive and one opened in response to the binding of isoproterenol, have been identified (Korn et al., 1991; Dousmanis & Pennefather, 1992; Weik & Spiess, 1992). RT-PCR has revealed the expression of hyperpolarisation-activated HCN1 channels (Tian & Shipston, 2000). Ca^{2+}-ATPase and the Na^+/Ca^{2+} transporter have been shown to help regulate intracellular $[Ca^{2+}]$ (Korn et al., 1991). Various subtypes of VGCCs have been seen in AtT20 cells. VGCC currents are primarily L-type, with over 60% of current blocked by the dihydropyridine-specific antagonist nifedipine. Other VGCC subtypes such as such as N, P/Q and T-type have also been detected by various VGCC blockers (Mackie et al., 1995).

Several questions remain to be answered over the generation of pacemaking in this cell line: Firstly, what do these other identified channel types contribute to the generation of pacemaking? Various potassium channels have been seen to control resting membrane potential and excitability *in-vivo* which has yet to be explored in AtT20 cells (Dousmanis & Pennefather, 1992). Subtypes of VGCCs have different activation properties and have been seen to control excitability in various cell types (Matschke et al., 2015) and Hodgkin-Huxley models of corticotroph excitability have suggested roles

for T-type channels that have not yet been seen experimentally (LeBeau et al., 1997). Secondly, the issue of whether secretion of ACTH is coupled to excitability in this cell line needs to be resolved and, if it is uncoupled, why is this the case?

Answering these questions will provide insight into the dysfunction of pacemaking in diseases of ACTH secretion. A summary of the ion channels involved in AtT20 pacemaking is shown in **Figure 1.6**

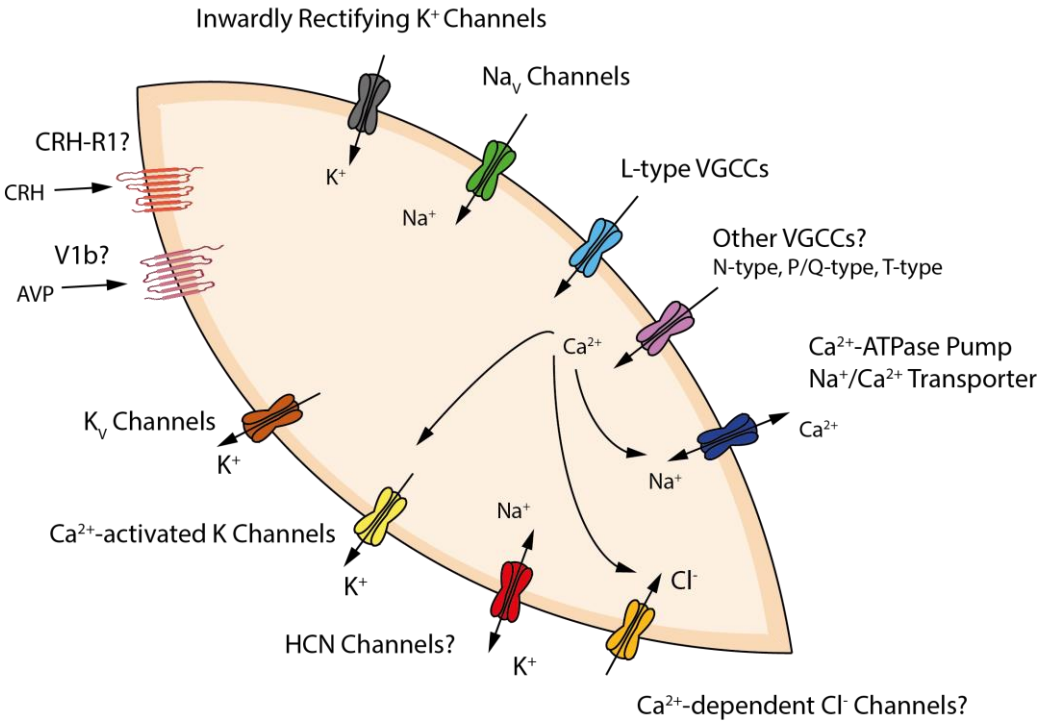

Figure 1.6. - Excitability in AtT20s. Intrinsic excitability is controlled by various ion channels. The frequency of Na_V-dependent action potentials is regulated by subthreshold membrane potential oscillations caused by L-type VGCCs. Action potential repolarisation and duration are regulated by K_V, VGCCs and Ca^{2+}-activated BK and SK channels. Inwardly rectifying K^+ channels, Ca^{2+}-ATPase pumps and Na^+/Ca^{2+} transporters maintain ionic concentration gradients. Channels with as yet unknown roles include HCN channels, N-type, P/Q-type and T-type VGCCs and Ca^{2+}-dependent Cl^- channels. Although they are present in AtT20s there is contradictory evidence over whether receptors for the ACTH secretagogues CRH and AVP have an effect on excitability (Diagram by M. Euston).

1.3 Pacemaking in Dopaminergic Neurons of the Substantia Nigra

1.3.1 The Role of SNc Dopaminergic Neurons *In-Vivo*

The substantia nigra pars compacta (SNc), located in the midbrain, is characterised by neurons that tonically release the neurotransmitter dopamine. There are roughly 12,000 dopaminergic (DA) neurons within the SNc of the adult rat, with each neuron making upwards of 100,000 synaptic connections (Francis et al., 2012). Neurons in the substantia nigra have two identified phenotypes in rats: large, fusiform cells with extensive dendritic trees; and smaller, polar cells with long axons coming from both poles that project towards regions of the basal ganglia (Richards et al., 1997) (**Figure 1.7A**).

1.3.1.1 SNc Projections to the Basal Ganglia

Axons from the SNc in rats mainly project along the nigrostriatal pathway to a region of the basal ganglia called the dorsal striatum. Projections to and from other regions of the basal ganglia including the globus pallidum, pars reticulata, pedunculopontine nucleus (PPN) and subthalamic nucleus (STN) have also been identified in mice (Matsuda et al., 2009; Watabe-Uchida et al., 2012). Projections from the PPN tegmental nuclei to the SNc have an excitatory effect on dopamine release. Excitatory postsynaptic potentials from this region can be blocked by application of the AMPA/kainate receptor blocker CNQX and muscarinic/nicotinic receptor blockers such as atropine and pirenzipine, indicating the involvement of glutamate and acetylcholine (Futami et al., 1995). GABAergic inputs from regions of the basal ganglia such as the neostriatum, globus pallidum and pars reticulata have been seen to act on SNc $GABA_A$ receptors to inhibit firing in SNc neurons (Petri et al., 2002; Lee & Tepper, 2009). This forms the basis of the nigral-striatal-nigral feedback loop, where SNc neurons activate their own GABAergic inhibitory neurons to regulate dopamine release. Dual patch clamp recordings show that stimulation of one SNc neuron can increase the firing rate of adjacent neurons, an effect that is likely caused by local neurotransmitter release (Vandecasteele et al., 2005). Application of D2-like receptor agonists decreases dopamine release, showing the presence of a dopamine negative feedback loop, with release of dopamine from dendrites in the SNc acting on D2-like auto receptors to inhibit the release of dopamine (Hooper et al., 1997).

1.3.1.2 Dopaminergic Control of Fine Motor Movement

Lesions of the SNc in animal models lead to motor deficits associated with fine motor control, while there is no deficit in cognitive function, memory and mood (which are associated with DA neurons in other regions of the basal ganglia). The most common symptoms were eyelid closure, bradykinesia, rigidity and postural tremor (Burns et al., 1983; Pioli et al., 2008). Administration of the dopamine precursor L-DOPA can temporarily reverse these effects (Burns et al., 1983). Stimulation of areas containing SNc projections can alleviate the symptoms caused by lesions of the SNc and lesions in downstream processing areas such as the thalamus can produce motor deficits similar to SNc lesions (Kumar et al., 2000; Jeljeli et al., 2003). This provides evidence for their role in expansive motor control pathways. These circuits are difficult to dissect due to the complex convergence of many pathways onto the basal ganglia, but can generally be broken down into two pathways (**Figure 1.7B**) (Calabresi et al., 2014):

1.) A direct pathway of SNc input to the dorsal striatum to inhibit the functions of the globus pallidum and pars reticulata, preventing their inhibition of the thalamus. This pathway contains large numbers of medium spiny neurons (MSNs) that express dopamine D1-like receptors (Keeler et al., 2014). The direct pathway has been proposed to facilitate the control and timing of motor actions.

2.) An indirect pathway of SNc input from the dorsal striatum to the external globus pallidum, resulting in disinhibition of the internal globus pallidum which in turn allows it to freely inhibit the thalamus. This pathway consists of MSNs that express dopamine D2-like receptors (Keeler et al., 2014). It has been suggested that this pathway is responsible for global inhibition of motor activity.

The thalamus is a mass of grey matter within the diencephalon that has important functions in relaying sensory and motor signals. Projections from the thalamic motor area connect to regions of the primary motor cortex, premotor cortex and the supplementary motor area (Kurata, 2005).

MSNs are GABAergic inhibitory neurons that are believed to be the primary site of action of DA neuron projections from the SNc. These cells typically form GABAergic synapses *in-vivo*, with the formation of dopamine synapses requiring a mismatch between DA pre-synaptic and GABAergic post-synaptic structures that is mediated by neuroligin-2 in mice (Uchigashima et al., 2016).

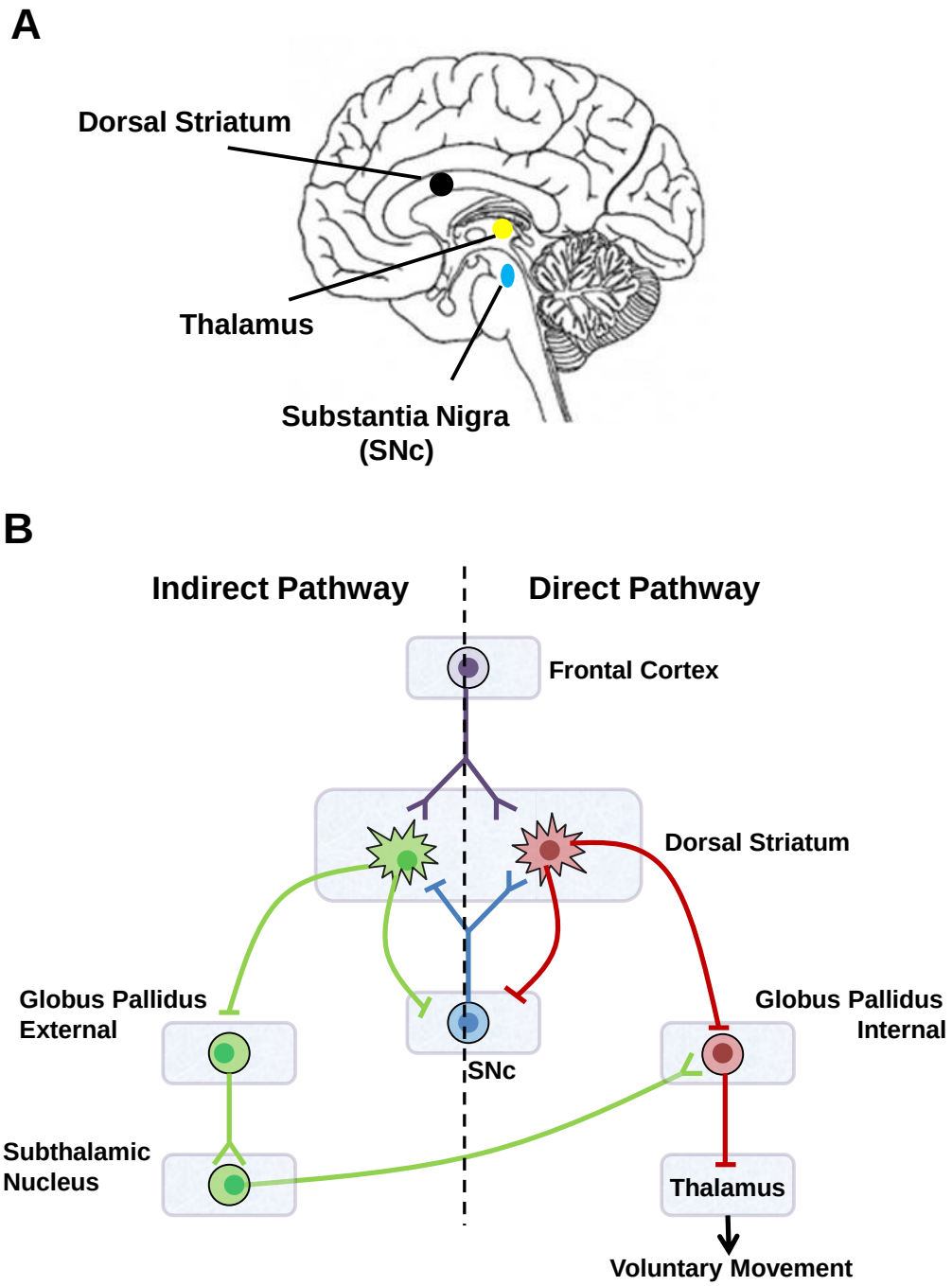

Figure 1.7 – **The principle components of the nigrostriatal pathway**. (A) Projections from the SNc to the dorsal striatum result in inhibition or dis-inhibition of the thalamus. (B) The two pathways of the nigrostriatal pathway. SNc neurons project onto GABAergic MSNs in the dorsal striatum. MSNs expressing D1 receptors make up a direct pathway to the internal globus pallidus (GPi) to prevent its inhibition of the thalamus. An indirect pathway involving MSNs expressing D2 receptors inhibits the thalamus through disinhibition of the GPi. GABAergic MSNs in the striatum project back to the SNc to provide negative feedback (Calabresi et al., 2014. Diagram by M. Euston).

Most dopamine receptors are slow-acting g-coupled receptors that produce either excitatory or inhibitory effects depending on their specific subtype. Various forms of these receptors are expressed throughout the nervous system, with various second messenger effects and physiological responses (Missale et al., 1998) (**Table 1.1**). Dopamine receptors can be broken down into two main types: D1-like (D1 and D5) and D2-like receptors (D2, D3 and D4). D1 receptors are typically excitatory via upregulation adenylate cyclase. This subsequently causes a membrane depolarisation via changes in the conductances of pacemaker-associated ion channels such as L-type VGCCs, HCN channels and Ca^{2+} dependent ion channels such as GIRK2. D2-like receptors are typically inhibitory via inhibition of adenylate cyclase. This in turn causes changes in the conductance states of the aforementioned ion channels and, notably through association with GIRK2, causes membrane hyperpolarisation (Missale et al., 1998).

These subtypes also differ in their affinities for dopamine, with D2-like receptors typically having a higher affinity than D1-like receptors. One such study, by performing a displacement assay using radioactive dopamine isotopes, found an IC_{50} value of 10.16 µM dopamine for D1-like versus 0.15 µM dopamine for D2-like receptors in the dorsal striatum (Marcellino et al., 2012). This can help explain the requirement for constant, pacemaker activation of the dorsal striatum by SNc neurons. Low concentrations of dopamine will result in a higher degree of activation of the inhibitory D2 pathway, while only continuous release of dopamine will result in a high enough concentration to activate the excitatory D1 pathway. D2 receptors can also be present in either high or low affinity forms depending on the splice variant of the receptor that is expressed. The abundance of each variant that is expressed on MSNs will also affect the concentration of dopamine required for activation of the D2 pathway (van Wieringen et al.,. 2013).

Dopamine action on MSNs therefore produces contradictory effects depending on the pathway involved. This allows for the inhibition or disinhibition of the thalamus and subsequent motor activity. Dopamine release onto MSNs has a concentration-dependent excitatory effect for those expressing D1-like receptors in rat striatal neurons, and a mainly inhibitory effect for those expressing D2-like receptors which depends upon the expression of different splice variants (Surmeier et al., 2007; Marcellino et al., 2012; Calabresi et al., 2014). D1- and D2- like receptors on interneurons are also activated to cause further inhibitory or excitatory changes in MSN membrane potential. Other neurotransmitters have been seen to modulate MSN activity through interneurons such

as GABA, acetylcholine, glutamate and neuropeptide Y (Do et al., 2013). It is the cumulative effect of all these inputs that decide if dopamine inhibits or excites an MSN in the striatum.

Family	Receptor	Transduction Mechanism	Expression
D1-like	D1	AC+ PLC+ L-type VGCCs+	Dorsal + ventral striatum, thalamus, hypothalamus
	D5	AC+	Hippocampus, hypothalamus, frontal cortex, cerebellum, midbrain
D2-like	D2	AC- K^+ conductance - Ca^{2+} conductance -	Dorsal + ventral striatum, thalamus, hypothalamus
	D3	AC- MAP Kinase+	Ventral striatum, islands of Calleja
	D4	AC- Ca^{2+} conductance-	Frontal cortex, midbrain, amygdala, cardiovascular system

Table 1.1 - Dopamine receptor classification. The 5 major subtypes of dopamine receptor, broken down according to their signalling pathways and regions of expression within an organism. Adenylate cyclase (AC), phospholipase C (PLC), voltage-gated calcium channels (VGCCs), mitogen-activated protein kinase (MAP Kinase). Increases and decreases are indicated by + and - symbols respectively. Adapted from the Tocris website (https://www.tocris.com/pharmacology/dopamine-receptors) and Missale et al., 1998.

1.3.2 Pacemaking in SNc Dopaminergic Neurons *In-Vivo*

Sustained dopamine release from SNc neurons is required for proper functioning of target structures such as the striatum. This is caused by an intrinsic pacemaking activity that generates tonic action potential firing. This activity was observed at a rate between 3-8 Hz in cultures of dissociated rat SNc neurons. This was observed to transition to arrhythmic bursting *in-vivo* in the presence of synaptic input, indicating the role of the local synaptic environment in control of their electrical activity (Grace & Bunney, 1984; Tepper et al., 1998; Guzman et al., 2009). Control of their excitability, through both intrinsic and agonist-induced means, is the central way in which dopamine is regulated (**Figure 1.8**).

1.3.2.1 Intrinsic Excitability in SNc Dopaminergic Neurons

SNc DA neurons have been seen firing *in-vivo* and *in-vitro* in animal models in the absence of any synaptic input, indicating the presence of intrinsic drivers of pacemaking (Grace & Bunney, 1984; Shen et al., 1994; Tepper et al., 1998). Pacemaking is thought to mainly be driven by voltage-gated cation channels for Na^+, Ca^{2+} and K^+. Block of Na_V channels in dissociated mouse SNc neurons prevents firing but leaves lower amplitude membrane oscillations at close to the pacemaker frequency. These were blocked by the removal of Ca^{2+} from the external medium (Puopolo et al., 2007). Ca^{2+} imaging has revealed this is driven by somatodendritic oscillations in their Ca^{2+} concentration (Guzman et al., 2009). Immunohistochemical analysis of somatodendritic ion channel expression in rat models has identified a huge range of channel types regulating their excitability including K_V channels (K_V1.3, K_V2.1, K_V3.2, K_V3.3, K_V4.3), Ca^{2+}-activated SK channels (SK1, SK2, SK3), HCN channels (HCN2, HCN4), L-type (Ca_V1.2, Ca_V1.3) and T-type VGCCs (Ca_V3.1, Ca_V3.3) (Dufour et al., 2014). Inside-out patch clamp recording has also identified Ca^{2+}-activated BK channels (Su et al., 2010).

K^+ channels (K_V, SK and BK) appear to control the action potential duration and size of the afterhyperpolarisation, though the differing kinetics of these channel types means they have different effects. Block of K_V2 increases action potential duration and decreases the afterhyperpolarisation while block of BK channels increases the amplitude of the afterhypolarisation. These contradicting effects are explained by the kinetics of both channels: BK channels activate and deactivate much quicker than the slowly activating and deactivating K_V channels. Block of either BK channels or K_V2 resulted in an instantaneous increase in the observed current passing through the other channel type that allowed pacemaking to continue. This was believed to be due to changes in action potential shape and suggests that these channel conductances have a limited ability to compensate for each other if one is lost (Kimm et al., 2015). Block of SK channels with the specific blocker apamin has been reported to have neuroprotective effects in a model of Parkinson's disease (PD), a disease characterised by death of neurons in the SNc (Alvarez-Fischer et al., 2013). SK channels also affect the afterhyperpolarisation following action potential firing, perhaps in response to an increase in intracellular Ca^{2+}. These channels may functionally couple to VGCCs, with the N-type blocker ω-conotoxin GVIA reducing SK currents by up to 40% (de Vrind et al., 2016).

The role of VGCCs in SNc pacemaking has been researched in detail over the last few years due to their purported role in the mechanism of SNc cell death in PD. In rats, L-type VGCC blockers such as nifedipine were reported to block somatodendritic Ca^{2+} oscillations and firing, leading to the conclusion that they generate a slow Ca^{2+} driven pacemaker potential to control pacemaking (Mercuri et al., 1994). SNc DA neurons in mice robustly express $Ca_V1.3$ mRNA (Chan et al., 2007). This VGCC subtype is rare within the brain with their expression only seen in around 10% of neurons. Unlike other L-type channels they open at relatively hyperpolarised, subthreshold membrane potentials making them ideal for pacemaking (Chan et al., 2007). It has since been discovered that the L-type antagonists used in previous experiments were used at such high concentrations as to antagonise other VGCC channel types. Subsequent experiments using the $Ca_V1.3$-selective antagonist isradipine show that this subtype is responsible for Ca^{2+} oscillations in SNc neurons but that their block alone is not enough to cause changes in cell excitability (Guzman et al., 2009). This has been backed up by $Ca_V1.3$-knockout mice which also show no effect on pacemaking (Chan et al., 2007). However, the ability for other genes to compensate for the knockout of others during development means that knockout models may not give a true indication of the role of $Ca_V1.3$ in pacemaking (Marschang et al., 2004). Conditional knockouts in adult mice would provide a better indicator of the importance of this channel in pacemaking in adult neurons. Roles for other VGCC subtypes have also been observed such as P/Q-type channels which, when blocked, slow the frequency of pacemaking (Puopolo, 2007).

Intrinsic pacemaking in SNc DA neurons is therefore a complicated and interconnected process. The observed robustness is an amazing example of homeostatic plasticity that is likely due to cross-regulation between the vast arrays of channel types involved which all have different kinetic properties. The changes in membrane properties caused by the loss of one or more channel types can cause alterations in other currents which result in a retention of pacemaker activity. It could be hypothesised then that knockout or block of several channel types simultaneously that do not affect excitability when blocked alone would have an effect on pacemaking. Indeed, this has been seen experimentally: Block of either HCN or $Ca_V1.3$ channels in mouse brain slices has no effect on excitability, yet block of both effectively stops all firing (Chan et al., 2007). $Ca_V1.3$ -/- mice show a shift in the importance of HCN channels, with them becoming critical for pacemaking. This is similar to the pacemaking seen in SNc neurons in

juvenile mice, where Na_V/HCN channels are critical. As the mice mature, observed $Ca_V1.3$ currents grow and the contribution of HCN currents diminishes due to a shift in its voltage activation. HCN channels are sensitive to allosteric regulation by cAMP. SNc DA neurons express the cAMP-producing enzymes adenylate cyclase 5 and 9, both of which are inhibited by Ca^{2+}. An increase in intracellular [Ca^{2+}] as a result of $Ca_V1.3$ expression could therefore decrease cAMP synthesis and downregulate HCN channel activity. $Ca_V1.3$ antagonism in mature SNc neurons does not block pacemaking by itself as its removal can increase cAMP synthesis and revert these cells back to a juvenile form of Na_V/HCN pacemaking (Chan et al., 2007). As previously noted, genetic compensation in response to gene knockout has been identified in other systems. Therefore another explanation that should be explored is whether developmental changes in response to the loss of $Ca_v1.3$ can upregulate HCN channel expression. A summary of the channels involved in intrinsic excitability is shown in **Figure 1.8**.

1.3.2.2 Agonist-Induced Excitability in SNc Dopaminergic Neurons

While intrinsic factors drive tonic firing it is synaptic inputs onto SNc DA neurons, both excitatory and inhibitory, that are believed to drive burst firing. Glutamatergic inputs from the STN, PPN and from within the SNc have been seen to form synapses onto SNc dendrites in mouse brain slices (Pearlstein et al., 2015). Analysis of mRNA expression and patch clamp recordings in rodent SNc neurons have identified AMPA-evoked currents mediated by GluA2-containing AMPA receptors, Kainate-evoked currents mediated by GluK3 and GluK5-containing Kainate receptors and NMDA-evoked currents mediated by GluN2B- and GluN2D-containing NMDA receptors (Gotz et al., 1997; Bischoff et al., 1997; Jones & Gibb, 2005). These are all ionotropic receptors, with NMDA receptors primarily passing Ca^{2+} and AMPA/Kainate receptors primarily passing Na^+ and K^+ (Hille, 2001). NMDA and AMPA receptors are localised to subpopulations of synapses within the dendrites of SNc neurons and are often found to co-localise (Chatha et al., 2000). The addition of antagonists to block NMDA and AMPA glutamate receptors in mice SNc neurons decreased cell activity while the addition of glutamate agonists caused high frequency burst activity. In the presence of NMDA/AMPA antagonists the afterhyperpolarisation following an action potential is decreased, suggesting a mechanism where burst firing is promoted by transiently inhibiting the ability of SNc neurons to repolarise (Blythe et al., 2007).

Two main types of inhibitory signalling affect SNc activity: A GABAergic feedback loop from the striatum and a local dopamine feedback loop. DA neurons form synapses with GABAergic neurons in the neostriatum, globus pallidum and pars reticulata which project back to the SNc (Lee & Tepper, 2009). Injection of GABA into the rat SNc inhibits dopamine levels in the striatum, indicating this feedback is inhibitory in nature (Reid et al., 1990). Immunohistochemistry on post-mortem SNc tissue identified a population of neurons expressing $GABA_A$ receptors (Petru et al., 2002). These are ionotropic Cl^- channels that produce inhibitory post-synaptic potentials upon receptor binding. Activation of $GABA_A$ receptors in the rat SNc inhibits burst firing and reverts the cells back to an intrinsic tonic modality (Hille et al., 2001; Tepper et al., 2002).

Whole cell current clamp recording in rat SNc neurons reveals that the application of dopamine or dopamine agonists has an inhibitory effect on their firing. This effect was reversed by the dopamine receptor antagonist trifluoperazine (Aghajanian & Bunney, 1977). Release of dopamine in mouse midbrain slices causes a hyperpolarisation of nearby neurons resulting in a temporary pause in firing (Beckstead et al., 2004). This effect was localised to the action of D2-like receptors within the dendrites and soma (Cragg & Greenfield, 1997). These are believed to play a key role in dopamine release by providing feedback inhibition that controls cell firing. D2 receptors are g-coupled receptors that inhibit adenylate cyclase and cAMP synthesis (Hille, 2001). Aside from this, they also activate g-protein activated inward rectifying potassium (GIRK) channels. SNc neurons in mice express both GIRK2 and GIRK3, though D2-receptors appear to couple specifically to GIRK2 (Davila et al., 2003). These likely form a pre-coupled complex that, upon dopamine binding, liberates the D2 $G\beta\gamma$ subunit. This allows it to bind and cause a conformational change in GIRK2. Activation of this channel at resting membrane potentials causes a membrane hyperpolarisation that prevents cell firing (Riven et al., 2006).

Similar to intrinsic excitability, agonist-induced excitability in SNc DA neurons is complex. Multiple excitatory and inhibitory systems are in place and it is believed the balance of these inputs is an important determinant of cell excitability. For example, burst firing in SNc neurons can be induced by the activation of NMDA receptors even in the presence of inhibitory GABAergic input. Models of SNc synaptic inputs show that it is the cumulative effect of these excitatory and inhibitory inputs that decide whether a cell fires, depending on which conductance dominates (Lobb et al., 2010; Morozova et al., 2016).

Overlap also exists between intrinsic and agonist-induced excitability. Increasing the firing rate of SNc neurons from mice causes Ca^{2+} influx through glutamate receptors to increase, increasing their sensitivity to synaptic inputs (Hage & Khaliq, 2015). Activation of T-type VGCCs may also be involved in certain SNc populations, acting in an excitatory manner in response to D2-activation. These channels open at hyperpolarised membrane potentials, hence subthreshold currents generated by D2-activated hyperpolarisation may open these channels and cause a counter-acting depolarisation. This is proposed to be a mechanism by which cells within the SNc can transmit dopamine signals differentially based on their ion channel composition (Evans et al., 2017). The ion channels involved in agonist-induced excitability are summarised in **Figure 1.8**.

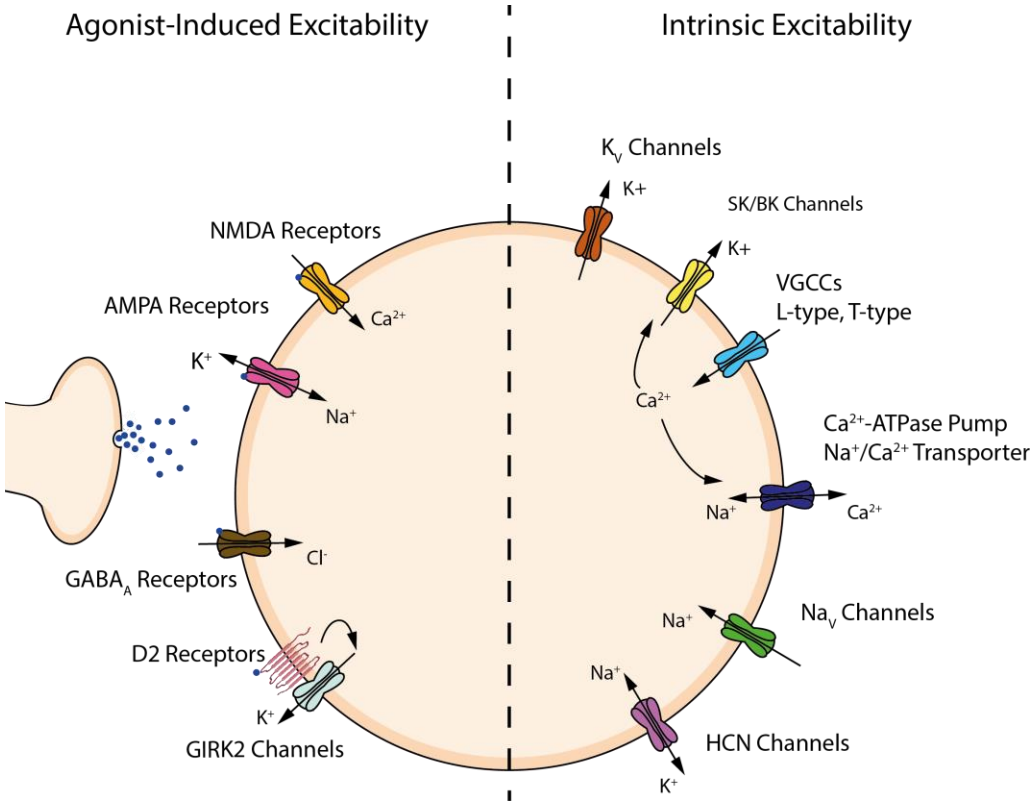

Figure 1.8 - Excitability in animal models of SNc DA neurons. Pacemaking involves the complex interaction of many ion channel populations. Subthreshold VGCC dependent Ca^{2+} waves underlie Na_V dependent action potentials. Action potential duration and repolarisation are controlled by K_V, BK and SK channels and VGCCs. HCN channels are believed to be involved in pacemaking in developing SNc neurons. Ca^{2+}-ATPase pumps and Na^+/Ca^{2+} transporters maintain ionic concentration gradients. Various neurotransmitters also affect pacemaking. These include excitatory inputs through NMDA and AMPA receptors, and inhibitory inputs through $GABA_A$ and dopamine D2 receptors (which activate a K^+ conductance through GIRK2 channels) (Diagram by M. Euston).

Although the mechanisms of pacemaking in SNc neurons *in-vivo* are relatively well studied, a major problem with current research is the lack of availability of human models. The majority of studies have been performed on animals such as primates, rats and mice. These have used either brain slices, dissociated cells or *in-vivo* recordings (Blesa & Przedborski, 2014). Differences between human and animal models are common across the scientific literature (Shanks et al., 2009), hence by translating data from animal models there is a risk of providing an incorrect representation of how SNc pacemaking functions in humans. Post-mortem examination of the SNc in PD patients has provided some insight into these cells in humans but models for healthy adult neurons or for the development of pacemaking are lacking. The requirement for relevant human models of SNc DA neurons is a huge bottleneck in this area of research, especially given the importance of this cell type in the pathology of PD.

1.3.3 SNc Neurons in Parkinson's Disease

Parkinson's disease (PD) is a neurodegenerative disorder of the central nervous system that is second only to Alzheimer's in terms of prevalence. In industrialised countries this is estimated to be 0.3%. Prevalence increases with age, with a huge increase in those aged 60 and over, with men slightly more likely to develop PD than women (de Lau & Breteler, 2006).

There are some genetic and environmental risk factors for PD but the majority of cases are idiopathic, that is to say, with no known cause. The disease increasingly affects quality of life and eventually causes severe disability. This leaves sufferers dependent on others for the performance of everyday tasks. Patients have more need for nursing home placements, have a greater incidence of hospital visits and a higher mortality rate than the general population. The mean duration of death from the onset of the disease is estimated at 6.9 to 14.3 years, with age and the co-presence of dementia being the highest predictors of mortality (de Lau & Breteler, 2006).

PD is characterised by the death of DA neurons within the SNc. This is accompanied by a reduced signal intensity in MRI scanning (Sasaki et al., 2014; Sveinbjornsdottir, 2016). Other regions are also affected such as the medulla oblongata, olfactory bulb and neocortex. Affected cells typically form abnormal protein aggregates, termed 'Lewy Bodies,' which begin to form at defined induction sites. These have been identified by histological staining to be comprised of a protein called alpha-synuclein. Lewy bodies

form in a predictable topographical sequence with the medulla and olfactory bulb first affected. Formation then appears in the midbrain, including the SNc, before finally spreading to the neocortex in the later stages of the disease. Neurons affected with Lewy bodies eventually degenerate and die, causing the main symptoms of the disease (Sveinbjornsdottir, 2016).

The degeneration of DA SNc neurons with Lewy bodies is regarded as the primary neuropathological correlate to PD's symptoms. These are in line with motor symptoms seen in animal models with SNc lesions. PD was first described as having 'palsy-like' symptoms by James Parkinson in 1817 and is characterised by resting tremor, slowness of movement (bradykinesia) and festinating gait (Parkinson, 1817). Symptoms often start on one side of the body before the other. Body posture becomes stooped with limb rigidity, shuffling gait and lack of arm swing while walking becoming apparent. Bradykinesia is common, leading to expressionless face and noticeably smaller hand writing (micrographia). Postural instability can occur either early or late in the disease and falls in the elderly affected with PD are common. Problems with slurred or hurried speech and difficulty swallowing have been identified in 40-80% of patients. Around 80% of patients have a resting tremor between 4-6 Hz. This is usually noticed in the hands but can also affect the legs leading to gait festination, where steps become progressively smaller and more rapid. Dystonia, an abnormal sustained muscle contraction, is another major symptom which can lead to abnormal movements and postural deformities such as forward flexion of the head and neck or scoliosis (Sveinbjornsdottir, 2016)**.**

Non-motor symptoms of the disease are associated with the degeneration of other affected brain regions. Dysfunction of the central and peripheral postganglionic autonomous nervous system can result in orthostatic hypotension, constipation, lack of urinary control and excessive sweating in certain patients. Sleep disturbances are common, affecting two thirds of patients. The most common are constant waking, daytime sleepiness and obstructive sleep apnoea. Psychotic symptoms are common in late stages of the disease, with patients experiencing paranoid visual hallucinations associated with deterioration of the hippocampus and amygdala. Associated dementia is also common. Sensory symptoms include a loss of sense of smell, tingly sensations and neuropathic pain (Sveinbjornsdottir, 2016).

There is currently no cure for PD, though treatment of the symptoms is possible. L-dopa, a precursor to dopamine, is the most widely used treatment and is effective at

treating the early to mid-stages of the disease. Dopamine receptor agonists and glutamate receptor antagonists have similar effects. Monoamine oxidase inhibitors can also prevent the breakdown of dopamine. The problem with these treatments is that they do not stop nor prevent the pathological course of the disease, hence they become ineffective once cell death has progressed past a critical point. Drug targets to halt or delay the progression of cell death in PD are being explored, such as enzyme inhibitors to prevent the formation of Lewy bodies (SYN-118) and the Na_V and T-type VGCC blocker Zonisamide. These clinical avenues are promising but so far show limited effectiveness (Schapira et al., 2014).

Transplantation of stem cells or stem cell-derived DA neurons into the SNc has been able to improve the motor symptoms of SNc ablated rats. However, these transplanted neurons show low levels of tyrosine hydroxylase immunostaining and the survival rate for transplanted cells is currently too low to be an effective treatment. iPSC-derived DA neurons have shown similar clinical improvements and produce cells that do not form Lewy bodies once transplanted. However, it has been suggested that these cells may be more susceptible to PD than others due to mutations and epigenetic markers. This field is still in its infancy so it remains to be seen whether stem cell transplantation can become an effective strategy to prevent or replace cell death in PD (Fu et al., 2015).

It is clear then that to provide effective strategies for the prevention of cell death in PD that the cellular mechanisms underlying specific cell death need to be explored.

1.3.4 The Role of Excitability in Parkinson's Disease

The predominant theory behind specific cell death in PD is that of mitochondrial dysfunction. This has been speculated to lead to the release of mitochondrial Ca^{2+}, reactive oxygen species (ROS) and the mishandling of damaged proteins which in combination lead to the death of specific subsets of neurons. The causes of mitochondrial dysfunction are still under debate but Ca^{2+} entry through VGCCs, specifically $Ca_v1.3$, has been proposed as a possible instigator (Surmeier, 2007). Various genetic risk factors have been identified in specific cases of PD with those with a family history of PD being twice as likely to develop the disease as those without. Environmental risk factors such as smoking, obesity and exposure to pesticides are linked to an increase in the incidence of PD (de Lau & Breteler, 2006).

The presence of one, or even several, of these genetic and environmental risk factors is not indicative of a person developing the disease. Also, current treatments that target the suspected mechanism of cell death fail to halt the disease and only slow its progression. It is therefore suspected, in most cases of PD, that cell death is due to the innate properties of the cell type involved in combination with specific mutations and environmental factors. A summary of the information in the following sections is shown in **Figure 1.9**.

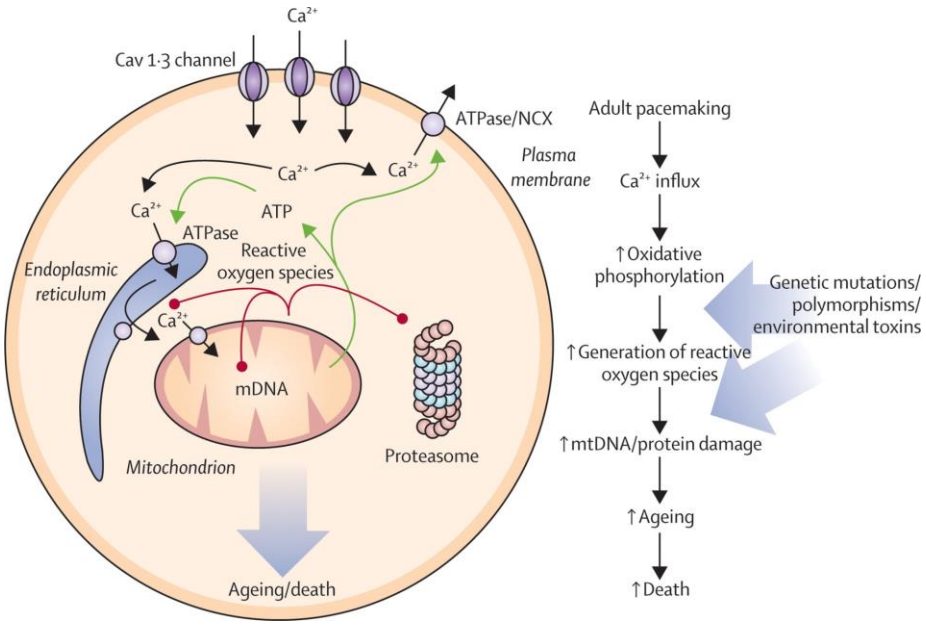

Figure 1.9 - Excitability and cell death in PD. SNc pacemaking leads to excessive Ca^{2+} influx. Ca^{2+} is uptaken by mitochondria, resulting in ROS production. ROS cause numerous effects within the cell, including mitochondrial DNA damage, protein phosphorylation, alpha synuclein accumulation and promotion of apoptosis. This, in combination with ageing and genetic/environmental risk factors, leads to selective death of SNc neurons in PD (From Surmeier, 2007).

1.3.4.1 The Role of Mitochondrial Stress

A role for mitochondrial dysfunction in PD was first identified in opiate addicts in the 1970s and 1980s. Patients that inadvertently injected 1-methyl-4-phenyl-1,2,5,6-tetrahydropyridine (MPTP), a by-product of opiate synthesis, showed symptoms remarkably similar to PD (Ballard et al., 1985). This was linked to aggregation of the active form of MPTP, MPP+, in the mitochondrial matrix leading to inhibition of complex I of the electron transport chain (Kopin, 1992). Post-mortem SNc tissue from

PD patients also show decreased complex I activity (Schapira et al., 1990) and mouse SNc neurons have been seen to selectively die in response to MPTP (Jackson-Lewis et al., 1995).

Cells within the body require mitochondria to produce sufficient ATP to meet their energy demands. For neurons in particular, this demand is high due to the energy requirement of maintaining the transmembrane ionic gradients that underlie excitability. This is carried out by ATP-dependent transmembrane ion pumps, leaving neurons with a lower reserve of ATP and increasing the chance of failure of cellular systems through ATP shortage (Surmeier & Schumaker, 2013).

Mitochondrial dysfunction also results in impaired Ca^{2+} homeostasis. Mitochondria play important roles in Ca^{2+} signalling through the sequestration and release of Ca^{2+}. The mitochondrial respiratory chain, through proton pumps in the inner membrane, establishes an inner membrane potential difference of around -180 mV. This establishes a strong thermodynamic force favouring the sequestration of cations (Murphy, 2009). Ca^{2+} is imported across the outer and inner mitochondrial membrane via various transporters: voltage-dependent anion channels in the outer membrane; Ca^{2+} uniporters and H^{+}/Ca^{2+} or Na^{+}/Ca^{2+} exchangers in the inner membrane. Failure of the mitochondrial membrane potential leads to a massive release of Ca^{2+}, increasing cytosolic levels up to 500 µM (Pan et al., 2013). This causes Ca^{2+}-dependent release of cytochrome c from the inner mitochondrial membrane, leading to activation of caspases which are responsible for protein degradation and apoptosis (Jenner, 2003).

1.3.4.2 The Role of Reactive Oxygen Species

Mitochondria are known to be a primary source of ROS within cells, producing species such as hydrogen peroxide and superoxide in isolated mitochondria as a result of complex I and III activity (Jensen, 1966).

Abnormal levels of oxidative damage to proteins, lipids and DNA has been identified in post-mortem samples of PD patients (Floor & Wetzel, 1998). The use of fluorescent superoxidase dyes in rat brain has identified increased levels of mitochondrial ROS production in response to the addition of rotenone, a complex I inhibitor which produces parkinsonian symptoms. ROS production could be further increased by hyperpolarisation of the mitochondrial membrane (Votyakova & Reynolds, 2001). All

of this suggests that ROS production in PD is linked to the availability of electron donors within complex I of the electron transport chain.

Overproduction of ROS is believed to cause a cascade of biochemical changes that eventually lead to the death of DA neurons. ROS-protein interactions have been seen to increase levels of lipid hydroperoxidases, malondialdehyde and protein carbonyls in the SNc. It is suggested that these oxidised proteins may not be adequately ubiquitinated and hence accumulate within cells (Jenner, 2003). 4-hydroxynonenal (HNE), a product of lipid peroxidation, shows increased levels in rat models of PD. This protein can cause DNA fragmentation and induce apoptosis through the induction of caspases-3, -8 and -9 (Liu & Kato, 2000).

Abnormalities in the ubiquitin-proteasome system, responsible for protein degradation, have also been identified within the SNc in animal models. This could be due to altered coding of the PA28 and PA700 regulatory caps of the 26S proteasome in the SNc, but oxidation by free radicals and HNE are more likely (Jenner, 2003). HNE can bind directly the 26S proteasome to inhibit protein degradation, and levels of HNE that don't inhibit cell viability have been seen to inhibit the processing of ubiquitinated proteins (Okada et al., 1999). Treatment of cultured cell lines with HNE causes apoptosis through an increase of ubiquitinated proteins leading to mitochondrial stress followed by ROS and caspase activation (Hyun et al., 2002). This also provides evidence of a positive feedback loop, where the effects of ROS production cause mitochondrial dysfunction leading to further ROS production.

The effects of protein oxidation by ROS in PD are numerous and the extent to which individual proteins affect cell death is still mostly speculative. More research needs to be carried out to find specific products of oxidation that affect cell survival in PD. Evidence also exists for oxidative stress only occurring late in the disease, with patients caught early showing little signs of protein oxidation (Jenner, 2003). From this it has been speculated that ROS production is an effect, not a cause, of cell death in PD. The circular nature of the causes of PD, where mitochondrial dysfunction causes effects that lead to further mitochondrial dysfunction, likely means that ROS production is simply accelerated in the latter stages of the disease and is not easily detected until this stage.

1.3.4.3 The Role of Alpha Synuclein

Inhibition of protein degradation through the ubiquitin-proteasome system provides a link between the mechanisms of cell death and the build-up of alpha-synuclein plaques in PD. Immunohistochemical staining of sections from PD patients post-mortem show that alpha-synuclein aggregates in clumps called Lewy bodies (Spillantini et al., 1998). Triplication of the alpha synuclein gene, *SCNA*, has been shown to cause a form of PD, and single nucleotide polymorphisms in this gene can increase the likelihood of developing the disease (Maraganore et al., 2006; Fuchs et al., 2007). It is clear then that alpha-synuclein build-up plays an important role in PD.

Part of the synuclein family, alpha-synuclein is found in association with synaptic vesicles on the membrane of neurons. Fluorescent labelling revealed this protein moves away from vesicles following action potential firing before rapidly returning. From this it is suggested its natural function is to regulate vesicle fusion through aiding the formation of the SNARE complex (Fortin et al., 2005). Alpha-synuclein can switch from an alpha helix conformation to beta-sheet oligomers in solution (Conway et al., 2000). Beta sheet aggregation can be induced by oxidation following the addition of mitochondrial inhibitors such as HNE and appears to drive its oligomerisation (Qin et al., 2007). This promotes the idea that ROS production in PD causes alpha synuclein aggregation.

The effects of alpha-synuclein aggregation are numerous due to its ability to bind to a variety of proteins. Through these interactions various pro-apoptotic effects have been identified. Alpha-synuclein oligomers have been seen to form pores in cell membranes and alter the function of VGCCs, both of which can lead to excessive Ca^{2+} influx (Hettiarachchi et al., 2009). They also inhibit 26S proteasome function during their own degradation. This effect is exaggerated in mutant forms of alpha-synuclein, leading to proteasomal dysfunction and increased sensitivity to apoptosis (Emmanouilidou et al., 2010).

A proportion of alpha-synuclein in wild type and overexpressed mice localises to mitochondria. This aggregation causes mitochondrial fragmentation and impaired complex I function, hence linking alpha-synuclein aggregation with mitochondrial dysfunction in PD. Overexpression of alpha-synuclein increases ROS production, which can be protected against through the antioxidant glutathione (Clark et al., 2010).

A more worrying aspect of alpha-synuclein in PD is its potential to show prion-like effects. Nearby cells can uptake secreted alpha-synuclein which in turn seeds the formation of Lewy bodies (Volpicelli-Daley et al., 2011). This ability to migrate to other brain regions can help to explain the progression of PD. Advancement from the medulla and olfactory bulb to the midbrain and neocortex could potentially be due to alpha-synuclein migration and seeding of Lewy bodies in these regions as the disease progresses.

Lowering of alpha-synuclein levels has been explored as a possible avenue for protection against PD. However, siRNA down-regulation leads to severe neurotoxicity in rats (McCormack et al., 2010). Methods to upregulate endogenous protein degradation, such as overexpression of the beclin-1 gene, can lead to protein clearance and neuroprotective effects (Spencer et al., 2009).

1.3.4.4 The Role of $Ca_V1.3$ Voltage Gated Calcium Channels

The question remains then: why are DA neurons within the SNc innately susceptible to degeneration? The VGCC subtype $Ca_V1.3$ has been implicated as a possible cause, providing a link between pacemaking and PD. Inhibition of $Ca_v1.3$ channels in mice can protect against the toxic effects of MPTP, rotenone and 6-hydroxydopamine (6-OHDA) at concentrations that would normally cause cell death in DA neurons (Chan et al., 2007). Use of L-type antagonists for hypertension is associated with a 30% reduction in the risk of developing PD and slows the progression of the disease even when initiated after diagnosis (Gudala et al., 2015). Due to these effects, clinical trials for $Ca_V1.3$-specific antagonists, such as isradipine, are in progress to determine if there is a clinical benefit to their use in PD (Biglan et al., 2017).

Autonomous pacemaking in SNc neurons uses slow, broad action potentials which maximise Ca^{2+} entry through VGCCs. $Ca_V1.3$ channels have faster kinetics and open at more hyperpolarised membrane potentials than other L-type VGCCs. Due to the innate properties of SNc neurons it is suspected that a proportion of these channels are always active during the pacemaking cycle. This results in a sustained elevation of Ca^{2+} into the cell. It is this increase in the intracellular Ca^{2+} concentration that is suspected to cause SNc vulnerability (Surmeier et al., 2017).

This influx results in elevated Ca^{2+} uptake by mitochondria at junction sites with the endoplasmic reticulum. This has been suggested to stimulate ATP production, ensuring

energy demands are met. However, when ATP demand is low it causes a concentration-dependent hyperpolarisation of the mitochondrial membrane which results in ROS production during complex I of the electron transport chain (Votyakova & Reynolds, 2001; Pacelli et al., 2015).

Ca^{2+} can also promote the aggregation of alpha-synuclein through the Ca^{2+}-dependent protease calpain. Calpain cleaves the C-terminus region of the protein to promote its aggregation. Inhibition of calpain in mice results in a reduction of aggregation and neuronal toxicity (Mishizen-Eberz et al., 2003).

$Ca_v1.3$ is therefore suspected to cause SNc vulnerability through sustained elevation of Ca^{2+} in the cytoplasm. This leads to mitochondrial stress, ROS production and aggregation of alpha-synuclein.

1.3.4.5 Genetic & Environmental Components

Although the majority of cases of PD are idiopathic, a proportion (~10%) are familial in nature (de Lau & Breteler, 2006). Specific gene mutations have been identified as risk factors and these have been used to shed further light on the causes of idiopathic PD.

Multiplication mutations in the SCNA gene that encodes for alpha synuclein have been identified in various cases of familial PD, leading to symptoms similar to the idiopathic form of the disease. Mutations in genes involved in the ubiquitin-proteasomal pathway, such as Parkin and UCHL1, lead to a slow or late onset form. Recessive mutations in mitochondrial function or ROS stress responses, such as PINK1 and DJ-1, have also been associated with the disease (de Lau & Breteler, 2006).

Apart from direct genetic causes in familial PD, a lot of research has gone into identifying genetic risk factors in the idiopathic form of the disease. A handful of genes are associated with a higher incidence of PD than others. These include those associated with dopamine degradation (MAOB) ROS inhibition (GSTT1) and plaque formation (APOE and Tau). These studies and meta-analyses have found only a very weak correlation between suspected susceptibility genes and PD, likely due to the complex, multi-factorial nature of the disease. This means the contribution of any one gene is relatively small or requires interaction with other genes and environmental factors (Tan et al., 2000; Healy et al., 2004; Huang et al., 2004).

Various environmental risk factors have been associated with PD (reviewed in de Lau & Breteler, 2006). Exposure to herbicides and pesticides such as paraquat and rotenone are suggested to be able to increase the likelihood of developing PD through their complex I inhibitory activity. Exposure to heavy metals such as zinc, copper and lead are suspected to be a risk factor through the accumulation of metals in SNc neurons leading to ROS production. Studies looking at the effects of tobacco and coffee consumption have concluded that they are associated with a reduced incidence. Proposed neuroprotective mechanisms include stimulation of dopamine production or nicotine acting as an antioxidant. Caffeine is known to inhibit adenosine A2 receptors which are important for dopamine release and supplementing PD rats with caffeine improves their motor deficits. Other Dietary habits are suspected to play a role in susceptibility to PD. Antioxidants such as vitamin C and E can reduce ROS damage and studies have found an association between vitamin E consumption and reduced risk of PD. It has been hypothesised that dietary iron could reduce ROS formation and that fatty acids could increase ROS formation through lipid peroxidation. Studies looking at these effects have opposing results and no such correlation between dietary iron or fatty acids and the incidence of PD has yet been identified (de Lau & Breteler, 2006).

Most cases of PD are therefore caused by the complex interaction of innate cell properties with genetic and environmental risk factors. Ca^{2+} influx through $Ca_V1.3$ VGCCs leads to uptake of Ca^{2+} into mitochondria. This can overload the buffering capacity of SNc neurons, leading to complex I dysfunction and ROS production. ROS production leads to protein damage including those involved in the proteasomal system, leading to reduced clearance of defective proteins. Alpha-synuclein, aided by Ca^{2+} and ROS damage, is allowed to aggregate and migrate which causes further damage and spread of the disease. These factors eventually lead to cell death. This is aided by genetic and environmental factors that cause further susceptibility through reduced mitochondrial function or ROS production. Each stage of this mechanism is a possible therapeutic target for treatment of the disease. The majority of this research, however, has been performed using animal models of the disease. It is clear that for effective strategies for the treatment for PD to be developed that more research into human models of the disease needs to be performed.

1.3.5 hiPSC-Derived Dopaminergic Neurons as a Human Model for Parkinson's Disease

1.3.5.1 Animal Models of PD

The majority of research into PD has been performed in animal models of the disease. The most commonly used *in-vivo* models are neurotoxic lesions caused by DA neuron specific toxins. Exposure of primates and mice to MPTP and 6-OHDA causes selective SNc death and parkinsonian symptoms, though Lewy body formation that is typical in human forms of PD is not present in these animals. To this day, MPTP lesioned primates remain the gold-standard for pre-clinical testing of therapeutic strategies for PD (Tieu, 2011).

Genetic models in animals are also a promising strategy. Knockout mouse models with mutations in Parkin and PINK1 have been shown to cause SNc degeneration. Two specific mutations in SCNA, A53T and A30P, have been used to create transgenic mice that show severe motor deficits similar to those seen in PD (Dawson et al., 2010). In the last few years a mouse model known as MitoPark has been used to specifically research the mechanisms of cell death in the SNc. This model was designed to test the hypothesis that mitochondrial dysfunction in the SNc causes parkinsonian symptoms by cell type-specific inactivation of mitochondrial transcription factor A. MitoPark mice exhibit many of the motor symptoms of PD, which can be alleviated by administration of L-DOPA (Ekstrand & Galter, 2009).

A major drawback of animal models is that they may not adequately mimic the mechanisms occurring in the human form of PD. Post-mortem brain slices have been used but these are only able to give insight into very late stages of the disease once severe degeneration has already occurred. *In-vivo* at least, animal models are the best we have available. In recent years, however, human induced pluripotent stem cell (hiPSC) derived DA neurons have come to the forefront as an *in-vitro* model of PD.

1.3.5.2 hiPSC-Derived Dopaminergic Neurons

Induced pluripotent stem cells (iPSCs) were first described in 2006 by Shinya Yamanaka and Kazutoshi Takahashi. By introducing certain reprogramming factors (Oct3/4, Sox2, c-Myc and Klf4) they were able to re-programme mouse fibroblasts into

an embryonic stem cell-like state. When transplanted into mice they were capable of differentiating to a wide range of cell types, similar to embryonic stem cells. It was soon discovered that these could also be generated from human fibroblasts, opening up a new field of possible stem cell therapies and disease models (Takahashi & Yamanaka, 2006; Takahashi et al., 2007).

Over the last few years the ability to differentiate iPSCs into specific cell types has been developed, DA neurons among them. iPSCs can be directed down a neural floor plate lineage through dual SMAD inhibition, then directed to a midbrain DA neuron fate through exposure to the transcription factors SHH and FGF8 (Kriks et al., 2012). This method has been used to produce neurons that express tyrosine hydroxylase, the rate-limiting enzyme in the production of dopamine (Hartfield et al., 2014). When transplanted into animal models of PD these neurons can relieve some of the motor symptoms of the disease (Wang et al., 2015). However, the discovery that iPSCs retain epigenetic markers from their previous lineage has halted most attempts at clinical trials in humans (Kim et al., 2010). Instead, human induced pluripotent stem cells (hiPSCs) have become important disease models for the study of various aspects of PD.

The electrical properties of hiPSC-derived DA neurons are relatively under-explored, with only one main study being produced that looked at this in any detail. This study found that these neurons in culture stain for markers characteristic of SNc DA neurons *in-vivo*. They produced ~10 Hz pacemaker activity in culture, receiving excitatory synaptic inputs and firing robust spike trains in response to current injection. These properties took 6 weeks to develop and continue to increase in frequency until 10-12 weeks. Ca^{2+} imaging revealed Ca^{2+} waves in both their soma and processes. This study also showed these neurons were susceptible to damage by mitochondrial toxins such as MPTP (Hartfield et al., 2014).

Various questions remain to be answered over the electrical excitability of hiPSC-derived DA neurons. Firstly, whether or not pacemaking is $Ca_V1.3$ dependent in these cells is unknown and needs to be researched to determine if they are suitable for modelling PD. Secondly, is the observed activity truly spontaneous? No study has, as of yet, determined whether the activity in these cells is intrinsic or driven by synaptic input. Thirdly, cell death in cultures containing hiPSC-derived DA neurons has been identified in response to SNc specific toxins, but, considering only up to 20-30% of the culture has been identified as being DA neurons in previous studies (Hartfield et al., 2014), are they more susceptible to death than other neuron types in culture, and does

$Ca_V1.3$ expression increase their susceptibility to cell death? Answering these questions will better inform future studies into PD by providing more information on the suitability of hiPSC-derived DA neurons as an *in-vitro* PD model.

1.4 Conclusion

Neurons and neuroendocrine cells throughout the nervous system exhibit pacemaker activity. This is used to control regular processes such as breathing, repetitive movement and consistent hormone release. Pacemaking is controlled by two overlapping systems: intrinsic excitability, which involves the balance of ion channel populations to produce rhythmic membrane potential changes; and agonist-induced excitability, which involves modulation of firing patterns by synaptic inputs. Two diseases that occur in cell types that exhibit pacemaker activity are Cushing's disease in pituitary corticotrophs and PD in SNc DA neurons.

Cushing's disease results in HPA-axis dysfunction. Subsequent symptoms including osteoporosis, obesity, diabetes and depression. An *in-vitro* model for this disease is the tumour cell line AtT20. These cells show pacemaker activity dependent on L-type VGCCs. A role for other VGCCs has been identified in models of their excitability but needs to be determined experimentally.

PD is caused by the selective death of DA neurons in the SNc. This is believed to be caused by mitochondrial dysfunction due to Ca^{2+} influx through $Ca_V1.3$ VGCCs. These are not critical for the pacemaker process in SNc neurons, with other channel types able to compensate for their loss. Human models for the disease are lacking but in the last few years hiPSC-derived DA neurons have come to the foreground. They have been seen to produce pacemaker activity *in-vitro* and show susceptibility to the mitochondrial toxin MPTP. Apart from this the electrical properties of these neurons are relatively underexplored. It is important to know if they have similar activity and synaptic inputs to SNc neurons *in-vivo* and whether or not they express $Ca_V1.3$ as this will better inform their suitability as a model for PD.

1.4.1 Motivation for the Research

PD and Cushing's disease are conditions that occur in neuronal and neuroendocrine cell types that exhibit robust pacemaking.

Cushing's disease affects around 100 000 people worldwide per year, 70% of which are women. The symptoms can cause crippling physical and psychological problems for sufferers, including obesity, osteoporosis, diabetes and depression. Treatment is either through surgery to remove pituitary tumours or through drugs to target the tumour or treat the symptoms. It is an expensive disease to treat, with the cost of one such drug, Pasireotide, estimated to cost £50 000 per patient per year (McKeage, 2013).

PD affects around 1 in 500 people worldwide, with an estimated 127 000 sufferers in the UK alone. The disease is more common in the elderly, causing symptoms including resting tremor, slowness of movement, shuffling gait and the co-presence of dementia. Patients have higher need for nursing home placements, have a greater incidence of hospital visits and a higher mortality rate than the general population. The mean duration of death from the onset of the disease is estimated at 6.9 to 14.3 years. The disease is currently incurable, with a few drugs available to treat or reduce the onset of symptoms (de Lau & Breteler, 2006). It is estimated to cost the NHS between £449 million and £3.3 billion per year, mostly due to the demand for inpatient care and nursing home placements (Findley, 2007).

In-vitro models are often used to study the mechanisms of these diseases, or to test new treatments prior to clinical trials. Studying how pacemaking is controlled and how it develops in these models will provide information about how similar or different these models are to those *in-vivo*. It is hoped this will inform future studies that use these cell types as model disease systems. In turn this will lead to a deeper understanding of pacemaking and more targeted, efficient research into the cellular mechanisms behind these diseases and any future treatments.

1.4.2 Aims of the Research

The research performed in this thesis has focussed on two *in-vitro* disease models: AtT20 D16v-F2 and hiPSC-derived DA neurons. In both of these models research is focused on the electrical properties of pacemaking, how it develops and how these properties compare to their *in-vivo* counterparts. The main questions for each cell type are outlined below:

1. **AtT20: What are the roles of different VGCC subtypes in pacemaking?**
    a. What are the roles of L-type VGCCs?
    b. What are the roles of N-type VGCCs?
    c. What are the roles of T-type VGCCs?
    d. Is the secretion of ACTH coupled to excitability?

2. **hiPSC-derived dopaminergic neurons: Are pacemaking properties the same or different from SNc dopaminergic neurons *in-vivo*?**
    a. Is spontaneous activity intrinsic or agonist-induced?
    b. What are the main synaptic inputs onto these neurons?
    c. Do they express $Ca_v1.3$?
    d. Are they susceptible to 6-OHDA and glutamate toxicity?
    e. When during development do the above properties develop?

In the following chapters I aim to answer these questions using techniques such as whole cell electrophysiology, immunostaining and fluorescence imaging. In AtT20 pituitary corticotrophs this provides a greater understanding of the general mechanisms of pacemaking and how its dysfunction could lead to problems of ACTH secretion. In hiPSC-derived DA neurons this quantifies any differences in excitability from SNc DA neurons in animal models.

By comparing differences and similarities in pacemaking between these models and their *in-vivo* counterparts it allows for an assessment of their suitability as models of their respective diseases that is more informed than any of the previous literature. It also allows for a comparison between the two models, giving further insight into the general mechanisms of pacemaking in the nervous system.

Chapter 2

The Mechanism of Pacemaking in AtT20 Anterior Pituitary Corticotrophs

Abstract

The murine pituitary tumour cell line AtT20 can be used as a model for normal corticotroph function and for related diseases such as Cushing's disease. This chapter has focused on the use of electrophysiology and Ca^{2+} imaging to dissect the roles of voltage-gated calcium channel (VGCC) subtypes that were previously unexplored in AtT20 pacemaking. Through these techniques I show that AtT20s spontaneously produce action potentials in culture. These were driven by underlying rhythmic changes in the cytoplasmic Ca^{2+} concentration, termed "Ca^{2+} waves," confirming previous literature. Unlike previous literature, however, two modalities of cytoplasmic Ca^{2+} waves were found to underlie AtT20 pacemaking that were able to maintain Ca^{2+} influx at similar levels despite changes in cell excitability: Fast waves that were tetrodotoxin (TTX) dependent and slow waves that were TTX-independent. Both modalities were found to be blocked by the L-type VGCC antagonist nifedipine. A novel role for T-type VGCCs in AtT20 pacemaking was identified, with the T-type antagonist ML218 blocking all pacemaker activity. N-type VGCCs did not appear to play a role in pacemaking. This research improves our understanding of the complex ion channel interactions that underlie pacemaking in corticotrophs and their associated diseases.

2.1 Introduction

AtT20 is a mouse anterior pituitary corticotroph tumour cell line that is commonly used for the study of exocytosis and hormone secretion due to their robust secretion of adrenocorticotropic hormone (ACTH). Similar to corticotrophs *in-vivo*, AtT20's *in-vitro* have been shown to display pacemaking activity in culture (Adler et al., 1983). This provides us with a useful model to study the mechanism of corticotroph pacemaking and its relationship to diseases of hormone secretion.

Research into the mechanisms of AtT20 pacemaking has been limited, mainly focusing on the use of ion channel blockers, electrophysiology and fluorescent Ca^{2+} imaging. Both corticotrophs *in-vivo* and AtT20s *in-vitro* have shown various rhythmic firing patterns with proportions of cells tonically firing single action potentials, firing in plateau-like bursts or showing complete quiescence under current clamp (Zemkova et al., 2016). The addition of the L-type VGCC antagonist nifedipine abolishes pacemaking in AtT20s, indicating these channels are a critical component of their pacemaking mechanism. Strengthening this hypothesis, loading of AtT20s with fluorescent Ca^{2+} dyes reveals regular increases in their intracellular Ca^{2+} concentration that are also blocked by nifedipine (Adler, 1983). Antagonists against other VGCC subtypes have revealed the presence of small populations of N-type and P/Q-type channels in AtT20s (Mackie et al., 1995). Modelling predictions have also suggested a role for T-type channels in firing pattern generation (LeBeau et al., 1997). Experimental evidence for the involvement of these channel types in pacemaking is lacking, in part due to a past lack of specific antagonists for different VGCC subtypes. With specific blockers for all major subtypes now available, it affords the opportunity to re-examine pacemaking in AtT20s to determine the roles of these other channels.

The research in this chapter has focused on determining the roles of L-, N- and T-type VGCCs in the generation of pacemaking in an AtT20 subtype, D16v-F2. Through the use of electrophysiology and fluorescent Ca^{2+} imaging I show that L-type and T-type channels have distinct roles. L-type VGCCs are critical for pacemaking and the generation of subthreshold Ca^{2+} waves. T-type channels are also critical for pacemaking and, although not critical for the generation of Ca^{2+} waves, may be involved in shaping their amplitude and duration. N-type channels on the other hand did not appear to be involved in pacemaking. This research improves our understanding of the complex ion channel interactions that underlie pacemaking in corticotrophs and their associated disease models, leading to a better understanding of diseases such as Cushing's disease.

2.2 Methods

2.2.1 Cell Culture

The AtT-20/D16v-F2 cell line was kindly gifted by Rory Duncan and associates from the Life Sciences Interface Laboratory at Heriot-Watt University, Edinburgh. Cells were incubated at 37^{o}C and 5% CO_2. All media products were obtained from ThermoFisher unless stated.

Murine-derived pituitary corticotroph tumour cells (AtT20) were plated onto sterile tissue culture treated 75 cm^2 flasks at 40% confluency. Once 80% confluency was reached the cells were washed with 5 ml Versene and detached using 5 ml TrypLE Express for 5 minutes at room temperature (21^{o}C) before passage. Cell media consisted of (v/v): 10% FBS, 1% sodium pyruvate, 1% GlutaMAX, 1% penicillin/streptomycin in DMEM lacking glucose and sodium pyruvate supplemented with Phenol Red. Prior to experimentation the cells were passaged onto 35 mm coverslips pre-coated with 100 µg/ml Poly-D-lysine in cell media lacking Phenol Red and incubated for 48-72 hours.

2.2.2 Electrophysiology

Recordings were performed in the whole cell configuration at room temperature (21^{o}C). Data was acquired using Clampex 10 software on an Axopatch 200B patch clamp amplifier with a 16 bit Digidata 1440A digital acquisition system (Molecular Devices) at 20 kHz with a 10 kHz low pass filter. Microelectrodes were pulled from borosilicate glass using a Flaming/Brown P-87 micropipette puller to a resistance of 3-8 MΩ. The extracellular solution contained (mM): 140 NaCl, 2.5 KCl, 2 MgCl2, 2 CaCl2, 10 HEPES, 10 Glucose, 15 D (+)-Saccharose, pH 7.4; 320 mOsm/kg. The intracellular solution contained (mM): 100 K-Gluconate, 20 KCl, 1 $CaCl_2$, 1 $MgCl_2$, 10 HEPES, 3 Phosphocreatine Na_2, 11 EGTA, 9 D (+)-Sucrose, 4 ATP-Mg_2; pH 7.2; 295 mOsm/kg. For calcium current recordings intracellular K-gluconate/KCl was replaced with 120 mM Cs-Gluconate and 10 mM $CaCl_2$/1 µM TTX were added to the bath prior to recording. Cells with more than 100 pA of leak current from a holding potential of -60 mV were rejected. The liquid junction potential (LJP) was calculated to be -2.4 mV (K internal) and -8.9 mV (Cs internal). Recordings were adjusted for these values during analysis**.** Whole cell capacitance was corrected during voltage clamp recording and series resistance compensation was applied to a minimum of 60%. The following

compounds were added where stated: TTX (1 µM), tetraethylammonium (TEA) (10 mM) Nifedipine (10µM), ω-conotoxin GVIA (1 µM), ML218 (1 µM), Bay K8644 (1 mM), corticotropin releasing hormone (CRH) (500 ng/ml).

The protocols used are outlined below:

1. **Current density and I/V relationships**: A holding potential of either -60 mV or -80 mV was applied in the voltage clamp configuration. +10 mV steps up to +80 mV were applied, with the holding potential being applied between steps. Each step lasted 200 milliseconds with 1 second between sweeps. P/4 leak subtraction was applied pre-recording.

2. **Firing frequency**: Recording was performed gap-free for up to 10 minutes in the current clamp configuration. No current was injected during recording and no leak subtraction was applied.

3. **Action potential properties:** Consecutive current steps of 10 pA were applied up to 100 pA from a holding potential of -60 mV. Each step lasted 200 ms with a 1 second gap between sweeps. No leak subtraction was applied.

4. **Continuous capacitance recording.** An estimate of whole cell capacitance was recorded using the membrane test feature of Clampfit 10. 4x 500 ms voltage steps from -80 to +10 mV were applied mid-recording with 500 ms gaps between steps. A full explanation of this approach is described in **Supplementary 2.1.**

2.2.3 Analysis of Recordings

All data was analysed using Clampfit 10 and Excel. For experiments involving channel agonists or antagonists, recordings were performed on the same cell before and after the addition of a compound.

Current Clamp: Firing rate was determined for each cell in each drug condition using the 'Threshold Search' mode in Clampfit 10. Resting potential, firing threshold, amplitude, peak depolarisation, peak hyperpolarisation, time to peak, repolarisation time, area under the graph and action potential duration were calculated for each cell in each drug condition using the statistics feature of Clampfit 10. Mean values and standard errors were calculated using Excel.

Voltage Clamp: Recordings were filtered offline using a 3 point lowpass boxcar filter. I/V relationships were generated in Clampfit 10 using the Quick-Graph feature. Data was exported to Excel and the mean peak current and S.E.M. were calculated for each drug condition. Whole cell capacitance was recorded from the membrane test feature in Clampex 10 prior to compensation.

2.2.4 Calcium Imaging

Calcium green-1 AM (ThermoFisher) was loaded into cells to assess changes in cytoplasmic Ca^{2+} concentration. A 1 mg/ml stock solution of Calcium Green-1 AM was formulated in loading medium containing 48 µl DMSO (Sigma) and 2 µl 20% w/v Pluronic F-127 (Sigma). 2-3 days after passage, AtT20 cells were loaded with a final concentration of 5 µg/ml Calcium Green-1 AM for 20 minutes at 37ºC in culture medium. Cells were washed 5 times with PBS pre-warmed to 37ºC and transferred to 35 mm culture dishes. Recording was performed in extracellular solution (as formulated in **2.2.2**) at room temperature (21ºC) using an Olympus IX71 microscope (10x objective, NA 0.3) and a 470 nm pE-100 light emitting diode (CoolLED). Fields of cells were recorded for 40 seconds using a Qi Click USB camera (QImaging) at 5 frames per second with a gain of 20. Data was collected using WinFluor v3.8. To investigate calcium spiking in different conditions the following drugs were added where stated: TTX (1 µM), Nifedipine (10 µM), ω-conotoxin GVIA (1 µM), ML 218 (1 µM).

Data Analysis: Manual regions of interest were drawn around cells in ImageJ. Data was then imported to Clampfit 10 for the calculation of wave frequency, duration, amplitude and time between waves. Graphs were portrayed as the proportional change in fluorescence from baseline (ΔF/F). The area under the graph was calculated in Excel using the Riemann summing method of numerical integration using ΔF/F values. For all Calcium Green-1 experiments the means from each of 3 experiments were calculated from 50 cells in each experiment. These 3 values were then averaged to give an overall mean and S.E.M.

2.2.5 Simultaneous Electrophysiology & Fluorescence Imaging

Simultaneous cell attached recording and fluorescent calcium imaging was performed using an Axopatch 200B amplifier at a 10 kHz frequency using an miDAQ USB6002

digital acquisition system (Molecular Devices). Data was recorded using WinFluor v3.8. The experiment was repeated 6 times. Pipettes and the bath contained extracellular solution as described in **2.2.2** and were pulled to a resistance of 2-4 MΩ. Imaging was performed as described in **2.2.4**.

Data Analysis: Data was filtered off-line using a 60 Hz low pass filter. Data was exported from WinFluor to Excel for analysis. Fluorescence and current clamp data was normalised between 0 and 1 to allow for easier comparison. Spikes in membrane potential were identified by eye and data points from exactly 1 second before the spike to 3 seconds after were averaged to obtain a mean time course for both fluorescence intensity and spikes in membrane potential.

2.2.6 Immunofluorescence Staining

Coverslips containing AtT20 cells were washed in PBS pre-warmed to 37ºC before fixation in 4% paraformaldehyde for 10 minutes at room temperature (21ºC). 3 washes with ice cold PBS were performed before permeabilisation with 0.1% Triton X-100 for 10 minutes at 21ºC. Coverslips were washed for 3x 5 minute washes with PBS containing 0.1% Tween-20 at 21ºC before a 30 minute incubation at 21ºC in PBS containing 1% BSA and 0.1% Tween-20 to prevent non-specific antibody binding. Primary antibody incubation was performed at 21ºC for 1 hour in PBS containing 1% BSA and 0.1% Tween-20. Coverslips were washed 3x for 5 minutes with PBS containing 0.1% Tween-20 at 21ºC. Secondary antibody incubation was performed for 1 hour in the dark at 21ºC in PBS containing 1% BSA. All secondary antibodies were conjugated with AlexaFluor fluorescent dyes. Coverslips were then washed 3x for 5 minutes with PBS in the dark at 21ºC before mounting on glass microscope slides with the mounting medium Mowiol® 4-88 and sealing with nail polish. Slides were stored at 4ºC until analysis. All reagents were acquired from Sigma Aldrich and all antibodies were from Abcam unless stated. The antibodies used were: mouse anti-ACTH with a rabbit anti-mouse AlexFluor-488 secondary; rabbit anti-$Ca_V1.3$ with a goat anti-rabbit AlexaFluor-647 secondary.

2.2.7 Microscopy

Light & Fluorescence Microscopy: An IX71 fluorescent microscope (Olympus) was used in combination with either a white light or a pE-100 470 nm LED excitation source (CoolLED) and a 10x objective lens. Data was acquired using WinFluor v3.8.

Confocal Microscopy: Fixed coverslips were imaged using a TCS SP5 II confocal microscope (Leica) with a 63x oil objective (NA 1.3). Samples were excited using an argon or white light laser. Images were collected using a Hamamatsu camera with 3x frame averaging at a resolution of 1024x1024 pixels.

STED Microscopy: Fixed coverslips were imaged using a TCS SP5 II confocal microscope (Leica) with a STED module using a 100x objective lens (NA 1.4). An Argon laser at 488 nm was depleted using a 592 nm STED depletion laser. Pixel size was 19.92 nm. Vesicle diameter calculations were performed in ImageJ using manual areas of interest.

2.2.8 Drugs & Compounds

All drugs were diluted from concentrated stock solutions and pipetted directly into the bath solution or culture medium at concentrations determined from the literature. All were purchased from Tocris unless otherwise stated.

2.2.9 Graphs & Statistical Analysis

All graphs and curve fitting were performed using OriginPro 8.5. Statistical analysis was performed using an appropriate statistical test in Excel using the XLSTAT plugin (t-tests, ANOVAs or KS-tests). The exact test used and their associated significance values are reported in the text. Differences were considered statistically significant when $p < 0.05$. Asterisks (*) on graphs indicate statistical significance at this p-value. Errors bars in all graphs and ± values in the text use the standard error of the mean (S.E.M.) which was calculated in Excel.

2.3 Results

2.3.1 Characterisation of AtT20 Pacemaking

2.3.1.1 Confirmation of an AtT20 Phenotype

To confirm that the cells used during experimentation were functional AtT20s, antibody staining against ACTH was performed. Under a light microscope the cells showed a morphology typical of AtT20s, being either spindle shaped or triangular with short processes extending from each pole (**Figure 2.1A**). Fluorescent imaging revealed that all of the cells in culture stained for ACTH. Staining was primarily localised to a region near one pole of the cell (**Figure 2.1B**). Stimulated Emission Depletion (STED) microscopy, a technique to image below the diffraction limit, provided the resolution to see ACTH contained within distinct puncta located in regions proximal to the processes, analogous to the axon hillock of neurons (**Figure 2.1C**). The mean diameter of these puncta, which were likely to have been ACTH-containing secretory granules, was (±S.E.M.) 179 ± 7 nm. A histogram of granule size revealed that their diameter ranged from 60-280 nm, with distinct peaks at 80-100 and 160-180 nm (n=108 granules from 1 cell) (**Figure 2.1D**).

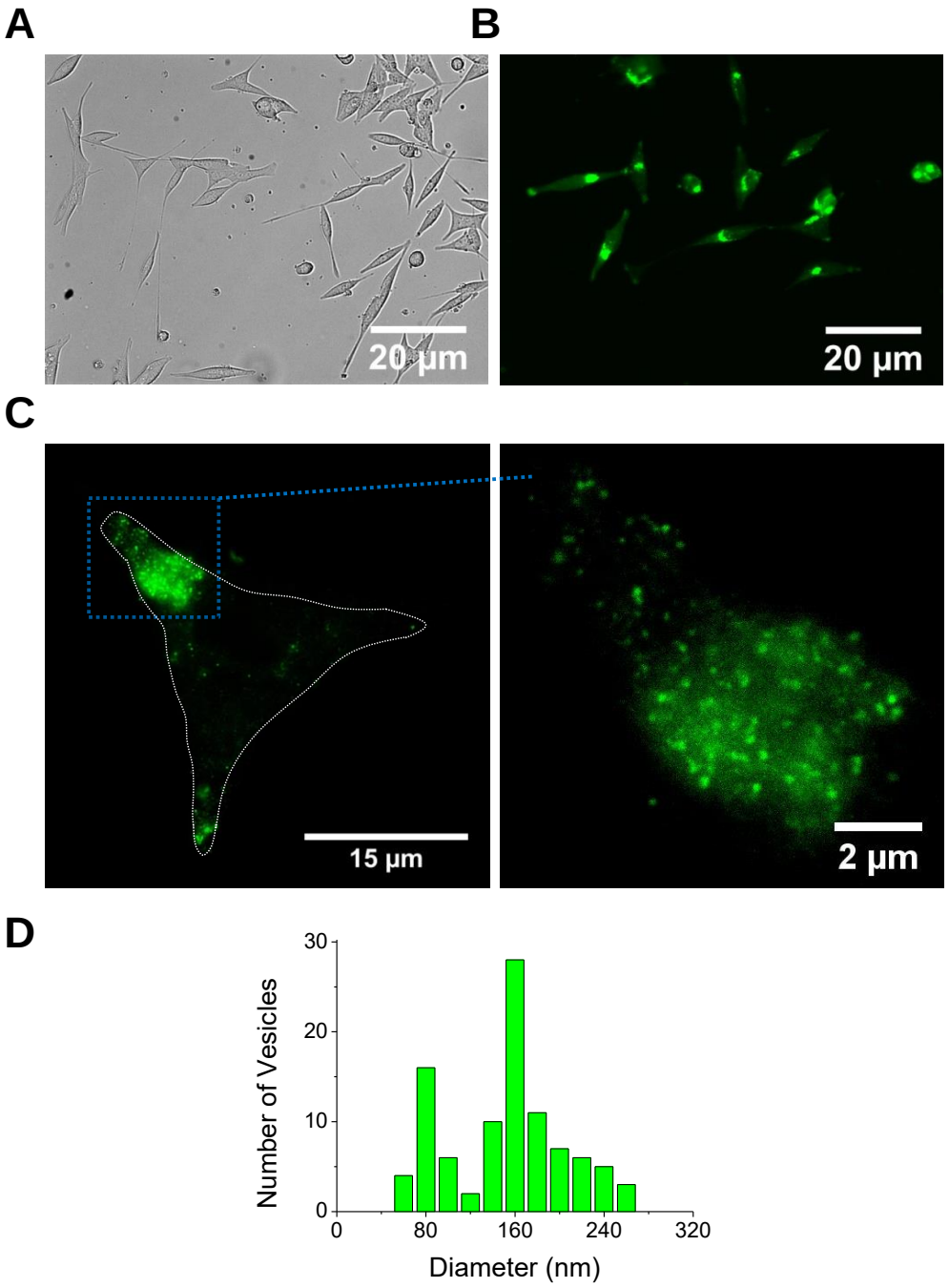

Figure 2.1 - **ACTH-containing secretory granules in AtT20s**. Representative images showing (A) AtT20s with a typical spindle or triangular morphology. (B) Cells stained for ACTH showing its localisation to a region near one pole of the cell. (C) STED microscopy revealing this region consists of small puncta that are likely to be ACTH-containing secretory granules. Image on the right is zoomed-in from the blue-outlined region in the left image. The white outline indicates the border of the cell. (D) A histogram of vesicle diameter from the STED image from C. Values are binned into 20 nm intervals, i.e. a value of 80 nm in the graph includes all vesicles with diameters between 80-99 nm.

2.3.1.2 Firing Properties of AtT20s

To determine the pacemaker properties of AtT20s, cells were analysed under whole cell current clamp. 66% of cells spontaneously fired action potentials in culture, with 2 rhythmic firing patterns being observed. Action potentials were defined as regenerative all-or-nothing membrane depolarisations that produced an overshoot beyond 0 mV. Cells were either quiescent (n=18), tonic (n=23) or burst firing (n=12) from 53 cells tested (**Figure 2.2**). Quiescent cells generally displayed a more depolarised resting membrane potential at -27.89 ± 3.09 mV than tonically firing cells at -38.01 ± 1.37 mV (Student's t-test, p=0.0025). Burst firing cells displayed a more hyperpolarised membrane potential at -47.2 ± 1.63 mV than tonic cells (Student's t-test, p=0.0002). Burst firing, at 0.54 ± 0.16 Hz, was significantly faster than tonic firing, at 0.29 ± 0.06 Hz (Student's t-test, p=0.02). Hyperpolarisation of quiescent cells could often induce firing, though burst firing could not be induced in tonically firing or quiescent cells.

Current injection elicited single action potentials in all cells tested (n=11) (**Figure 2.3A**) with a mean threshold for firing of -30.43 ± 2.16 mV and a mean peak of +21.18 ± 4.11 mV before hyperpolarising to -39.8 ± 2.71 mV. Action potentials were slow and broad, with the mean time from threshold to repolarisation being 44.7 ± 4.43 ms.

500 ng/ml of the ACTH stimulant corticotropin releasing hormone (CRH) exhibited no effect on membrane potential (Paired t-test, p=0.654) or firing frequency (Paired t-test, p=0.646) (n=4) and did not induce firing in quiescent cells up to 10 minutes after addition in all cells tested (n=2) (**Figure 2.3B, 2.3C**).

Uncertainty remains over whether ACTH secretion is coupled to or uncoupled from electrical activity in AtT20s (Surprenant, 1982; Zemkova et al., 2016). In an attempt to settle this uncertainty, whole cell capacitance was continuously recorded in whole cell voltage clamp from a holding potential of -80 mV. This method can identify secretory events via the increase in surface area associated with secretory granule fusion with the membrane. The application of 4x 500 ms voltage steps to +10 mV resulted in no change in capacitance in any of the cells tested (n=29) (**Figure 2.4A**). Addition of 1 mM of the L-type VGCC agonist Bay K8644, however, caused a response in every cell tested (n=5), with a mean increase in capacitance of 0.186 ± 0.058 pF (**Figure 2.4B**). Given the secretory granules were observed to be ~160 nm in diameter, this would indicate the fusion of ~231 granules, assuming a specific capacitance of 1 μF/cm^2 (Gentet et al., 2000).

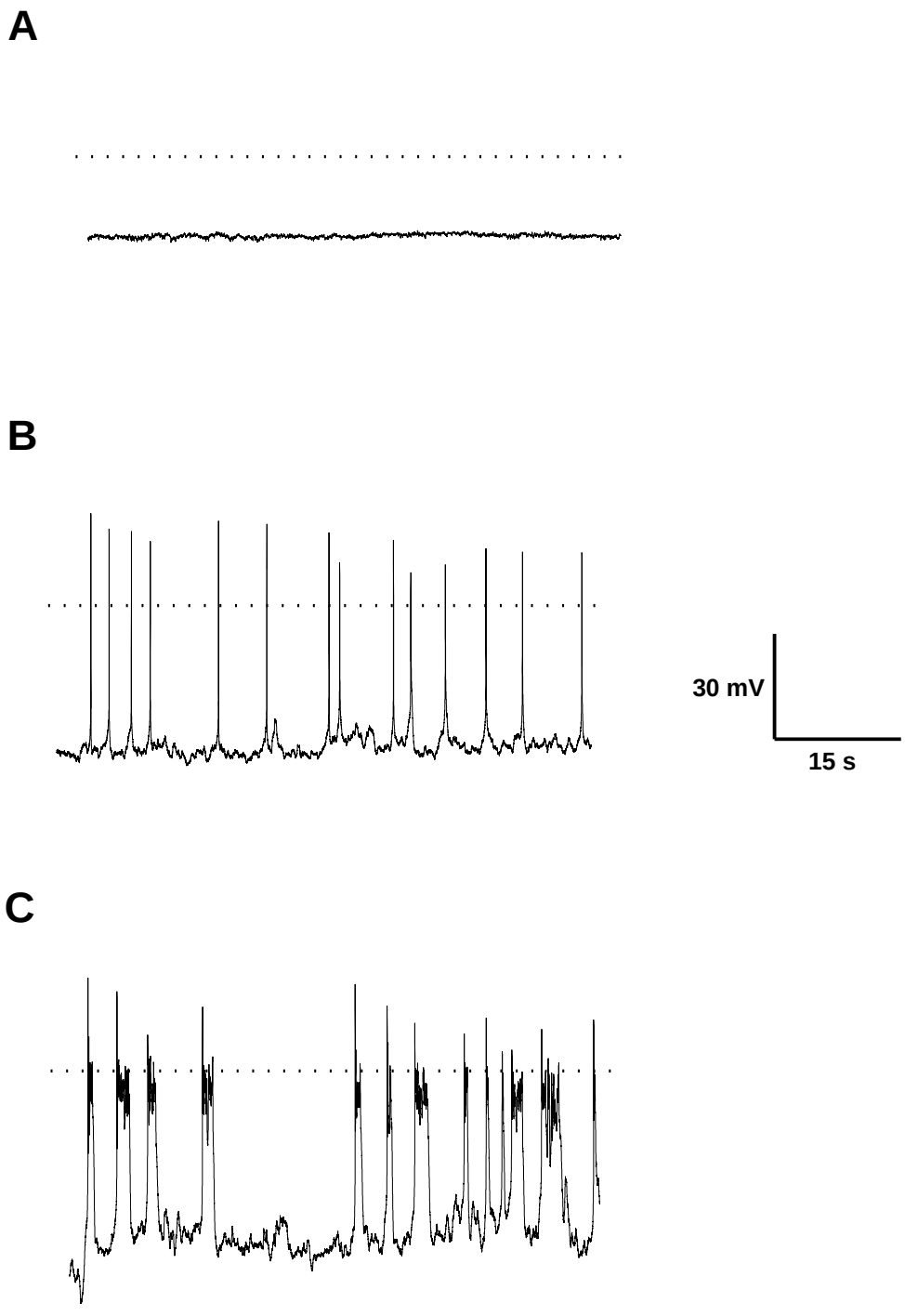

Figure 2.2 - Spontaneous firing patterns in AtT20s. Representative whole cell current clamp traces from (A) quiescent (B) tonic firing and (C) burst firing AtT20 cells in culture. Dotted lines indicate 0 mV.

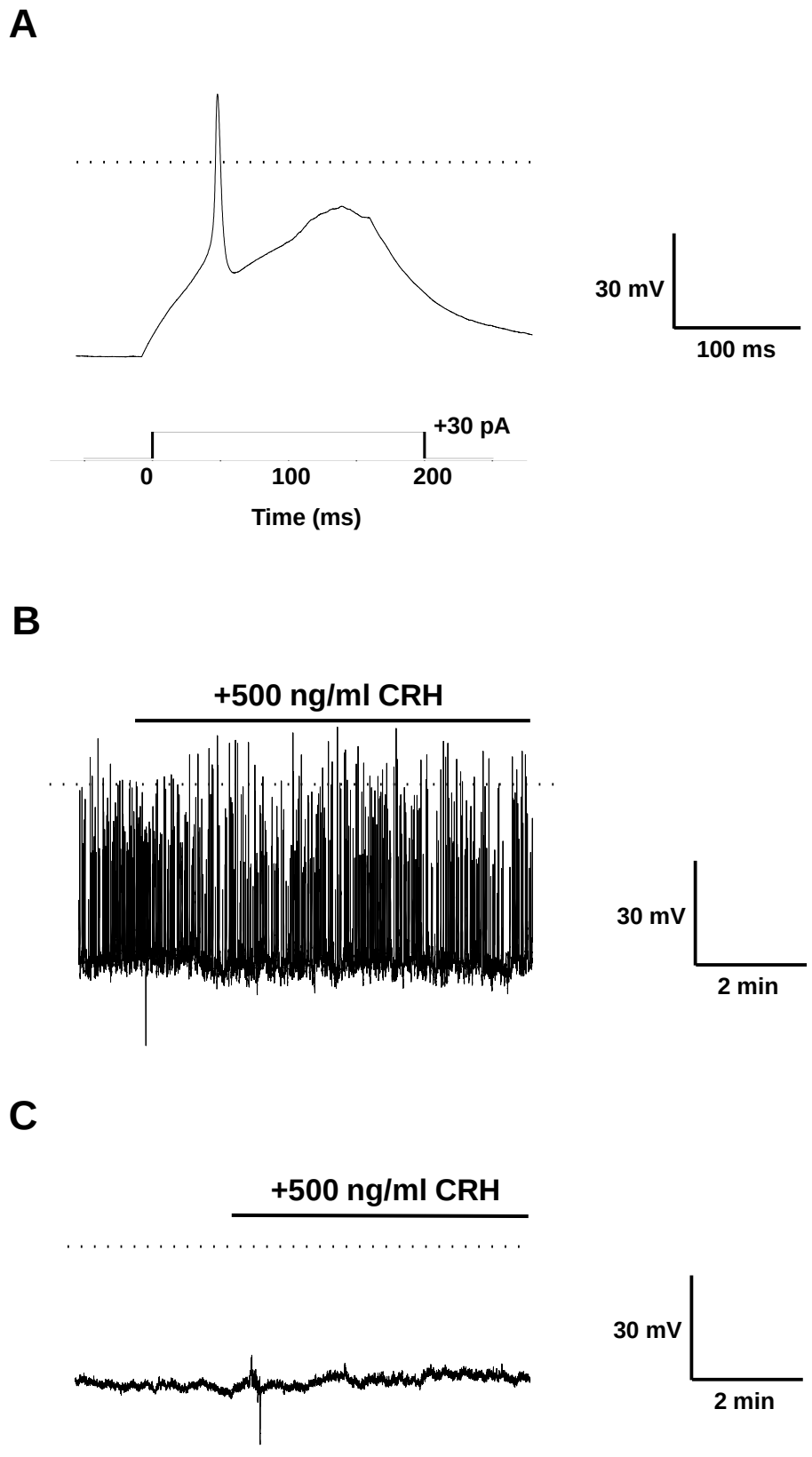

Figure 2.3 - Induced Excitability in AtT20s. (A) Representative whole cell current clamp recording from a holding potential of -60 mV showing a single action potential upon current injection. Representative whole cell current clamp recordings showing the addition of CRH in (B) a firing cell and (C) a quiescent cell. Dotted lines indicate 0 mV.

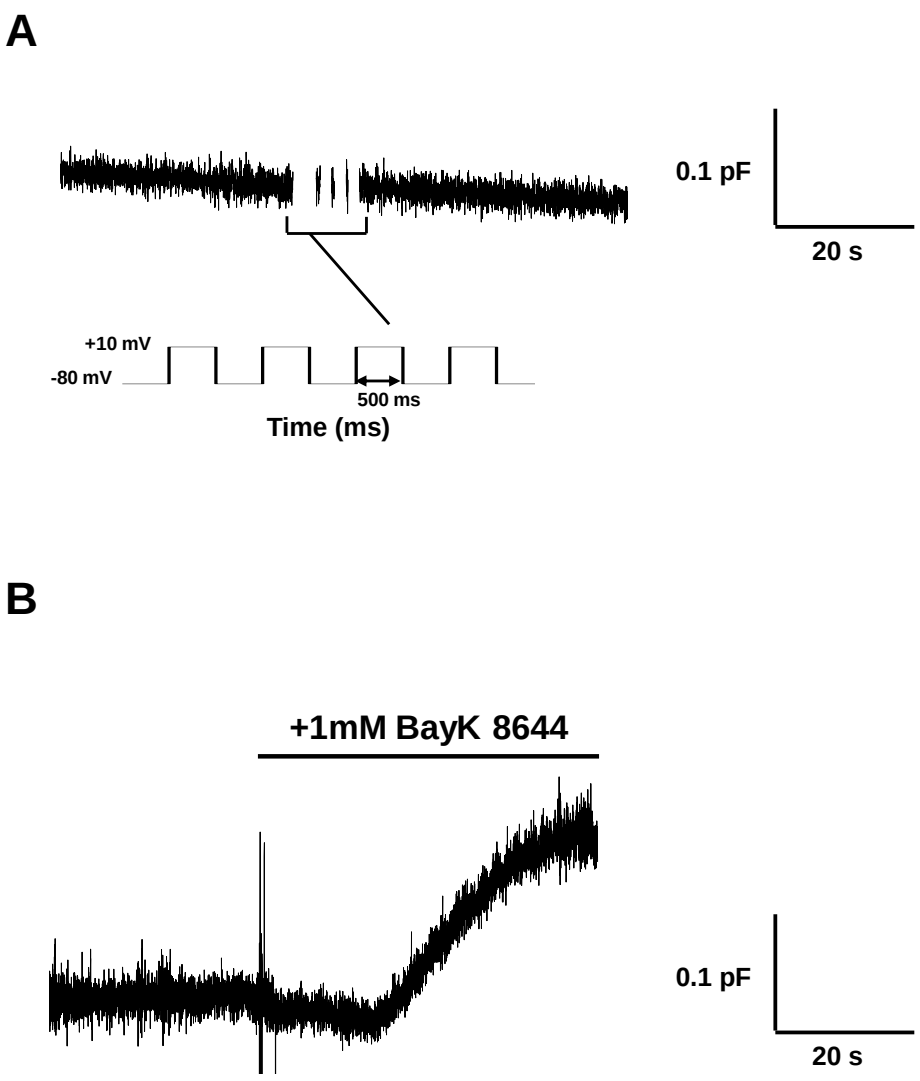

Figure 2.4 - Capacitance recordings in AtT20s. Representative whole cell voltage clamp recordings from a -80 mV holding potential showing changes in membrane capacitance in response to (A) 4x 500ms voltage steps to +10 mV and (B) 1 mM BayK 8644.

2.3.1.3 Voltage-Gated Ionic Currents in AtT20s

The voltage gated ionic currents underlying pacemaking were determined using whole cell voltage clamp. Mean whole cell capacitance was 14.91 ± 3.24 pF which indicates an average cell surface area of 1491 ± 324 μm^2 when assuming a specific membrane capacitance of 1 $\mu F/cm^2$ (n=11). All cells tested displayed voltage-gated sodium (Na_V) and voltage-gated potassium (K_V) currents in response to positive voltage steps from a holding potential of -80 mV (n=11) (**Figure 2.5A**). These were blocked by the addition of 1 µM TTX and 10 mM tetraethylammonium (TEA) respectively (**Figure 2.5B, 2.5C, 2.6A**). This revealed the presence of small Ca^{2+} currents that were blocked by 1 µM of the non-specific VGCC blocker $CoCl_2$ (**Figure 2.6A, 2.6B**).

To determine the VGCC subtypes that constitute this Ca^{2+} current density, VGCC antagonists were added under whole cell voltage clamp in the presence of 1µM TTX (extracellular) and 120 mM Cs-gluconate (intracellular) to block Na_V and K_V currents respectively (**Figure 2.6C**). Positive voltage steps from holding potentials of -60 and -80 mV were applied, with the results being analysed via a repeated measures ANOVA (n=12). A significant within-subjects difference was observed over the course of the experiment, indicating that the drugs were blocking statistically significant proportions of the mean peak current, without taking into account the different holding potentials ($F=97.981$, $p=0.0001$). The Mauchly test indicated that the condition of sphericity was not violated ($\chi 2=37.62$, $p<0.001$, $\varepsilon=0.508$). Peak current was denser at -80 mV than -60 mV though this was not significant ($F=0.874$, $p=0.36$). Addition of 10 µM of the L-type antagonist nifedipine blocked the majority of the peak current at -60 mV and -80 mV, with a significant difference in mean peak current still observed between the two ($F=12.383$, $p=0.002$). Subsequent co-addition of 1 µM of the N-type antagonist ω-conotoxin GVIA caused no identifiable difference in current at -60 mV but caused a further decrease in current at -80 mV versus nifedipine alone. A difference in peak current between -60 mV and -80 mV was still observed under these conditions ($F=10.394$, $p=0.004$). The I/V relationship at -80 mV was shifted towards a more hyperpolarised potential versus nifedipine alone (**Figure 2.6D**). Further addition of 1 µM of the T-type antagonist ML218 decreased the peak current at -60 mV and -80 mV versus ω-conotoxin and nifedipine combined. A significant difference in peak current between -60 and -80 mV was no longer identified ($F=4.001$, $p=0.058$).

A small proportion of the current remained after the addition of all 3 antagonists. This is likely comprised of P/Q type channels as these have been previously identified in

AtT20s (**Figure 2.6C**) (Mackie et al., 1995). **Figure 2.6E** shows the relative proportion of the peak current that is blocked by each VGCC antagonist from a -80 mV holding potential.

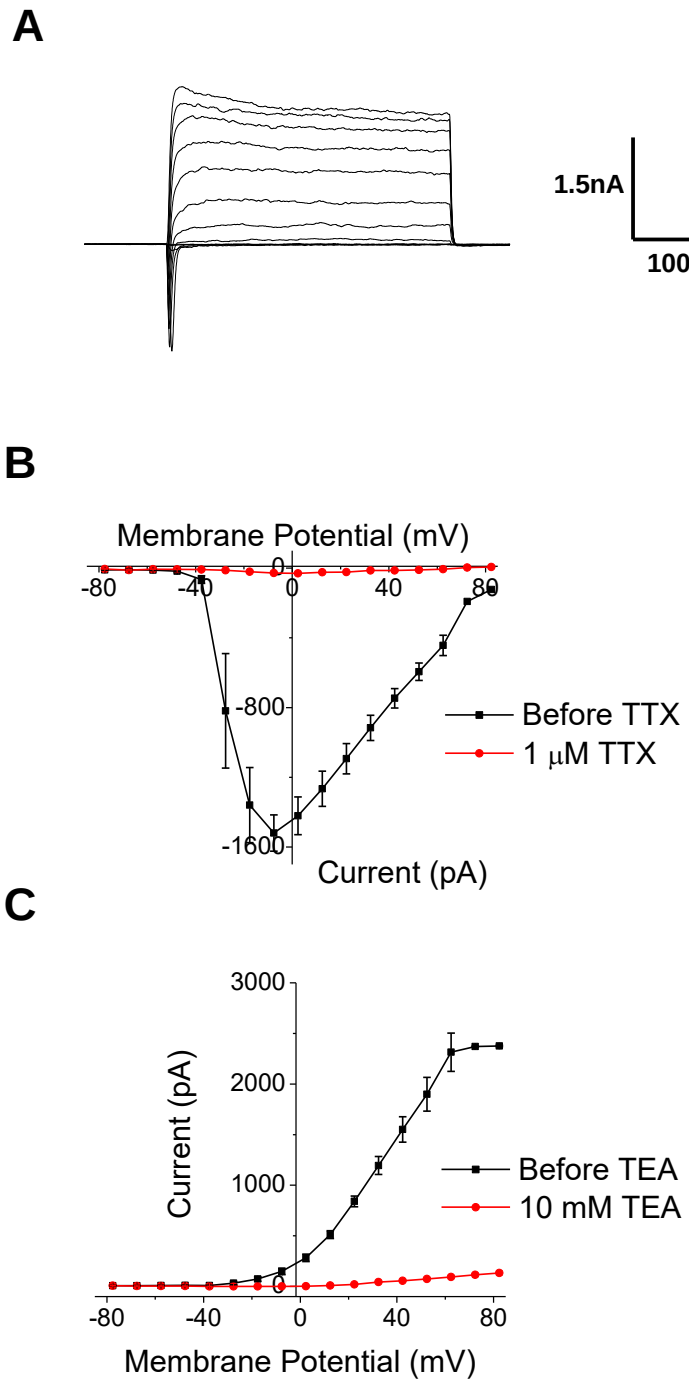

Figure 2.5 - Voltage-gated currents in AtT20s. (A) Representative whole cell voltage clamp recording showing voltage-gated currents in AtT20 cells (B) Negative peak current I/V relationship before and after the addition of 1 μM TTX. (C) Positive peak current I/V relationship before and after the addition of 10 mM TEA. N=11. Error bars ± S.E.M.

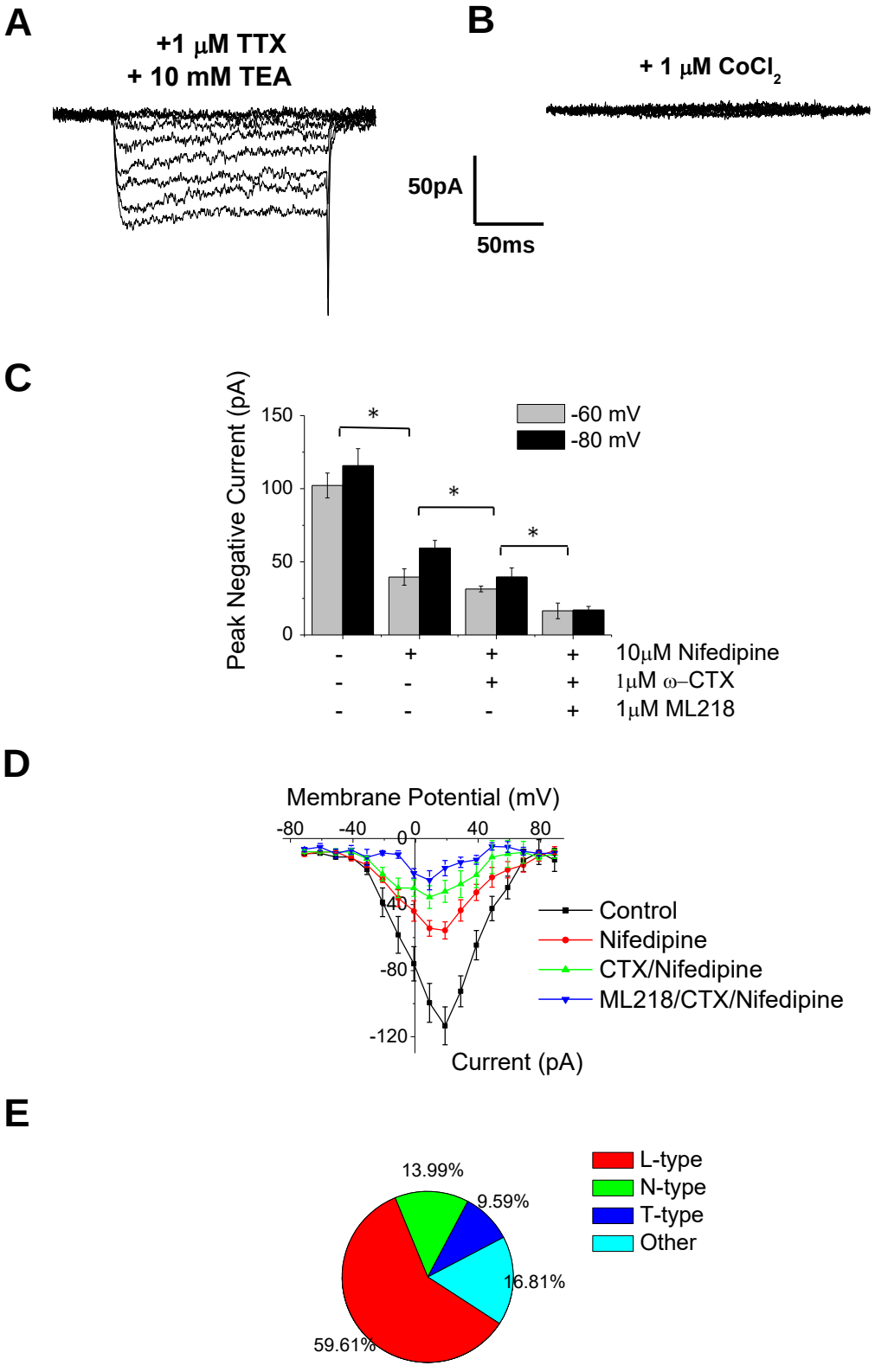

Figure 2.6 - VGCC currents in AtT20s. Representative whole cell current clamp recordings from a -80 mV holding potential from the same cell showing (A) a small inward current in the presence of TTX and TEA that (B) was blocked by $CoCl_2$ (C) Mean peak Ca^{2+} currents from two different holding potentials before and after block with various subtype-specific VGCC antagonists (n=12) (D) Mean I/V relationships from a -80 mV holding potential before and after addition of each antagonist (n=12) (E) Graphical representation of the percentage of peak current blocked by each antagonist from a -80 mV holding potential. Error bars ± S.E.M. *indicates statistical significance between subjects using a repeated measures ANOVA at $p<0.05$.

2.3.1.4 Calcium Waves in AtT20s

To determine the role of voltage-gated Ca^{2+} currents in pacemaking, AtT20 cells were loaded with the fluorescent cytoplasmic fluorescent Ca^{2+} indicator Calcium Green-1 (**Figure 2.7A**). During 40 second fluorescence intensity recordings 88 ± 1.8% of cells showed regular spikes in their intracellular Ca^{2+} concentration at a mean frequency of 0.19 ± 0.02 Hz (**Figure 2.7B**). This frequency showed no statistical difference from the frequency of action potential firing (Student's t-test vs tonically firing cells, p=0.193). These were termed "Ca^{2+} waves." 76 ± 3.6% of cells still produced waves after block of Na_V channels with 1 µM TTX in the extracellular solution. This addition caused a noticeable shift in wave properties (**Figure 2.7C**). Ca^{2+} waves decreased in frequency (Student's t-test, p=0.012) (**Figure 2.8A**), increased in amplitude (Student's t-test, p=0.045) (**Figure 2.8B**), increased in duration (Student's t-test, p=0.001) (**Figure 2.8C**) and had a longer inter-wave interval (**Figure 2.8D**) (Student's t-test, p=0.0004) than controls before the addition of TTX (n=3).

As an estimate of total Ca^{2+} influx, the area under the Ca^{2+} waves was calculated (n=3). The mean area under individual waves noticeably increased in the presence of 1 µM TTX compared to controls (Student's t-test, p=0.003) (**Figure 2.9A**). This was clearly seen after averaging the wave shape in both conditions (n=50 cells from 1 repeat) (**Figure 2.9B**). Interestingly, the mean area under the graph across the whole 40 second recording period was not statistically different from controls (Student's t-test, p=0.34) (n=3) (**Figure 2.9C**).

To determine whether TTX-dependent waves precede or follow an action potential, AtT20s were clamped in the cell attached configuration after Calcium Green-1 loading (**Figure 2.7D**). Current clamp revealed brief spikes in membrane potential that were followed by longer duration changes in Calcium Green-1 fluorescence. These transients started at the onset of a membrane potential spike, with no difference in onset time observed between the two (Student's t-test, p=0.28). Ca^{2+} waves lasted for a mean duration of 2.58 ± 0.6 seconds. Peak fluorescence intensity lagged behind the peak in membrane potential by a mean of 0.33 ± 0.08 seconds (n=6). The 0.2s frame rate and the response time of the dye should be taken into consideration. Despite this it seems unlikely that TTX-dependent Ca^{2+} waves are preceding action potentials, instead occurring simultaneously with or after their initiation.

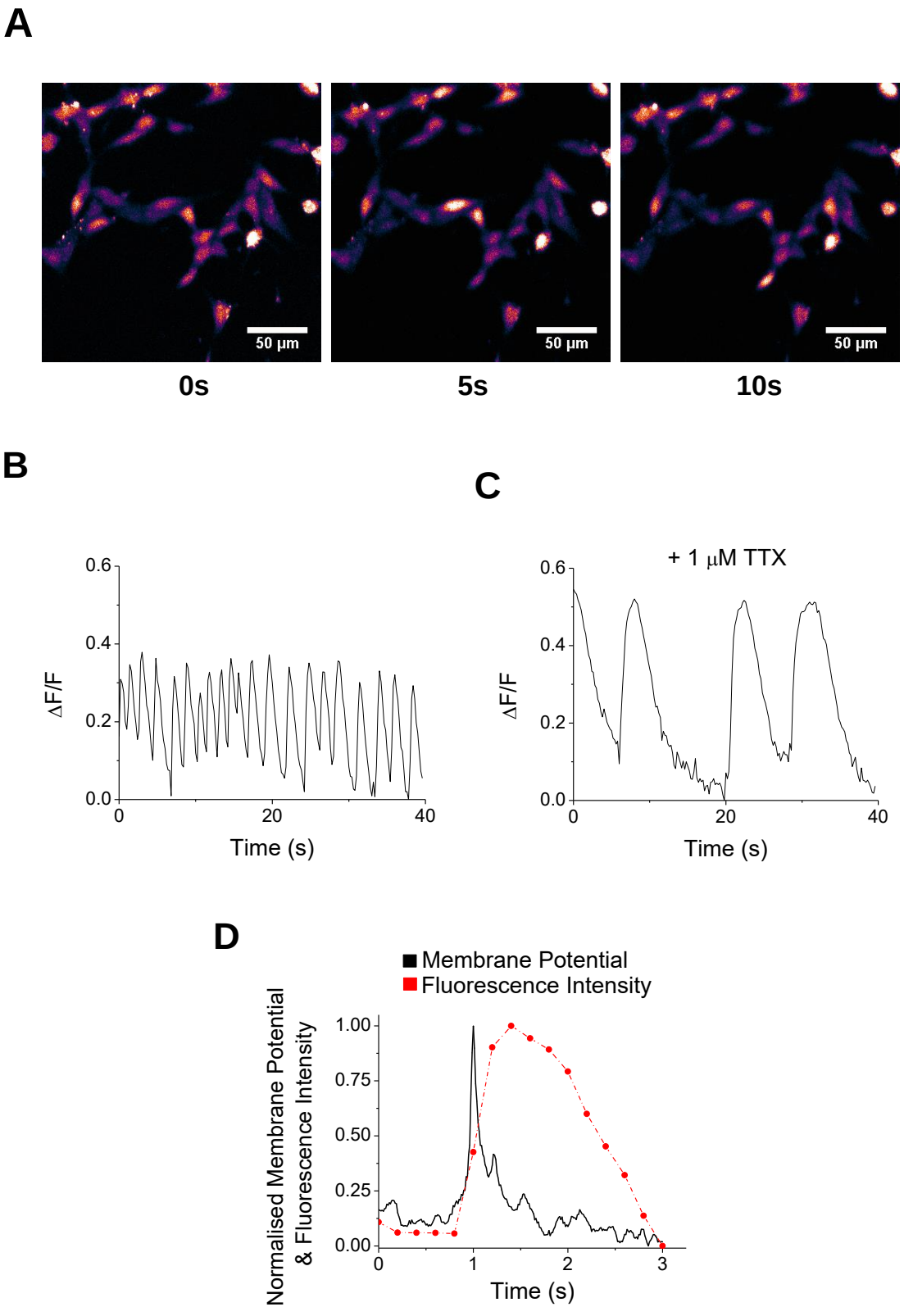

Figure 2.7 - Intracellular Ca^{2+} waves in AtT20s. (A) Representative fluorescence images from an AtT20 cell loaded with Calcium Green-1 that is producing a $Ca2^{+}$ wave. Representative bleach corrected ΔF/F traces from separate cells (B) before and (C) after the addition of 1µM TTX. (D) Graph showing the average shape and onset time of membrane potential changes and Ca^{2+} waves after Calcium Green-1 loading (n=6).

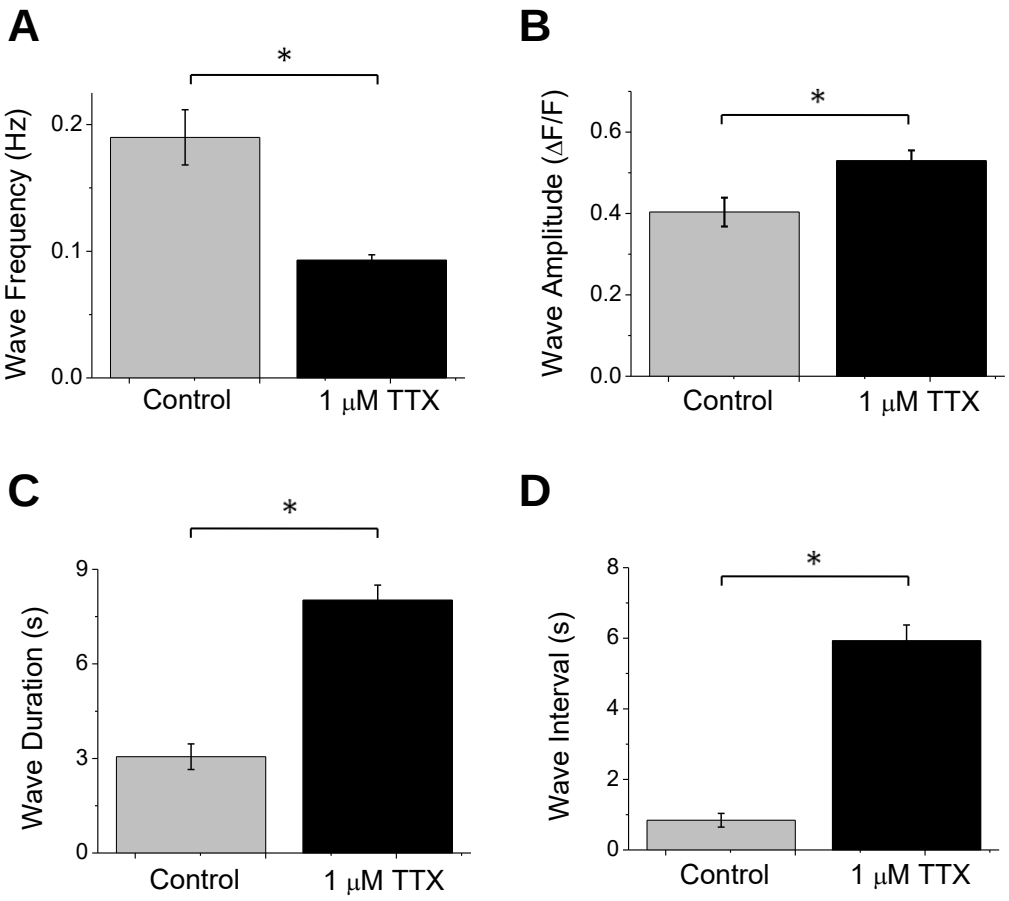

Figure 2.8 - The effect of TTX on Ca^{2+} waves - I. Graphs from AtT20 cells loaded with Calcium Green-1 showing means for (A) wave frequency (B) wave amplitude (C) wave duration and (D) the mean interval between waves before and after the addition of 1 μM TTX (n=3 for all conditions). Error bars ± S.E.M. *indicates statistical significance using two-way Student's t-tests at p=0.05.

.

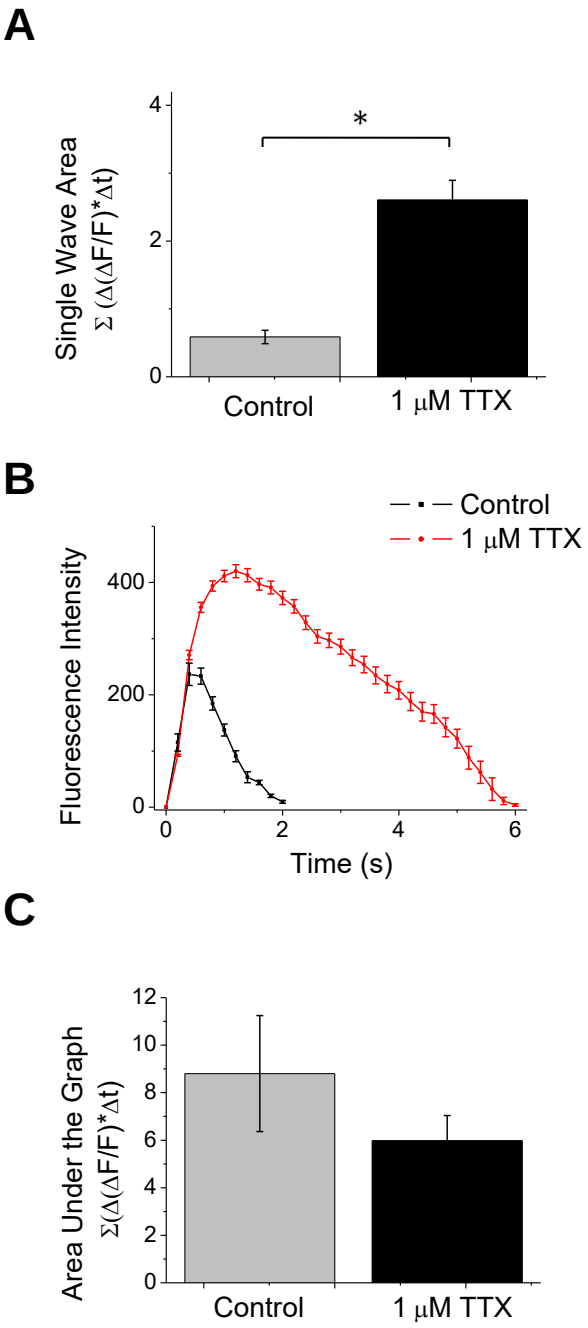

Figure 2.9 - The effect of TTX on Ca^{2+} waves - II. Graphs from AtT20 cells loaded with Calcium Green-1 showing (A) the mean area under individual Ca^{2+} waves (n=3) (B) the average wave shape from 1 experiment (50 cells from 1 repeat) and (C) the mean total area under the graph before and after the addition of 1 μM TTX (n=3). Error bars ± S.E.M. *indicates statistical significance two-way Student's t-tests at p=0.05.

2.3.2 The Role of L-, N- & T-type Channels in AtT20 Pacemaking

2.3.2.1 The Role of L-type Channels

To determine the role of L-type VGCCs in pacemaking, an L-type agonist and antagonist were applied to cells during whole cell current clamp recording. Addition of 10 μM of the L-type antagonist nifedipine caused a membrane hyperpolarisation that was found to not be statistically different from controls (Paired t-test, p=0.29) and caused action potential firing to cease in all cells tested (n=4) (**Figure 2.10A)**. Addition of 1 mM of the L-type agonist Bay K8644 caused an equal and opposite effect. A 17.5 ± 2.8 mV depolarisation of the membrane occurred that was statistically significant from controls (Paired t-test, p=0.024) and action potential firing ceased in all cells (n=3) (**Figure 2.10C**).

To determine whether Na_V and K_V currents were affected by the addition of the drug, positive voltage steps from a -80 mV holding potential were applied under whole cell voltage clamp. The addition of 10 μM nifedipine caused no change in Na_V current but caused a reduction in K_V current (n=4) (**Figure 2.10B**). No effect on the I/V relationships of Na_V or K_V channels was found upon the addition of 1 mM Bay K8644 (n=3) (**Figure 2.10D**).

To determine whether L-type VGCCs were driving Ca^{2+} waves, AtT20 cells were exposed to nifedipine after Calcium Green-1 loading. Addition of 10 μM nifedipine blocked Ca^{2+} waves observed during 40 second fluorescence intensity recordings in all cells tested (**Figure 2.11A, 2.11B**) and drastically reduced the mean total area under the graph (Student's t-test, p<0.001) (n=3) (**Figure 2.11C**).

The L-type subtype $Ca_V1.3$ is often expressed in pacemaker cell types. To determine whether these channels are present in AtT20s, cells were stained using an anti-$Ca_V1.3$ primary antibody (n=3). Fluorescence was identified in all AtT20 cells in culture, indicating the presence of $Ca_V1.3$ (**Figure 2.11D**). To ensure the observed fluorescence was not due to non-specific staining of either the primary or secondary antibody, controls were performed with the primary antibody only, secondary antibody only and with both antibodies + an antigen against $Ca_V1.3$. No staining was observed in any of the controls (**Supplementary 2.2**).

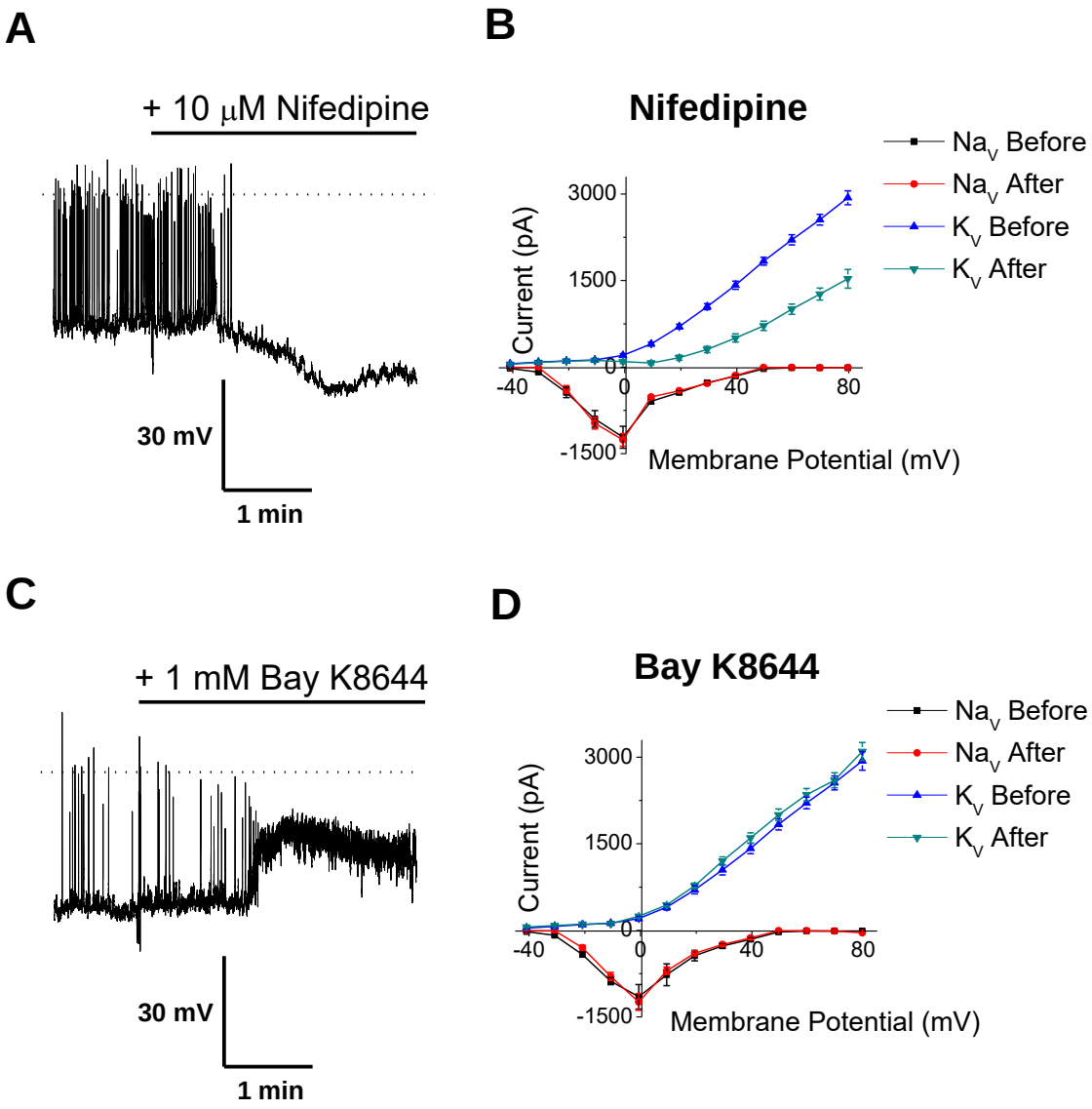

Figure 2.10 - The effect of nifedipine and Bay K8644 on pacemaking. Representative whole cell current clamp recordings showing (A) the addition of 10 μM nifedipine and (C) the addition of 1 mM Bay K8644. Mean I/V relationships for Na_V and K_V currents before and after the addition of (B) 10 μM nifedipine (n=4) and (C) 1 mM BayK8644 (n=3) Error bars ± S.E.M.

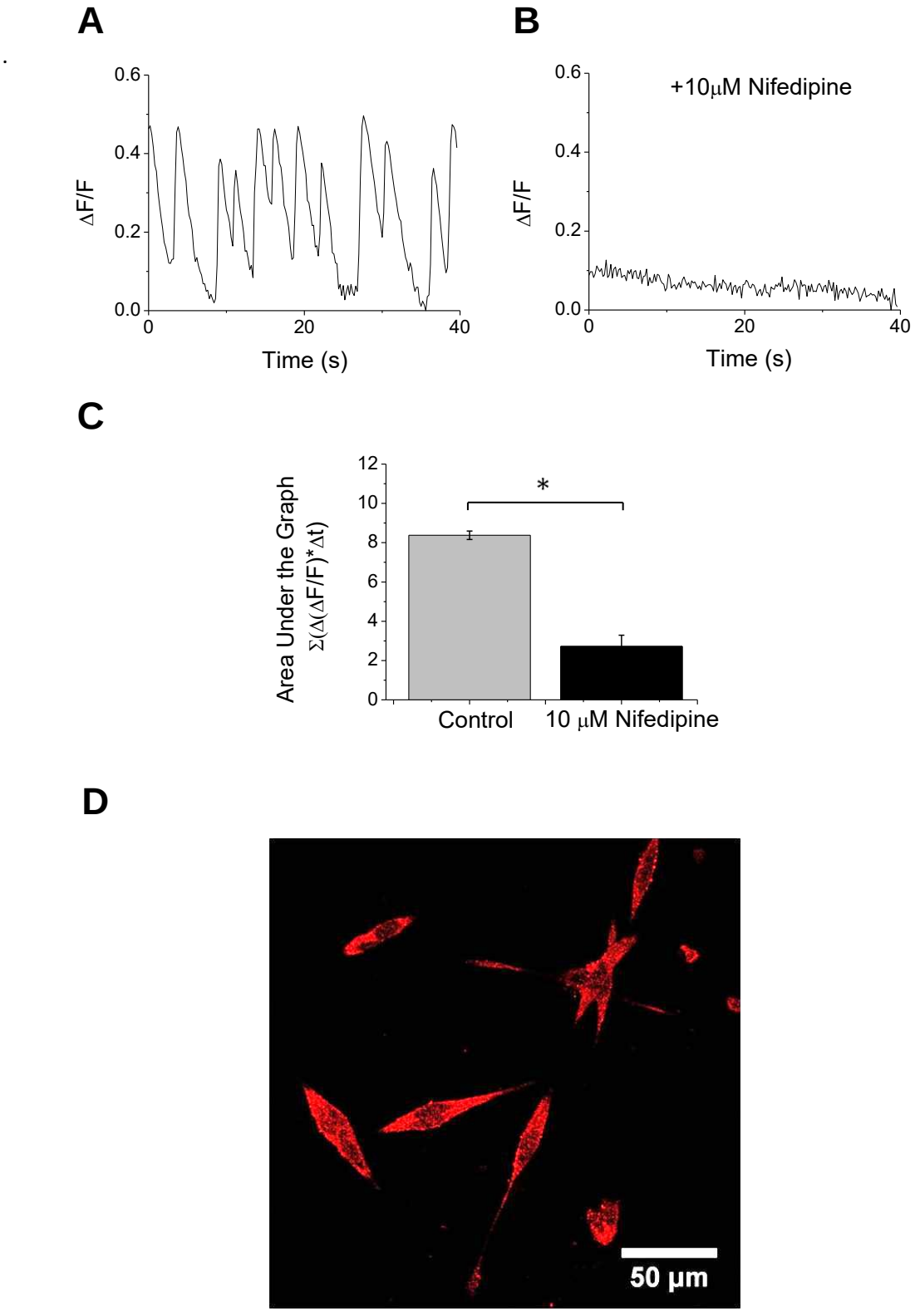

Figure 2.11 - Ca^{2+} waves are L-type dependent. Representative bleach corrected ΔF/F traces from AtT20 cells loaded with Calcium Green-1 showing Ca^{2+} waves in separate cells (A) before and (B) after the addition of 10 μM nifedipine. (C) The mean total area under the graph from bleach corrected fluorescence traces before and after the addition of 10 μM nifedipine (n=3). (D) Representative confocal image of AtT20 cells antibody stained against the L-type VGCC subtype $Ca_V1.3$. Error bars ± S.E.M. *indicates statistical significance using a two-way Students t-test at p=0.05.

2.3.2.2 The Role of N-Type Channels

The N-type selective VGCC antagonist ω-conotoxin GVIA was applied to AtT20 cells under whole cell current clamp to determine the role of N-type VGCCs in pacemaking (n=3) (**Figure 2.12A**). Addition of 1 µM of the drug caused no change in resting membrane potential (Paired t-test, p=0.997) or firing rate (Paired t-test, p=0.371) (**Figure 2.12B**). To determine the effect of ω-conotoxin GVIA on Na_V and K_V currents, positive voltage steps from a -80 mV holding potential were applied under whole cell voltage clamp**.** No effects on Na_V or K_V current density or I/V relationships were identified when compared to controls before the addition of the drug (n=3) (**Figure 2.12C, 2.12D**). **Figure 2.12E** and **2.12F** show example whole cell voltage clamp recordings from a -80mV holding potential before (in the presence of 10 µM nifedipine, 1 µM TTX and 120 mM Cs-gluconate) and after the addition of 1 µM ω-conotoxin GVIA, demonstrating the presence of an N-type current.

To determine the role of N-type channels in the generation of Ca^{2+} waves, AtT20 cells were loaded with Calcium Green-1. Waves continued in the presence of 1 µM ω-conotoxin GVIA (**Figure 2.13A, 2.13B**) with no statistical difference in mean frequency (p=0.109) (**Figure 2.13C**), amplitude (p=0.681) (**Figure 2.13D**), duration (p=0.587) (**Figure 2.13E**) or inter-wave interval (p=0.408) (**Figure 2.13F**) when tested using a two-way Student's t-test (n=3).

The area under individual Ca^{2+} waves upon the addition of 1 µM ω-conotoxin GVIA was not statistically different from controls before the addition of the drug (n=3) (Student's t-test, p=0.756) (**Figure 2.14A**), though a slight change in the average wave shape did appear to occur (n=50 cells from 1 repeat), which may be due to the slight differences in wave amplitude (**Figure 2.14B**). There was also no statistical difference in the mean total area under the graph when compared to controls before the addition of the drug (Student's t-test, p=0.97) (n=3) (**Figure 2.14C**).

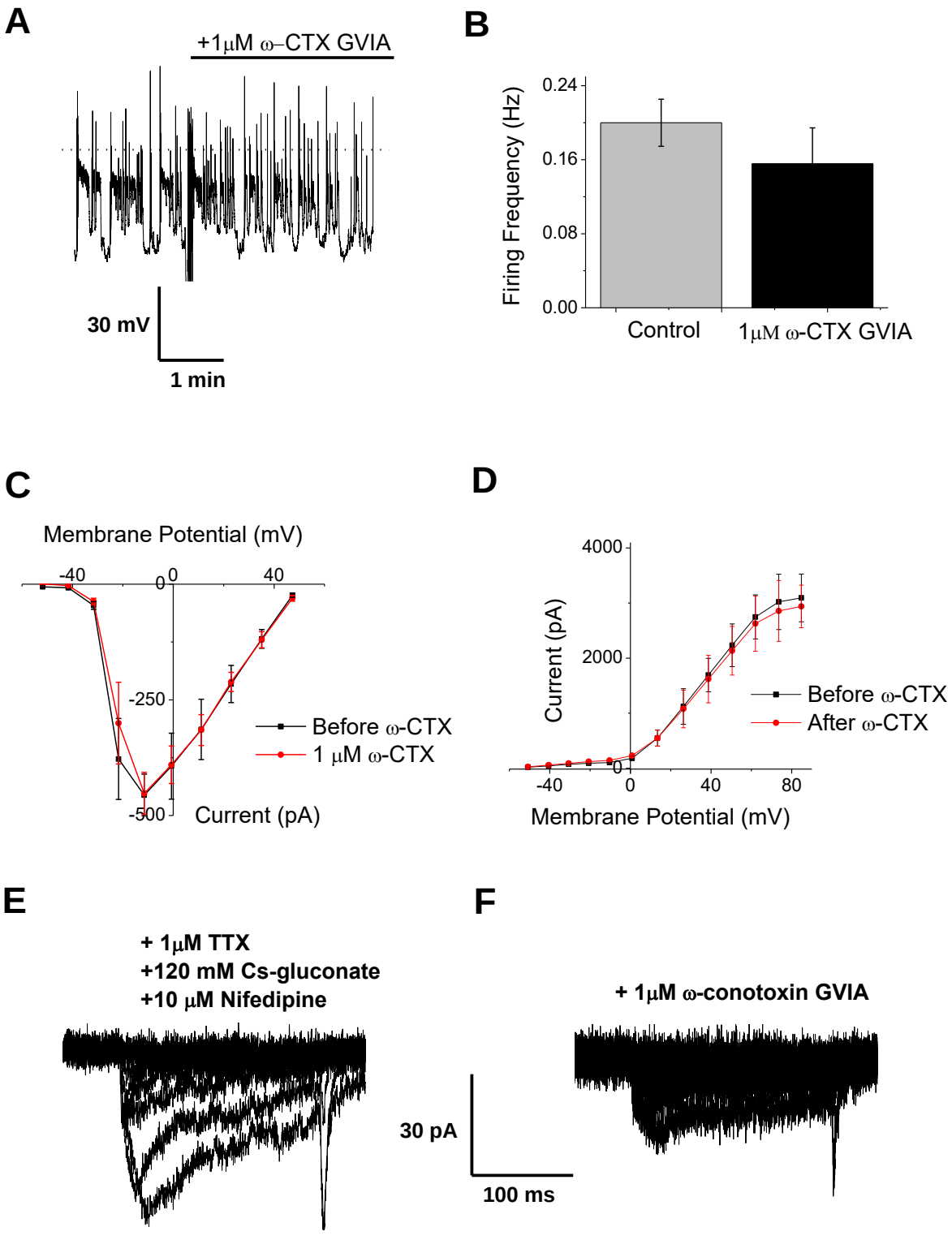

Figure 2.12 - The effect of ω-conotoxin GVIA on pacemaking. (A) Representative whole cell current clamp recording showing the addition of 1 μM ω-conotoxin GVIA. The dotted line indicates 0 mV. (B) Graph showing the mean firing frequency from cells before and after the addition of the drug (n=3). Mean I/V relationships for (C) Na_V currents and (D) K_V currents before and after addition of the drug (n=3). Representative whole cell voltage clamp recordings from a -80 mV holding potential showing the same cell (E) before and (F) after the addition of ω-conotoxin GVIA. Error bars ± S.E.M.

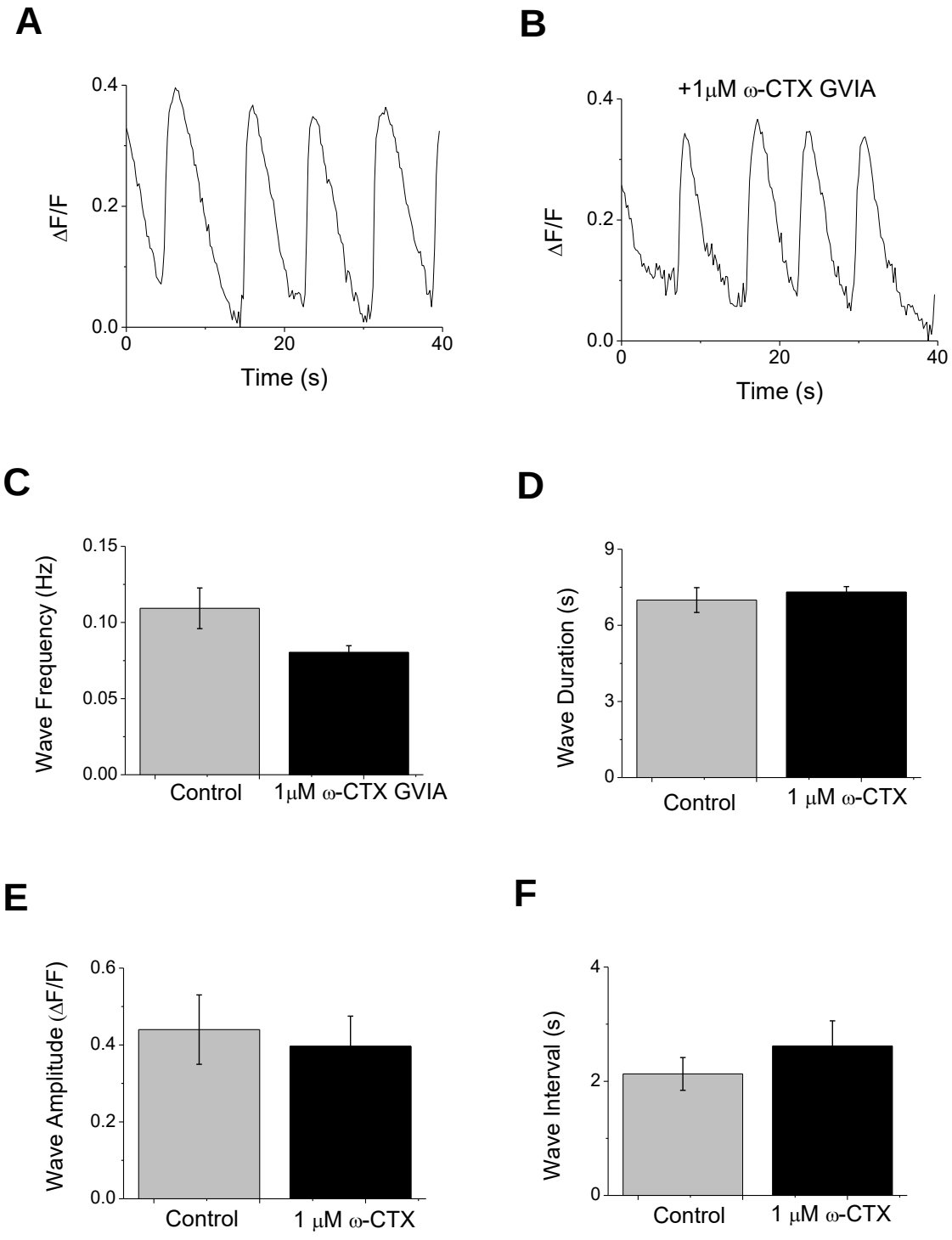

Figure 2.13 - The effect of ω-conotoxin GVIA on Ca^{2+} waves - I. Representative bleach-corrected ΔF/F traces from AtT20 cells after Calcium Green-1 loading (A) before and (B) after the addition of 1 μM ω-conotoxin GVIA (n=3). Graphs showing mean values for (C) wave frequency (D) wave duration (E) wave amplitude and (F) interval between waves before and after the addition of the drug (n=3 repeats). Error bars ± S.E.M.

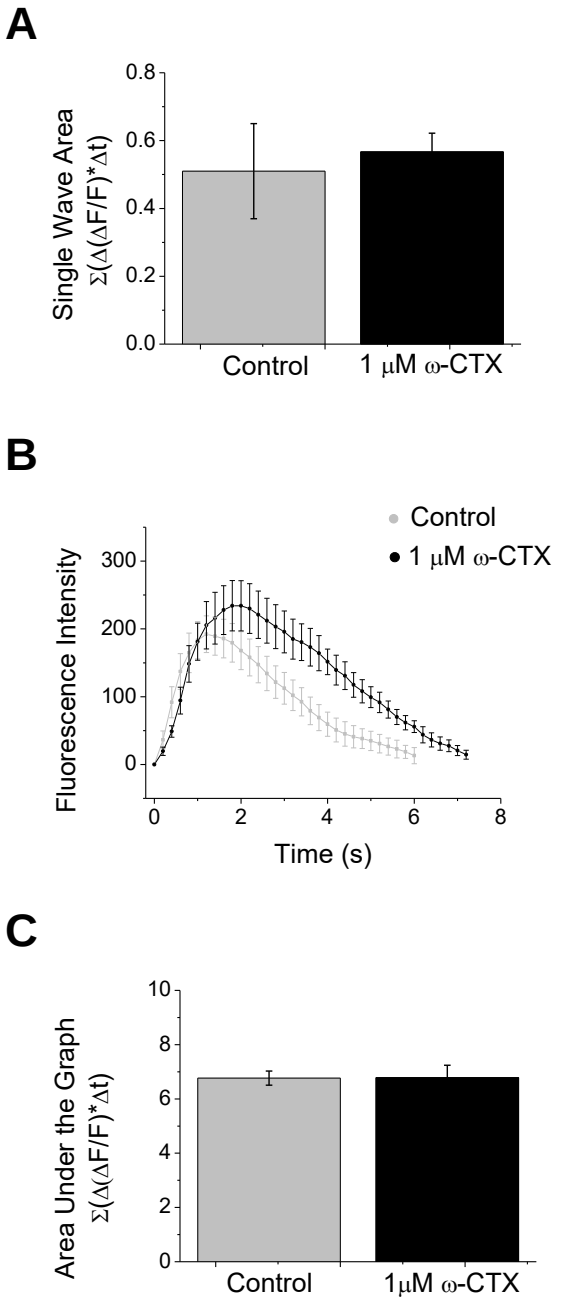

Figure 2.14 - The effect of ω-conotoxin GVIA on Ca^{2+} waves - II. Graphs from AtT20 cells loaded with Calcium Green-1 before and after the addition of 1 μM ω-conotoxin GVIA showing (A) the mean area under individual Ca^{2+} waves (n=3) (B) the average wave shape before and after addition of the drug (n=50 cells from 1 repeat) and (C) the mean total area under the graph (n=3). Error bars ± S.E.M.

2.3.2.3 The Role of T-Type Channels

The T-type antagonist ML218 was added during whole cell current clamp recording to determine the role of T-type VGCCs in AtT20 pacemaking (n=4). All action potential firing ceased within 2-3 minutes of the addition of 1 μM ML218 (**Figure 2.15A**). No effect on membrane potential was observed when compared to controls before the addition of the drug (Paired t-test, p=0.921).

To determine any effect of ML218 on Na_V and K_V currents, positive voltage steps from a -80 mV holding potential were applied under whole cell voltage clamp (n=4). No change in the I/V relationship was seen for Na_V or K_V currents after the addition of the drug. (**Figure 2.15B, 2.15C**).

As T-type currents have not previously been identified in AtT20s, attempts were made to isolate this current. Na_V and K_V currents were blocked with TTX (1 μM) and Cs-gluconate (120 mM in the intracellular solution) respectively. After block of L-type channels with nifedipine (10 μM) and N-type channels with ω-conotoxin GVIA (1 μM) the addition of ML218 (1 μM) caused a reduction in the remaining current, indicating the presence of T-type channels (**Figure 2.15D, 2.15E**).

To determine the role of T-type channels in the generation of Ca^{2+} waves, AtT20 cells were loaded with Calcium Green-1 AM (n=3). A shift in wave modality similar to the addition of TTX was seen upon the addition of 1 μM ML218 (**Figure 2.16A, 2.16B**). A decrease in the mean wave frequency compared to controls was observed (**Figure 2.17A**) while no clear change was observed in mean wave amplitude (**Figure 2.17B**), duration (**Figure 2.17C**) or interval between waves (**Figure 2.17D**) compared to controls before the addition of the drug.

Since blocking T-type channels prevented action potential firing it was hypothesised that block of Na_V channels would no longer have an effect on Ca^{2+} waves. Surprisingly, the co-addition of 1 μM TTX and 1 μM ML218 caused another shift in modality, with waves becoming disordered and smaller in amplitude (**Figure 2.16C**). One-way ANOVAs between controls and each drug condition showed a significant effect of drug condition on wave frequency ($F=13.391$, $p=0.006$), wave amplitude ($F=7.475$, $p=0.023$), wave duration ($F=7.578$, $p=0.023$) and time between waves ($F=8.907$, $p=0.016$). Performance of a Tukey comparison test showed a significant decrease in wave frequency between the controls and ML218 as well as controls and co-addition, but no significant difference between ML218 alone and co-addition (Control/ML218,

p=0.006; control/ML218+TTX, p=0.025; ML218/ML218+TTX, p=0.42) **(Figure 2.17A)**. Mean wave amplitude was not significantly different between controls and ML218 nor between ML218 and co-addition, but was significantly decreased between controls and co-addition (control/ML218, p=0.381; control/ML218+TTX, p=0.02; ML218/ML218+TTX, p=0.112) (**Figure 2.17B**). Mean wave duration was significantly decreased between controls and ML218 as well as controls and co-addition, but no significant difference was seen between ML218 and co-addition (controls/ML218, p=0.049; controls/ML218+TTX, p=0.026; ML218/ML218+TTX, p=0.865) (**Figure 2.17C**) Mean time between waves was not significantly different between controls and ML218, but was significantly increased between controls and co-addition and ML218 and co-addition (controls/ML218, p=0.862; controls/ML218+TTX, p=0.019; ML218/ML218+TTX, p=0.035) (**Figure 2.17D**) compared to ML218 alone was observed (n=3).

One-way ANOVAs were performed to determine the effect of drug condition on Ca^{2+} wave area. A statistically significant effect of drug condition was seen for both single wave area and mean total area under the graph (single wave area, F=4.376, p=0.015; total area, F=7.459, p=0.024). Performance of a Tukey comparison test showed that single wave area was not significantly different between controls and ML218 nor ML218 and co-addition, but was significantly decreased between controls and co-addition (controls/ML218, p=0.886; controls/ML218+TTX, p=0.06; ML218/ML218+TTX, p=0.018) (**Figure 2.18A**) (n=3). The mean total area under the graph was significantly decreased between controls and ML218, controls and co-addition and between ML218 and co-addition (controls/ML218, p=0.016; controls/ML218+TTX, p=0.002; ML218/ML218+TTX, p=0.043) (**Figure 2.18C**) (n=3). Averaging the Ca^{2+} wave shape in all conditions showed a slight decrease in amplitude in the presence of ML218 and a much larger decrease in amplitude upon the addition of both drugs (n=50 cells from 1 repeat) (**Figure 2.18B**).

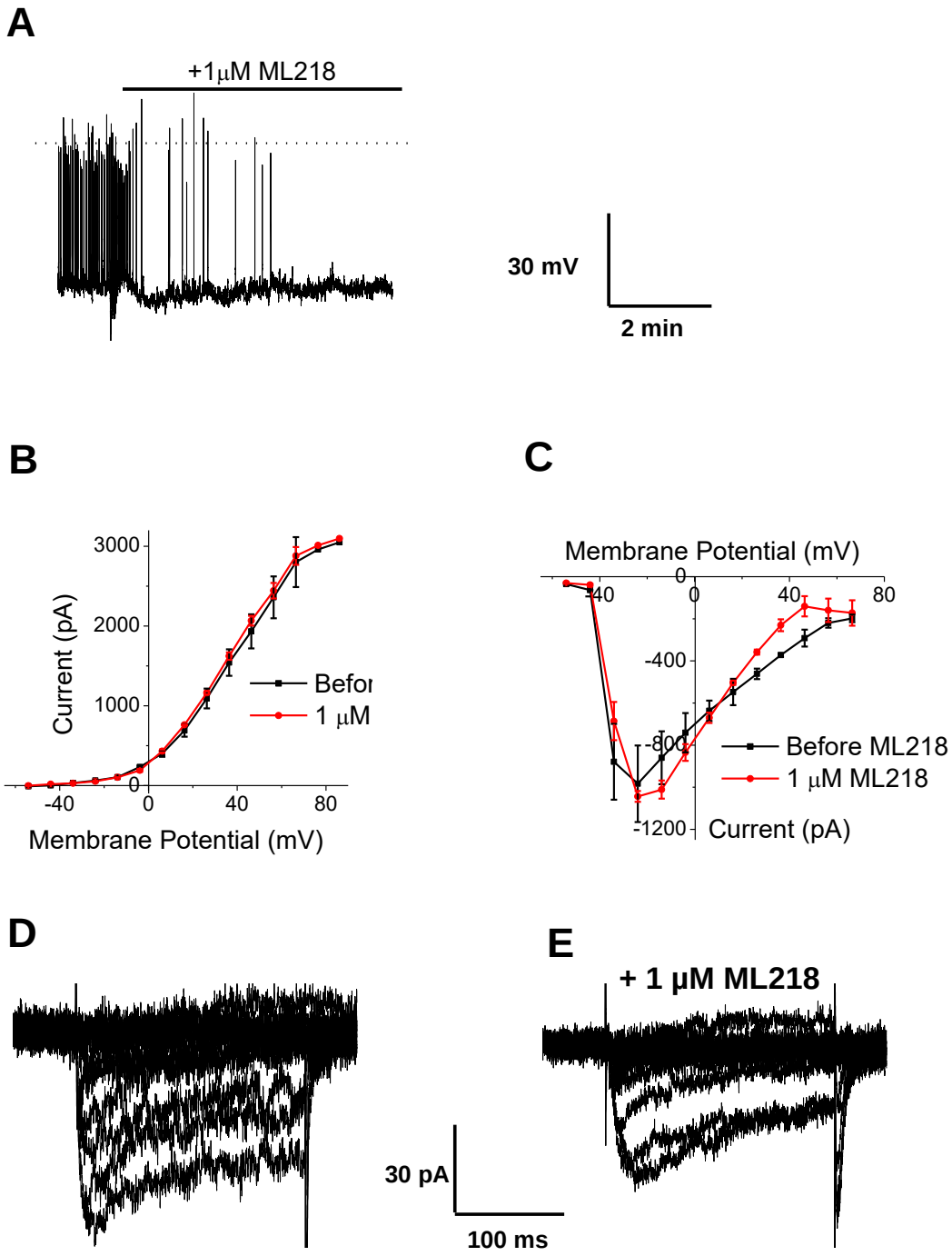

Figure 2.15 - The effect of ML218 on pacemaking. (A) Representative whole cell current clamp recording showing the cessation of pacemaking after the addition of 1 μM ML218. Dotted line indicates 0 mV. Mean I/V relationships before and after the addition of ML218 for (B) K_V currents and (C) Na_V currents (n=4). Error bars ± S.E.M. Representative whole cell voltage clamp recordings from a -80 mV holding potential showing Ca^{2+} currents from the same cell (D) before and (E) after the addition of ML218.

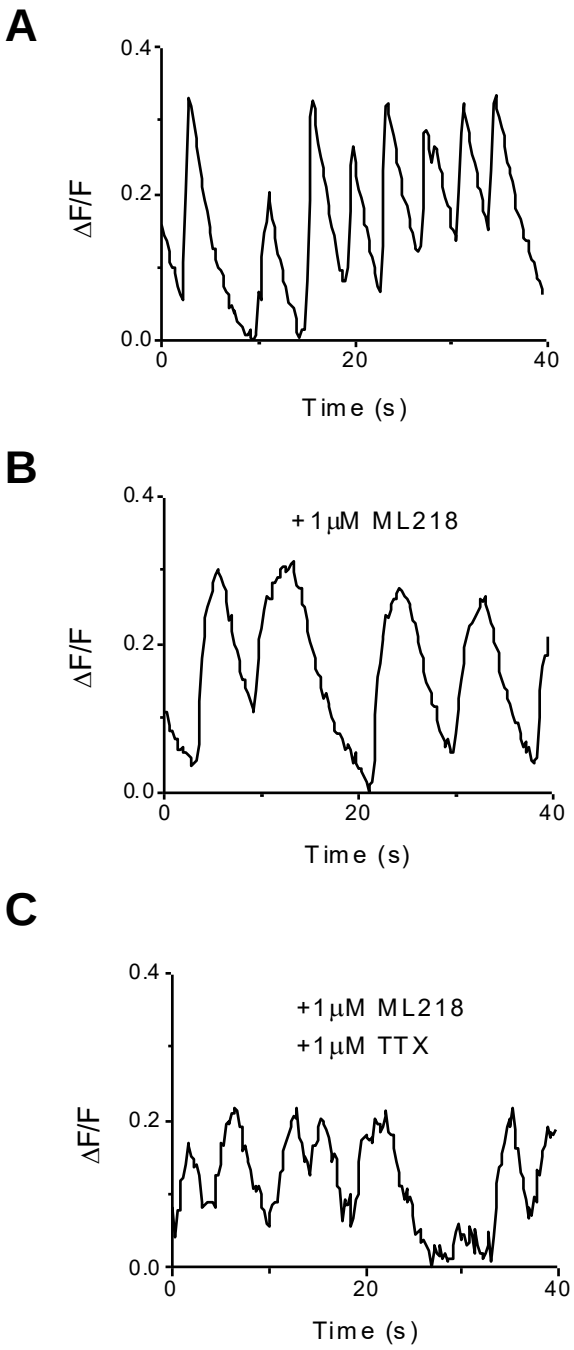

Figure 2.16 - The effect of ML218 on Ca^{2+} waves. Representative fluorescence recordings showing different cells (A) before and (B) after the addition of ML218, and (C) after the addition of ML218 and TTX.

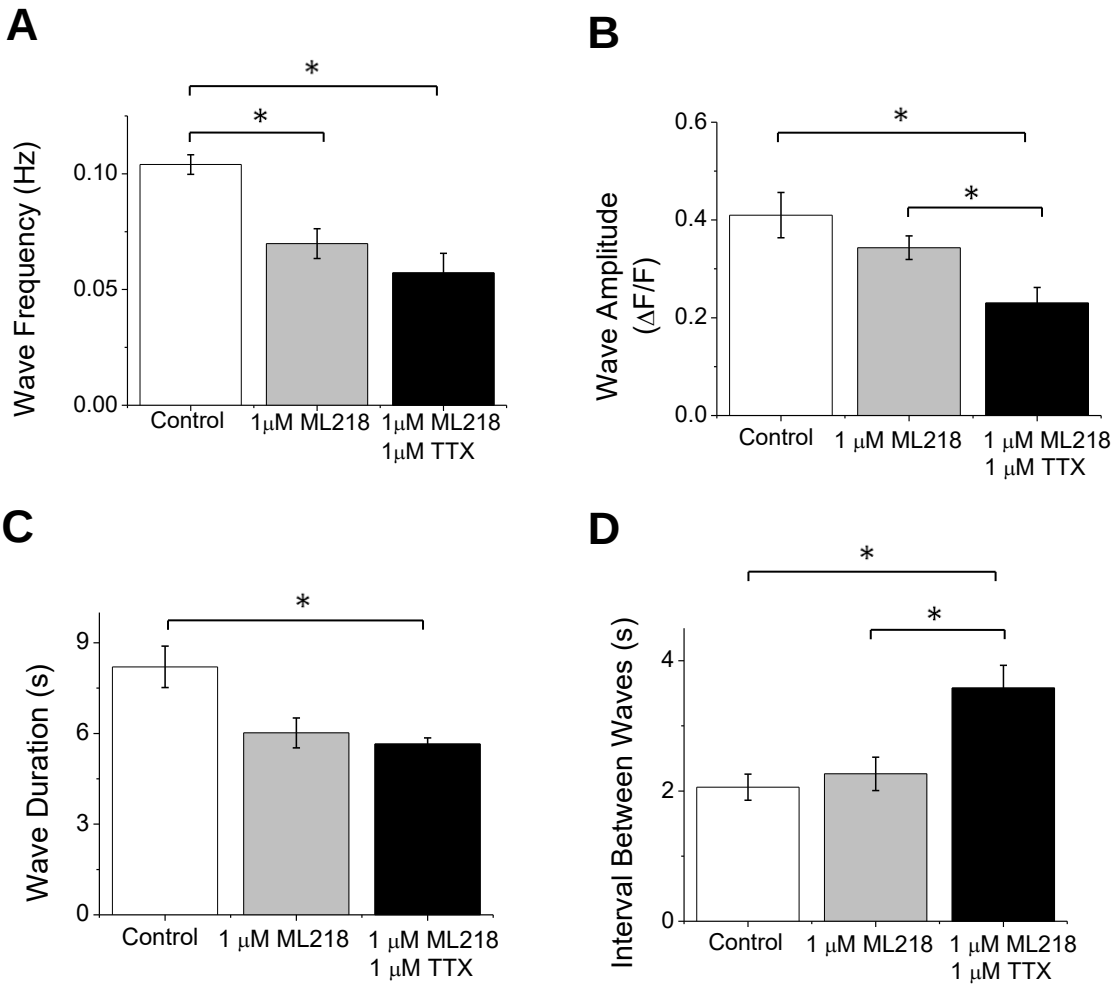

Figure 2.17 - The effect of ML218 on Ca^{2+} wave properties - I. Graphs showing mean values for (A) wave frequency (B) wave amplitude (C) wave duration and (D) interval between waves for AtT20 cells before and after the addition of ML218 alone or the co-addition of ML218 and TTX (n=3). Error bars ± S.E.M. *indicates statistical significance using a Tukey comparison test at p=0.05.

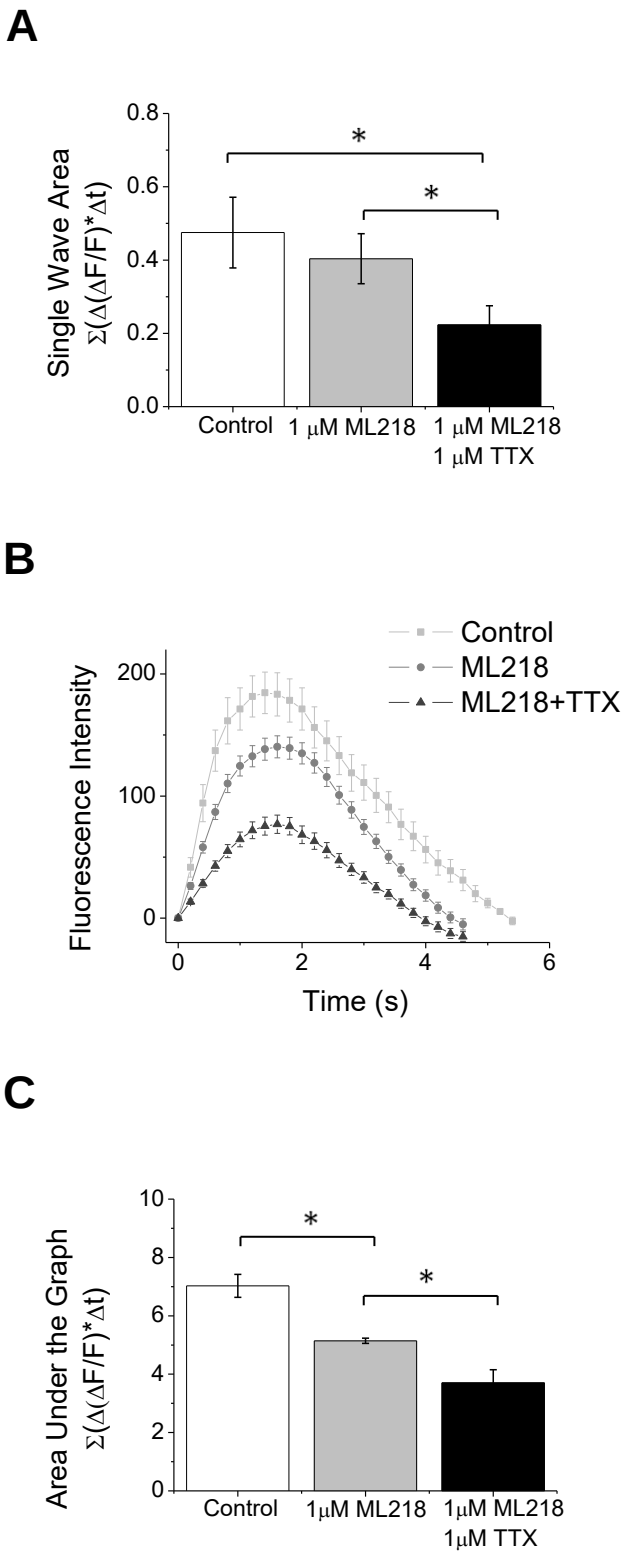

Figure 2.18 - The effect of ML218 on Ca^{2+} wave properties - II. Graphs showing (A) the mean area under individual Ca^{2+} waves (n=3) (B) the average wave shape (n=50 cells from 1 repeat) and (C) mean total area under the graph for AtT20 cells loaded with Calcium Green-1 (n=3 repeats for each condition). All graphs show cells before and after the addition of ML218 alone or the co-addition of ML218 and TTX. Error bars ± S.E.M. *indicates statistical significance using a Tukey comparison test at p=0.05.

2.4 Discussion

The experiments described here examined the role of various VGCC subtypes in generating pacemaking in AtT20 anterior pituitary corticotrophs. Through the data presented, I show that many AtT20s displayed spontaneous action potentials which were TTX and nifedipine sensitive, as has been previously described in the literature (Adler et al., 1983). The ACTH secretagogue CRH did not cause membrane potential changes, unlike the changes seen in corticotrophs *in-vivo*. This supports previous evidence suggesting that secretion is uncoupled from electrical activity in AtT20s (Surprenant, 1982). This is backed here by capacitance recordings which suggest that secretion is instead instigated by a general increase in intracellular Ca^{2+}.

Here I show that rhythmic increases in the cytoplasmic Ca^{2+} concentration, termed "Ca^{2+} waves," underlie pacemaking. Previous literature has suggested that these waves were not affected by the addition of TTX, hence the waves are action potential independent and occur below the threshold for firing (Fiekers & Konopka, 1996). My data dispute this, with TTX causing a shift in wave properties, increasing their amplitude and duration while decreasing their frequency. The finding that both modalities were nifedipine sensitive confirms previous studies that suggest pacemaking is L-type channel dependent.

Both N-type and T-type VGCCs were identified here in whole cell voltage clamp experiments. N-type and P/Q-type channels have previously been identified using a similar approach (Mackie et al., 1995), though the presence of T-type channels had only been suggested through simulations (LeBeau et al., 1997). Whether or not these subtypes are involved in AtT20 pacemaking had not been investigated. Here I identify a novel role for T-type VGCCs in AtT20 pacemaking, with them being critical for the generation of action potentials. Considering the voltage-activation properties of T-type channels are shifted towards hyperpolarised potentials, similar to $Ca_V1.3$ they are ideal for subthreshold activation (Perez-Reyes et al., 1998). Although T-type channels are not instigating Ca^{2+} waves in AtT20s (as block of L-type VGCCs completely eliminates them) they nevertheless have a small but critical role in their shaping as seen by the changes in wave shape and area upon the addition of ML218. In AtT20s these channels are likely opening close to the firing threshold, providing enough of a change in membrane potential to allow Na_V channel activation. In support, they have been identified in corticotrophs *in-vivo* and in other pacemaking cell types performing just this purpose (Guérineau et al., 1991; Matschke et al., 2015). A role for Na_V channels in

the subthreshold shaping of Ca^{2+} waves was also identified, as seen by the change in mean total area under the graph upon the co-addition of ML218 and TTX. N-type channels appeared to play no role in pacemaking. This subtype is rarely seen to contribute to pacemaking in other cell types and is most often associated with the process of exocytosis in neuronal cell types (Lévêque et al., 1994).

2.4.1 Characterisation of AtT20 Pacemaking

2.4.1.1 Confirmation of an AtT20 Phenotype

Before detailed characterisation of pacemaking could occur it was important to validate that the cell line being used displayed the correct phenotype. Antibody staining for ACTH was selected to determine this as corticotrophs (and AtT20's) are characterised by its expression. AtT20s have previously been shown to stain for ACTH at their poles and in the cell body near the start of processes (Baldini et al., 1998). The same observation was made here, indicating cells of the same phenotype. STED microscopy provided the resolution to see individual puncta, which were likely to be ACTH-containing secretory granules. This can be taken as an indicator that the cells are functional, as the production of ACTH along with the packaging, transportation and docking of a readily releasable pool of secretory granules requires a range of cellular processes to be in order.

Granule diameter appeared to be distributed into two main peaks at 80-100 nm and 160-180 nm. This could indicate the presence of two populations of "small" and "large" granules. Corticotrophs are known to contain large, dense-core granules that contain ACTH (Kurosumi et al., 1966). Pituitary cells also secrete other molecules such as beta-endorphin and beta-lipotropin (Gumbiner & Kelly, 1981). The granule sizes identified here may therefore represent different secretory cargoes. Another explanation for the peak at 80-100 nm is that vesicles below the STED diffraction limit (which is 30-50 nm in theory though is often higher in practice) are being diffraction-limited to a size of 80 nm, hence artificially inflating the number of 80-100 nm granules. No previous literature has demonstrated secretory granules in this cell type at STED resolution. Previous studies using electron microscopy have stated the presence of large, dense core secretory granules ranging in size from 500-1000 nm in primary corticotrophs

(Kurosumi & Kobayashi, 1996). The results here therefore provide new information on the size, number and location of secretory granules in AtT20s.

2.4.1.2 Firing Properties of AtT20s

Two modalities of AtT20 pacemaking, tonic firing and burst firing, have been previously described in the literature (Adler et al., 1983). The results here confirm that finding. These different modalities could also be identified by their resting potential, with quiescent cells having a more depolarised membrane than tonic cells and bursting cells having a more hyperpolarised membrane than tonic cells. Hyperpolarising quiescent cells could often induce firing, though tonic cells could not be made to burst fire. This indicates that membrane potential isn't the only determinant of firing modality. Complex variations in ion channel expression are a likely explanation, which is backed by computer-based models of excitability (LeBeau et al., 1997). The resting potentials described here are somewhat lower than those described in the literature, which has stated a resting potential of -55 mV. Bursting cells described here had a resting potential close to this at -47 mV. These discrepancies could be due to cell-cell variability, differences in temperature or differences in liquid junction potentials.

A previous study observed CRH-induced changes in membrane potential and firing rate in AtT20s (Zemkova et al., 2016). Here I found that CRH had no effect on pacemaking. It is worth noting that CRH has both long and short term effects in primary corticotrophs, stimulating the release and production of ACTH over minutes to hours. The 10 minute recording period used here may not have been enough to determine long term effects. A disconnect between excitability and hormone secretion in AtT20s has also been described in the literature, perhaps explaining the lack of effect of CRH (Surprenant, 1982). Capacitance recording was used to attempt to determine whether secretion of ACTH is coupled to electrical activity. Capacitance is a measure of membrane surface area, with membrane having a specific capacitance of between 0.8 and 1 $\mu F/cm^2$ (Gentet et al., 2000). Fusion of a number of small secretory granules can therefore be detected as an increase in capacitance. No capacitance changes were observed here in response to membrane depolarisation indicating that secretion is likely disconnected from electrical activity. BayK 8644, a VGCC agonist, did induce a change in capacitance. This has previously been reported in the literature (Heisler, 1985) and

indicates that secretion is likely coupled to the intracellular Ca^{2+} concentration rather than directly to pacemaking.

2.4.1.3 Voltage-Gated Ionic Currents in AtT20s

Here I show the presence of TTX-sensitive Na_V and TEA-sensitive K_V currents that underlie pacemaking. Various subtypes of VGCCs were also identified, such as L-type, N-type channels. These are of the same proportions of the total current to those seen in a similar study using channel antagonists (Mackie et al., 1995). A small T-type current was also identified in AtT20s, which although identified in primary corticotrophs has previously only been suggested through computer-based modelling (LeBeau et al., 1997; Matschke et al., 2015).

When determining the presence of VGCC subtypes it was important to take into account the selectivity of channel antagonists for other subtypes. ω-conotoxin GVIA for example, apart from selectivity for N-type channels, has a moderate selectivity for L-type channels (Mcleskey et al., 1987) and some T-type antagonists can have effects on Na_V channels (Strege et al., 2005). The concentrations of the antagonists used and the order they were applied were carefully selected in an attempt to minimise non-specific channel block, though its occurrence should not be discounted. K_V, Na_V and VGCC I/V relationships are shown in many figures in an to attempt to show transparency over this potential issue.

Two holding potentials were used in **Figure 2.5C** as further confirmation that the correct channel types were being blocked. N-type and T-type channels are activated from lower holding potentials than L-type channels (Nowycky et al., 1985; Perez-Reyes et al., 1998). Hence it was hypothesised that ω-conotoxin GVIA and ML218 should block a larger proportion of the current at -80 mV than at -60 mV, an effect that was observed in the results.

2.4.1.4 Calcium Spiking in AtT20s

Here I show that AtT20s exhibited high frequency spikes in their cytoplasmic Ca^{2+} concentration that decreased in frequency but increased in amplitude and duration upon the addition of TTX. This likely indicates that Ca^{2+} waves are entrained by the rate of action potential firing. This hypothesis is strengthened by simultaneous cell attached

recording and fluorescence imaging that showed the peak fluorescence intensity after loading with Calcium Green-1 started at the onset of a membrane potential spike and lasted for several seconds afterwards. This contradicts a previous study that showed TTX having no effect on Ca^{2+} waves (Fiekers & Konopka, 1996). The response time of the fluorescent dye could provide inaccuracies in this result. Calcium Green-1 has a relatively high affinity with a K_D of 190 nM (Thomas et al., 2000), indicating a relatively fast response time in the 10's of milliseconds at 37^{o}C. However the experiments here were performed at 21^{o}C. The expected response time would therefore be expected to increase. This, along with the 200 ms frame rate used, means this result should be looked at with caution as with a delay in fluorescence peak of 330 ms it may lie within the combined response time of the dye and frame rate in the conditions used. Given these potential errors it still seems unlikely that Ca^{2+} waves are occurring a long time before an action potential. What is more likely is that the peaks in membrane potential and fluorescence intensity lie in much closer proximity than has been identified here, with Ca^{2+} waves occurring simultaneously with or slightly after/before an action potential.

The fact that Ca^{2+} waves continued in the presence of TTX and were blocked by nifedipine indicates that rhythmic L-type waves underlie action potential firing. These are likely to be driving rhythmic firing as indicated by the block of pacemaking upon the addition of nifedipine.

Although Calcium Green-1 is not a ratiometric dye and cannot be used to determine an exact concentration, its fluorescence increases relatively linearly with Ca^{2+} binding at biological concentrations (Thomas et al., 2000). Hence by calculating the area under the graph any changes in the total influx of Ca^{2+} through VGCCs can be approximated. The surprising lack of change in the total area under the graph upon the addition of TTX despite a drop in wave frequency can be explained by a compensatory increase in single wave area, amplitude and duration. The reason for this change is likely related to the uncoupling of Ca^{2+} entry from action potential firing. The membrane hyperpolarisation caused by opening of K_V channels during an action potential would normally act to inactivate VGCCs, providing a tight window for Ca^{2+} influx. As this no longer occurs in the presence of TTX it means that Ca^{2+} influx is no longer restricted to entry during this window. This could lead to longer duration Ca^{2+} influx. It could also perhaps lead to Ca^{2+}-dependent Ca^{2+} release from intracellular stores, further increasing the size of intracellular Ca^{2+} waves. Ryanodine receptors have been implicated in secretion in

AtT20s, providing some evidence for this possibility (Yamamori et al., 2004). Block of VGCCs has previously been shown to reduce AtT20 viability in culture, suggesting that Ca^{2+} influx through these channels is important for cell survival (Loechner et al., 2009). Data here suggests the reason for this, where VGCCs are involved in a feedback mechanism that retains Ca^{2+} influx at a set physiological level despite changes in cell excitability. Considering that L-type VGCCs are the predominant component of the Ca^{2+} current in AtT20s and block of this channel type prevents all Ca^{2+} waves it is likely that these channels play a major role in this mechanism.

2.4.2 The Role of L-, N- & T-type Channels in AtT20 Pacemaking

2.4.2.1 The Role of L-type Channels

Data here shows that L-type VGCCs are critical for pacemaking, with their block completely abolishing all action potentials and Ca^{2+} waves. They are also involved in the maintenance of the resting membrane potential, shown through the corroborating effects of nifedipine (hyperpolarisation) and Bay K8644 (depolarisation). This could either be through low-level, persistent activation of L-type channels keeping the Ca^{2+} equilibrium at a point that results in a more depolarised membrane potential; or through an indirect effect on the activity of Ca^{2+}-activated K^+ channels. K^+ channels are known to be involved in maintaining the resting membrane potential in the majority of, if not all, excitable cells (Peterson & Maruyama, 1984) and Ca^{2+} dependent K^+ channels have previously been identified in corticotrophs and AtT20s (Adler et al., 1983; Duncan et al., 2015). A reduction in K_V current was noticed upon the addition of nifedipine, providing some evidence for an effect on Ca^{2+}-dependent K^+ channels. L-type channels have a major effect on total Ca^{2+} influx as seen via the area under the graph of the fluorescence traces. A decreased concentration of cytoplasmic Ca^{2+} could be reducing K^+ channel activity, resulting in membrane hyperpolarisation. However, nifedipine is also known to block K^+ channels, such as K_V and inwardly rectifying K^+ channels, with one study citing an effect at ~40 µM (Li et al., 2015). Whether the concentration used here, 10 µM, is high enough to affect K^+ channels is not known and may be difficult to separate from effects on Ca^{2+} activated K^+ channels. The membrane depolarisation seen upon the addition of Bay K8644 provides some evidence for the effect of nifedipine being due to an effect of Ca^{2+} channels as opposed to direct block of K^+ channels.

L-type channels in cardiac cells have been seen to display a 'window current' between -30 and 0 mV, i.e. voltages at which channels open but do not inactivate completely, therefore providing a constant current. This is suggested to be important for maintaining intracellular Ca^{2+} levels (Hirano et al., 1992). This could provide an explanation for their ability to generate Ca^{2+} waves in AtT20's, with a proportion of channels always in an activated state, driving subthreshold membrane potential changes to generate rhythmic electrical activity.

The expression of $Ca_V1.3$ in these cells has previously been seen in culture (Loechner et al., 2009). This subtype is considered ideal for pacemaking due to their activation occurring at potentials that are more hyperpolarised than other L-type VGCCs, making them ideal for subthreshold activation. They are found in other pacemaker cells, perhaps indicating a conserved feature across many pacemaker types.

2.4.2.2 The Role of N-type Channels

N-type channels had no statistically significant effects on action potential frequency, membrane potential or Ca^{2+} wave dynamics in the experiments performed here. This could be due to the relatively small proportion of the current density that they represent (13.99%). It also suggests that no coupling between N-type VGCCs and BK channels is occurring as has been identified in other cell types (Loane et al., 2007), as no effect on K_V current was observed. At this point the role of N-type channels in AtT20s is unknown. N-type channels have important roles in exocytosis in other neuronal cell types (Millán & Sánchez-Prieto, 2002), a possibility that could also be explored here. Performing capacitance measurements in combination with N-type antagonists would determine whether N-type VGCCs are involved in secretion in AtT20s.

2.4.2.3 The Role of T-type Channels

A role for T-type channels in pacemaking had previously been suggested in the literature (LeBeau et al., 1997) but had not been experimentally proven. Here I present direct evidence of a role for T-type channels in excitability in AtT20s. T-type channels have been observed to drive firing in corticotrophs *in-vivo* and in other cell types such as thalamic reticular neurons (Guérineau et al., 1991; Huguenard & Prince, 1992). The T-type specific antagonist ML218 prevented action potential firing without affecting the

membrane potential. T-type channels have different activation properties than the other subtypes described here, being fast activating/inactivating and having an opening probability shifted more towards hyperpolarised membrane potentials (Perez-Reyes et al., 1997). It is possible, but seems unlikely, that T-type channels are required for the generation of action potentials. What is more likely is that they simply enhance and shape Ca^{2+} waves when close to the threshold for firing. This, either by providing a larger depolarisation or by increasing dV/dt, acts to push the cell past threshold to cause Na_V channel activation and hence action potential firing. T-type VGCCs, similar to L-type, have been observed to produce a window current at hyperpolarised membrane potentials (Bijlenga et al., 2000). At resting membrane potentials the majority of channels are closed with a small number chronically activated. Slight depolarisations can result in massive activation that drives a cell to fire. This chronic activation, if present in AtT20s, would also produce a constant subthreshold current and could explain how they aid in shaping subthreshold Ca^{2+} waves. Performing current injection would have determined whether action potentials could still be induced in the presence of ML218, confirming or refuting a direct involvement of T-type channels in action potential generation.

Block of T-type channels caused changes in Ca^{2+} wave properties that were similar to the addition of TTX, with spiking able to continue at a reduced frequency. Unlike the addition of TTX alone, ML218 did not cause an increase in wave amplitude. Block of T-type channels would prevent their contribution to Ca^{2+} influx, perhaps offsetting this increase. The co-addition of TTX and ML218 did not cause a further decrease in frequency, further indicating that block of T-type channels prevents pacemaking. Combined addition did, however, reduce the amplitude, time between waves and the total area under the graph from ML218 alone. From this it can be postulated that subthreshold Na_V channel activation is helping to shape Ca^{2+} waves even when the cell is not firing. Persistent, subthreshold Na_V currents are present in cell types such as cerebellar Purkinje neurons, providing some evidence to back this possibility (Carter et al., 2012).

2.4.3 Conclusions

Data here allows for the roles of VGCCs in pacemaking in AtT20s to be described in greater detail than is currently in the literature. The likely mechanism is as follows:

In the absence of firing, L-type VGCCs, aided by T-type VGCCs and perhaps some subthreshold Na_V channel activation, produce rhythmic subthreshold Ca^{2+} waves. These waves retain cytoplasmic Ca^{2+} concentrations to within a set physiological level that promotes cell survival. They also generate membrane potential changes that bring the cell close to the firing threshold. When close to this threshold, T-type VGCCs activate. This increases the rate of change of membrane potential (dV/dt), allowing for the fast activation of TTX-sensitive Na_V channels and the generation of an action potential. The depolarisation during an action potential acts to open VGCCs, allowing further Ca^{2+} influx. This is followed by their rapid inactivation due to the action potential hyperpolarisation. This is caused in part by the Ca^{2+} influx itself, which may activate Ca^{2+} dependent BK and SK channels. This hyperpolarisation acts to decrease the time between Ca^{2+} waves by rapidly driving the membrane potential back to subthreshold values. Na_V and Ca^{2+} channels are therefore dependent on each other, with VGCCs required to maintain an underlying frequency, while Na_V channels then entrain Ca^{2+} waves to the rate of action potential firing to increase this frequency and maintain consistent, rhythmic firing. This mechanism also creates a tight window for Ca^{2+} entry into the cell during an action potential, which could also explain the observed disconnect between electrical activity and secretion. Since the levels of Ca^{2+} entering the cytoplasm remain relatively consistent whether a cell is active or inactive (due to changes in the shape and frequency of Na_V entrained vs non-entrained Ca^{2+} waves) there will be no large increase in Ca^{2+} to drive Ca^{2+}-dependent exocytosis, which is known to be required as shown by the effect of the VGCC agonist BayK 8644 on membrane capacitance. This proposed mechanism therefore encapsulates all of the results observed within this chapter and is summarised in **Figure 2.19**.

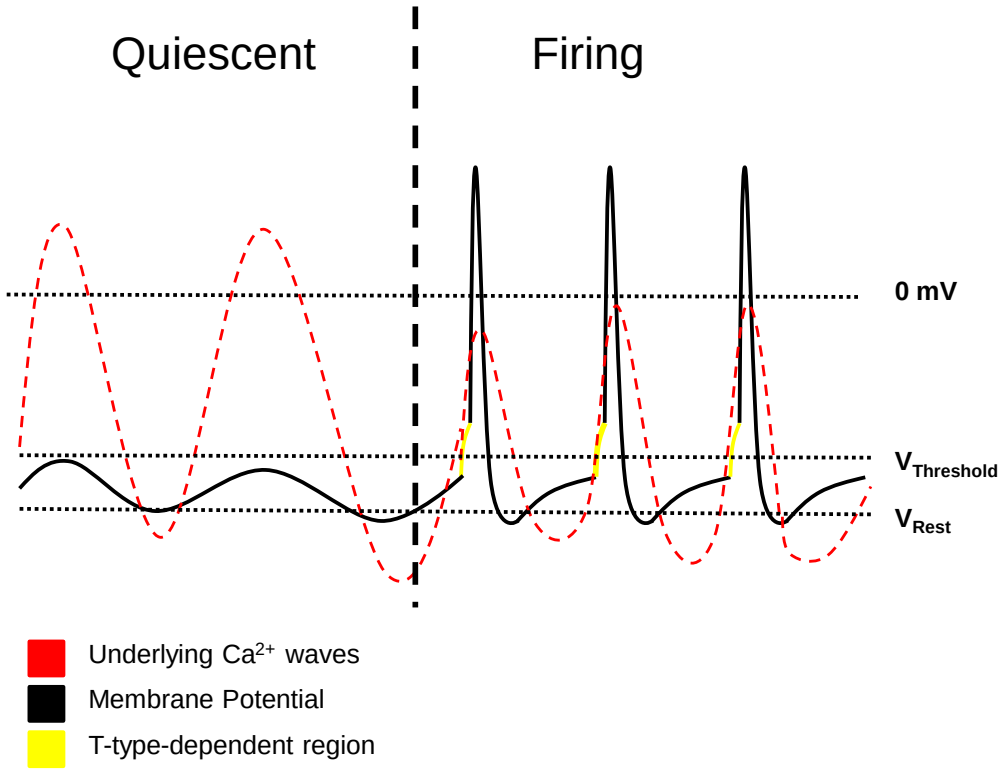

Figure 2.19 - The mechanism of pacemaking in AtT20s. Subthreshold Ca^{2+} waves generated by L-type VGCCs drive membrane potential changes close to the firing threshold. Near the threshold for Na_V channel opening, T-type VGCCs activate to drive the membrane past the threshold for Na_V channel opening, generating an action potential. This results in a fast after-hyperpolarisation generated primarily by K^+ channels that prevents further Ca^{2+} influx. This acts to decrease the time between Ca^{2+} waves, allowing consistent and rhythmic firing.

Chapter 3

The Development of Pacemaking in hiPSC-Derived Dopaminergic Neurons

Abstract

Dopaminergic (DA) neurons of the substantia nigra pars compacta display intrinsic pacemaking *in-vivo* which is believed to be an important factor in their selective death in Parkinson's disease (PD). Human induced pluripotent stem cell (hiPSC)-derived DA neurons are a human model of the disease that have previously been shown to display pacemaking *in-vitro*, though the early development of this activity and whether it is truly intrinsic rather than synaptically driven has not been determined. Here I have used electrophysiology and Ca^{2+} imaging in combination with pharmacological block of ion channels to follow the early development of pacemaking in hiPSC-derived DA neurons up to 6 weeks after the onset of differentiation from neural progenitors. The results show that pacemaker-like activity developed from 2 weeks post-differentiation, though after 6 weeks their electrical properties remained relatively immature. Firing could be blocked by glutamate and dopamine D2 receptor antagonists indicating it is driven by synaptic input rather than their intrinsic electrical properties. hiPSC-derived DA neurons did, however, display a more excitable phenotype than the non-DA cells in the same culture, being more likely to fire action potentials and producing spike trains that were dependent upon L-type voltage-gated calcium channels (VGCCs). Cultures containing hiPSC-derived DA neurons developed regular spikes in their intracellular Ca^{2+} concentration that were sensitive to the voltage-gated sodium channel antagonist tetrodotoxin (TTX). These data provide a deeper understanding of pacemaking in this disease model, hopefully leading to more targeted, efficient research into the cellular mechanisms of PD and any future treatments.

3.1 Introduction

A bottleneck in PD research has been the lack of human models of the disease. Although decades of research using rodent and primate models has occurred, we still know little about human DA neurons. With the discovery of hiPSCs and their ability to be differentiated into various lineages, hiPSC-derived DA neurons have become a promising *in-vitro* model (Takahashi et al., 2007). Performing a detailed electrophysiological characterisation of these neurons will potentially provide valuable information into the mechanisms of *in-vivo* cell death in human forms of PD.

Substantia nigra pars compacta (SNc) DA neurons are characterised by their pacemaker activity. This is primarily tonic in nature, with regular single action potentials at 3-8 Hz being seen in rat neurons in-vitro. Their activity also appears to be modulated by synaptic input, with phasic burst firing seen in the presence of a large quantity of synaptic inputs (Grace & Bunney, 1984; Tepper et al., 1998; Guzman et al., 2009). These neurons also produce multiple slow, oscillatory action potentials, termed "spike trains," in response to current injection in rat models (Grace & Onn, 1989).

A wide range of ion channels have been implicated in controlling their excitability in rat models. This includes voltage-gated sodium (Na_V) channels, voltage-gated potassium (K_V) channels ($K_V1.3$, $K_V2.1$, $K_V3.2$, $K_V3.3$, $K_V4.3$), Ca^{2+}-activated SK channels (SK1, SK2, SK3), BK channels, HCN channels (HCN2, HCN4), L-type ($Ca_V1.3$) and T-type ($Ca_V3.1$, $Ca_V3.3$) VGCCs (Dufour et al., 2014). Subthreshold cytoplasmic Ca^{2+} waves are suspected to act as a driver for this intrinsic excitability (Guzman et al., 2009). Inputs onto these cells in rat and guinea pig brain slices are a mix of excitatory glutamatergic and inhibitory GABAergic transmission, with D2 autoreceptors allowing local negative feedback (Cragg & Greenfield, 1997; Gotz et al., 1997; Lee & Tepper, 2009).

Characterisation of pacemaking in hiPSC-derived DA neurons is limited to one major study (Hartfield et al., 2014). This study found that these neurons displayed pacemaker activity *In-vitro* that appeared to be spontaneous. They also produced trains of action potentials in response to current injection within 6- 12 weeks of differentiation. This was accompanied by the development of Ca^{2+} waves and excitatory spontaneous postsynaptic currents (ESPSCs) within the same period. It was suggested by the authors that the observed activity is intrinsic, though whether it is instead driven by synaptic input was not investigated. Study of these cells from 0-6 weeks post differentiation has

also not been performed. It is unknown, for example, when voltage-gated ion channel populations characteristic of DA neurons develop or what the synaptic inputs onto these neurons are in culture and at what stage they appear and mature. Whether the observed activity was specific to DA neurons and not all of the neurons in culture was also not considered in this previous study.

This chapter focuses on how hiPSC-derived DA neurons develop into excitable cells capable of pacemaking. Characterisation of electrical activity, Ca^{2+} spiking, voltage-gated ion channel currents and synaptic inputs was performed on DA neurons that were positively identified as expressing tyrosine hydroxylase (TH). TH is the rate limiting enzyme in the production of dopamine, being responsible for the hydroxylation of tyrosine into the dopamine precursor L-DOPA. This can then be converted to dopamine via aromatic amino acid decarboxylase (Daubner et al., 2011). This experiment was performed weekly from 0- 6 weeks post-differentiation from hiPSC-derived neural progenitor cells (hNPCs) to produce a time course of their early electrical development.

My results show that spontaneous firing that is characteristic of SNc DA neurons began to develop from 1- 2 weeks post-differentiation. Underlying this excitability was the development of voltage gated Ca^{2+} currents and Ca^{2+} waves. These waves were found to be TTX-sensitive and therefore action potential dependent rather than the subthreshold waves that have been reported in primary DA neurons (Puopolo et al., 2007). Firing was found to be dependent upon glutamate receptors and dopamine D2 receptors. Excitatory spontaneous postsynaptic currents (ESPSCs) were identified from week 2 and were blocked by glutamate receptor antagonists. All of this indicates that electrical activity during the first 6 weeks of development was not being intrinsically driven. All of the above traits showed a clear shift in maturity at week 6, perhaps indicating the development of mature synaptic networks at this time point.

By assessing any differences from DA neurons *In-vivo* this chapter provides information on the strengths and limitations of hiPSC-derived DA neurons as a model for PD. It also acts to improve our understanding of pacemaking in human DA neurons, leading to more targeted, efficient research into the cellular mechanisms of PD and any future treatments.

3.2 Methods

3.2.1 Culture & Expansion of Human Neural Progenitors

The protocols for culture and expansion followed the product description guidelines from Axol Bioscience, detailed below. Cells and reagents were from Axol unless otherwise stated. Human iPSC-derived neural progenitor cells (hNPCs) originating from female new-born cord blood were expanded on sterile 12 well tissue culture plates (Corning) pre-coated with SureBond-XF at a density of 80 000/cm^2 in plating-XF medium. 24 hours after plating, media was replaced with neural expansion-XF medium supplemented with 20 ng/ml FGF2 and 20 ng/ml EGF. Cells were passaged every 5 days and expanded until an optimal quantity were obtained for differentiation. Cells were incubated at 37ºC and 5% CO_2.

3.2.2 Differentiation of hNPCs to Dopaminergic Neurons

hNPCs were passaged in expansion-XF medium and plated at a density of 30 000/cm^2 onto coverslips pre-coated with SureBond-XF. 24 hours after passage, media was changed to STEMdiff™ dopaminergic neuron differentiation medium (STEMcell) supplemented with 200ng/ml sonic hedgehog (SHH) (Millipore). Media was changed daily for 14 days. The cells were then passaged and plated at a density of 20 000/cm^2 onto glass coverslips pre-coated with SureBond-XF. Media was changed to STEMdiff™ dopaminergic neuron maturation medium 1 (STEMcell). Full media changes were performed every 48 hours for 5 days. Media was then changed to maturation medium 2 (STEMcell) and replaced every 48 hours up to a total culture time of 6 weeks. Cells were incubated at 37ºC and 5% CO_2. **Figure 3.1** shows a graphical representation of the steps involved in differentiation and the theory behind this approach.

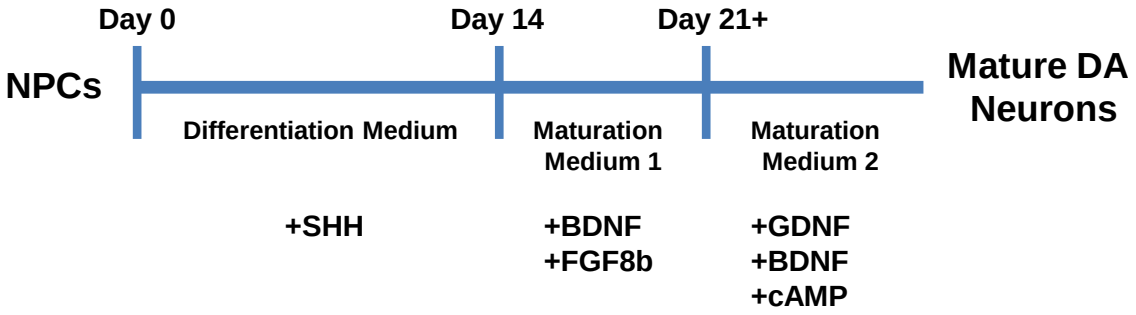

Figure 3.1 - Directed differentiation of NPCs to DA neurons via a neural floor plate lineage. DA neurons within the SNc express the floor plate marker LMX1A and roof plate marker FOXA2. hiPSC-derived NPCs, which are equivalent to cells of the neural tube during embryonic development, can be differentiated into DA neurons via the addition of sonic hedgehog (SHH). This promotes expression of LMX1A. Subsequent addition of FGF8b induces the co-expression of FOXA2, leading to the generation of a DA lineage. Factors such as BDNF, GDNF and cAMP are added to support cell growth and survival. (Kriks et al., 2012).

3.2.3 Electrophysiology

Recordings were performed on 0- 6 week differentiated neurons in the whole cell configuration at room temperature (21^{o}C). Data were acquired using Clampex 10 software on an Axopatch 200B patch clamp amplifier with a 16 bit Digidata 1440A digital acquisition system (Molecular Devices) at 20 kHz with a 5 kHz low pass filter. Microelectrodes were pulled from borosilicate glass using a Flaming/Brown P-87 micropipette puller to a resistance of 3-8 MΩ. Extracellular and intracellular solutions were formulated identically to those used previously in the literature (Hartfield et al., 2014): Extracellular (mM): 129 NaCl, 5 KCl, 2 $CaCl_2$, 1 $MgCl_2$, 30 Glucose, 25 HEPES, pH 7.4, 310 Osm/kg. Intracellular (mM): 120 K-Gluconate, 25 KCl, 4 MgATP, 2 NaGTP, 10 EGTA, 1 $CaCl_2$ and 10 HEPES, 295 Osm/kg, pH 7.2. For calcium current recordings KCl/Gluconate was replaced with 145 mM Cs-gluconate in the intracellular solution and carried out in the presence of 1 µM TTX (Tocris) and 10 mM $CaCl_2$. 1 mg/ml Lucifer Yellow (Sigma) was added to the intracellular solution immediately prior to recording to mark neurons for later cytochemical characterisation. An image of each Lucifer Yellow filled cell was taken using an Olympus IX71 microscope with a 470 nm LED (CoolLED), with data collection using WinFluor v3.8 with a QiClick USB camera

(QImaging). This allowed recordings to be sorted into TH-positive and TH-negative categories after immunostaining. Cells with more than 50 pA of leak current were rejected. P/4 leak subtraction was applied pre-recording to compensate for leak current in all accepted cells during voltage clamp recordings. Whole cell capacitance compensation was applied prior to recording in voltage clamp recordings and series resistance was compensated to a minimum of 60%. The liquid junction potentials were found to be +1.1 mV (K-Gluconate internal) and -6.1 mV (Cs-Gluconate internal) and were corrected after recording. To determine which neurotransmitters and receptors were involved in driving electrical activity, various agonists and antagonists were added directly to the bath. A full list of compounds and the concentrations used can be found in **3.2.8**.

Four protocols were used to acquire relevant data:

1.) Voltage clamp recording from a holding potential of -80 mV to +60 mV in 200 millisecond +10 mV steps. This was used to acquire current-voltage (I/V) relationships and current densities for Na_V, K_V and Ca^{2+} channels.
2.) Continuous voltage clamp recording from a holding potential of -80 mV. This was used to detect the presence of synaptic inputs.
3.) Continuous current clamp recording without current injection. This was used to determine the presence of spontaneous action potentials, subthreshold potentials and the resting membrane potential.
4.) Current clamp recording from a holding potential of -80 mV, with a 20 pA current step. This was used to determine the ability of a cell to fire action potentials upon current injection. Steps were 1 second in duration.

Data Analysis: Firing frequency, membrane potential, peak current and area under the graph (for ESPSCs) were calculated in Clampfit 10.

3.2.4 Immunofluorescence Staining

Coverslips were washed in PBS pre-warmed to 37^{o}C before fixation in 4% paraformaldehyde for 10 minutes at room temperature (21^{o}C). 3 washes with ice cold PBS were performed and cells were permeabilised with 0.1% Triton X-100 for 10 minutes at 21^{o}C. Coverslips were washed for 3x 5 minute washes with PBS containing 0.1% Tween-20 at 21^{o}C before a 30 minute incubation at 21^{o}C in PBS containing 1% BSA and 0.1% Tween-20 to prevent non-specific antibody binding. Primary antibody

incubation was performed at 21ºC for 1 hour in PBS containing 1% BSA and 0.1% Tween-20. Coverslips were washed 3x for 5 minutes with PBS containing 0.1% Tween-20 at 21ºC. Secondary antibody incubation was performed for 1 hour in the dark at 21ºC in PBS containing 1% BSA. All secondary antibodies were conjugated with AlexaFluor fluorescent dyes. Coverslips were then washed 3x for 5 minutes with PBS in the dark at 21ºC before mounting on glass microscope slides with the mounting medium Mowiol® 4-88 and sealing with nail polish. Slides were stored at 4ºC until analysis. All reagents were acquired from Sigma Aldrich and all antibodies were from Abcam unless stated. A full list of the antibodies used and their dilutions can be found in **Table 3.1**.

Antibody	Description	Concentration Used	Secondary	Concentration Used
Anti-NeuN	Species: Mouse. Antibody against **Neu**ronal **N**uclei	1:50	Donkey anti Mouse AlexaFluor-488	1:500
Anti-PSD95	Species: Mouse. Antibody against a human postsynaptic marker associated with NMDA receptors	1:1000	Donkey anti Mouse AlexaFluor-488	1:500
Anti-Synaptophysin	Species: Rabbit. Antibody against a ubiquitously expressed presynaptic marker	1:1000	Goat anti Rabbit AlexaFluor-647	1:500
Anti-TH	Species: Rabbit, Chicken. Antibody against a dopaminergic neuron marker, Tyrosine Hydroxylase	1:500	Goat anti Rabbit AlexaFluor-647 Goat anti Chicken AlexaFluor 568	1:500 1:500

Table 3.1 - Primary and secondary antibodies. Table illustrating the antibodies used during experimentation, their uses and the dilutions used.

3.2.5 Confocal Microscopy

Fixed coverslips were imaged using a TCS SP5 II confocal microscope (Leica) with a 63x oil objective (NA 1.3). Samples were excited using an argon or white light laser. Images were collected using a Hamamatsu camera with 3x frame averaging at an image resolution of 1024x1024 pixels.

Data Analysis: Images were analysed in ImageJ. Percentages of stained cells was performed semi-automatically using the Analyse Particle function in ImageJ. Colocalisation of synaptic markers was performed using the NeuronJ and SynapCountJ plugins for ImageJ. Cells identified after confocal microscopy as TH -positive and -negative were manually matched to their corresponding Lucifer Yellow images from electrophysiological recordings based on their morphology.

3.2.6 Calcium Imaging

Calcium green-1 AM (ThermoFisher) was loaded into cells to assess changes in cytoplasmic Ca^{2+} concentration. A 1 mg/ml stock solution of Calcium Green-1 AM was formulated in loading medium containing 48 µl DMSO and 2 µl 20% w/v Pluronic F-127 (Sigma). 0- 6 week differentiated neurons were loaded with a final concentration of 5 µg/ml Calcium Green-1 AM for 20 minutes at 37ºC in culture medium. The cells were washed 5 times with PBS pre-warmed to 37ºC and the coverslips were transferred to 35 mm culture dishes. Recording was performed in dopaminergic neuron external solution (as formulated in **3.2.3**) at 21ºC using an Olympus IX71 microscope (10x objective, NA 0.3) and a 470 nm pE-100 light emitting diode (CoolLED). Fields of cells were recorded for 40 seconds using a Qi Click USB camera (QImaging) at 5 frames per second with a gain of 20.

Data Analysis: Regions of interest were drawn manually around cells in ImageJ. Fluorescence data was then imported into Clampfit 10 for the calculation of wave frequency using the threshold and template search features. Area under the graph was calculated manually in Excel using the Riemann summing method of numerical integration. Recordings were manually bleach corrected in Clampfit 10. For all graphs, changes in fluorescence were expressed as the proportional change in fluorescence from baseline ($\Delta F/F$). For all Calcium Green-1 experiments the means from each of 3 experiments were calculated from 50 cells in each experiment. These 3 values were then averaged to give an overall mean and S.E.M.

3.2.7 Drugs & Compounds

In various experiments ion channel agonists/antagonists and other solutions were applied to the cells. All drugs were diluted from concentrated stock solutions and pipetted directly into the bath at concentrations determined from the literature. All were purchased from Tocris unless otherwise stated. The compounds used and their concentrations are: TTX (1 µM), TEA (10 mM, Sigma), nifedipine (1 µM), $CoCl_2$ (1 µM, Sigma), CNQX (5 µM), D-AP5 (50 µM), picrotoxin (1 µM), L-glutamic acid (1 mM, Sigma), $CaCl_2$ (10 mM), SCH23390 (10 nM), nemonapride (10 nM).

3.2.8 Graphs & Statistical Analysis

All graphs and curve fitting were performed using OriginPro 8.5. Statistical analysis was performed using an appropriate statistical test in Excel using the XLSTAT plugin (t-tests, ANOVAs or KS-tests). The exact test used and their associated significance values are reported in the text. Differences were considered statistically significant when $p < 0.05$. Asterisks (*) on graphs indicate statistical significance at this p-value. Errors bars in all graphs and ± values in the text use the standard error of the mean (S.E.M.) which was calculated in Excel.

3.3 Results

3.3.1 Confirmation of a Dopaminergic Neuronal Phenotype

DA neurons in culture and *in-vivo* express tyrosine hydroxylase (TH), the rate limiting enzyme in the dopamine production pathway. To determine whether the differentiation protocol used was producing hiPSC-derived DA neurons from hNPCs, co-staining using antibodies against the neuron-specific marker NeuN and against TH was performed from 0 weeks (hNPCs) to 6 weeks post-differentiation (n=4). TH-positive neurons were identified from 1 week, with the number of positive neurons increasing as a percentage of the total population each week until reaching a steady level of ~25% at 4-6 weeks post-differentiation (**Figure 3.2A, 3.2B**). Counterstaining with the nuclei stain DAPI revealed NeuN staining in over 80% of counterstained nuclei at all weeks tested (**Figure 3.2C**). This finding was surprising as NeuN was only expected to be present in mature neurons in later weeks of development. NeuN staining did, however, become more prominent in later weeks, clearly staining the cell bodies and processes of neurons as they matured in culture (**Figure 3.2A**). Almost 100% of TH-positive cells were NeuN-positive at all weeks tested (**Figure 3.2C**). Control experiments performed with only the secondary antibodies used during the TH and NeuN staining confirmed that the observed staining was not due to non-specific binding of the secondary antibody (**Supplementary 3.1**). Non-specific binding of the primary antibody, though unlikely due to the presence of NeuN negative cells within the cultures, should not be discounted as a possible reason for this unexpected NeuN staining.

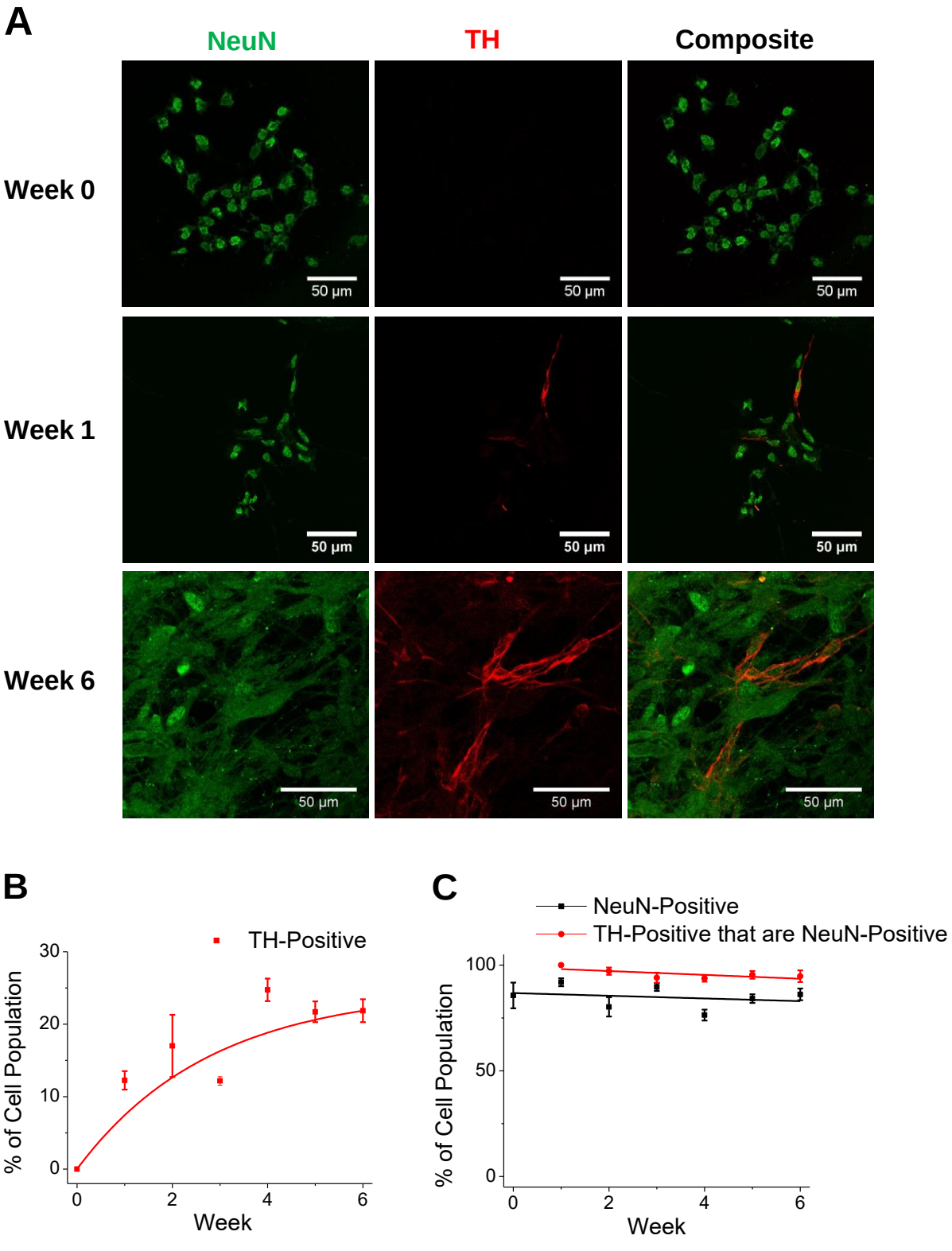

Figure 3.2 - TH-positive neurons develop in culture. (A) Cultured neurons at 0, 1 and 6 weeks post-differentiation that were immunostained for the neuron-specific marker NeuN (green) and the DA marker TH (red). Graphs showing the mean percentages of the total cell population that were (B) TH-positive and (C) NeuN-positive up to 6 weeks post-differentiation (n=4). Error bars ± S.E.M.

3.3.2 The Development of Excitability

SNc DA neurons *in-vivo* and *in-vitro* are characterised by their ability to produce spontaneous pacemaker activity (Shen et al., 1994; Guzman et al., 2009). To determine whether hiPSC-derived DA neurons become excitable and at what stage in development this occurs, whole cell current clamp recording was performed from 0 to 6 weeks post-differentiation with 1 mg/ml Lucifer Yellow added to the intracellular solution to mark cells for later cytochemical identification (n=3 to 8 TH-positive or TH-negative cells per time point) (**Figure 3.3**). Action potentials were defined as regenerative all-or-nothing membrane potential depolarisations that produced an overshoot beyond 0 mV. Recordings from human neural progenitor cells (hNPCs) prior to differentiation revealed no action potential firing in any cells tested (n=18). Lucifer Yellow identification first revealed spontaneous action potential firing in TH-positive cells from 2 weeks post-differentiation. The percentage of 4-6 week TH-positive cells that were firing was significantly higher than in week 4-6 TH-negative cells (n=3) (**Figure 3.4A**) Two modalities of spontaneous firing were observed: tonic firing (**Figure 3.4B**) and burst firing (**Figure 3.4C**).

From 0-6 weeks post-differentiation several changes in excitability occurred. The mean resting membrane potential in all cells became increasingly hyperpolarised (**Figure 3.4D**). The performance of one-way ANOVAs revealed that there was a significant effect of time in culture on the resting membrane potential (TH-positive, $F=9.947$ $p=0.0001$; TH-negative, $F=3.203$, $p=0.011$). The mean resting potential of TH-positive cells was more hyperpolarised than TH-negative cells from weeks 3 to 6, though no statistical difference was identified between the two groups ($F=4.112$, $p=0.115$). A two-sided Dunnett test showed that the resting potential statistically differed from controls from week 2 in both TH-positive cells and TH-negative cells (TH-positive: week 1, $p=0.643$; week 2, $p=0.04$; week 3-5, $p<0.0001$) (TH-negative: week 1, $p=0.646$; week 2, $p=0.02$; week 3-5, $p<0.05$).

The frequency of spontaneous firing remained similar in all cells until week 6, when a large increase in firing frequency was observed in both TH-positive and TH-negative cells (**Figure 3.4E**). The performance of one-way ANOVAs showed a statistically significant effect of time in culture on firing frequency (TH-positive, $F=9.453$, $p<0.0001$; TH-negative, $F=6.851$, $p<0.0001$). No statistical difference was observed between TH-positive and TH-negative cells ($F=8.322$, $p=0.292$). A two-sided Dunnett test showed that firing frequency was statistically difference from week 0 at week 6 but

not at prior weeks for both TH-positive and TH-negative cells (TH-negative: week 1-5, $p>0.3$; week 6, $p<0.0001$) (TH-positive: week 1-5, $p>0.1$; week 6, $p<0.0001$).

hiPSC-derived DA neurons have previously been shown to produce trains of rhythmic action potentials upon current injection once they reach maturity (Hartfield et al., 2014). To confirm this, a 20 pA current injection was applied to cells under whole cell current clamp from 0 to 6 weeks post-differentiation. At Week 0, 6 of 18 hNPCs produced single action potentials upon current injection with the remaining cells showing no ability to fire. Early signs of spike train development were seen from week 2. Spikes became more pronounced and the number of spikes per train increased from 2 to 6 weeks post-differentiation (**Figure 3.5A**). The percentage of TH-positive cells producing these trains at weeks 4-6 was significantly higher than in TH-negative cells during the same time period (n=3) (**Figure 3.5B**).

Pacemaking in the SNc neurons of animal models has been found to be L-type VGCC dependent (Guzman et al., 2009). To determine whether pacemaking in hiPSC-derived DA neurons was also L-type dependent, the L-type VGCC antagonist nifedipine was applied to week 4-6 cells under whole cell current clamp. Unfortunately, only one week 5 TH-positive cell survived through the antibody staining and identification process. The addition of 10 μM nifedipine to this cell abolished all action potential firing within 1 minute of addition (**Figure 3.6A**). Firing could still be induced via current injection, though membrane potential depolarisations no longer crossed the threshold of 0 mV required to be defined as an action potential. This cell, which was able to produce spike trains prior to the addition of nifedipine, could only produce single spikes after the addition of the drug (**Figure 3.6B**).

Neurotransmitters such as glutamate, GABA and dopamine have been implicated in the regulation of pacemaking in SNc DA neurons *in-vivo* (Blythe et al., 2007). To determine their involvement in hiPSC-derived DA neurons, the effect of various receptor antagonists on action potential firing was determined in week 4-6 TH-positive cells. The general glutamate receptor antagonist Kynurenic acid blocked action potential firing in 3 out of 5 cells (**Figure 3.7A, 3.7E**), with the remaining 2 cells capable of firing action potentials in its presence. The $GABA_A$ receptor antagonist Picrotoxin (n=3) caused a slight decrease in firing frequency that was not found to be statistically significant (Paired t-test, p=0.373) (**Figure 3.7B, 3.7E**). The dopamine D1 receptor antagonist SCH 23390 (n=3) had no effect on firing frequency (Paired t-test, p=0.267) (**Figure 3.7C, 3.7E**) while the D2/D3 receptor antagonist Nemonapride (n=4) caused a

membrane depolarisation of 11.32 ± 4.2 mV and a decrease in firing frequency that was statistically significant from controls (Paired t-test, p=0.022) (**Figure 3.7D, 3.7E**).

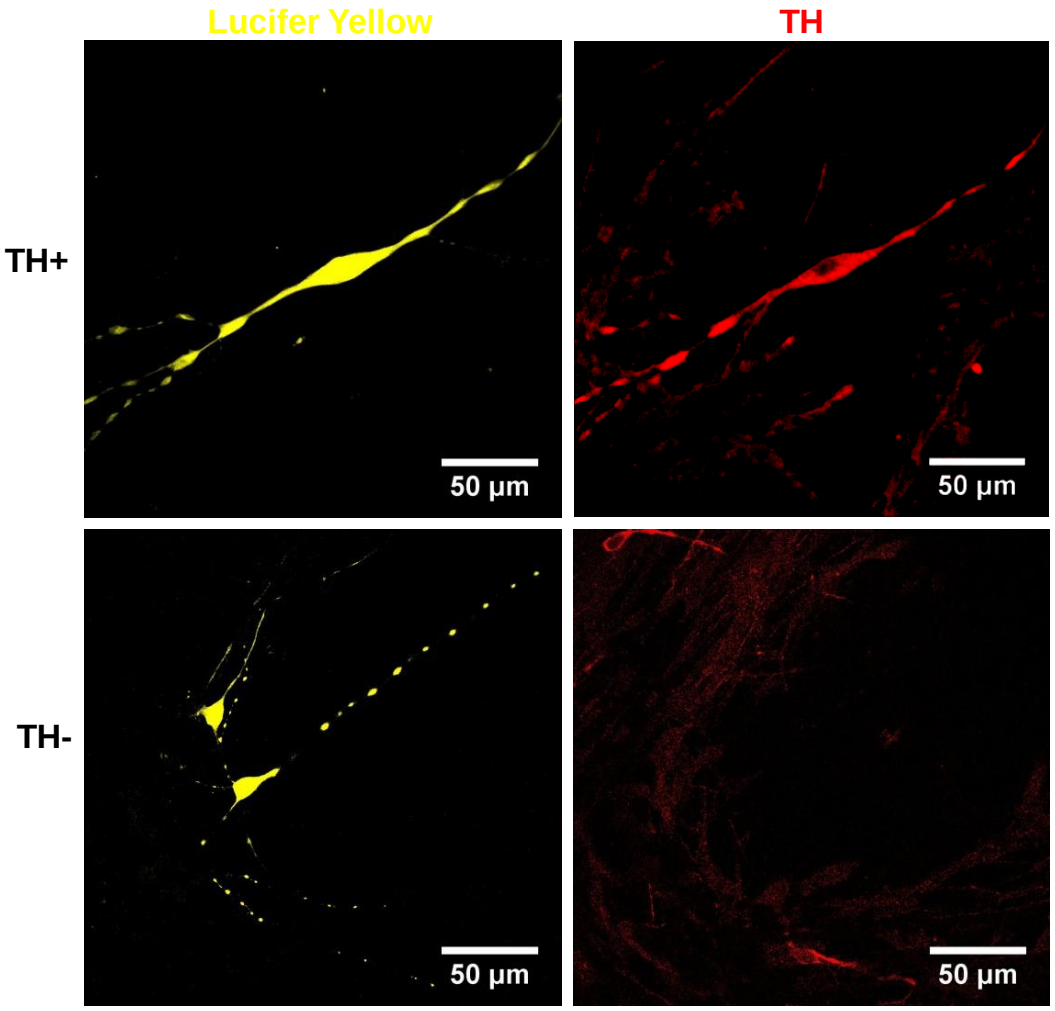

Figure 3.3 - Lucifer Yellow identification of neurons. Representative confocal images of cells 5 weeks post-differentiation that were pipette-loaded with the fixable fluorescent dye Lucifer Yellow during whole cell recording. Images were taken before and after immunostaining for the DA-specific marker TH and show TH-positive (upper) and TH-negative (lower) cells in culture.

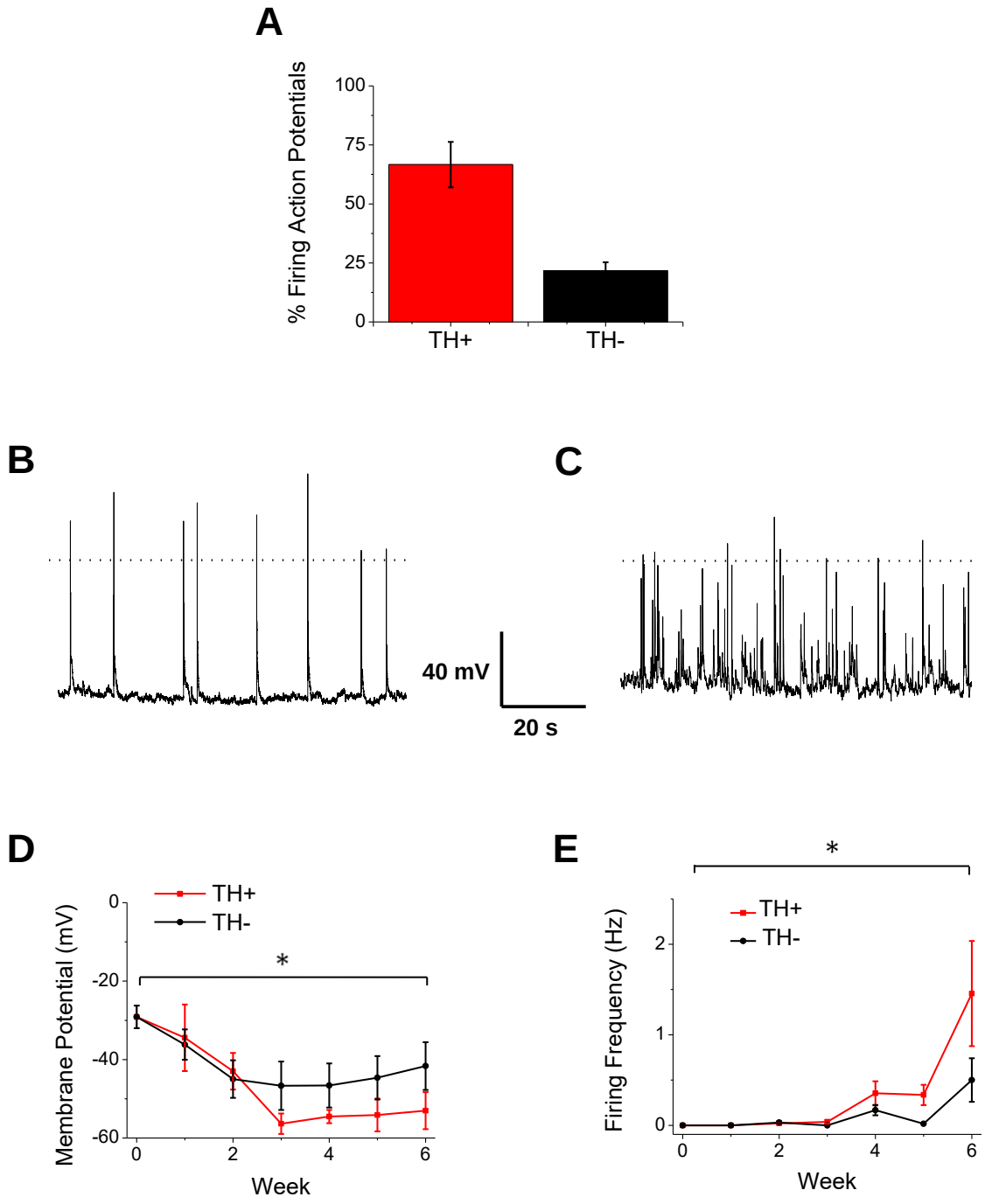

Figure 3.4 - TH-positive neurons fire action potentials in culture. (A) Pooled data from weeks 4-6 showing the percentage of TH-positive and TH-negative cells that fired spontaneous action potentials. Representative whole cell voltage clamp recordings showing the two modalities of firing that were identified: (B) rhythmic tonic firing and (C) arrhythmic burst firing. Dotted lines indicate 0 mV. Graphs showing (D) mean membrane potential and (E) mean firing frequency in TH-positive and TH-negative cells from 0 to 6 weeks post-differentiation. Error bars ± S.E.M. *indicates statistical significance using a one-way ANOVA at p=0.05.

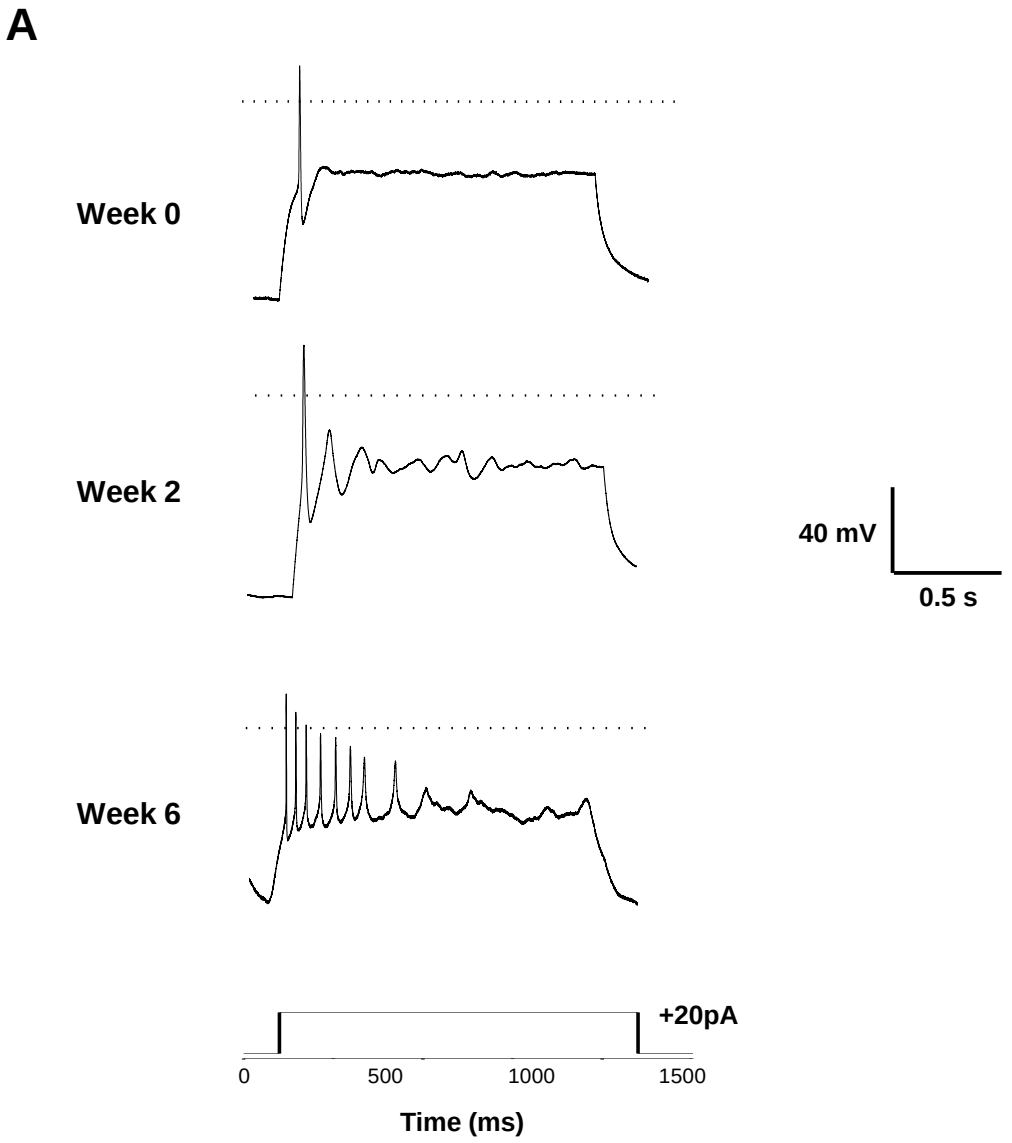

Figure 3.5 - TH-positive neurons develop spike trains in culture. (A) Representative whole cell current clamp recordings from week 0, week 2 and week 6 showing TH-positive cells developing the ability to fire multiple action potentials in response to a 20 pA current step. (B) Pooled data from weeks 4-6 showing the percentage of TH-positive and TH-negative cells that were able to produce more than one action potential upon current injection. Error bars ± S.E.M.*indicates statistical significance using a two-way Student's t-test at p=0.05.

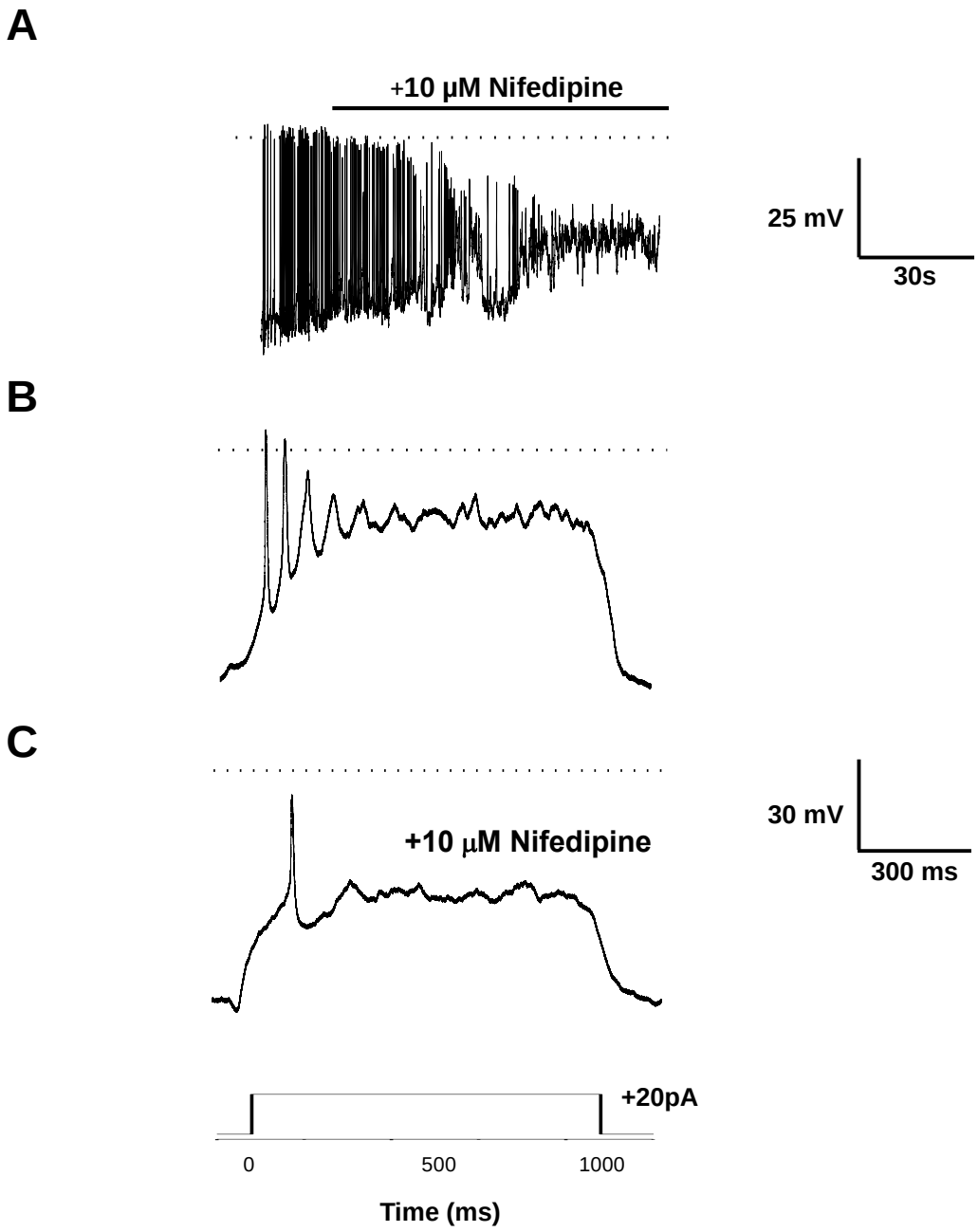

Figure 3.6 - The effect of nifedipine on pacemaking in a TH-positive neuron. Representative whole cell current clamp recordings from a week 5 TH-positive cell showing the effect of nifedipine on (A) action potential firing and the ability to produce spike trains (B) before and (C) after the addition of the drug from a -80 mV holding potential.

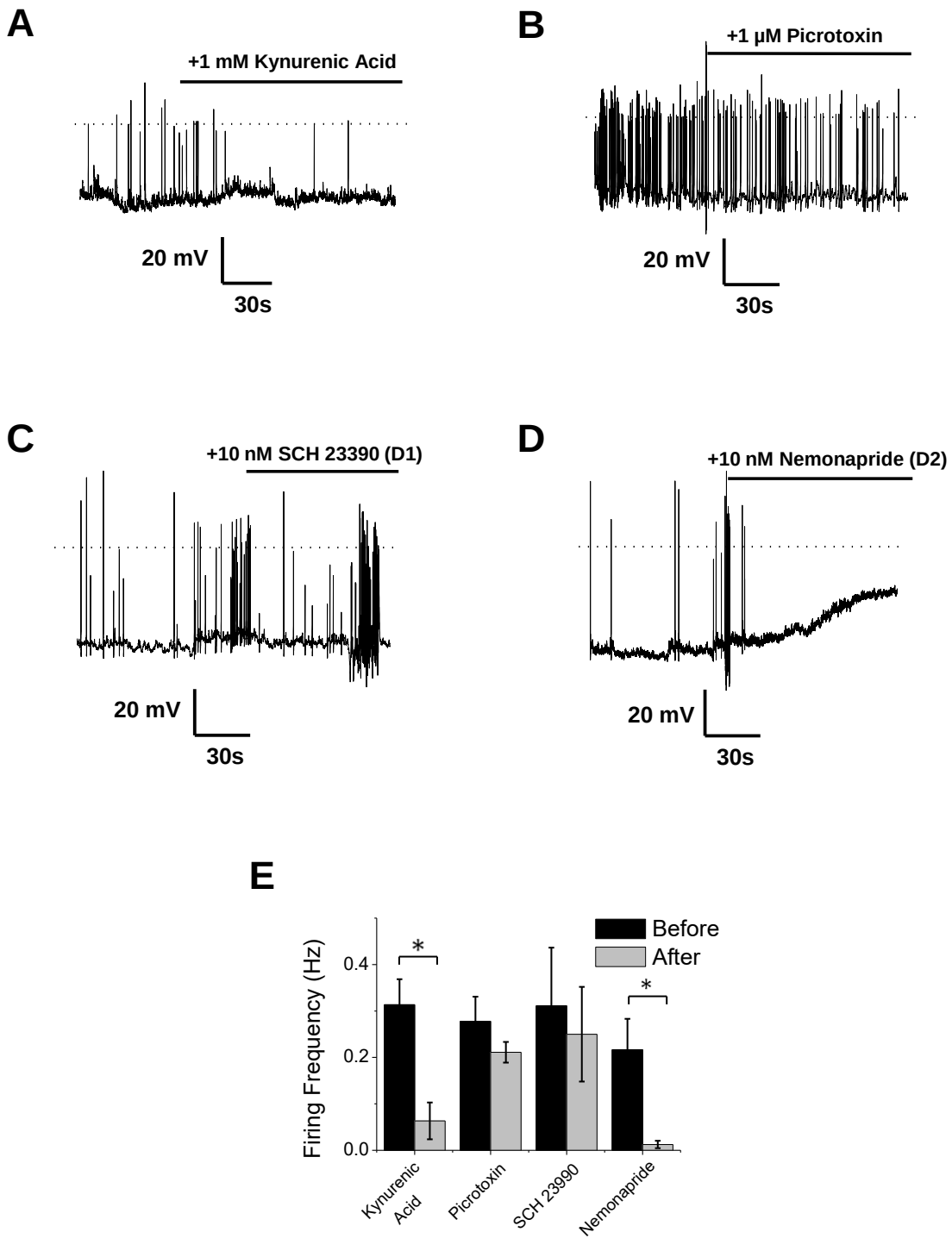

Figure 3.7 - Action potential firing is dependent on synaptic input. Representative whole cell current clamp recordings from week 4-6 TH-positive cells showing the effect of extracellular addition of (A) Kynurenic acid (B) Picrotoxin (C) SCH23390 and (D) Nemonapride. (E) Graph showing the mean firing frequency before and after the addition of each antagonist (n=3-5). Error bars ± S.E.M. *indicates statistical significance using a two-way paired t-test at p=0.05.

3.3.3 The Development of Ion Channel Populations

To characterise changes in ion channel expression that accompany the development of excitability, whole cell voltage clamp was performed using the fixable fluorescent dye Lucifer Yellow (n=3 to 8 TH-positive or TH-negative cells per time point). Whole cell capacitance increased from 0-6 weeks post-differentiation in TH-positive and TH-negative cells, likely indicating an increase in cell size and complexity (**Figure 3.8A**). Performance of one-way ANOVAs revealed that these increases were statistically significant across the 6 week time course (TH-positive: $F=12.794$, $p<0.0001$; TH-negative: $F=11.714$, $p<0.0001$). No statistical difference was observed between TH-positive and TH-negative cells ($F=0.881$, $p=0.32$). A two-sided Dunnett test against week 0 showed that whole cell capacitance first statistically differed from week 0 at week 3 for TH-positive cells (week 1-2, $p>0.5$; week 3, $p=0.02$, week 4-6, $p<0.001$) and week 4 for TH-negative cells (week 1-3, $p>0.1$; week 4, $p=0.022$; week 5-6, $p<0.0001$).

The mean access resistance showed a decrease in TH-positive cells but remained consistent in TH-negative cells (**Figure 3.8B**). Performance of one-way ANOVAs showed that no statistical change occurred over the 6 week time course for either group (TH-positive: $F=0.727$, $p=0.63$; TH-negative, $F=0.072$, $p=0.998$). No statistical difference was found between TH-positive and TH-negative cells ($F=2.107$, $p=0.177$).

Voltage-sensitive currents were identified in all cells from week 0 to week 6 (**Figure 3.9A, 3.9B**). These were blocked by the addition of 1 µM TTX and 10 mM tetraethylammonium (TEA) to the extracellular solution (**Figure 3.9C**). When corrected for whole cell capacitance these currents increased in density from weeks 0-6, with TH-positive cells developing larger peak currents than TH-negative cells (**Figure 3.10A, 3.10C**). The performance of one-way ANOVAs revealed that for voltage-gated sodium (Na_V) currents the effect of time in culture on current density was not significant for TH-negative but was significant for TH-positive cells (TH-negative: $F=0.819$, $p=0.563$; TH-positive: $F=4.821$, $p<0.0001$). No statistical difference was observed between TH-positive and TH-negative cells at week 6 ($F=1.186$ $p=0.326$). A two-sided Dunnett test showed that, for positive cells, they statistically differed from week 0 at weeks 5 and 6 (week 5, $p=0.008$; week 6, $p=0.002$; other weeks, $p>0.1$).

For voltage-gated potassium (K_V) currents, one-way ANOVAs revealed that the effect of time in culture on current density was also not significant for TH-negative but was significant for TH-positive cells (TH-negative, $F=1.897$, $p=0.11$; TH-positive, $F=4.141$,

p=0.003). No statistical difference was observed between TH-positive and TH-negative cells (F=1.679, p=0.252). A two-sided Dunnett test showed that, for TH-positive cells, current density statistically differed from week 0 only at week 6 (p=0.029).

No shift in the IV relationship for either current was observed between TH-positive (n=4) and TH-negative cells at week 6 (n=3) (**Figure 3.10B, 3.10D**).

Since VGCCs are believed to be involved in the selective death of SNc DA neurons in PD, the development of Ca^{2+} currents was investigated. After the addition of 1 µM TTX and 10 mM $CaCl_2$ to the extracellular solution and 120 mM Cs-gluconate to the intracellular solution, no currents were observed in hNPCs at week 0 (n=11) (**Figure 3.11A**).

Capacitance-corrected currents increased weekly up to 4 weeks post-differentiation before reaching a plateau (**Figure 3.11B, 3.11D**). These were blocked by 1 µM of the non-specific VGCC blocker $CoCl_2$ (**Figure 3.11C**). The performance of one-way ANOVAs showed there was a statistically significant effect of time in culture on current density for both TH-negative and TH-positive cells (TH-negative, F=3.335, p=0.013; TH-positive, F=8.122, p<0.0001). TH-positive and TH-negative cells were found to statistically differ from each other (F=7.049, p=0.033). A two-sided Dunnett test showed that for TH-negative cells current density statistically differed from week 0 at weeks 4 and 5 (week 4, p=0014; week 5, p=0.027; week 6, p=0.085; other weeks, p>0.05) while it statistically differed at all weeks except week 2 in TH-positive cells (week 1, p= 0.017; week 2, p=0147, other weeks, p<0.001).

The I/V relationship for these currents was slightly shifted towards negative potentials for TH-positive compared with TH-negative cells at week 6 (n= 3 to 5 TH-positive or TH-negative cells per week) (**Figure 3.11E**).

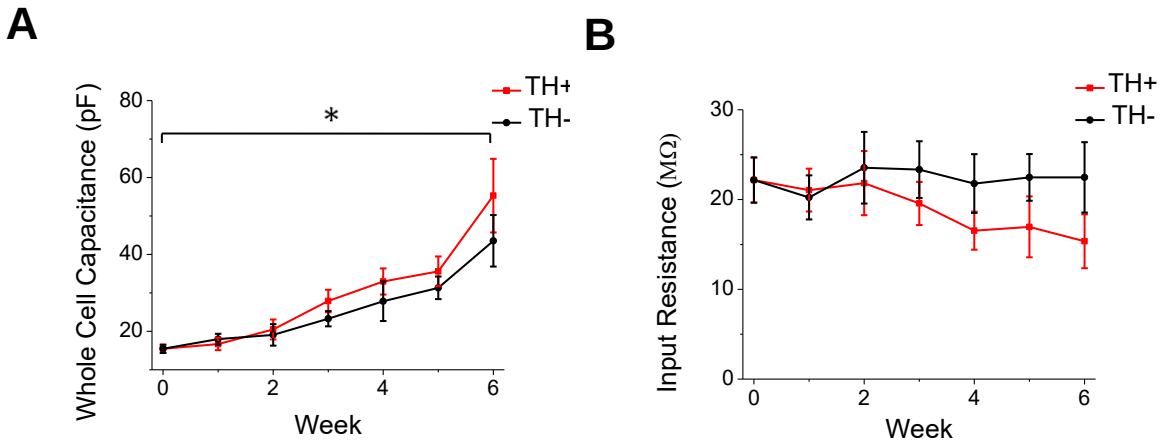

Figure 3.8 - Time-dependent changes in passive membrane properties. Graphs showing changes in (A) whole cell capacitance and (B) input resistance in TH-positive and TH-negative cells from 0 to 6 weeks post-differentiation. Error bars ± S.E.M. *indicates statistical significance using a one-way ANOVA at p=0.05.

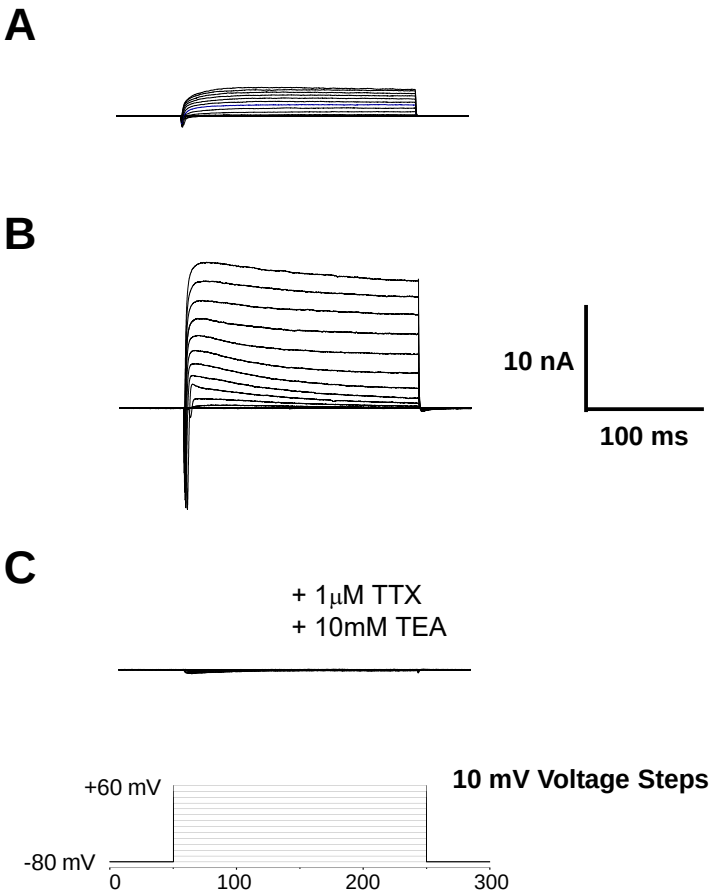

Figure 3.9 - Voltage-dependent currents in hiPSC-derived dopaminergic neurons. Representative whole cell voltage clamp recordings showing voltage-dependent currents at (A) 0 weeks and (B) 6 weeks (TH-positive) post-differentiation. (C) Representative whole cell voltage clamp recording after the addition of TTX and TEA. The experimental protocol used is shown in the bottom panel.

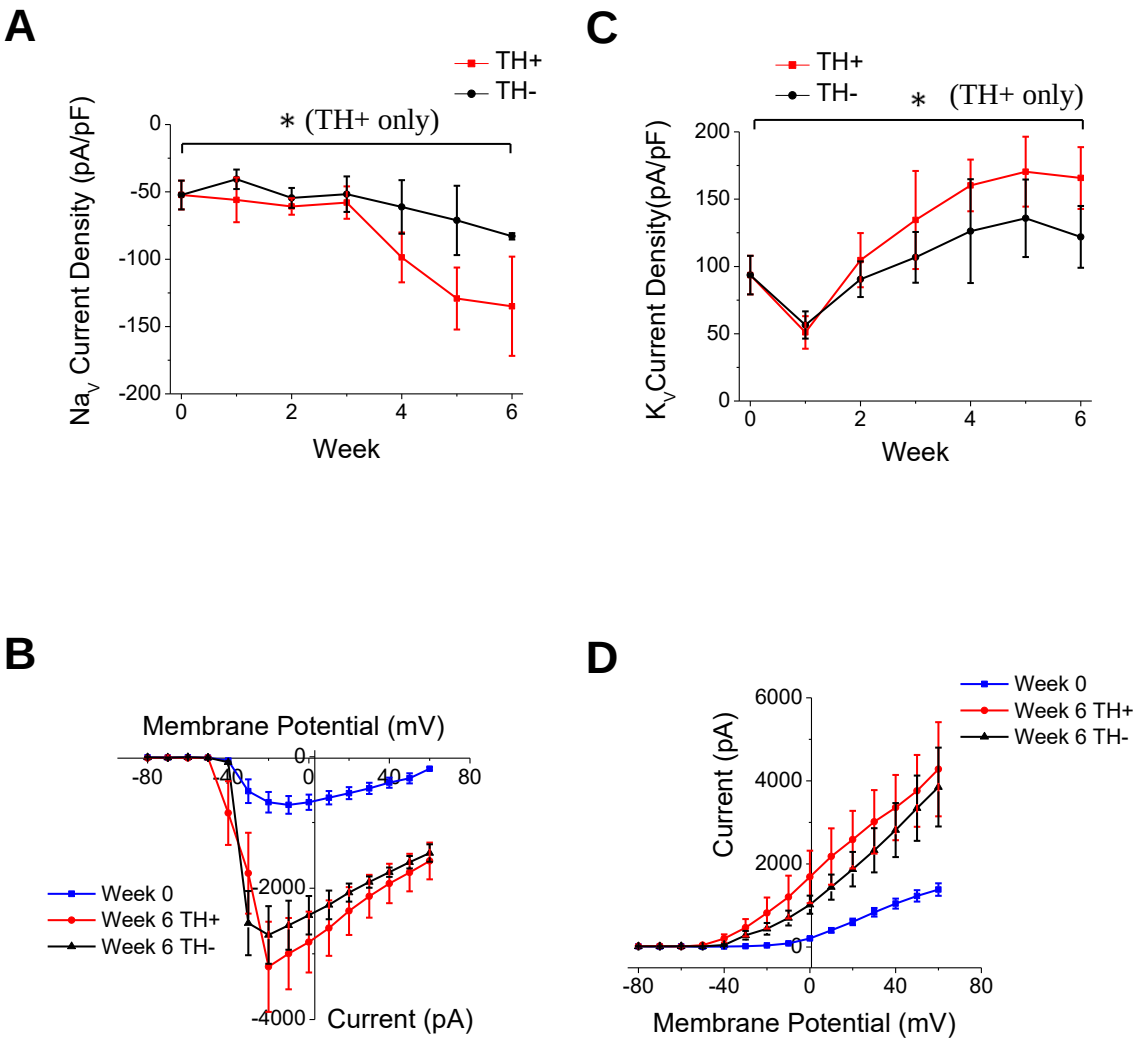

Figure 3.10 - Na_V and K_V current properties in hiPSC-derived dopaminergic neurons. Graphs showing (A) mean current densities for Na_V currents for TH-positive and TH-negative cells from 0-6 weeks post-differentiation and (B) Na_V I/V relationships for week 0 and week 6 TH-positive/TH-negative cells. Graphs showing (C) mean current densities for K_V currents for TH-positive and TH-negative cells from 0-6 weeks post-differentiation and (D) K_V I/V relationships for week 0 and week 6 TH-positive/TH-negative cells. Error bars ± S.E.M. *indicates significance using a one-way ANOVA at p=0.05.

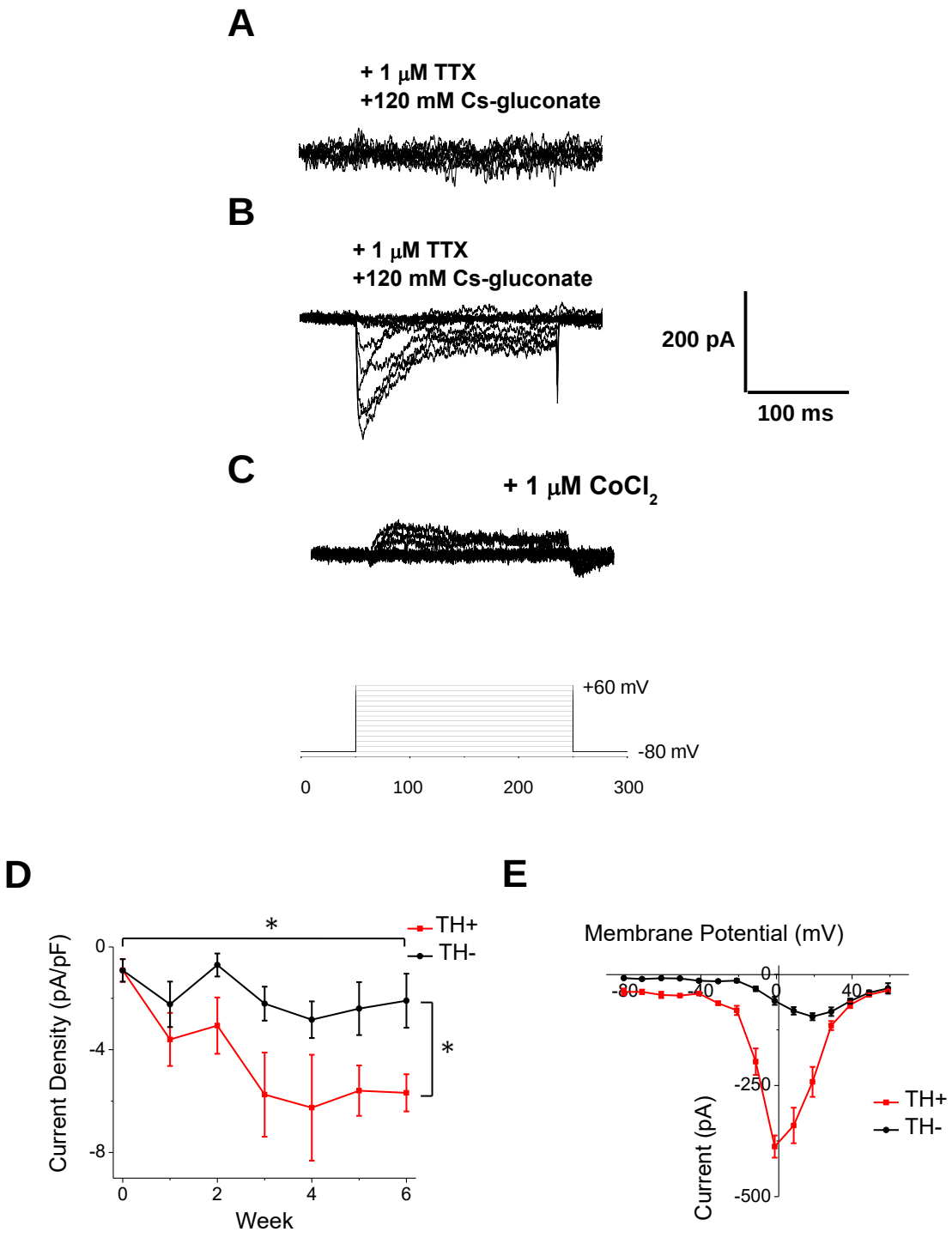

Figure 3.11 - Voltage-dependent Ca^{2+} currents in hiPSC-derived dopaminergic neurons. Representative whole cell voltage clamp recordings from a -80 mV holding potential for neurons (A) 0 weeks and (B) 4 weeks (TH-positive) post-differentiation. (C) Same cell from B in the presence of $CoCl_2$. The experimental protocol used is shown in the bottom panel. Graphs showing (D) the mean current density from weeks 0-6 (n=3-5 per time point) and (E) The mean Ca^{2+} I/V relationships for TH-positive (n=3) and TH-negative cells (n=5) at week 6. Error bars ± S.E.M. * indicates statistical significance using a one-way ANOVA at p=0.05.

3.3.4 The Development of Synaptic Inputs

Synaptic input plays a role in the regulation of firing rate in SNc DA neurons *in-vivo* (Blythe et al., 2007). To determine whether hiPSC-derived DA neurons form synapses *in-vitro*, cells were co-stained for the presynaptic marker synaptophysin, the NMDA receptor associated protein PSD-95 and the DA marker TH at 6 weeks post-differentiation. Staining was seen for both PSD-95 and Synaptophysin in TH-positive cells (**Figure 3.12A**). Regions of co-localisation between PSD-95 and Synaptophysin could be identified, indicating the formation of synapses in culture (**Figure 3.12B**). The mean number of synapses per TH-positive cell was estimated to be 31.9 ± 4.2 (n=12) using the ImageJ plugin SynapCountJ.

To determine the presence of synaptic currents, cells were held at a -80 mV holding potential in the whole cell voltage clamp configuration from 0-6 weeks post-differentiation. Lucifer Yellow was added to the internal solution to allow cytochemical identification of TH-positive cells (n=3-8 TH-positive or TH-negative cells per time point). From Week 2 onwards, excitatory spontaneous postsynaptic currents (ESPSCs) were identified in the majority of cells, including those that were TH-positive (**Figure 3.13A, 3.13B**). As an estimate of total ion flux during these ESPSCs the area under the graph was calculated for 60 second recordings. The mean total area under the graph remained consistent until week 6, when a drastic increase in area was observed for both TH-negative and TH-positive cells (**Figure 3.13C**). The performance of one-way ANOVAs showed that there was a statistically significant effect of time in culture on area under the graph for both TH-positive and TH-negative cells (TH-negative, $F=11.346$, $p<0.0001$; TH-positive, $F=11.771$, $p<0.0001$). No statistical difference was observed between TH-negative and TH-positive cells at any time point ($F=8.434$, $p=0.233$). A two-sided Dunnett test showed that, for both TH-negative and TH-positive cells, area under the graph statistically differed from week 0 only at week 6 ($p<0.0001$ for both).

To determine which neurotransmitters and receptors were producing these currents, various post-synaptic receptor antagonists were added to the extracellular solution during whole cell voltage clamp recording from a -80 mV holding potential. The results below are only from TH-positive cells that are between 4-6 weeks post-differentiation, as identified by Lucifer Yellow staining. Addition of 1 mM of the general glutamate receptor antagonist kynurenic acid blocked ESPSCs in TH-positive cells within 10 minutes of addition (**Figure 3.14A**) and reduced the area under the graph during 60

second recordings when compared to controls before the addition of the drug (n=5) (**Figure 3.14F**). This reduction in area was found to be statistically significant (paired t-test, p=0.01). 50 µM of the NMDA receptor antagonist D-AP5 (n=4) or 5 µM of the AMPA/Kainate receptor antagonist CNQX (n=4) both partially blocked ESPSCs (**Figure 3.14B, 3.14C**) and reduced the mean total area under the graph (**Figure 3.14F**). These changes in area were not statistically significant when compared to controls (paired t-test, CNQX: p=0.066, D-AP5: p=0.063). The addition of both antagonists blocked ESPSCs similar to the addition of kynurenic acid (n=5) (**Figure 3.14D, 3.14F**). The decrease in total area under the graph that was observed upon the addition of both antagonists was found to be statistically significant compared to controls (paired t-test, p=0.009). Averaging the shape of ESPSCs from before (n=332 ESPSCs from 4 cells) and after the addition of 50 µM D-AP5 (n=227 ESPSCs from 4 cells) revealed a reduction in ESPSC duration after the addition of the drug (**Figure 3.14E**).

Small amplitude ESPSCs remained in the presence of kynurenic acid or D-AP5/CNQX. Calculation of the equilibrium potential for Cl^- for the extracellular and intracellular solutions used gave a value of -42.12 mV. This is more depolarised than the typical Cl^- equilibrium potential for neurons which lies around -80 to -90 mV. From the holding potential of -80 mV used, Cl^- currents would therefore appear as excitatory currents rather than the inhibitory currents typically carried by Cl^-. The remaining ESPSCs could therefore represent GABAergic outward currents, though time constraints meant this was not tested experimentally.

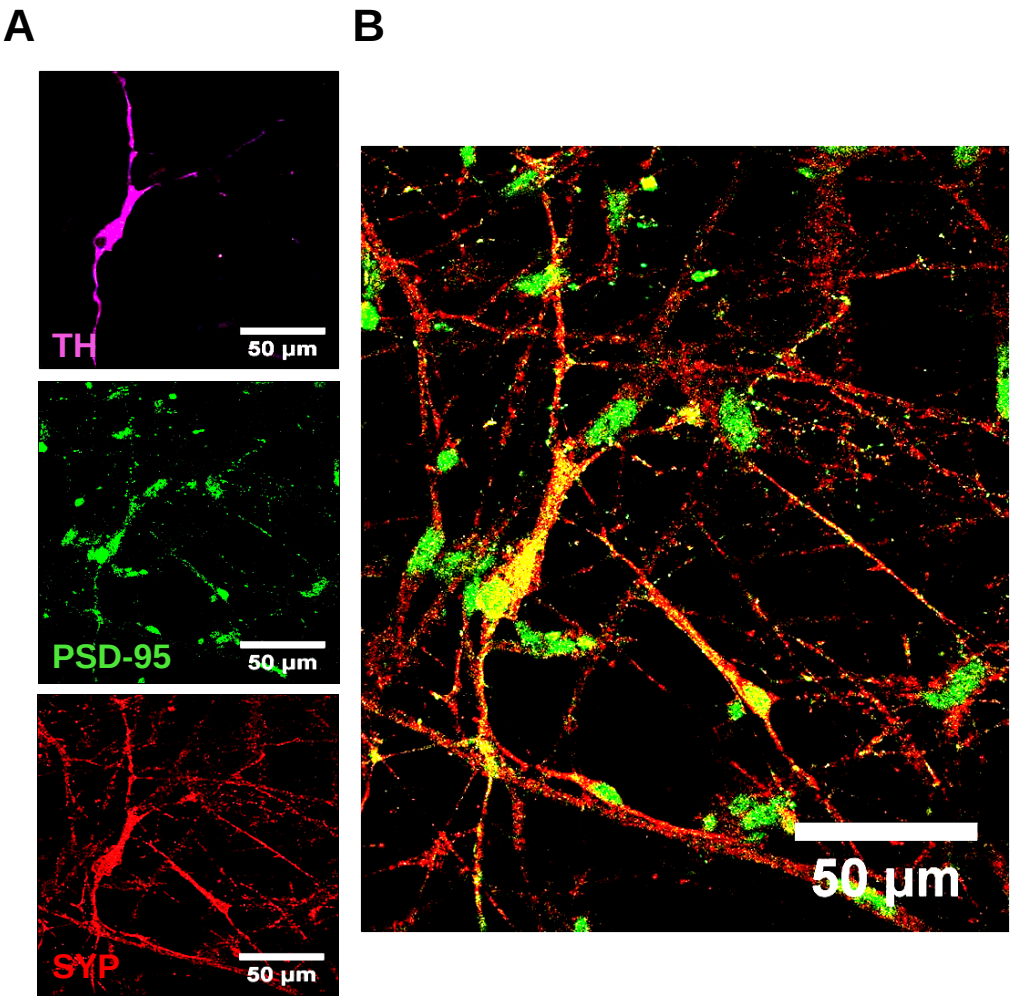

Figure 3.12 - TH-positive neurons form synapses in culture. (A) Representative confocal images of the same field of week 6 cells stained for (top to bottom) TH, PSD-95 (postsynaptic marker) and Synaptophysin (presynaptic marker). (B) A composite image of the PSD-95 and Synaptophysin staining from A. Regions of co-localisation are shown in yellow.

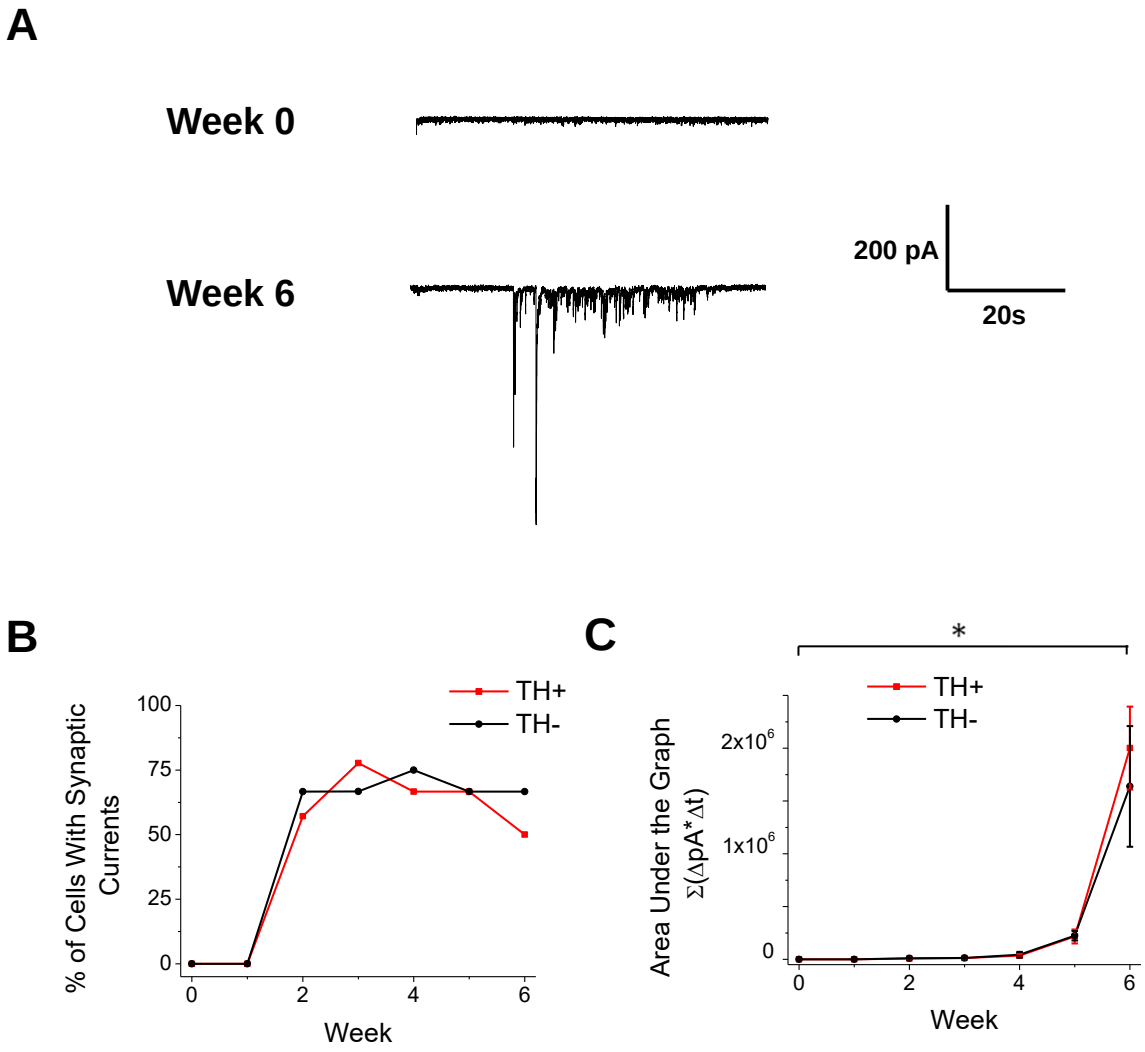

Figure 3.13 - Synaptic currents in hiPSC-derived neurons. (A) Representative whole cell voltage clamp recordings from a holding potential of -80 mV in week 0 and week 6 cells showing the development of ESPSCs. Graphs showing (B) the percentage of TH-positive and TH-negative cells that displayed synaptic currents and (C) the mean total area under ESPSCs during 60 second recordings from 0-6 weeks post-differentiation (n=3-8 per week). Error bars ± S.E.M. *indicates statistical significance using a one-way ANOVA at p=0.05.

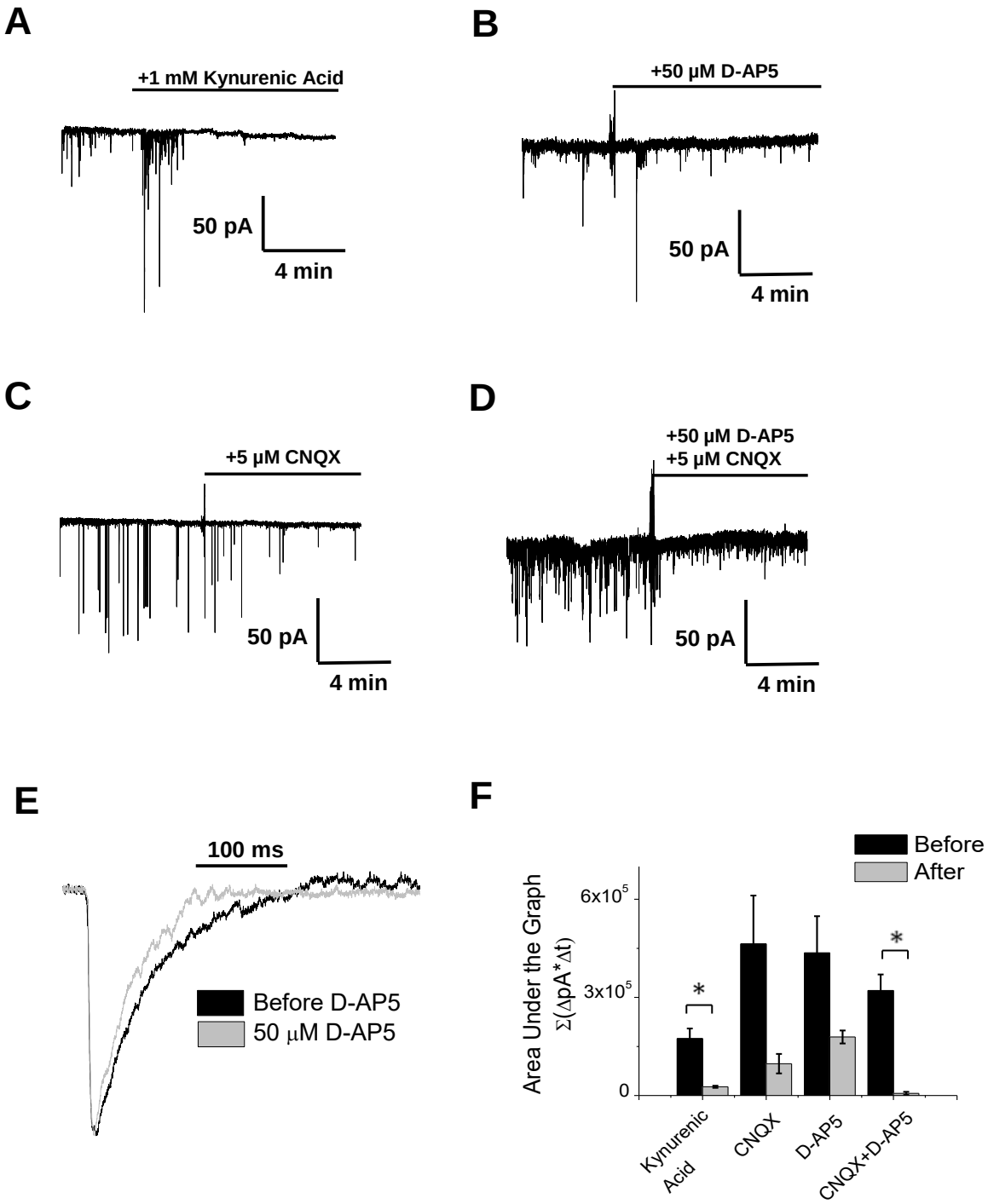

Figure 3.14 - Synaptic inputs in TH-positive neurons. (A) Representative whole cell voltage clamp recordings from a -80 mV holding potential showing the effects of (A) kynurenic acid (B) CNQX (C) D-AP5 and (D) CNQX + D-AP5 on ESPSCs in TH-positive cells from 4-6 weeks post-differentiation. (E) The average ESPSC shape in TH-positive cells before and after the addition of D-AP5. Current values were normalised to allow for easier comparison (F) Graph showing the mean total area under the graph during 60 second recordings before and after the addition of the receptor antagonists listed above. Error bars ± S.E.M. *indicates significance using a two-way paired t-test at p=0.05.

3.3.5 The Development of Calcium Waves

SNc DA neurons control pacemaking partially via Ca^{2+} influx through VGCCs (Chan et al., 2007). To determine whether Ca^{2+} waves develop in hiPSC-derived DA neuron-containing cultures, cells were loaded with the fluorescent Ca^{2+} dye Calcium Green-1 each week from 0-6 weeks post-differentiation (**Figure 3.15A**). In all experiments the results are obtained from 40 second fluorescence intensity recordings (n=3, with 50 cells tested per repeat). The results here look at the general cell population and therefore do not distinguish between TH-positive and TH-negative cells.

Calcium Green-1 fluorescence was observed in all the cells in the cultures. Fluorescence was seen in both the soma and dendrites, with soma being noticeably brighter. Ca^{2+} waves were present from week 0 in a small percentage of cells, with the percentage exhibiting waves increasing from week 0 to week 6 (**Figure 3.15B, 3.15C**). Waves were initially disordered but became regular in frequency between week 0 and week 6, with week 6 cells often displaying waves in regularly spaced bursts (**Figure 3.15B, 3.16**). The frequency of Ca^{2+} waves initially increased, between weeks 0 and 1, then remained consistent until week 6 (**Figure 3.15D**). The performance of a one-way ANOVA showed a statistically significant effect of time in culture on Ca^{2+} wave frequency ($F=6.303$, $p=0.002$). A Tukey comparison showed that frequency was statistically different from week 0 at week 1, then did not statistically differ from the previous week at each subsequent week (week 0 vs 1, $p=0.007$; week 1 vs 2, $p=0.933$, week 2 vs 3, $p=0.845$; week 3 vs 4, $p=0.66$; week 4 vs 5, $p=0.551$; week 5 vs 6, $p=0.487$).

Since Ca^{2+} influx is implicated in the pathology of PD, the mean total area under the graph was calculated as an estimate of total Ca^{2+} influx. The mean total area under the graph remained consistent from weeks 0 to 5, with a massive increase being observed at week 6 (**Figure 3.15E**). The performance of a one-way ANOVA showed there was a statistically significant effect of time in culture on the mean total area under Ca^{2+} waves ($F=5.502$, $p=0.004$). A two-sided Dunnett test showed that mean total area only differed from week 0 at week 6 (weeks 1-5, $p>0.9$; week 6, $p=0.002$). These data suggest that a large increase in Ca^{2+} influx was occurring at week 6. This ties in with the observed increases in action potential firing frequency and area under synaptic events, likely indicating that a shift in maturity is occurring at week 6 in culture.

Ca^{2+} waves can be dependent on or occur independently of action potential firing (Moreno-Juan et al., 2017; Stellwagen et al., 1999). To determine whether Ca^{2+} waves

in hiPSC-derived DA neurons are action potential dependent, recordings were taken before and after the addition of the Na_V antagonist TTX. Addition of 1 µM TTX to the extracellular solution prevented Ca^{2+} waves in the majority of week 4-6 cells (**Figure 3.17A**). Isolated waves still occurred in a small percentage of cells (**Figure 3.17B**). It was hypothesised that spontaneous synaptic events could be producing these TTX-insensitive waves. To determine whether glutamate receptor activation could cause Ca^{2+} waves, 1 mM L-glutamic acid was added to cells during Ca^{2+} imaging. All cells tested displayed a large peak in fluorescence upon L-glutamic acid addition in the presence of TTX which was followed by a decrease in fluorescence from baseline (**Figure 3.17C**).

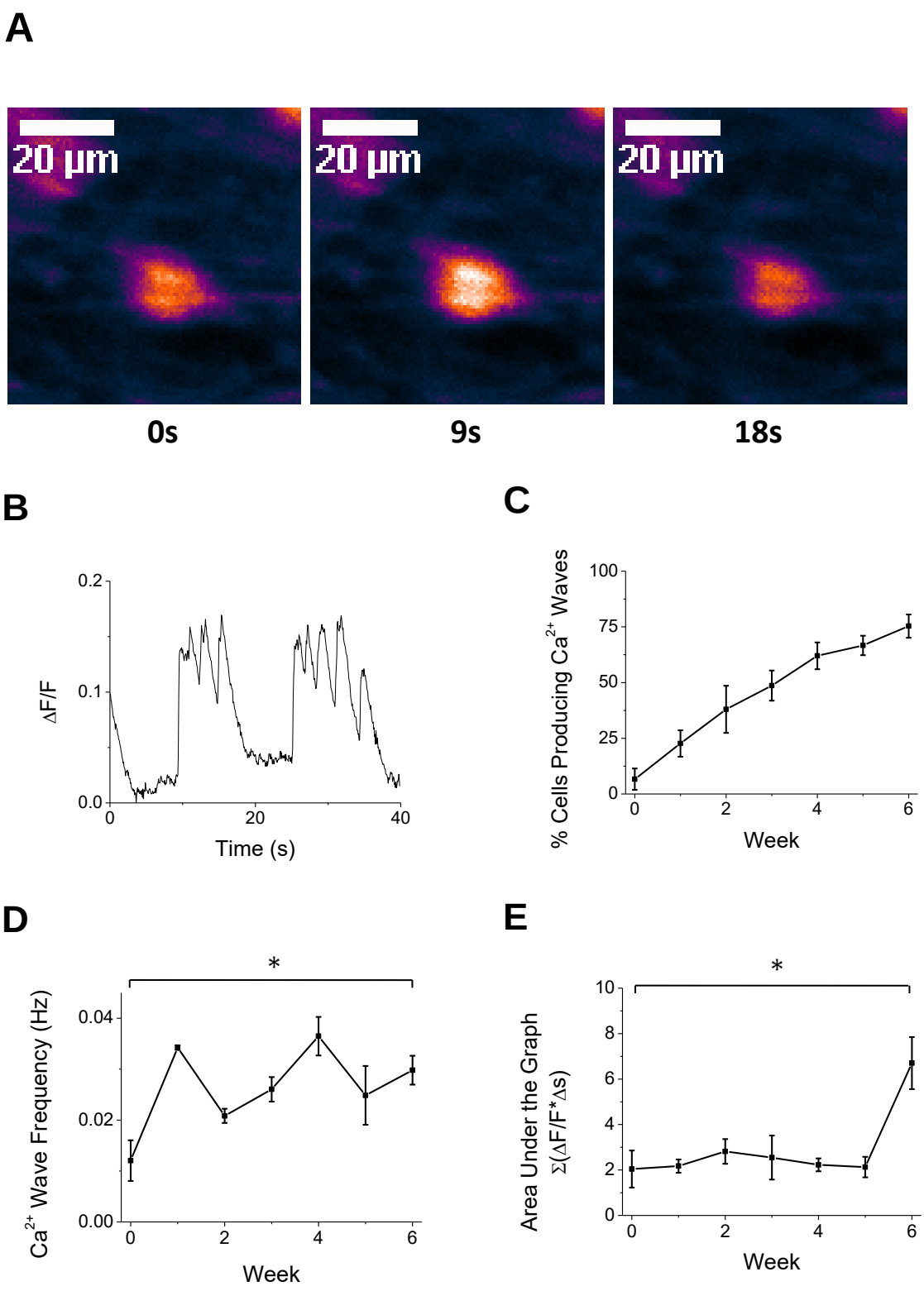

Figure 3.15 - The development of Ca^{2+} waves in hiPSC-derived dopaminergic neuron-containing cultures. (A) Representative false colour fluorescence image of a week 6 cell loaded with Calcium Green-1 that is exhibiting a Ca^{2+} wave (B) Representative fluorescence intensity recording from a week 6 cell producing Ca^{2+} waves. Graphs showing (C) the percentage of cells that were producing Ca^{2+} waves (D) the mean wave frequency and (E) the mean total area under the graph for cells from 0-6 weeks post-differentiation. Error bars ± S.E.M. *indicates statistical significant using a one-way ANOVA at p=0.05.

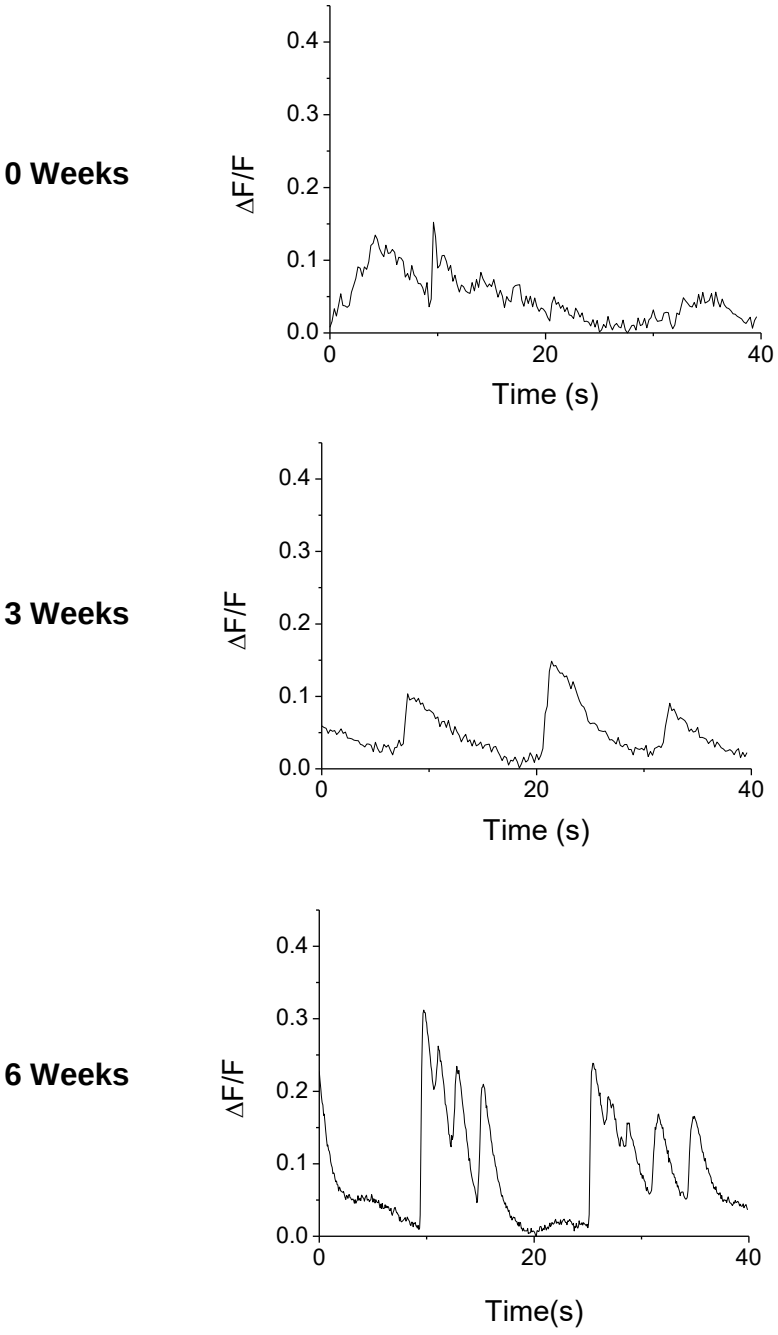

Figure 3.16 - The maturation of Ca^{2+} waves in cultures containing hiPSC-derived dopaminergic neurons. Representative fluorescence intensity recordings from cells loaded with Calcium Green-1 at 0, 3 and 6 weeks post-differentiation. Changes in fluorescence expressed as ΔF/F.

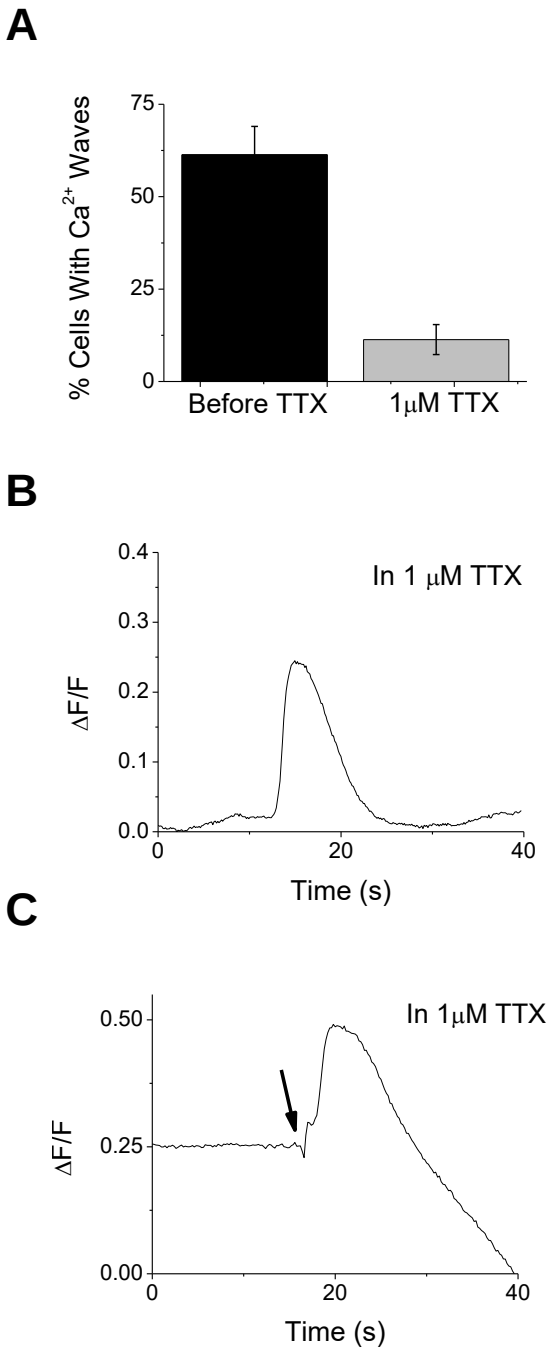

Figure 3.17 - The action potential dependence of Ca^{2+} waves. (A) Graph showing the mean percentage of week 4-6 cells that were producing Ca^{2+} waves before and after the addition of TTX. Representative fluorescence recordings from week 4 Calcium Green-1 loaded cells in the presence of TTX showing (B) waves still occurring in the presence of TTX and (C) the addition of L-glutamic acid in the presence of TTX. The arrow indicates the addition of 1 mM L-glutamic acid. Error bars ± S.E.M. *indicates statistical significance using a two-way Student's t-test at p=0.05.

3.4 Discussion

This chapter has focused on the early electrical development of hiPSC-derived DA neurons in culture. A previous study of these neurons found that spontaneous pacemaking, synaptic currents and Ca^{2+} waves developed between 6-12 weeks post-differentiation from hiPSCs (Hartfield et al., 2014). The results I present here compliment that work, looking instead at the early period of development from 0 to 6 weeks post-differentiation from hiPSC-derived neural progenitors.

Here I show that many phenotypic traits that are typical of DA neuron electrophysiology developed at earlier time points than previously described. Spontaneous action potential firing that resembled pacemaker activity was observed, though by examining in detail the effects of neurotransmitter receptor blockers on this excitability it was revealed that very little, if any, truly intrinsic activity had developed after 6 weeks in culture. Instead, activity was seen to be driven by activation of ionotropic glutamate receptors and D2 receptors. The presence of other inputs such as metabotropic glutamate and GABA receptors also cannot be discounted.

Despite this lack of intrinsic activity, TH-positive cells in these cultures displayed a natural propensity towards excitable states, being significantly more likely to fire action potentials and produce spike trains than TH-negative cells. SNc DA neurons *in-vivo* display a similar inclination towards excitability that is thought to be partially due to the expression of $Ca_V1.3$ VGCCs (Chan et al., 2007; Guzman et al., 2009). Data here provide evidence suggesting that excitability in hiPSC-derived DA neurons is also L-type VGCC dependent, with action potential firing being blocked by the L-type VGCC antagonist nifedipine in one TH-positive cell. Since this was performed in only one cell, whether this is representative of the general population cannot be concluded.

TH-positive cells also developed significantly larger voltage-dependent Ca^{2+} currents than TH-negative cells by week 6, possibly explaining their increased excitability. The I/V relationship for Ca^{2+} currents was shifted towards a more negative potential in TH-positive cells compared to TH-negative cells, perhaps indicating that Ca^{2+} currents in these two populations are comprised of different channel types. $Ca_V1.3$ channels are known to open at more negative potentials than other L-type channels (Zampini et al., 2010), which, if they are expressed in these neurons in culture, could explain the shift. Whether or not $Ca_V1.3$ is expressed in these cells is investigated in Chapter 4. $Ca_V1.3$ channels have previously been described as "ideal for pacemaking" due to their

activation and inactivation properties (Chan et al., 2007). They have been shown to be responsible for slow, subthreshold Ca^{2+} waves in SNc neurons that help control pacemaker activity (Guzman et al., 2009). Data here shows that Ca^{2+} waves were seen in cells in culture, though these were TTX-dependent and not subthreshold. It is worth noting that I investigated Ca^{2+} waves in the cell body and not in dendrites, hence the presence of subthreshold waves increasing cell excitability in these regions in culture should not be discounted. A previous study of these neurons in culture identified Ca^{2+} waves in dendrites (Hartfield et al., 2014).

All of these traits (excitability, VGCC currents, synaptic currents, and Ca^{2+} waves) began developing from roughly 1-2 weeks in culture and clearly showed a major shift in maturity between weeks 5 and 6. All in all, there is evidence to suggest that the increased excitability of TH-positive cells in these cultures was likely due to the development of VGCC currents, a trait that is critical to pacemaking in SNc DA neurons in animal models.

3.4.1 Confirmation of a Dopaminergic Neuronal Phenotype

A previous study and manufacturer data have described differentiated cultures using the STEMdiff protocol as containing 15-30% TH-positive neurons, >90% expressing neuronal markers, with <10% of the population expressing astrocyte markers (Hartfield et al., 2014). Here I confirm this, with ~25% TH-positive neurons and >80% NeuN positive cells after 6 weeks in culture. The remaining NeuN-negative cells may therefore represent astrocytes present in the cultures.

The relatively small percentage of the total population that is TH-positive meant that, without a method to positively identify cells that had undergone electrophysiological characterisation, the majority of cells analysed would likely not be TH-positive and would provide an inaccurate analysis. Lucifer Yellow staining was chosen as a method to identify cells as TH-positive or TH-negative after immunostaining, allowing them to be matched to their corresponding electrical recordings. Even with Lucifer Yellow staining, many of the experiments suffer from relatively low N numbers. This is due to the random nature of selecting cells for whole cell recording and the loss of ~50% of Lucifer Yellow loaded cells during the immunostaining procedure. Cells at later weeks (weeks 5-6) were also far more likely to detach from the coverslips during transfer to the extracellular solution used for electrophysiological recording. The "hit rate" of TH-

positive cells could be increased to ~40-50% by selecting cells for whole cell recording based on their morphology (See Chapter 4) and the experiments were repeated as many times as possible in an attempt to increase numbers. Time constraints have still left many of the results relatively statistically underpowered, though in many experiments the differences were still clear enough to draw meaningful conclusions.

It is worth noting that the TH-negative population likely contains a mixture of neuronal and non-neuronal cell types, as seen by NeuN staining. Differences in excitability and current density may therefore be explained by the presence of non-excitable cells in the results. Attempts at NeuN staining to discount non-neuronal cell types were attempted but could not be distinguished from Lucifer Yellow staining.

The neuronal nuclei marker NeuN is not expected to stain neural progenitors as it is typically a marker for mature differentiated neurons (Gusel'nikova & Korzhevskiy, 2015). hNPCs here, however, clearly showed NeuN staining at concentrations lower than those previously used in the literature, which have typically used NeuN antibodies at concentrations of 1:10 or 1:20 compared to the 1:50 dilution used here (Eriksson et al., 1998). This could be a consequence of the differentiation protocol used to derive them from hiPSCs, with them being further towards maturation than typical NPCs *in-vivo*. It could also possibly be a retention of a phenotype from a previous lineage. The cells used here, hiPSC-derived hNPCs, were originally derived from cord blood which are unlikely to have been expressing NeuN. The change in staining that was observed in later weeks, with the cell body and processes showing NeuN staining, suggests the staining of NPCs was not due to non-specific staining. This is backed up by the fact that NeuN did not stain all of the nuclei in culture. This finding suggests at a difference between the hiPSC-derived NPCs used here and NPCs *in-vivo* in terms of their expression of typically mature neuronal markers. NeuN antibodies stain for a protein called Fox-3, which is downregulated by expression of doublecortin during NPC division (Kim et al., 2009). hiPSC-derived NPCs staining for NeuN could suggest that they were no longer dividing, perhaps due to the high density of the population at the time of staining, or that progenitor formation and cell division in these neurons is controlled through other mechanisms that are different from neuronal development *in-vivo*. Staining for a second neuronal marker such as beta III tubulin or MAP2 would have solved whether this was specific for NeuN or the NeuN antibody or whether these NPCs were generally more mature than expected.

3.4.2 The Development of Excitability

Here I show that TH-positive cells began to spontaneously fire action potentials in culture from 2 weeks post-differentiation. *In-vivo,* SNc neurons have been described as firing tonically, with burst firing seen in response to a large quantity of synaptic input (Grace & Bunney, 1984; Tepper et al., 1998; Guzman et al., 2009). Both of these modalities were seen here. TH-positive cells here were more likely to be firing action potentials and more likely to produce multiple action potential "trains" in response to current injection, indicating an innate inclination towards more excitable states. These trains have previously been seen in both animal models and hiPSC-derived DA neurons (Bayer et al., 2007; Hartfield et al., 2014). Here I show that the firing frequency and resting membrane potential were no different between TH-positive and TH-negative cells, though this could be due to low N numbers and a subsequent lack of statistical power.

Spontaneous action potential firing in hiPSC-derived DA neurons has previously been described in the literature (Hartfield et al, 2014). However, whether the observed activity was intrinsically or synaptically driven was not investigated. Here I show that spontaneous firing was not intrinsic, being dependent on glutamatergic and D2/3 DA input. Glutamatergic inputs and D2 autoreceptors have been seen regulating firing in the SNc neurons of mice and guinea pigs respectively (Cragg & Greenfield, 1997; Pearlstein et al., 2015), along with an inhibitory GABAergic feedback loop in rats (Grace & Bunney, 1985). Data here represents the first direct evidence for glutamatergic and DA input in hiPSC-derived DA neurons. No clear regulation of firing frequency by $GABA_A$ receptors was identified here in TH-positive cells in culture, though a small non-significant decrease in firing frequency compared to controls was observed that may or may not become significant with higher statistical power. Considering the calculated -42 mV equilibrium potential for Cl^-, which is the major ion flowing through GABA receptors (Siegel et al., 1999), it is unlikely that any effect of GABA receptors would be seen here in whole cell current clamp experiments. This is due to the membrane potential of the cells tested often resting around the equilibrium for Cl^-, meaning there would be little to no driving force through GABA receptors.

Two TH-positive cells were identified here that fired action potentials in the presence of a glutamate receptor antagonist. Several reasons can be proposed for this: incomplete block of glutamate receptors was allowing firing to continue; other neurotransmitters such as dopamine or GABA were responsible for firing in these cells; or these cells are

innately exhibiting pacemaking independently of outside input. Given the identified inclination of TH-positive cells towards excitability, it is possible that given more time in culture these neurons have the ability to develop intrinsic pacemaker activity. Synaptic activity is critical for the correct development of neuronal networks *in-vivo* (Donovan, 1999). It could therefore be the case that synaptic input is required for the development of intrinsic pacemaking in hiPSC-derived DA neurons.

L-type VGCCs are critical for pacemaking in SNc DA neurons *in-vivo* (Chan et al., 2007; Guzman et al., 2009). Attempts were made here to determine whether the same is true of hiPSC-derived DA neurons. Unfortunately, due to loss of cells during immunostaining only one TH-positive cell could be recovered. This cell, however, displayed activity that was L-type dependent. Whether this is representative of all the DA neurons in culture cannot be determined, yet it still represents some of the first direct evidence for L-type VGCC-dependent excitability in hiPSC-derived DA neurons in culture.

All in all, the results presented here point to many similarities (excitability, L-type dependence, glutamatergic and dopaminergic input) and differences (little to no intrinsic pacemaking, perhaps no GABAergic feedback) between hiPSC-derived DA neurons and SNc neurons in animal models. Given the observed differences in excitability and synaptic connectivity, care should be taken over the translation of results to *in-vivo* models. Many of these phenotypic properties continued to mature with time in culture and, along with the finding that TH-positive cells showed a tendency towards more excitable states, there is evidence to suggest that truly intrinsic activity may develop with more time in culture.

3.4.3 The Development of Ion Channel Populations

Voltage-gated ion channels underlie excitability in all neuronal cells, with differential expression of channel types responsible for the range of excitable phenotypes seen in the body (Prinz et al., 2003). It was important to investigate any changes in voltage-gated ion channel currents in TH-positive cellss post-differentiation to determine if they are the likely cause of TH-positive cells being more inclined towards excitability that TH-negative cells in culture.

It was important, firstly, to identify changes in passive cell properties. Whole cell capacitance is a measure of cell surface area, assuming a specific capacitance of 0.8-1.0

$\mu F/cm^2$. It was therefore important to correct for cell capacitance to determine true changes in current density. Here I show that input resistance was lower in TH-positive cells than TH-negative cells, though this was not significant perhaps due to low statistical power. Lower input resistance would indicate a decrease in responsiveness to synaptic inputs, since Ohm's law would give lower changes in membrane potential in response to current input. It also decreases with an increase in whole cell capacitance (due to more open channels and higher membrane leak) and can be explained by the slightly higher, though once again not statistically significant, increase in whole cell capacitance in TH-positive cells.

Here I show that Na_V and K_V current densities increased weekly but showed no difference between TH-positive and TH-negative cells, indicating they are likely not responsible for the excitability differences between the two. Changes in channel distribution were not investigated and cannot be discounted as a possible cause of differences in excitability. Space clamp issues could also prevent proper clamping of current or voltage within axons and dendrites meaning that large current densities in these regions may not be identified. Ca^{2+} current densities were significantly larger in TH-positive cells and, given that $Ca_V1.3$ channels underlie excitability in SNc neurons *in-vivo*, could explain the increased excitability of hiPSC-derived TH-positive cells in culture. The negative-shifted voltage-activation of $Ca_V1.3$ channels is also a likely explanation for the negative-shifted IV relationship for VGCC currents identified in TH-positive cells here (Zampini et al., 2010) though could also be due to T-type channels which are dendritically expressed in SNc DA neurons in rats (Dufour et al., 2014). $Ca_V1.3$ distribution is investigated in Chapter 4. This negative shift allows increased Ca^{2+} influx at subthreshold membrane potentials. This provides subthreshold oscillations in membrane potential, heightening sensitivity to other near-threshold stimuli. The increased excitability in TH-positive cells may therefore be due to an increased VGCC current density that acts to heighten their sensitivity to other stimuli, though the observed differences in current density could also be due to the presence of non-neuronal cells within the TH-negative population.

3.4.4 The Development of Synaptic Inputs

Synaptic inputs are an important regulator of pacemaking in the SNc neurons of animal models (Blythe et al., 2007). In experiments here, co-localisation of the presynaptic

marker synaptophysin, a protein that is ubiquitously expressed at the presynaptic terminal, with the postsynaptic marker PSD-95, an NMDA receptor-associated protein, was used to indicate the formation of synapses in TH-positive cells in culture. Regions of co-localisation were identified in TH-positive cells, indicating that these cells likely form synapses in culture. The co-localisation method used involved creating a mask of the TH-positive region before semi-automated co-localisation in SynapCountJ was performed. The number of counted synapses was highly dependent upon the intensity of staining and the threshold values selected for each channel, therefore rather than being used as a definite indicator of the presence of synapses or their numbers it was instead used as supporting evidence to justify an electrophysiological characterisation of synaptic currents. Despite this, the number of synapses counted roughly correlates to those found in a previous study on synapses in cortical neurons that used a similar staining method. This previous study suggested a count of 5 synapses per neuron after 1 week in culture, with the number increasing 30 fold after 3 weeks (Cullen et al., 2010). They also found that numbers were highly dependent upon plating density. The plating density here (20 000/cm^2) was lower than that used in this previous study (50 000/cm^2) which may explain the lower numbers observed here at later weeks compared to this previous study.

Here I show that excitatory spontaneous postsynaptic currents (ESPSCs) were first observed from 2 weeks post-differentiation. The amplitude and frequency of events was highly variable and did not give clear indications of differences between weeks. Area under the events was selected as an indicator of changes. It has been previously used in the literature as it is sensitive to all factors including amplitude, frequency and the duration of events, giving an indication of the total ion flux during the measured period (Potapenko et al., 2011). A large increase in area at week 6 was identified in all cells, possibly due to an increase in the number or strength of synapses or other developmental changes that occur at this time. This likely indicates a maturation of the synapses in culture.

NMDA and AMPA/Kainate receptors may be responsible for the observed ESPSCs under the conditions tested, with data here showing that the simultaneous addition of antagonists for these receptors almost completely abolishing ESPSCs. Small excitatory currents remained in the presence of these antagonists, which could be accounted for by excitatory GABA currents caused by the -42 mV equilibrium potential. Due to time constraints this could not looked at in any depth. Further evidence for the presence of

NMDA and AMPA receptors comes from two sources: First, from PSD-95 staining, which associates with NMDA receptors in postsynaptic regions. Second, from the change in ESPSC shape upon the addition of an NMDA receptor antagonist. AMPA and NMDA receptors have different kinetic properties with AMPA-associated ESPSCs being of shorter duration than the extended decay time seen with NMDA-associated currents (which are often AMPA-dependent) (Jeun et al., 2009). This effect was identified here, with the addition of the NMDA receptor antagonist D-AP5 reducing the duration of ESPSCs.

Given that cells begin to fire action potentials from 2 weeks in culture and this activity is largely dependent on glutamate receptors, it is likely that the development of ESPSCs is an instigator of this activity. Cultures here likely began to form mature networks at week 6, as seen by the large increase in the area under synaptic events that occurred at this time point. This correlates with the large increase in action potential firing frequency that occurred after the same time in culture.

Co-expression of AMPA and NMDA receptors is common throughout the nervous system and is critical to processes such as synaptic plasticity (Shi et al., 1999). Since NMDA receptors are ligand and voltage-gated while AMPA receptors are simply ligand-gated, NMDA receptors require a depolarisation for their activation (Bliss & Lomo, 1973). Therefore, they are often co-localised AMPA receptors and the two receptor types are able to alter the electrical response of a neuron based on their expression. Evidence has shown that block of NMDA receptors can increase firing frequency in spinal neurons by reducing background NMDA activity (Thaweerattanasinp et al., 2016). It has also been shown that block of AMPA receptors can have a similar effect in models of DA neurons depending on which other currents are present (Zakharov & Kuznetsov, 2015). These differing roles are backed by their kinetic properties. AMPA receptors typically allow the flow of Na^+/K^+ over Ca^{2+} (though this differs based on subunit composition), are fast activating and inactivating, and have a large unitary conductance. NMDA receptors are typically slower to inactivate and have a smaller unitary conductance (Hille, 2001). The balance of these receptor currents therefore appears to be important for determining the electrical response of a synapse and/or neuron. AMPA and NMDA receptors have long been known to shift their numbers and localisation in response to electrical activity, providing the basis for synaptic plasticity. This allows the strengthening or weakening of specific synapses (Lau & Zukin, 2007; Malinow & Malenka, 2002). AMPA receptors

are believed to be responsible for short term changes in synaptic strength while NMDA receptors, through Ca^{2+} dependent processes, control changes in long term potentiation (Rao & Finkbeiner, 2007). Synaptic plasticity is known to be critical during the development of mature neuronal networks (Shi et al., 1999), therefore the increase in firing frequency and synaptic currents observed in this thesis is likely to be due to increases in the expression of AMPA and NMDA receptors as these neurons mature. Ca^{2+} influx through NMDA receptors is known to be critical for synaptic plasticity (Rao & Finkbeiner, 2007). The increase in Ca^{2+} influx seen via Ca^{2+} imaging at week 6 provides further evidence for synaptic activity occurring due to increased expression and/or localisation of NMDA receptors.

3.4.5 The Development of Calcium Waves

Somatodendritic Ca^{2+} waves have been identified in rat SNc neurons *in-vivo* and in hiPSC-derived TH-positive cells in culture. These are believed be an underlying driver for pacemaker activity (Guzman et al., 2009; Hartfield et al., 2014). Here I confirm these previous studies, with hiPSC-derived DA neuron-containing cultures producing Ca^{2+} waves in their soma that increase in definition and rhythmicity up to 6 weeks post-differentiation. Once again, I use the area under the graph as a measure of changes in total ion flux. A large increase in Ca^{2+} influx at week 6 was observed and, since an increase in ion flux due to synaptic events was also observed at this time point, is likely to be due to synaptic activity. This provides further evidence for the formation of mature neuronal networks at this time point.

These waves have previously been described as subthreshold, i.e., occurring below the threshold for action potential firing. Here, in all cultures tested, Ca^{2+} waves were TTX-sensitive in all but a small proportion of cells. This indicates that the majority of Ca^{2+} influx was not sub-threshold and was dependent upon action potential firing. It was hypothesised that the remaining cells were producing waves innately or due to spontaneous neurotransmitter release. The addition of glutamate and dopamine receptor antagonists would have determined whether the remaining cells produced Ca^{2+} waves intrinsically, but due to time constraints this experiment has not yet been performed. Addition of L-glutamic acid caused an increase in intracellular Ca^{2+} and, although a crude manipulation, demonstrates that Ca^{2+} waves can also be generated by glutamate

receptor activation. This also provides further evidence for the presence of glutamate receptors, specifically NMDARs, as they pass Ca^{2+} in response to glutamate activation.

The results presented here confirm that these cells develop Ca^{2+} waves in culture as they do *in-vivo*, though they are likely driven by action potential firing and synaptic input. The hyperpolarised activation potential of $Ca_V1.3$ could be allowing subthreshold activation as a cell approaches threshold, increasing the likelihood of a cell reaching the threshold for firing. The majority of Ca^{2+} influx then occurs in a wave-like fashion following an action potential. Previous studies in SNc DA neurons have found that Ca^{2+} influx during action potentials acts to control the shape and timing of pacemaking (Surmeier et al., 2017). It is important to note that Ca^{2+} waves here were investigated in the soma and not in dendrites. Subthreshold waves in dendrites have been previously described in the literature and cannot be discounted. Many classes of voltage-gated ion channels are dendritically expressed in rat SNc neurons, hence there are likely differences in electrical properties between the soma and the dendrites of these neurons (Dufour et al., 2014). It is also possible, given the relatively short time in culture, that subthreshold waves begin to develop in more mature differentiated neurons. As such it can be concluded that sub-threshold Ca^{2+} waves did not develop in the soma up to 6 weeks post-differentiation.

Chapter 4

$Ca_V1.3$ Expression and Selective Cell Death in hiPSC-Derived Dopaminergic Neurons

Abstract

$Ca_V1.3$ L-type voltage gated calcium channels (VGCCs) in dopaminergic (DA) neurons of the substantia nigra pars compacta (SNc) are believed to contribute towards their selective cell death in Parkinson's disease (PD), though whether human induced pluripotent stem cell (hiPSC) -derived DA neurons express this channel had not been established. In this chapter I have characterised $Ca_V1.3$ immunostaining in this cell type during the first 6 weeks post-differentiation from hiPSC-derived neural progenitor cells (hNPCs). Whether $Ca_V1.3$-positive cells were more vulnerable to cell death in response to the DA-specific toxin 6-hydroxydopamine (6-OHDA) or in response to glutamate-induced excitotoxicity was then investigated. The results show that two morphologically distinct populations of hiPSC-derived DA neurons could be identified that were either $Ca_V1.3$-positive or $Ca_V1.3$-negative. A novel, single-stain cell death assay was then characterised and used to show that 6-OHDA toxicity developed specifically in neurons expressing the DA marker tyrosine hydroxylase (TH). All cells in culture displayed a resistance to excitoxicity at concentrations of extracellular glutamate that have previously been seen to induce cell death in neuronal cell types. No differences in cell death between $Ca_V1.3$-positive and $Ca_V1.3$-negative DA neurons were identified indicating that, at least during the 0-6 week development period investigated, the presence of $Ca_V1.3$ does not increase the susceptibility of hiPSC-derived DA neurons to cell death in response to 6-OHDA or extracellular glutamate. Data here provides valuable information on the suitability of hiPSC-derived DA neurons for use as an *in-vitro* human PD model, hopefully lead to more targeted, efficient design of PD studies that use these neurons.

4.1 Introduction

The selective vulnerability of SNc DA neurons in PD is believed to be partially due to Ca^{2+} influx through VGCCs during pacemaking. VGCC-dependent pacemaking in these neurons causes excessive Ca^{2+} influx into the cytosol. This extra Ca^{2+} is removed by mitochondria at special junction sites with the endoplasmic reticulum. This causes a concentration-dependent hyperpolarisation of the mitochondrial membrane which results in reactive oxygen species (ROS) production during complex I of the electron transport chain (Pacelli et al., 2015). This in turn leads to a number of ROS-protein interactions that are damaging to the cell, including oxidised protein products such as 4-Hydroxynonenal (HNE), damage to the ubiquitin-proteasome system leading to alpha-synuclein aggregation, and promotion of apoptosis through caspase activation (Okada et al., 1999; Liu & Kato, 2000; Hyun et al., 2002).

SNc DA neurons express a relatively rare class of L-type VGCC, known as $Ca_V1.3$. The negative-shifted voltage-activation of $Ca_V1.3$ channels compared to other L-type VGCCs has seen them described as "ideal for pacemaking" and they are believed to be responsible for subthreshold somatodendritic Ca^{2+} waves that help sustain SNc pacemaking *in-vivo* (Chan et al., 2007; Guzman et al., 2009). Inhibition of $Ca_V1.3$ channels can protect DA neurons from the toxic effects of the mitochondrial toxins 1-methyl-4-phenyl-1,2,3,6-tetrahydropyridine (MPTP), rotenone and 6-OHDA at concentrations that would normally cause cell death (Chan et al., 2007). The use of L-type antagonists for the treatment of hypertension is associated with a 30% reduction in the risk of developing PD and slows the progression of the disease even when initiated after diagnosis (Gudala et al., 2015). Due to these effects, clinical trials for $Ca_V1.3$-specific antagonists such as isradipine are in progress to determine if there is a clinical benefit to their use in PD (Biglan et al., 2017).

Studies into the mechanism of selective cell death in PD have used hiPSC-derived DA neurons as a model system in recent years (Woodard et al., 2014) but $Ca_V1.3$ expression in this cell type has not been characterised. Selective susceptibility of hiPSC-derived DA neurons to MPTP has been demonstrated through its effects on the mitochondrial membrane potential (Hartfield et al., 2014). However, whether susceptibility to these toxins results in an increase in cell death, or if the effect is selective for DA neurons within a mixed population culture, has only been demonstrated at lower concentrations (Nguyen et al., 2011) and no information is available over whether $Ca_V1.3$ expression affects their susceptibility to 6-OHDA. SNc DA neurons have also shown susceptibility

to glutamate excitotoxicity in the presence of MPTP, though whether hiPSC-derived DA neurons show a similar susceptibility has not been investigated (Meredith et al., 2009).

Research in this chapter has focused on whether hiPSC-derived DA neurons showing immunostaining with antibodies specific for $Ca_V1.3$ in culture. If and when these neurons show selective death in response to the DA specific toxin 6-OHDA or in response to extracellular glutamate was then characterised in cells from 0-6 weeks post-differentiation at the level of the general cell population, in DA neurons and in $Ca_V1.3$-positive DA neurons to determine any differences in susceptibility between these cell populations.

My results show that $Ca_V1.3$ staining is ubiquitous across the majority of cells in culture from week 0 hNPCs to week 6 differentiated neurons. Morphologically distinct populations of $Ca_V1.3$-positive and $Ca_V1.3$-negative TH-positive neurons were identified from week 1 that may correspond to populations of SNc neurons that have previously been identified in rat models (Robertson et al., 1991; Richards et al., 1997). 6-OHDA toxicity was found to be more specific for TH-positive neurons than TH-negative neurons, with no difference in toxicity between $Ca_V1.3$-positive and $Ca_V1.3$-negative phenotypes. In contrast, all neurons in culture from 0-6 weeks post-differentiation displayed a resistance to glutamate-induced excitotoxicity at concentrations that have previously been reported to result in cell death in other neuronal cell types in culture (Kritis et al., 2015).

By performing this characterisation, valuable information on whether early stage (0-6 week) hiPSC-derived DA neurons are suitable for studying the mechanisms involved in selective cell death in PD has been gained. The benefits and limitations of using these cells to model PD will be better understood, hopefully lead to more targeted, efficient design of PD studies that use hiPSC-derived DA neurons.

4.2 Methods

4.2.1 Culture & Expansion of Human Neural Progenitors

The protocols for culture and expansion followed the product description guidelines from Axol Bioscience. Cells and reagents were obtained from Axol unless otherwise stated. Human iPSC-derived neural progenitor cells (hNPCs) were expanded on sterile 12 well tissue culture plates (Corning) pre-coated with SureBond-XF at a density of 80 000/cm^2 in plating-XF medium. 24 hours after plating, media was replaced with neural expansion-XF media supplemented with 20 ng/ml FGF2 and 20 ng/ml EGF. Cells were passaged every 5 days and expanded until an optimal quantity were obtained for differentiation. Cells were incubated at 37^{o}C and 5% CO_2.

4.2.2 Differentiation of hNPCs to Dopaminergic Neurons

hNPCs were passaged in expansion-XF medium and plated at a density of 30 000/cm^2 onto coverslips pre-coated with SureBond-XF. 24 hours after passage, media was changed to STEMdiff^{TM} dopaminergic neuron differentiation medium (STEMcell) supplemented with 200ng/ml sonic hedgehog (SHH) (Millipore). Media was changed daily for 14 days. The cells were then passaged and plated at a density of 20 000/cm^2 onto glass coverslips pre-coated with SureBond-XF. Media was changed to STEMdiff^{TM} dopaminergic neuron maturation medium 1 (STEMcell). Full media changes were performed every 48 hours for 5 days. Media was then changed to maturation medium 2 (STEMcell) and replaced every 48 hours up to a total culture time of 6 weeks. Cells were incubated at 37^{o}C and 5% CO_2.

4.2.3 Immunofluorescence Staining

Coverslips were washed in PBS pre-warmed to 37^{o}C before fixation in 4% paraformaldehyde for 10 minutes at room temperature (21^{o}C). 3 washes with ice cold PBS were performed and cells were permeabilised with 0.1% Triton X-100 for 10 minutes at 21^{o}C. Coverslips were washed for 3x 5 minute washes with PBS containing 0.1% Tween-20 at 21^{o}C before a 30 minute incubation at 21^{o}C in PBS containing 1% BSA and 0.1% Tween-20 to prevent non-specific antibody binding. Primary antibody

incubation was performed at 21ºC for 1 hour in PBS containing 1% BSA and 0.1% Tween-20. Coverslips were washed 3x for 5 minutes with PBS containing 0.1% Tween-20 at 21ºC. Secondary antibody incubation was performed for 1 hour in the dark at 21ºC in PBS containing 1% BSA. All secondary antibodies were conjugated with AlexaFluor fluorescent dyes. Coverslips were then washed 3x for 5 minutes with PBS in the dark at 21ºC before mounting on glass microscope slides with the mounting medium Mowiol® 4-88 and sealing with nail polish. Slides were stored at 4ºC until analysis. All reagents were acquired from Sigma Aldrich and all antibodies were from Abcam unless stated.

The antibodies used were I.) rabbit anti- $Ca_V1.3$ (Alomone Labs, 1:500) with a goat anti-rabbit AlexFluor-488 secondary (1:500) and II.) chicken anti-Tyrosine Hydroxylase (1:500) with a goat anti-chicken AlexFluor-568 secondary (1:500).

4.2.4 Confocal Microscopy

Fixed coverslips were imaged using a TCS SP5 II confocal microscope (Leica) with a 63x oil objective (NA 1.3). Samples were excited using an argon or white light laser. Images were collected using a Hamamatsu camera with 3x frame averaging at an image resolution of 1024x1024 pixels.

Data Analysis: Images were analysed in ImageJ. Calculation of the percentages of immunostained cells was performed manually using the cell count plugin. Mean values are from 5-10 fields of view per experimental repeat. Cell length, area and number of projections were calculated from TH-immunostained images. Cell length was calculated as a straight line between the two furthest visible points of the cell. Cell area was taken as the total 2D surface area (including soma and processes) and was calculated using the analyse particle feature. Number of processes was analysed by drawing a circular region of interest around the soma of each cell and manually counting the number of processes that cross the circle.

4.2.5 Toxicity Assay

Confirmation of the staining protocol: 0-6 week differentiated neurons were incubated at 37ºC, 5% CO_2 in 24 well plates with 100 µM Etoposide for 1 hour to induce cell death. Cells were stained with the live cell nuclei stain Hoechst 33342 (1 µM). In some experiments the cells were co-stained using the dead cell nuclei stain

propidium iodide (1 µM). Staining was performed for 10 minutes at 37ºC, 5% CO_2. Cells were then washed 5 times with PBS pre-warmed to 37ºC before imaging at room temperature (21ºC). This confirmed that dead cells were stained brighter than live cells using Hoechst, hence Hoechst alone could be used to indicate the proportion of cell death using the bright: total nuclei ratio. This approach was used in the subsequent experiments.

Toxicity Assay: 0-6 week differentiated neurons were taken weekly and incubated at 37ºC, 5% CO_2 for 24 hours with varying concentrations of 6-OHDA or L-glutamic acid. The cells were then washed 5x using PBS pre-warmed to 37ºC before staining with Hoechst 33342 (1 µM) for 10 minutes at 37ºC, 5% CO_2. The cells were then washed 5 times with PBS pre-warmed to 37ºC before imaging. After imaging, cells were immunostained for $Ca_V1.3$ and TH as described in **4.2.3**. Images were once again taken after staining.

Imaging: Images were collected using a FLoid Cell Imaging Station USB microscope with a 20x objective (NA 0.45) at room temperature (21ºC). Imaging data for cells 0-6 weeks post-differentiation for Hoechst (Ex: 390 nm, Em: 446 nm) and after immunostaining for Hoechst, $Ca_V1.3$ (Ex: 482 nm, Em: 532 nm) and TH (Ex: 586 nm, Em: 646 nm) were collected from 3-10 fields of view for each concentration of each drug and analysed in ImageJ. Each concentration was repeated a minimum of 3 times to allow for statistical analysis, with pooling of data from multiple weeks required to achieve this where necessary.

Data Analysis: Semi-automatic nuclei counting for Hoechst and/or Propidium iodide was performed using ImageJ. First, images were threshold adjusted to remove artefacts within the image. For Hoechst staining the process was repeated separately using two different thresholds: I.) one that removed artefacts but left all Hoechst nuclei in the image intact; and II.) one that removed artefacts and dim nuclei, leaving only bright Hoechst nuclei in the image intact. This allowed for ratiometric counting of live/dead nuclei (**Supplementary 4.1**). The watershed function was used to separate conjoined nuclei. The analyse particle function was then used to automatically count nuclei using a 10 pixel particle exclusion filter. Nuclei on the edges of the images were excluded. Nuclei counting from Hoechst images after immunostaining was manually matched to the TH and $Ca_V1.3$ immunostained images to determine if individual TH or $Ca_V1.3$ positive or negative cells displayed dim/bright nuclei. Calculation of means and S.E.M was performed in Excel. The percentage of bright nuclei vs total nuclei for the whole

cell population, for TH-positive cells only, for TH-negative cells only and for TH-positive+$Ca_V1.3$ positive cells was used as an indicator of the percentage of cell death in each population.

4.2.6 Graphs & Statistical Analysis

All graphs and curve fitting were performed using OriginPro 8.5. Statistical analysis was performed using an appropriate statistical test in Excel using the XLSTAT plugin (t-tests, Pearson's R tests, ANOVAs or KS-tests). The exact test used and their associated significance values are reported in the text. Differences were considered statistically significant when $p < 0.05$. Asterisks (*) on graphs indicate statistical significance at this p-value. Errors bars in all graphs and ± values in the text use the standard error of the mean (S.E.M.) which was calculated in Excel.

4.3 Results

4.3.1 $Ca_V1.3$ Expression in hiPSC-Derived Dopaminergic Neurons

SNc DA neurons *in-vivo* express $Ca_V1.3$ L-type VGCCs. This subtype is believed to be involved in the selective death of these neurons in PD. To determine whether hiPSC-derived DA neurons express $Ca_V1.3$ in culture, cells were immunostained against the DA neuron marker TH and against $Ca_V1.3$ from 0-6 weeks post-differentiation. $Ca_V1.3$ staining was seen in all hNPCs at week 0, with near ubiquitous staining seen in both TH-positive and TH-negative neurons from 1 to 6 weeks post-differentiation (**Figure 4.1A**). Positive and negative controls using human $Ca_V1.3$ antigen and lacking primary/secondary antibodies confirmed the specificity of the antibody for $Ca_V1.3$ and proved staining was not due to non-specific antibody binding (**Supplementary 4.2**).

From week 1 onwards, a population of TH-positive cells was identified as $Ca_V1.3$-negative. These comprised a small proportion of the TH-positive population (**Figure 4.1B**). Interestingly, the presence of $Ca_V1.3$ could be predicted based on cell morphology. $Ca_V1.3$-positive TH-positive cells were typically elongated with spindle shaped somas and long processes extending from both poles (**Figure 4.2**). $Ca_V1.3$-negative cells appeared to have larger somas and a greater number processes (**Figure 4.3**). To quantify these observed differences in morphology, the mean cell length, 2D surface area and number of processes was calculated for both phenotypes, with data pooled from weeks 1-6 to allow for statistical analysis (n=6). The mean whole cell surface area was 341.93 ± 42.57 μm^2 for $Ca_V1.3$-positive versus 341.504 ± 39.6 μm^2 for $Ca_V1.3$-negative cells. The mean surface area of the soma was 98.16 ± 13.58 μm^2 for $Ca_V1.3$-positive versus 154.43 ± 21.59 μm^2 for TH-negative cells. No statistical difference in surface area was observed between phenotypes (Student's t-test, whole cell: p=0.989, soma: p=0.519) (**Figure 4.4A**). Mean cell length was 150.56 ± 14.72 µm for $Ca_V1.3$-positive versus 115.53 ± 6.33 µm for $Ca_V1.3$-negative cells, with no significant difference between the two (Student's t-test, p=0.054) (**Figure 4.4B**). However, the mean number of processes was significantly lower in $Ca_V1.3$-positive cells at 2.3 ± 0.06 compared to $Ca_V1.3$-negative TH-positive cells at 4.42 ± 0.62 (Student's T-test, p=0.007) (**Figure 4.4C**). A histogram of the number of processes (n=81 $Ca_V1.3$-positive, 29 $Ca_V1.3$-negative) showed that $Ca_V1.3$-negative cells displayed greater variance in their number (**Figure 4.4D**). The Kolmogorov-Smirnov test to compare differences between distributions showed there was a significant difference between the distributions of the two groups (D=0.558, p<0.0001).

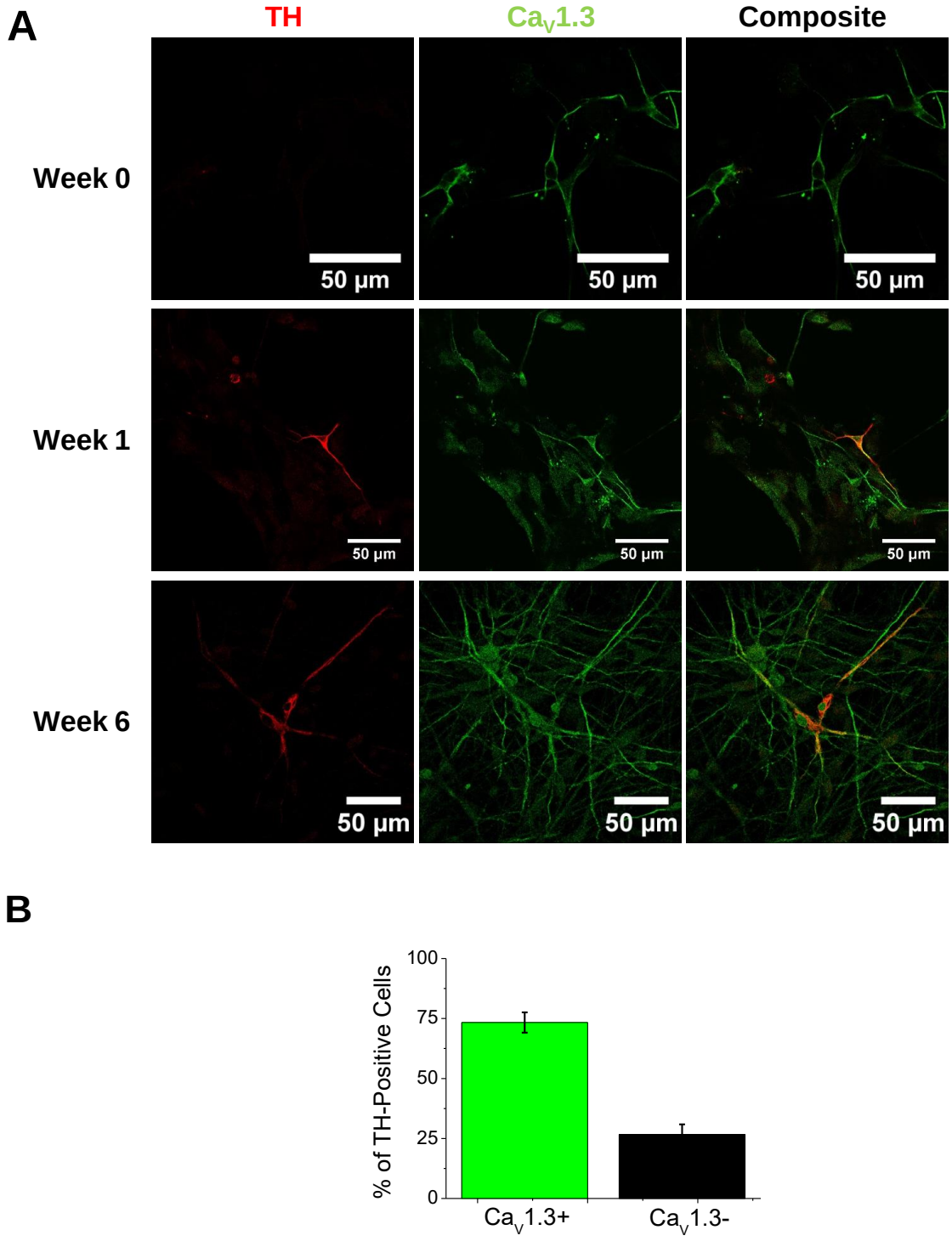

Figure 4.1 - $Ca_V1.3$ immunostaining in cultures containing hiPSC-derived DA neurons. (A) Representative confocal images from neurons 0, 1 and 6 weeks post-differentiation that were immunostained for TH (red) and $Ca_V1.3$ (green). (B) Graph showing the percentage of TH-positive neurons that are $Ca_V1.3$-positive (green) and $Ca_V1.3$-negative (black). Data is pooled from 1-6 weeks post-differentiation (n=6). Error bars ± S.E.M.

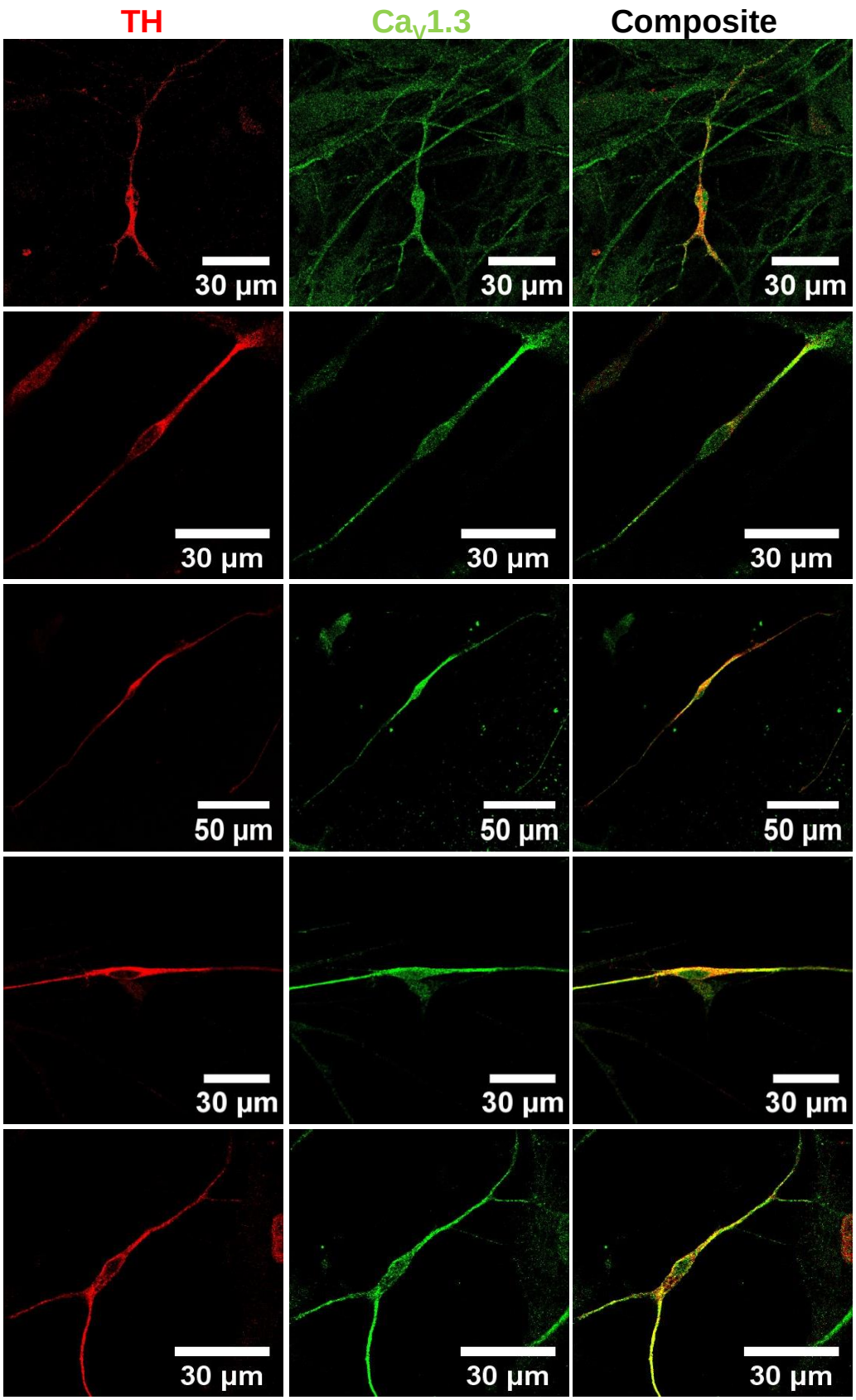

Figure 4.2 - $Ca_V1.3$ positive hiPSC-derived dopaminergic neurons. Representative confocal images from 5 TH-positive neurons from 1-6 weeks post-differentiation that were immunostained for TH (red) and $Ca_V1.3$ (green).

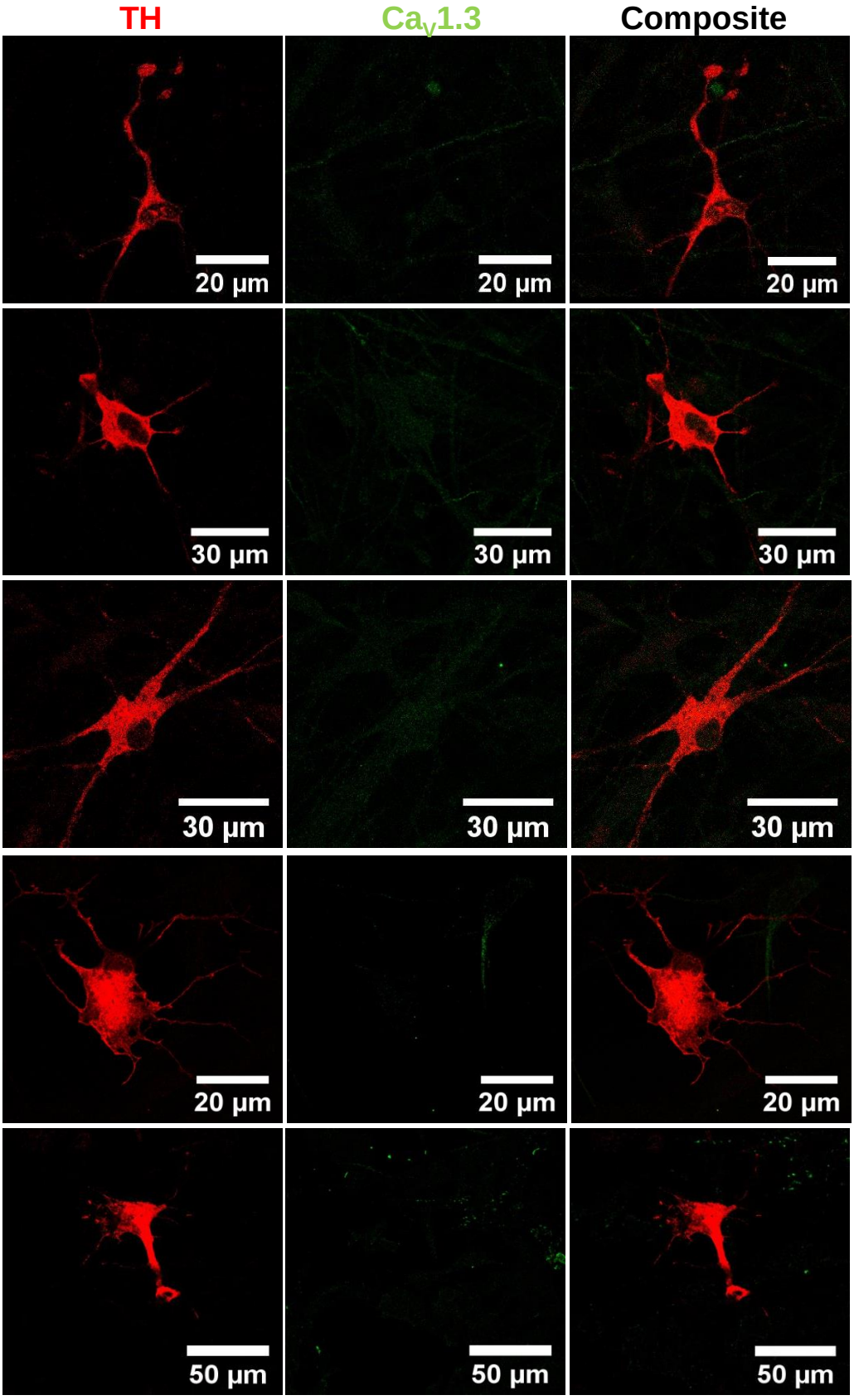

Figure 4.3 - Ca$_V$1.3 negative hiPSC-derived dopaminergic neurons. Representative confocal images of 5 TH-positive neurons from 1-6 weeks post-differentiation that were immunostained for TH (red) and Ca$_V$1.3 (green).

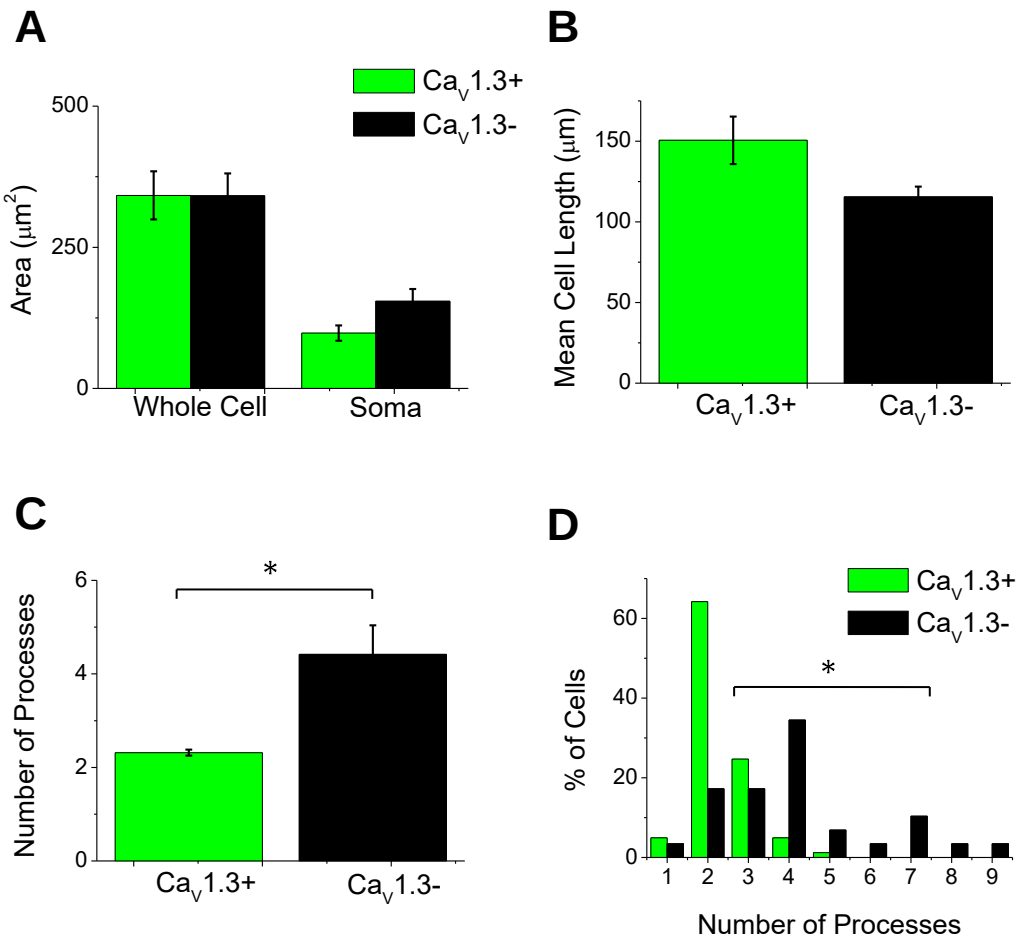

Figure 4.4 - Morphological characterisation of Cav1.3-positive and Cav1.3-negative hiPSC-derived DA neurons. Graphs from week 1-6 TH-positive neurons showing (A) the mean 2D surface area from the whole cell and soma (n=6). (B) The mean cell length between the two furthest poles (n=6). (C) The mean number of processes originating from the soma (n=6). (D) Histogram of data showing the percentage of cells that have each number of processes (Cav1.3+, n=81. Cav1.3-, n=29). Error bars ± S.E.M. *indicates statistical significance at p=0.05 using a two-way Student's t-test (A) (B) (C) or a Kolmogorov-Smirnov test (D).

4.3.2 Selective 6-OHDA Susceptibility in hiPSC-Derived Dopaminergic Neurons

DA neurons *in-vivo* are selectively killed by 6-OHDA, a toxin that causes oxidative damage and dysfunction of mitochondrial metabolism after uptake through dopamine reuptake transporters. This susceptibility is often exploited to model PD *in-vivo* using lesioned animal models (Schwarting & Huston, 1996). If hiPSC-derived DA neurons are to be used as a human model of PD then they must be able to show a similar susceptibility to 6-OHDA. To determine whether this susceptibility exists and whether it is specific to TH-positive neurons in culture, cells were exposed to various concentrations of 6-OHDA for 24 hours from 0-6 weeks post-differentiation.

To act as a cell death assay, cells were co-stained with the live cell nuclei stain Hoechst 33342 and the dead cell nuclei stain Propidium iodide (PI). To validate this method, week 4-6 differentiated neurons were incubated with Etoposide, a toxin which induces cell death through DNA breaks. More PI staining was identifiable in toxin-incubated cells compared to controls (**Figure 4.5A**). An unexpected result was that Hoechst staining was at least 3 fold brighter in PI stained cells than non-PI stained cells (n=3) (Student's t-test, p=0.016) (**Figure 4.5A, 4.5B**). This effect persisted when cells were stained for Hoechst alone, with identifiable 'bright' nuclei and 'dim' nuclei (n=3) (Student's t-test, p=0.015) (**Figure 4.6A, 4.6B**). This effect was also able to survive through fixation and permeabilization, though with a reduced intensity (n=3) (Student's t-test, p=0.007) (**Figure 4.6A, 4.6C**). Staining was seen in nuclei stained for PI alone, confirming that the PI staining seen while co-staining with Hoechst was due to cell death and not an artefact due to fluorescence bleed through from high intensity Hoechst-stained nuclei (**Figure 4.6B**).

To determine whether Hoechst alone could be used to calculate the percentage of cell death in a culture (and hence allow the PI excitation channel to be used for antibody staining), co-localisation analysis of Hoechst-stained 'bright' nuclei and PI-stained nuclei was performed. Little co-localisation was seen between PI and Hoechst when comparing whole fields of cells, with a mean Pearson's R-value of 0.42 ± 0.11 (n=3) (**Figure 4.7A**). When co-localisation analysis was restricted to only 'bright' Hoechst nuclei a higher degree of linear correlation was seen, with a mean Pearson's R-value of 0.83 ± 0.07 (n=3) (**Figure 4.7B**).

No difference in the mean percentage of cell death in neurons incubated with Etoposide or in controls was identified when using either the PI:total Hoechst nuclei ratio or the

'bright' Hoechst:total Hoechst nuclei ratio (Student's t-test, Etoposide: p=0.899, control: p=0.605) (n=5) (**Figure 4.7B**). From this it was concluded that Hoechst staining alone can be used to determine the percentage of dead cells in a culture and was at least as accurate as co-staining with PI and Hoechst. This single staining method was used in all subsequent cell death assays.

To determine whether selective cell death occurs in response to DA toxins, neurons were incubated with varying concentrations of 6-OHDA from 0-6 weeks post differentiation to generate dose-response curves based on percentage of cell death (n=3 to 4 per concentration). More Hoechst staining was seen in week 1-6 neurons compared to week 0 neurons at high concentrations of 6-OHDA (**Figure 4.8A**). Pooled data from weeks 1-6 could be fitted with a Boltzmann function and the concentration at which 50% of the population displayed cell death (LD50) was shifted towards lower concentrations compared to week 0 (**Figure 4.8B**). Cell death was still seen in week 0 neurons though higher concentrations were required to elicit an effect, perhaps indicating a general toxicity of 6-OHDA at higher concentrations (**Figure 4.8B**). Performance of one-way ANOVAs showed a significant effect of concentration on % cell death ($F=23.695$, $p<0.0001$) and a Tukey comparison test showed a significant statistical difference between week 0 and week 1-6 cells ($p<0.0001$). The percentage of cell death in controls incubated without 6-OHDA remained consistently below 15% and dropped between weeks 0 and 6 (**Figure 4.8C**). Cell death in week 1-6 neurons appeared to plateau at ~60% of the general population (**Figure 4.8B**), suggesting that 6-OHDA was selective for a subpopulation of neurons.

To determine whether TH-positive neurons were being selectively destroyed, week 1-6 6-OHDA incubated neurons were immunostained against TH and $Ca_V1.3$ after Hoechst staining (**Figure 4.9A**). TH-positive neurons were selectively destroyed, with almost 100% cell death at 100-200 µM 6-OHDA compared to ~60% for TH-negative cells at 200 µM (**Figure 4.9B**). 6-OHDA incubated TH-positive neurons typically displayed small, condensed nuclei typical of apoptosis/necrosis which were seen in fewer TH-negative neurons. The performance of one-way ANOVAs showed a statistically significant effect of concentration on % cell death for both conditions (TH-positive: $F=117.863$, $p<0.0001$; TH-negative: $F=55.973$, $p<0.0001$). A significant effect was found between TH-positive and TH-negative cells ($F=11.181$, $p<0.0001$).

Both $Ca_V1.3$-positive and $Ca_V1.3$-negative TH-positive neurons were affected by 6-OHDA, with one-way ANOVAs showing a statistically significant effect of

concentration on % cell death ($Ca_V1.3$+: F=37.411, p<0.0001; $Ca_V1.3$-: F=10.221, p<0.0001) (**Figure 4.9C**). The dose-response curves for $Ca_V1.3$-positive and $Ca_V1.3$-negative TH-positive neurons displayed little difference, and a one-way ANOVA showed no statistical difference between subjects (F=0.106 p=0.751), indicating that $Ca_V1.3$ expression does not increase the susceptibility of week 1-6 TH-positive neurons to cell death in response to 6-OHDA.

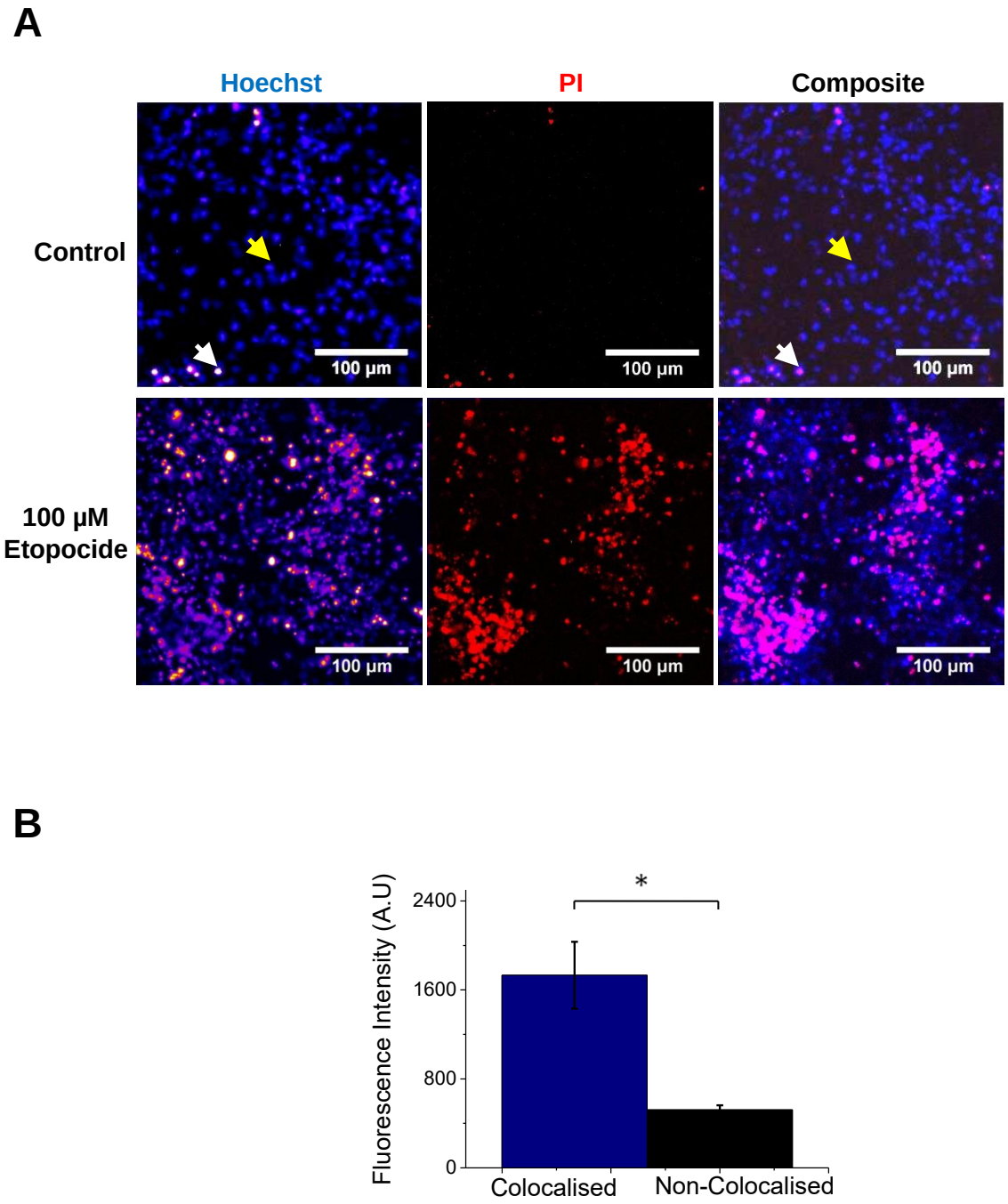

Figure 4.5 - Hoechst 33342 as a differential live/dead cell dye. (A) Representative false-colour fluorescence images from Hoechst/PI-stained week 4 neurons before and after 1-hour incubation with 100 µM Etoposide. Arrows indicate 'bright' (white arrow) and 'dim' (yellow arrow) nuclei, showing that 'bright' nuclei also stain for PI. In composite images, magenta indicates regions of overlap between the two dyes. (B) Graph showing mean fluorescence intensity for Hoechst-stained nuclei that were co-localised or not co-localised with PI (n=3). Error bars ± S.E.M. *indicates statistical significance using a two-way Student's t-test at p=0.05.

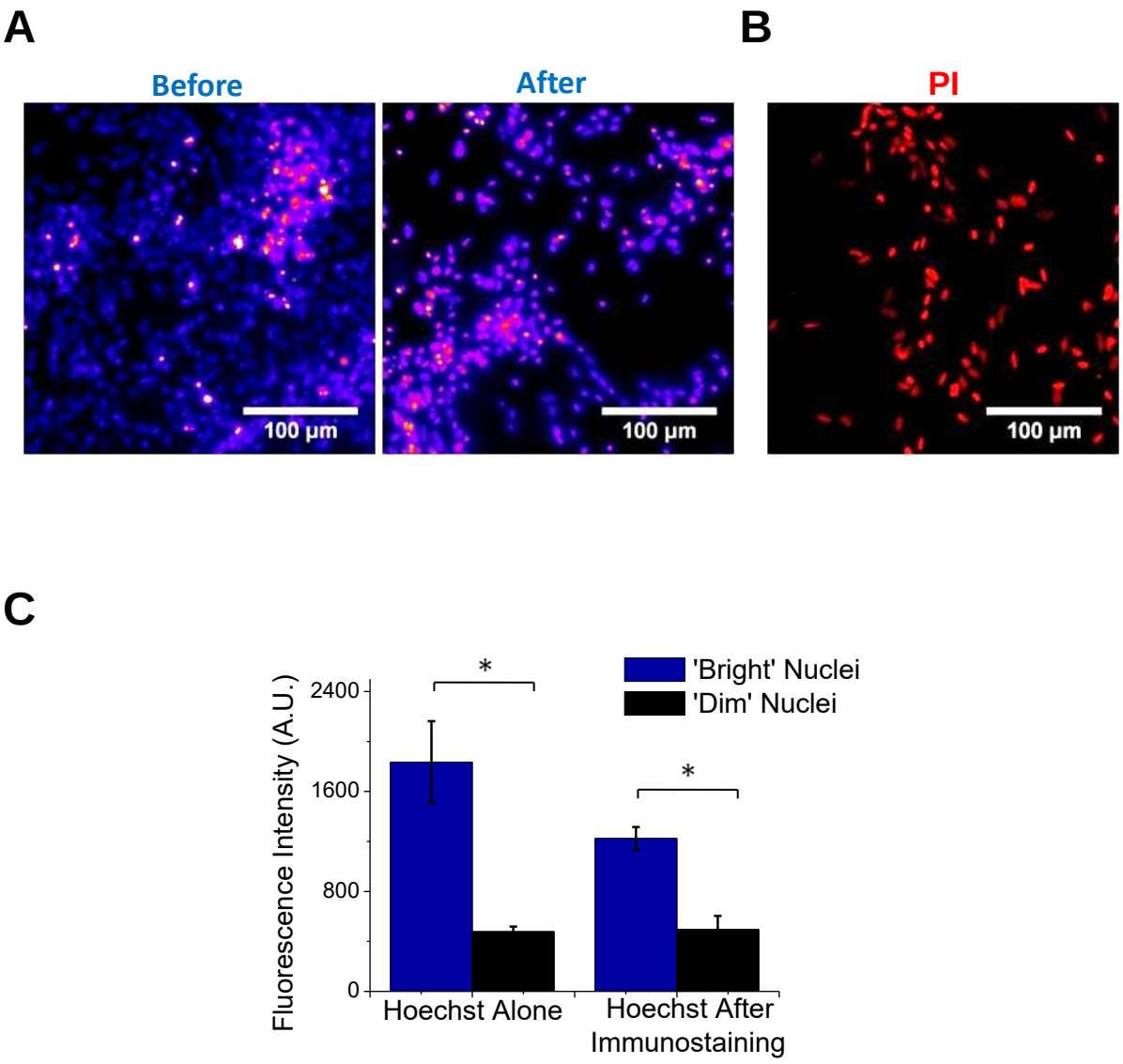

Figure 4.6 - Hoechst 33342 live/dead identification could be performed after fixation. (A) Representative fluorescence images from week 4-6 differentiated neurons incubated with Etoposide for 1 hour showing Hoechst staining (left, left panel) before and (left, right panel) after fixation/permeabilization and (B) a separate experiment showing PI staining alone before fixation/permeabilization. (C) Graph showing the mean fluorescence intensity of 'bright' and 'dim' Hoechst-stained nuclei before and after fixation and permeabilization (n=3). Error bars ± S.E.M. *indicates statistical significance using a two-way Student's t-test at p=0.05.

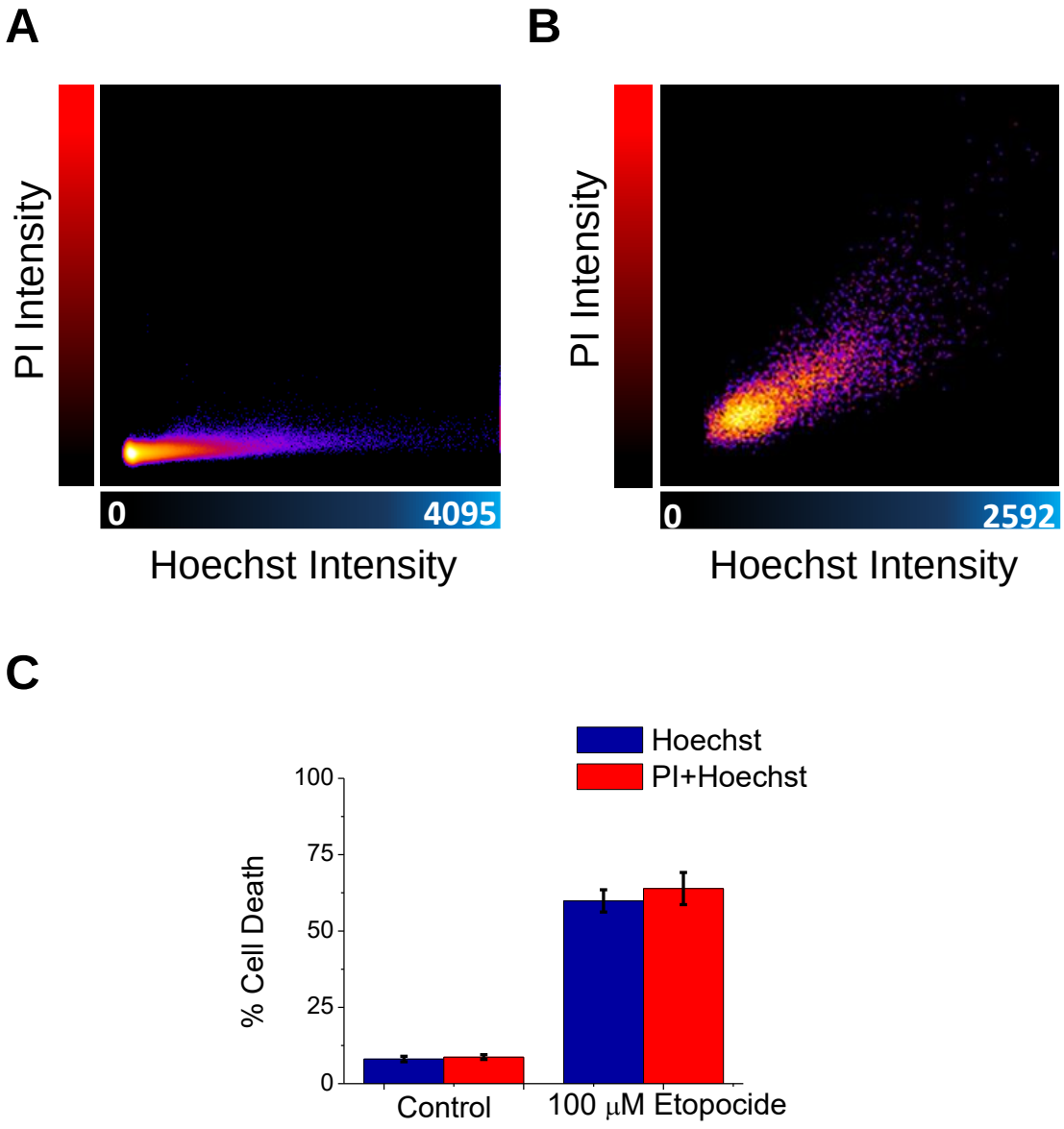

Figure 4.7 - Co-localisation of Hoechst 33342 and PI. Representative 2D intensity scatter plots from week 1-6 differentiated neurons incubated with 100µM Etoposide showing (A) a whole field of view of Hoechst and PI stained cells and (B) a region of interest from A containing only 'bright' Hoechst nuclei. (C) Graph comparing the mean percentage of cell death in neurons with and without Etoposide incubation when using the 'bright' vs total Hoechst nuclei ratio (blue) or the PI-stained nuclei vs total Hoechst nuclei ratio (red) (n=5). Error bars ± S.E.M.

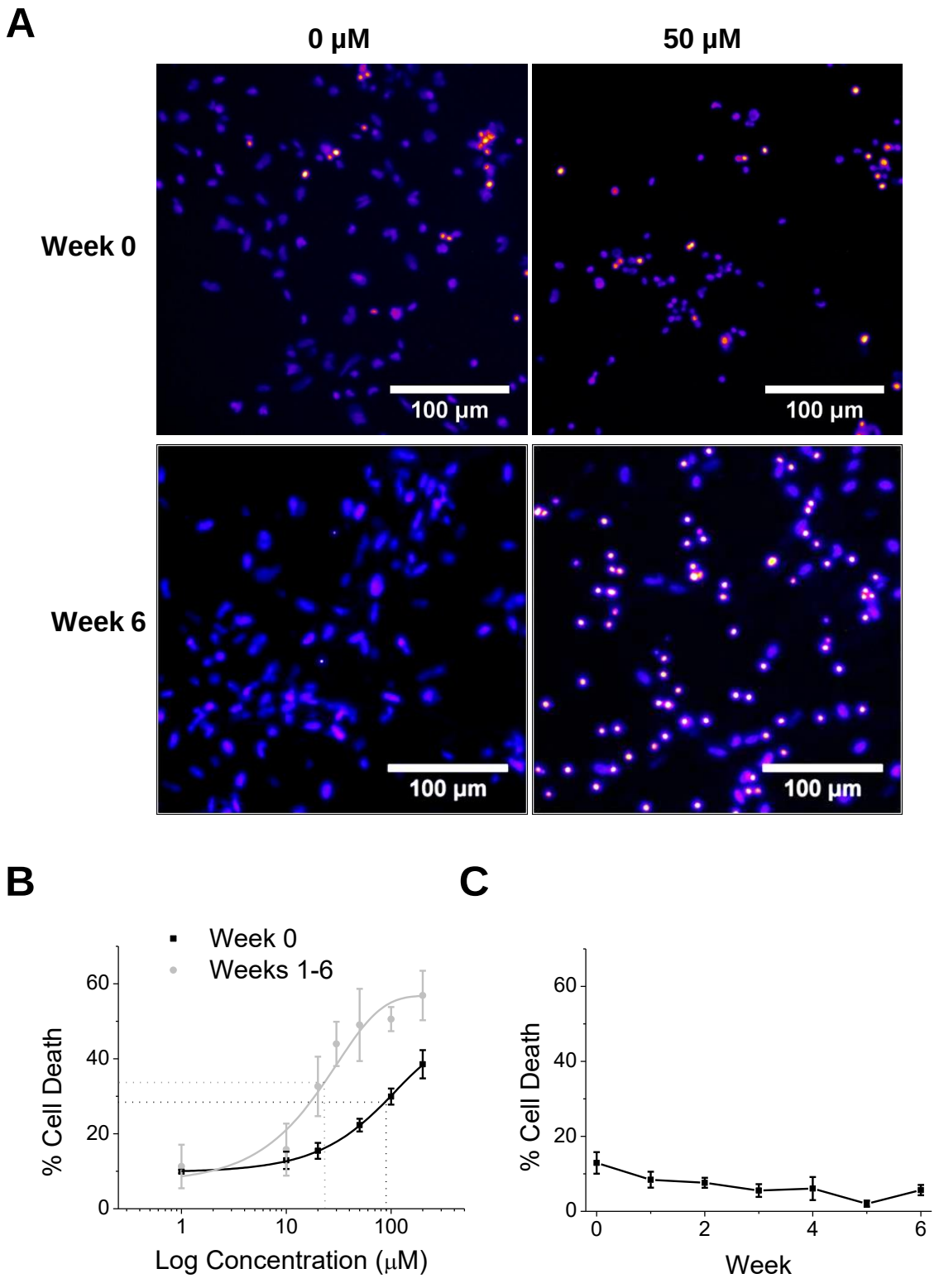

Figure 4.8 - 6-OHDA toxicity develops in cultures containing hiPSC-derived DA neurons. (A) Representative fluorescence images from week 0 and week 6 neurons before and after incubation with 50 µM 6-OHDA for 24 hours. Graphs showing (B) the mean percentage of cell death after 24 hour incubation with 6-OHDA in week 0 and week 3-6 neurons. Dotted lines indicate LD50. Data points are fitted using Boltzmann functions. (C) The mean percentage of cell death in controls incubated for 24 hours without 6-OHDA from weeks 0-6. n=3 to 4 per concentration/time point. Error bars ± S.E.M.

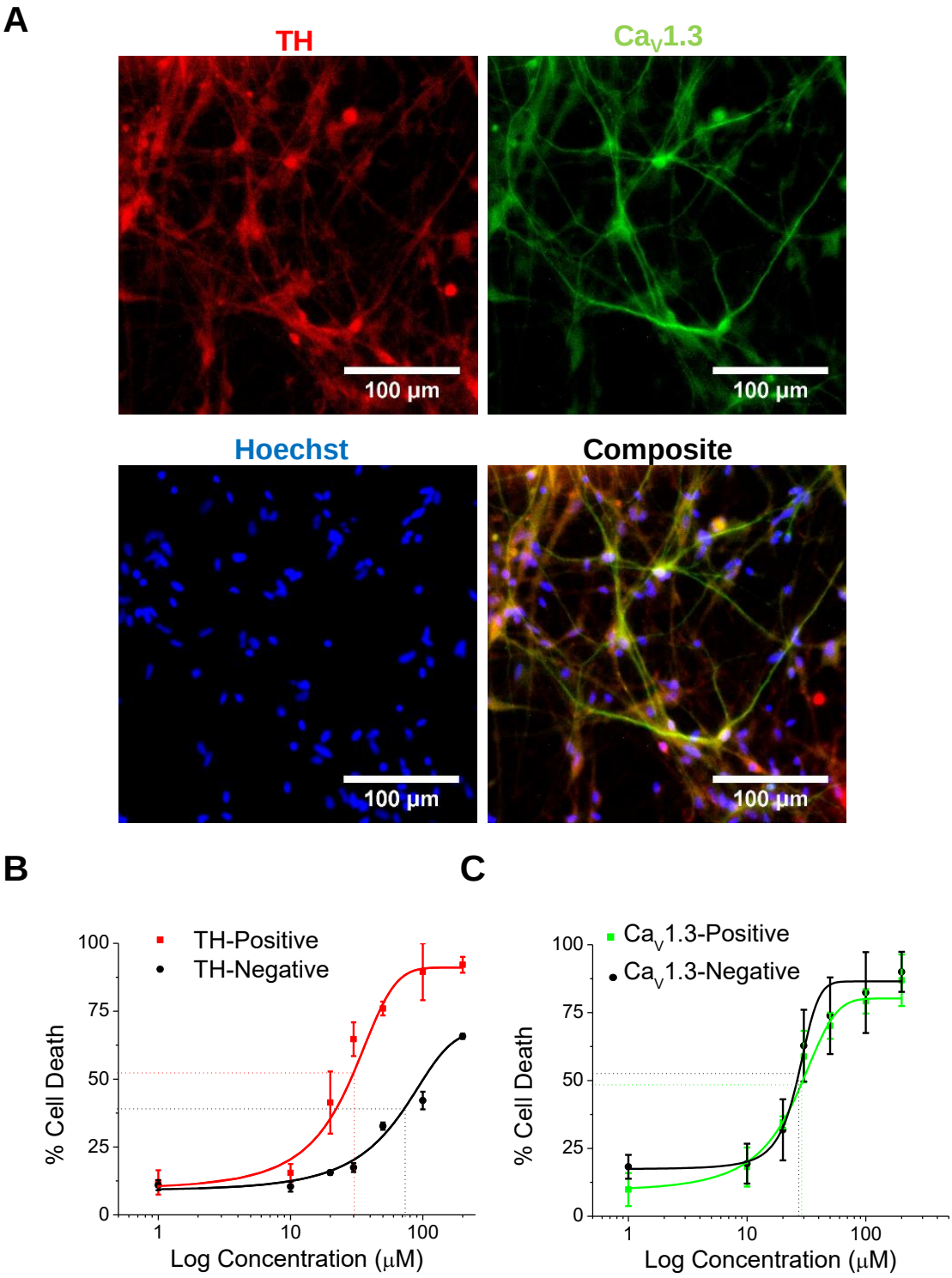

Figure 4.9 - TH-positive neurons are selectively susceptible to 6-OHDA. (A) Representative fluorescence images of neurons 6 weeks post-differentiation that were immunostained for TH (red) and $Ca_V1.3$ (green) after staining with 1 µM Hoechst 33342. Graphs of the mean percentage of cell death using pooled dated from week 1-6 neurons following 24 hours 6-OHDA incubation showing (B) TH-positive vs TH-negative neurons and (C) $Ca_V1.3$-positive vs $Ca_V1.3$-negative TH-positive neurons. n=3-5 per concentration. Dotted lines indicate LD50. Error bars ± S.E.M.

4.3.3 Glutamate Excitotoxicity in hiPSC-Derived Dopaminergic Neurons

It has previously been shown that glutamate excitotoxicity plays a role in the selective death of SNc DA neurons in PD. Excessive activation of glutamate receptors, such as NMDARs and AMPARs, results in an increased cytosolic Ca^{2+} concentration which results in a cascade of effects that lead to cell death (Gupta et al., 2013). Whether hiPSC-derived DA neurons are susceptible to glutamate excitoxicity and whether or not there is any difference in susceptibility between TH-positive and TH-negative neurons in culture has not been identified.

To determine whether hiPSC-derived DA neurons display glutamate excitotoxicity, cultures were incubated for 24 hours with varying concentrations of L-glutamic acid from 0-6 weeks post-differentiation (n=3-6 per concentration). Hoechst staining revealed no increase in cell death in week 0 neurons or in pooled data from weeks 3-6 at L-glutamic acid concentrations ranging from 100 µM to 10 mM **(Figure 4.10A, 4.10B)**. These concentrations have previously been reported as toxic to various neuronal cell types in culture (Kritis et al., 2015). Addition of 100 mM L-glutamic acid increased cell death in week 3-6 but not week 0 cells (**Figure 4.10B**). The performance of one-way ANOVAs showed no statistical effect of concentration on % cell death for week 0 or week 3-6 cells (week 0: F=0.884, p=0.47; weeks 3-6: F=2.189, p=0.129). No statistical difference was observed between week 0 and week 3-6 neurons (F=0.18, p=0.683). Cell death in controls incubated without L-glutamic acid was high at week 0 (26.36 ± 7.45%) but dropped in the following weeks to 4.43 ± 1.89% at week 6 (**Figure 4.10C**).

To determine any differences in susceptibility to glutamate excitotoxicity between TH-positive and TH-negative neurons, cells were immunostained for TH and $Ca_V1.3$ following Hoechst staining (**Figure 4.11A, 4.11B**). One-way ANOVAs showed a significant effect of concentration on % cell death in both TH-positive and TH-negative cells (TH+: F=3.87, p=0.041; F=3.641, p=0.048). No difference was observed between the dose-response curves for TH-positive and TH-negative neurons (F=0.515, p=0.504).

Separating TH-positive cells into CaV1.3-positive and CaV1.3 negative cells showed a similar trend to previous populations (**Figure 4.11B**). One-way ANOVAs showed no statistically significant effect of concentration on % cell death for $Ca_V1.3$-positive nor $Ca_V1.3$-negative TH-positive neurons ($Ca_V1.3$+: F=0.585, p=0.636; $Ca_V1.3$-: F=0.089, p=0.965). No significant difference was observed between $Ca_V1.3$-positive and $Ca_V1.3$-negative cells (F=0.025, p=0.88).

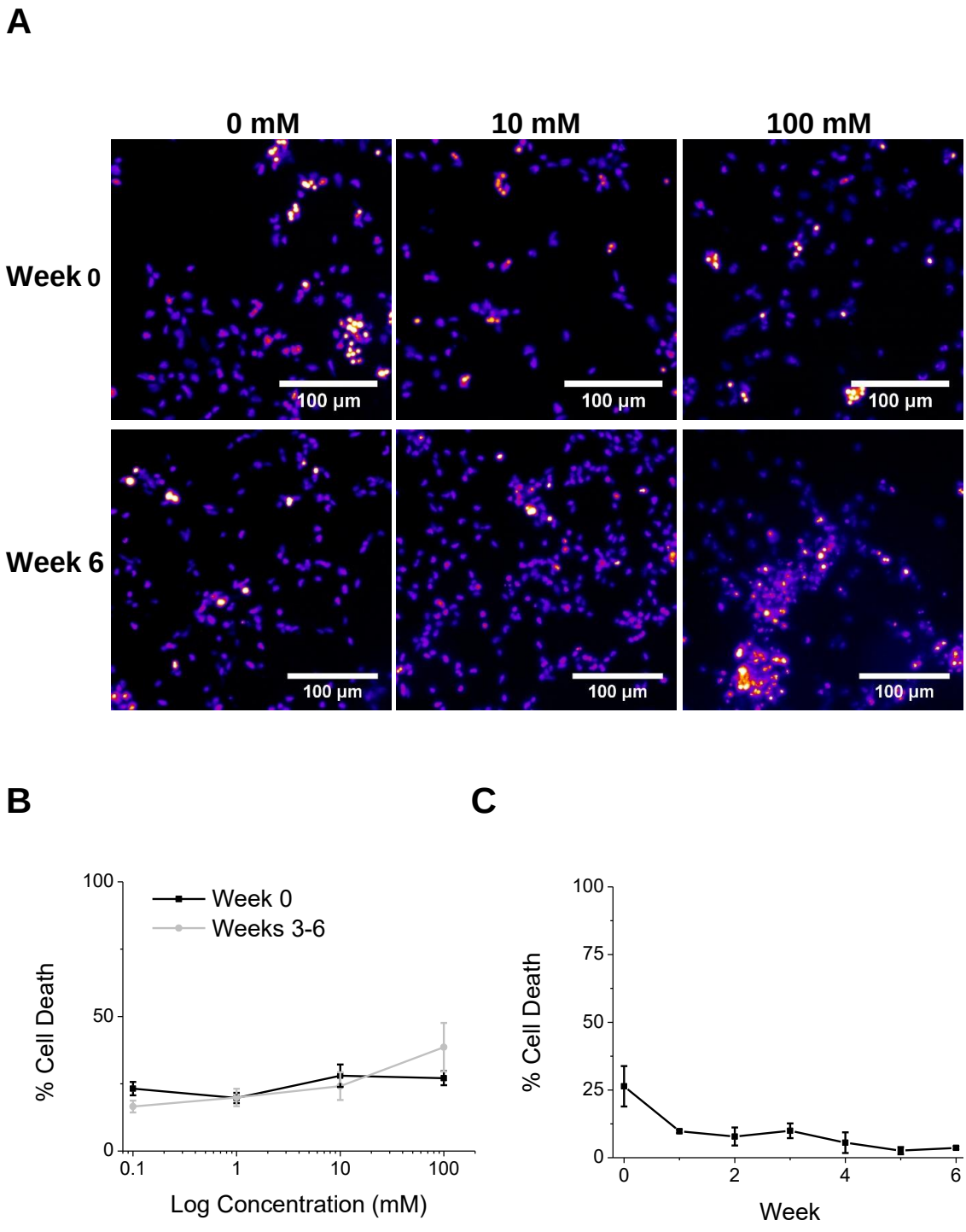

Figure 4.10 - Glutamate excitotoxicity in cultures containing hiPSC-derived dopaminergic neurons. (A) Representative Hoechst-stained fluorescence images showing neurons 0 and 6 weeks post-differentiation that have been incubated with 0, 10 or 100 mM L-glutamic acid for 24 hours. (B) Graph showing the mean percentage of cell death in week 0 and week 3-6 differentiated neurons after incubation with varying concentrations of L-glutamic acid (n=3 to 6 per concentration). (C) Graph showing the mean percentage of cell death each week post-differentiation in controls incubated without L-glutamic acid. n=3 to 4 per week. Error bars ± S.E.M.

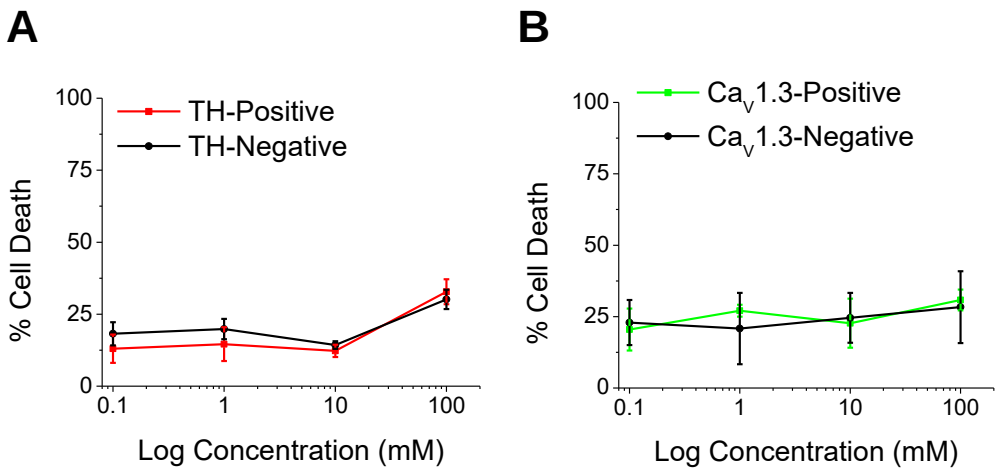

Figure 4.11 - TH-positive neurons are not selectively susceptible to glutamate excitotoxicity. Graphs showing the mean percentage of cell death in (A) TH-positive vs TH-negative neurons and (B) Ca$_V$1.3-positive vs Ca$_V$1.3-negative TH-positive neurons in response to 24 hour incubation with increasing concentrations of L-glutamic acid. Data was pooled from 3-6 weeks post-differentiation. Error bars ± S.E.M.

4.4 Discussion

The L-type VGCC subtype Ca$_V$1.3 is believed to play a role in the selective death of SNc DA neurons *in-vivo* by increasing cytoplasmic Ca^{2+} levels during pacemaking. This in turn leads to accumulation of Ca^{2+} in mitochondria and, in combination with other stressors, leads to a collapse of the mitochondrial membrane potential (Pacelli et al., 2015). Whether Ca$_V$1.3 is expressed in hiPSC-derived DA neurons had not been investigated. This chapter has focused on characterising Ca$_V$1.3 immunostaining in hiPSC-derived TH-positive cells. Here I show that Ca$_V$1.3 was identified at all stages of development in the majority of cells in culture and that its expression precedes differentiation to different phenotypes. It has previously been reported that Ca$_V$1.3 is expressed in NPCs in mice and may be critical for their development and differentiation (Marschallinger et al., 2015).

Two distinct populations of TH-positive cells were identified here. Ca$_V$1.3-positive cells made up the majority of TH-positive cells. These were spindle shaped and typically had two processes extending from both poles of the cell. Ca$_V$1.3-negative cells composed a

small proportion of the TH-positive population. These had a more varied number of processes and a slight tendency towards larger cell bodies. Rat studies of the SNc *in-situ* have identified long, spindle shaped neurons projecting towards the basal ganglia while short, diffuse neurons were seen projecting locally (Richards et al., 1997). Projections to other regions of the substantia nigra such as the pars reticulata have also been identified, with these cells displaying dendritic release of dopamine (Robertson et al., 1991). The two subpopulations of DA neuron I have identified here may therefore correspond to some of these previously observed populations.

Previous studies on hiPSC-derived DA neurons have shown that they are susceptible to the effects of mitochondrial toxins such as MPTP and 6-OHDA (Nguyen et al., 2011; Hartfield et al., 2014). Whether this susceptibility results in an increased incidence of cell death had only previously been investigated at lower concentrations of 6-OHDA than those used here (Nguyen et al., 2011). It was also not known whether $Ca_V1.3$ expression increases the susceptibility of TH-positive neurons to 6-OHDA. Here I show, by incubating week 0-6 cultures with 6-OHDA, that cell death is selective for TH-positive cells, with general toxicity occurring at higher concentrations perhaps due to the fact that 6-OHDA auto-oxidises to release free radicals in solution (Padiglia et al., 1997). This also provides further evidence of the DA phenotype of these cells. No increase in cell death in $Ca_V1.3$-positive vs $Ca_V1.3$ negative TH-positive cells was seen over the course of 6 weeks. This does not discount the possibility that an increase in cell death would be seen at later stages of maturity when synapses have fully developed or that $Ca_V1.3$ expression in these neurons increases susceptibility to other mitochondrial toxins such as MPTP, as has been seen recently in primary neurons (Wang et al., 2017).

Glutamate excitotoxicity has been observed in SNc neurons, an effect that is increased after exposure to low levels of mitochondrial complex IV inhibitors. This has led to the idea that excitotoxicity may be involved in the selective cell death of SNc DA neurons in PD (Meredith et al., 2009). The presence of glutamate excitotoxicity in hiPSC-derived DA neurons had not previously been investigated. Here I show that all of the cells in culture, whether week 0 or week 6, showed a remarkable resistance to cell death in response to L-glutamic acid. Studies investigating glutamate excitotoxicity in various neuronal cell types in culture have reported variable concentrations, from 0.1 to 100 mM, and variable timescales, from 1 to 72 hours, for death to occur (Kritis et al., 2015). The results observed here do not discount several possibilities: that more mature hiPSC-derived DA neurons develop toxicity to glutamate; that incubation with L-glutamic acid

for an extended period may elicit an effect; or that glutamate excitotoxicity in these cell types requires other stressors to occur, as has previously been identified in primary SNc neurons (Meredith et al., 2015).

The results from this chapter suggest that hiPSC-derived DA neurons immunostain for $Ca_V1.3$ in a similar fashion to SNc DA neurons *in-vivo*, though staining was not restricted to TH-positive subpopulations. TH-positive cells, as expected, were selectively susceptible to 6-OHDA. hiPSC-derived DA neurons, however, may not be suitable for the study of glutamate excitotoxicity in PD as they showed a remarkable resistance to its effects. $Ca_V1.3$-positive cells did not display an increased susceptibility to cell death in response to either toxin, at least during the early development period tested.

4.4.1 $Ca_V1.3$ Expression in hiPSC-Derived Dopaminergic Neurons

SNc DA neurons *in-vivo* express $Ca_V1.3$, a relatively rare subtype of L-type VGCC that are believed to be involved in the mechanism of selective cell death of SNc neurons in PD. This was demonstrated by $Ca_V1.3$-/- mice, whose SNc neurons developed pacemaking normally via the compensatory effect of HCN channels but developed a resistance to mitochondrial toxins when compared to wild type mice (Chan et al., 2007). Here I demonstrate that $Ca_V1.3$-negative and $Ca_V1.3$-positive hiPSC-derived DA neurons develop in culture when using the differentiation protocol used here. The $Ca_V1.3$-positive cells were observed to be elongated with long projections from both poles while the $Ca_V1.3$-negative cells typically had a more varied number of projections.

A previous study of rat nigral neurons *in-vivo* found phenotypes similar to those identified here, with spindle shaped cells producing long projections to regions of the basal ganglia and short, diffuse GABAergic neurons projecting to cells in their local environment (Richards et al., 1997). Local SNc projections to other regions of the substantia nigra such as the pars reticulata have also been identified, with these cells displaying dendritic release of dopamine (Robertson et al., 1991). Other regions of the midbrain, such as the ventral tegmental area, contain $Ca_V1.3$-negative DA neurons that instead rely on Na_V channels to control pacemaking (Khaliq & Bean, 2010). Here I provide evidence for a potential link between these previous studies, suggesting that the morphologically distinct populations seen in these *in-vivo* studies possibly correspond

to cells that are positive or negative for $Ca_V1.3$. The spindle shaped cells with long projections seen *in-vivo* projecting to the basal ganglia may correspond to $Ca_V1.3$-positive cells, while the diffuse $Ca_V1.3$-negative cells with many projections may correspond to neurons that are closer in phenotype to either the locally projecting GABAergic neurons, ventral tegmental area neurons or to those that project to the pars reticulata. The presence of D2 autoreceptors on SNc neurons *in-vivo* suggests that local release of dopamine may aid in the regulation of pacemaking (Hooper et al., 1997). For this to occur, projections from DA neurons to nearby cells must occur. The short, diffuse, $Ca_V1.3$-negative DA neurons identified here could correspond to the *in-vivo* variants of these cells and suggests that hiPSC-derived DA neuron cultures contain cells that correspond to more than one *in-vivo* phenotype. Co-release of GABA and dopamine has also been seen in other neuronal cell types so, although little to no GABAergic input was seen in chapter 3 (perhaps due to the solutions used) and GABA co-release hasn't been identified in the SNc *in-vivo*, it is a possibility that is at least worth consideration (Richards et al., 1997; Tritsch et al., 2016).

Another possibility is that these $Ca_V1.3$-negative cells may not be neuronal in nature. TH has been identified in non-neuronal cell types such as pancreatic islet progenitors, though considering the cultures here are differentiated from NPCs it seems unlikely that these cell types could be generated (Teitelman et al., 1993). Another suggestion is that these cells could be other, non-DA neurons. TH is involved in the production of catecholamines other than DA such as adrenaline and noradrenaline so these types of neurons could result in false-positive TH-staining. Although rare, adrenergic and noradrenergic input has been identified in the SNc so this possibility should perhaps be investigated in future studies (Mejías-Aponte et al., 2009).

The specificity of the antibodies should be considered when interpreting the results. The epitope for the $Ca_V1.3$ antibody used corresponds to amino acids 859-875 of rat $Ca_V1.3$. This region lies between the alpha subunit domains II and III and is conserved between species such as human, mouse, hamster and chicken. This region is specific to $Ca_V1.3$, and is not found in other common subtypes such as $Ca_V1.2$ (Hui et al., 1991; Soldatov, 1994) (Alomone labs website, http://www.alomone.com/p/anti-cav1.3/acc-005/1023). The antibody used here has previously been used to differentiate between the expression of $Ca_V1.2$ and $Ca_V1.3$ in cell types such as the cultured DA cell line SH-SY5Y, mouse cortical astrocytes and mouse spiral ganglion neurons (Lv et al., 2014; Cheli et al., 2016; Sun et al., 2017). Control experiments were performed here, with no fluorescence

being identified when the $Ca_V1.3$ primary antibody was first incubated with the $Ca_V1.3$ epitope. Other control experiments confirmed that the primary antibody did not display auto-fluorescence and that the secondary antibody did not display non-specific binding. Data here, in combination with data from previous studies, demonstrates that the $Ca_V1.3$ antibody used appears to be specific for $Ca_V1.3$ over other VGCC subtypes.

Time constraints meant that an in-depth time course of $Ca_V1.3$ immunostaining in culture could not be performed. To acquire enough data for statistical analysis, data from weeks 1-6 was pooled together. This could have the effect of masking morphological differences due to changes in cell length, area and number of processes in the general population as the cells mature. Therefore, only gross differences are likely to have been identified. Despite this, differences were observed between phenotypes and whether a TH-positive neuron stained for $Ca_V1.3$ or not could be predicted with a reasonably high degree of accuracy based on its morphology.

The results here confirm that hiPSC-derived DA neurons are suitable for studies into the role of $Ca_V1.3$ pacemaking in PD, though care must be taken to ensure that $Ca_V1.3$-positive cells and not the $Ca_V1.3$-negative variants are being investigated.

4.4.2 Selective 6-OHDA Susceptibility in hiPSC-Derived Dopaminergic Neurons

SNc neurons *in-vivo* are selectively destroyed by 6-OHDA, a toxin that produces ROS after entering the cell through dopamine reuptake transporters. One study in rats found a loss of ~10-15% of TH-positive neurons in the SNc after 7 days of 100 µM 6-OHDA incubation (Zhang et al., 2012). Here I confirm the same selective cell death is present in hiPSC-derived DA neuron-containing cultures and is specific for TH-positive cells. This selectivity has previously been identified in these neurons *in-vitro*, though only at low concentrations that resulted in a low occurrence of cell death in culture (Nguyen et al., 2011). This previous study used concentrations from 1-10 µM 6-OHDA, identifying ~15% of TH-positive neurons expressing the cell death marker Caspase-3 compared to ~6% of TH-negative cells and ~3-5% of controls incubated without 6-OHDA after 35 days in culture. Here I confirm this, with a similar selectivity seen in TH-positive neurons (~15% compared to ~10% of TH-negative at 10 µM). My data go further, showing selectivity of 6-OHDA hiPSC-derived TH-positive cells at concentrations up to 200 µM. Data here also shows that this selectivity is not present in hNPCs, instead developing after differentiation.

The death of TH-negative cells could be attributed to several factors. 6-OHDA is rapidly oxidised in solution if not in the presence of an anti-oxidant (Padiglia et al., 1997). To prevent or slow down oxidation, the anti-oxidant ascorbic acid was added to all solutions and cell media containing 6-OHDA. Despite this, oxidation likely still occurred at a slower rate, releasing ROS into the media resulting in toxic effects. A proportion of "TH-negative" cells may also be expressing low levels of TH that are not easily detected through immunostaining and fluorescence imaging. A less likely reason is that the TH-negative cells have a limited capability to uptake 6-OHDA, either through the expression of dopamine uptake transporters or through other means such as endocytosis. A previous study on hiPSC-derived DA neuron-containing cultures found that these neurons are susceptible to mitochondrial membrane potential changes in response to MPTP, a mitochondrial toxin that is often used in animal models to induce Parkinsonian-like symptoms (Tieu, 2011). Though this was not investigated, my data provide a link to this study by suggesting that the observed mitochondrial membrane potential changes may be the cause of the selective death of TH-positive cells in response to exposure to 6-OHDA.

Block of $Ca_V1.3$ channels has previously been found to reduce DA cell death in disease models and reduce the incidence of PD in clinical trials (Chan et al., 2007; Gudala et al., 2015). However, in the experiments performed here, $Ca_V1.3$-positive cells were not found to be more susceptible to cell death than $Ca_V1.3$-negative cells. Since Ca^{2+} influx due to $Ca_V1.3$ VGCCs is linked to pacemaking and a previous study on hiPSC-derived DA neurons that looked at their later development (6-12 weeks) found an increased frequency and rhythmicity to their pacemaking at later weeks (Hartfield et al., 2014), it could be that hiPSC-derived DA neurons at 0-6 weeks in development have not yet developed fully mature pacemaking and hence are not yet susceptible to $Ca_V1.3$-related mitochondrial stress. This is supported by data from Chapter 3 that suggests there is a developmental shift at 6 weeks post-differentiation that likely indicates the beginning of the formation of mature neuronal networks.

The use of dedicated live/dead cell dyes to assess cell death was considered, though the difference in brightness between live and dead nuclei made it difficult to assess both in fluorescent images using the imaging tools that were available. Therefore the common two-staining method of using the live nuclei stain Hoechst 33342 and the apoptotic nuclei stain PI was used with the idea of using the ratio of the two as an indicator of cell death. The finding that Hoechst staining was several fold brighter in dead cells and

could therefore distinguish between live/dead nuclei was an unexpected result. Upon discovery, this effect was extensively characterised to determine whether it was suitable for use as a single-stain cell death marker. The relative difference in brightness between live and dead nuclei using this method was much lower (3x compared to 50x) than commercially available live/dead cell dyes and therefore allowed analysis of all nuclei in a single image without saturation while also allowing immunostaining at the excitation wavelength where PI would have been used. If higher concentrations of Hoechst or longer incubation times were used no difference in brightness was observed. It has been suggested in the literature that Hoechst has a lower rate of diffusion than other nuclei stains such as DAPI and, although live cell permeable, it is slow to pass through living membranes (Park et al., 1985). All of this suggests that the observed effect was highly dependent upon the concentration, incubation time and cell type used. Considering that PI is known to stain late apoptotic and necrotic cells rather than early apoptotic cells, it was assumed from the results that bright Hoechst nuclei were also late apoptotic/necrotic. "Dead" is therefore used as a term that encompasses both apoptotic and necrotic as differences between the two were not assessed. It is worth mentioning that this Hoechst approach likely does not distinguish between live and early apoptotic cells and may therefore miss cells that are starting to undergo apoptosis in response to 6-OHDA and glutamate incubation.

The use of a ration method to calculate cell death in Hoechst-stained cells was a novel approach I designed during these experiments. By calculating the number of bright "dead" nuclei as a percentage of the total number of stained nuclei it gives the percentage of dead cells in each condition. This method was relatively robust, with the brightness difference in live-stained cells being capable of surviving fixation and immunostaining. The effect was, however, very dependent upon the Hoechst concentration and time of incubation, with periods longer than 10 minutes at 37ºC tending to saturate the nuclei, and periods of less than 8 minutes leaving the brightness difference too small to accurately quantify. With careful consideration of these facts, along with some degree of optimisation for different cell types, I believe this assay can be a simple, cheap and effective way of determining late stage cell death in cultures.

The results here show that hiPSC-derived DA neurons are selectively destroyed by 6-OHDA similar to SNc neurons *in-vivo* and primary neurons in culture. $Ca_V1.3$ expressing hiPSC-derived DA neurons were not more susceptible to 6-OHDA than their $Ca_V1.3$-negative variants during the first 6 weeks post-differentiation. The results also

suggest that Hoechst 33342 can be used as a live/dead cell dye depending on the concentration, incubation time and cell type studied.

4.4.3 Glutamate Excitotoxicity in hiPSC-Derived Dopaminergic Neurons

Many neuronal cell types display excitotoxicity where, in the presence of high extracellular concentrations of the neurotransmitter glutamate, excessive glutamate receptor activation results in increased cytosolic Ca^{2+} concentrations. This leads to cell death either through apoptosis or autophagy (Kritis et al., 2015). Previous studies have suggested that SNc DA neurons are vulnerable to glutamate excitotoxicity and become increasingly susceptible in the presence of mitochondrial toxins such as MPTP (Meredith et al., 2009). Whether hiPSC-derived DA neurons in culture display excitotoxicity in response to high concentrations of extracellular glutamate had not been investigated.

Here I have shown that hiPSC-derived DA neurons are resistant to excitotoxicity at concentrations that are toxic to various other neuronal cell types in culture. Excitotoxic death in PC12 and NT-2 cells has been reported at glutamate concentrations of 10 µM to 10 mM respectively at timescales from 0.5 to 72 hours (Kritis et al., 2015). Due to the reliance of glutamate excitotoxicity on the expression of glutamate receptors, data from weeks 3-6 was pooled as the development of ESPSCs that were blocked by glutamate receptor antagonists was first observed at around this time point in culture. No difference between week 0 hNPCs and week 3-6 differentiated neurons was observed here, neither were TH-positive cells nor $Ca_V1.3$-positive/TH-positive cells more susceptible.

NPCs have previously been reported to have a high resistance to glutamate excitotoxicity (Suzuki et al., 2006), perhaps due to differences in glutamate receptor expression compared to mature neurons.

Several reasons for the resistance of differentiated neurons to glutamate excitotoxicity can be proposed. During these experiments, cultures were incubated with L-glutamic acid for 24 hours. In certain cell types toxicity was seen after as long as 72 hours. It could be that further incubation is needed to see an effect.

Astrocytes are known to play an important role in excitotoxicity, being mainly responsible for the uptake of released extracellular glutamate *in-vivo*. They can also

promote excitotoxicity through the reversal of their Na^+-Glutamate transporters when extracellular glutamate concentrations are above a critical level (Schousboe & Waagepetersen, 2005). Considering that ~85% of the cells in culture stained for neuronal markers (**Figure 3.2C**) it is possible that astrocytes make up a significant proportion of the remaining cells. Astrocytes are also believed to interact directly with synapses in what is known as a "tripartite synapse." This close association allows for cross-talk between neurons and glia and is believed to be critical for excitotoxicity *in-vivo* (Rudy et al., 2015). It could be predicted then that the astrocytes in hiPSC-derived DA cultures would promote excitotoxicity. Since excitotoxicity was not seen in culture, it could indicate either the lack of formation of these tripartite synapses or that there are too few astrocytes present to induce excitotoxicity. An interesting experiment for future studies would be to add glia such as astrocytes and oligodendrocytes to these cultures to see if excitotoxicity develops.

Another possibility is that synapses in these cultures have not yet reached full maturity. Data from chapter 3 suggests at a shift in synaptic maturity at 6 weeks post-differentiation, though this may indicate the onset of maturity rather than its completion. NMDA receptors are believed to be critical for excitotoxicity in hiPSC-derived neurons (Gupta et al., 2013). Changes in NMDA receptor expression, localisation and trafficking are associated with synaptic plasticity and maturation (Yashiro & Philpot, 2008). Excitotoxicity may therefore develop with more time culture.

Previous studies have suggested that dopamine can reduce the cytosolic Ca^{2+} increases associated with exposure to high concentrations of extracellular glutamate (Vaarmann et al., 2013). The presence of dopamine in the extracellular medium could therefore be having a protective effect on all the cells in culture.

It has previously been shown that neurons with a compromised mitochondrial membrane potential are protected against the toxic effects of excessive glutamate receptor activation. This is due to their inability to accumulate Ca^{2+} into mitochondria as efficiently as other neurons (Nicholls & Budd, 1998). Since the mitochondrial membrane potential is known to be vulnerable in SNc DA neurons (Schapira et al., 1990) it could be that the vulnerable phenotype associated with these neurons is providing a degree of neuroprotection against glutamate excitotoxicity. This theory does, however, contradict evidence that suggests SNc DA neurons are more susceptible to glutamate excitotoxicity in the presence of mitochondrial toxins (Meredith et al., 2009).

AMPA receptors expressing the GluR2 subunit have been shown to protect against excitotoxicity due to their reduced permeability for Ca^{2+} (Iihara et al., 2001). If this subunit is expressed in these cells it could explain the resistance, though this would need to be experimentally determined.

NPCs have also been shown to protect neurons against the toxic effects of glutamate through the release of neurotrophic factors (Lladó et al., 2004). The cells in these cultures have been differentiated from NPCs. If a proportion of the cells in culture have not gone through differentiation, or if they have retained certain phenotypic traits typical of NPCs due to their relative immaturity, they may provide neuroprotection to neurons in culture.

Interestingly, resistance to glutamate-induced excitotoxicity has been identified in other PD models *in-vitro*. The human neuroblastoma cell line SH-SY5Y, which displays phenotypic traits typical of DA neurons, has been shown to be sensitive only to high extracellular glutamate concentrations ranging from 8 to 80 mM (Xie et al., 2010).

Through the experiments performed here I have shown that hiPSC-derived DA neurons, during the first 6 weeks post-differentiation from hNPCs, display a resistance to excitoxicity at concentrations of extracellular glutamate that cause death in other neuronal cell types. This resistance was not specific to TH-positive cells and the presence of $Ca_V1.3$ did not influence susceptibility. These neurons may therefore not be suitable for the study of excitotoxicity in PD.

Chapter 5

General Discussion

Abstract

In this thesis I have presented data that fills in gaps in our knowledge of pacemaking in two *in-vitro* models of human diseases. This allows for a comparison of pacemaking between these models and their *in-vivo* counterparts to be performed and for their suitability for modelling the role of excitability in these diseases to be assessed. For AtT20s, I show that their intrinsic properties are similar to corticotrophs *in-vivo*. They do, however, appear to be disconnected from agonist-induced effects on excitability and from action potential-evoked release of adrenocorticotropic hormone. They are therefore suitable for investigating the mechanisms of intrinsic pacemaking but not for the study of the role of excitability in hormone release. For human induced pluripotent stem cell derived dopaminergic neurons, I show that excitable properties that are characteristic of the dopaminergic neurons of the substantia nigra pars compacta that die in Parkinson's disease develop during early maturation in these cultures. Overall, however, excitability in these neurons appeared relatively immature. They are therefore not suitable or require extended maturation times before they can be used to model mature pacemaking and cell death in Parkinson's disease.

5.1 Conclusions

Pacemaking in neuronal and neuro-endocrine cell types provides a mechanism for the entrainment of action potential firing to a particular frequency. This in turn allows for the control of rhythmic processes such as breathing, hormonal cycles and fine motor control (Pike et al., 1999).

Two examples of diseases that occur in cell types known for their pacemaker activity are Cushing's disease and Parkinson's disease (PD). Cushing's disease is caused by corticotroph tumours within the anterior pituitary, resulting in excess secretion of adrenocorticotrophic hormone (ACTH) and subsequently cortisol from the adrenal cortex (Nelson et al., 1960). PD is caused by the selective death of substantia nigra pars compacta (SNc) dopaminergic (DA) neurons, in part due to Ca^{2+} influx through $Ca_V1.3$ voltage-gated calcium channels (VGCCs) during pacemaking (Chan et al., 2007; Sveinbjornsdottir, 2016).

Both cell types have *in-vitro* models that can be used to study their relevant diseases. AtT20 is a neuroendocrine cell line derived from mouse pituitary tumours and are known for their robust secretion of ACTH (Woods et al., 1960). Human induced pluripotent stem cell (hiPSC)-derived DA neurons are a promising new *in-vitro* model for PD (Swistowski et al., 2010). However, whether the mechanisms of pacemaking in these models truly mimic their respective *in-vivo* counterparts is not fully known.

The research in this thesis has focused on gaps in the understanding of pacemaking in both models. For AtT20s the role of L-type, N-type and T-type VGCCs was investigated. For hiPSC-derived DA neurons the early development of pacemaking and selective vulnerability to cell death were investigated. This allows for two types of comparison to be made: Differences and similarities between the models and their respective *in-situ* counterparts can be assessed; and differences and similarities between the two models can be assessed to compare the mechanisms of pacemaking between cell types.

5.1.1 Pacemaking in AtT20s

Various VGCC subtypes have previously been identified in AtT20s, including L-type, N-type, T-type and P/Q-type channels (Mackie et al., 1995). The role of many of these in AtT20 pacemaking had not been studied. The results from chapter 2 show that L-type

VGCCs are critical for pacemaking in AtT20s, being required for action potential firing and the generation of subthreshold Ca^{2+} waves. This has previously been reported in the literature (Adler et al., 1983). One important new finding that I present is the relationship of two modalities of Ca^{2+} waves to pacemaking: TTX-dependent waves and slower, larger amplitude TTX-independent waves. It has previously been reported that TTX has no effect on Ca^{2+} waves in this cell type (Fiekers & Konopka, 1996). Here, by looking at the form of Ca^{2+} waves before and after the addition of TTX, I show that although they are not abolished by Na_V channel block they are significantly altered. There was no statistical difference in total nominal Ca^{2+} influx upon the addition of TTX, with the increased duration and amplitude of the waves compensating for their significantly reduced frequency. This points to a mechanism whereby L-type VGCCs and Na_V channels synergistically shape the frequency and amplitude of spontaneous Ca^{2+} waves. During loss of Na_V currents, L-type VGCCs compensate for and prevent a decrease in cytosolic Ca^{2+} in quiescent cells that would normally enter the cell during pacemaking. L-type VGCCs have previously been reported as critical for proliferation and cell survival in AtT20s (Loechner et al., 2009), a role that can be explained by this compensatory mechanism.

The L-type subtype $Ca_V1.3$ is often found in pacemaker cells due to its activation properties being favourable for subthreshold activation (Zampini et al., 2010). Here I show that AtT20s immunostain for $Ca_V1.3$, partly confirming the presence of this subtype in these cells. This has been previously seen in the literature, with this channel type being critical for the proliferation and survival of AtT20s (Loechner et al., 2009). No molecular identification of $Ca_V1.3$ channels through the detection of, for example, *CACNA1D* RNA transcripts via RT-PCR, has been performed either here or in the literature. Although it seems relatively clear that it is present, performing this experiment would eliminate any doubt over the presence of $Ca_V1.3$ in AtT20s.

T-type VGCCs have previously been suggested to be involved in AtT20 pacemaking by way of computer-based modelling (LeBeau et al., 1997), however direct evidence for their presence or involvement was lacking. Here I show that T-type channels are critical for pacemaking in AtT20s, though they play a different role to L-type channels. The T-type antagonist ML218 blocked all pacemaking without affecting the membrane potential. It also caused a shift in the modality of Ca^{2+} waves that was exacerbated by the addition of the Na_V antagonist TTX. This suggests that T-type channels are required for action potential generation and that T-type and Na_V channels are synergistically

involved in the shaping of but not the generation of subthreshold Ca^{2+} waves. T-type channels are found in many pacemaker cell types due to their negative-shifted activation properties being favourable for their subthreshold activation (Perez-Reyes, 2003; Matschke et al., 2015). A major difference from $Ca_V1.3$ is that T-type channels are fast and transiently activated. This makes them ideal for aiding in action potential generation by shifting dV/dt when close to the firing threshold. This observed role for T-type channels in AtT20s has not previously been described in the literature.

N-type VGCCs did not appear to be involved in pacemaking in AtT20s, with the N-type antagonist ω-conotoxin having no significant effect on action potential firing or Ca^{2+} wave properties. This finding was not surprising considering the lack of N-type channel pacemaking in the literature. This channel type is more closely associated with exocytosis in neurons, having previously been found to lie close to exocytotic protein complexes (Millán & Sánchez-Prieto, 2002). N-type channels may even contain a binding site to allow for direct interaction with the exocytotic proteins syntaxin, SNAP-25 and synaptotagmin (Sheng et al., 1997).

All in all, the results here allow for the conclusion that VGCCs and Na_V channels generate pacemaking in this model. L-type VGCCs, with input from other VGCCs subtypes and perhaps a degree of subthreshold Na_V channel activation, produce subthreshold oscillations in membrane potential that bring the cell close to the firing threshold. Near threshold, T-type VGCCs increase the rate of change of the membrane potential substantially to activate Na_V channels, generating an action potential. The following hyperpolarisation then acts to quickly inactivate VGCCs, keeping Ca^{2+} entry locked to a tight window during an action potential.

Data here also provides the first super-resolution analysis of secretory granule size in an AtT20 cell, with them likely having a diameter of 160-180 nm. Secretion of these granules appeared to be disconnected from their excitability, however, with membrane potential changes unable to induce capacitance changes associated with secretion. Capacitance could be increased by addition of an L-type agonist, indicating that secretion is likely linked to increases in intracellular Ca^{2+}. In addition, no changes in excitability were observed upon the addition of the ACTH secretagogue corticotropin releasing hormone (CRH). Whether or not excitability is linked to secretion in this cell type has remained ambiguous, with contradictory evidence being published on the matter. One study identified a membrane depolarisation and increase in firing rate upon

the addition of CRH (Zemkova et al., 2016). Another found that changes in excitability had no effect on secretion, with it instead being linked to increases in intracellular Ca^{2+}. (Surprenant, 1982). The experiments here, along with those in previous studies, require the addition of chelators such as EGTA to buffer unwanted changes in intracellular Ca^{2+}. This could have undesired effects on Ca^{2+} increases after CRH addition or during action potential firing. The true effect of excitability on secretion is therefore difficult to determine under these conditions, with studies that avoid this buffering required to draw a more meaningful conclusion.

Figure 5.1 summarises the ion channels that were investigated during the course of this thesis, highlighting those for which new roles in pacemaking in AtT20s were identified.

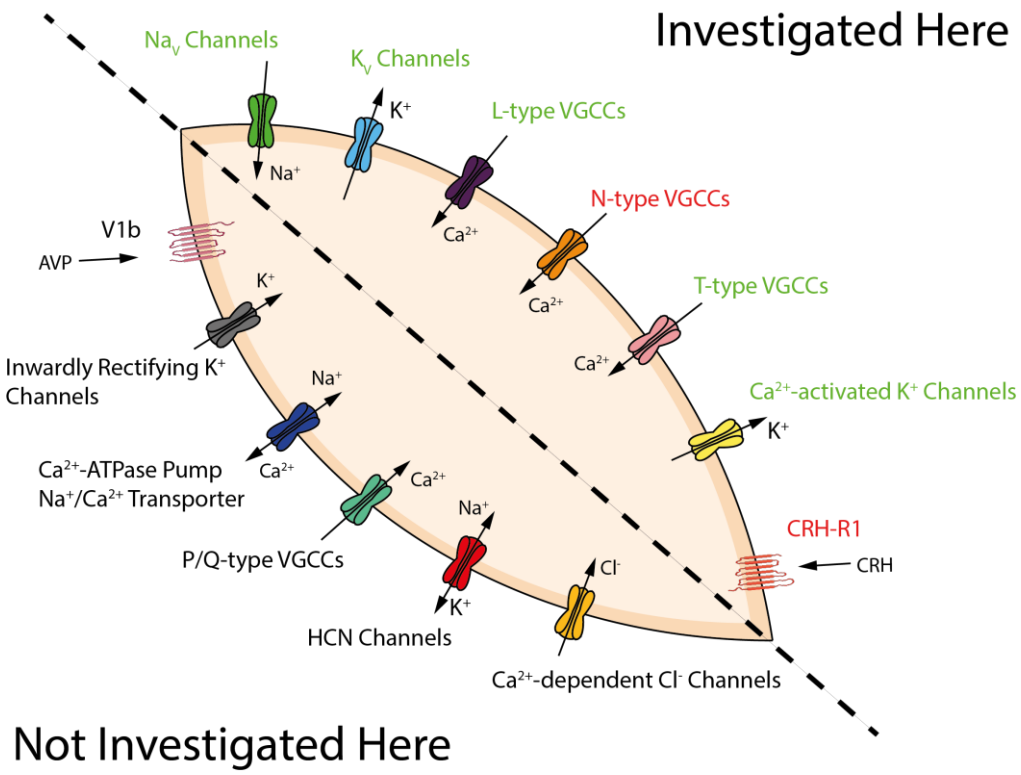

Figure 5.1 – The ion channels investigated in AtT20s. A graph showing the ion channels that were (bottom) and weren't (top) investigated in AtT20s during this research. Green highlights channels that were found to be involved in pacemaking in novel ways: Na_V channels supported Ca^{2+} waves in a subthreshold manner along with T-type VGCCs; L-type VGCCs maintained intracellular Ca^{2+} to within physiological levels despite changes in activity; K^+ channels help shape Ca2+ waves. Red highlights channels that were found to not be involved in pacemaking: N-type channels played no role; CRH-1 had no role despite having a role in corticotrophs in-vivo.

5.1.2 Pacemaking in hiPSC-Derived Dopaminergic Neurons

By identifying cells as tyrosine hydroxylase (TH)-positive or negative, data presented in chapters 3 and 4 shows that hiPSC-derived DA neurons begin to develop an excitable phenotype typical of SNc DA neurons from 1-2 weeks post-differentiation from hiPSC-derived neural progenitor cells (hNPCs). Action potential firing was observed in cells from 2 weeks in culture. TH-positive cells had a tendency towards more excitable states, being more likely to be firing action potentials and more likely to produce spike trains in response to depolarisation than cells that were TH-negative. This result is likely confounded by the presence of non-neuronal/non-excitable cell types within the TH-negative population, considering that 10-15% of cells in the cultures were identified as NeuN-negative. Neurons in culture also developed Ca^{2+} waves that increased in amplitude and rhythmicity up to 6 weeks post-differentiation. All of this has been previously described in the only study that has looked at excitability in these neurons in-depth (Hartfield et al, 2014). This study described the development of action potentials and Ca^{2+} waves from 6-12 weeks post-differentiation from hiPSCs rather than from younger hiPSC-derived NPCs as has been performed in this thesis. Considering the different starting points, where it takes ~2 weeks to develop hNPCs from hiPSCs, excitability and Ca^{2+} waves developed several weeks earlier than described in this previous study, though likely continue to mature past 6 weeks as previously described (Hartfield et al., 2014).

Here I show that action potential firing and spike trains were L-type VGCC dependent, though only in one TH-positive cell. This is the first time L-type dependence has been investigated and identified in a hiPSC-derived DA neuron. Only a single TH-positive cell could be identified due to time constraints and the loss of Lucifer Yellow marked cells during immunostaining. This marks a good starting point, however, for further analysis of the role of L-type VGCCs in pacemaking in hiPSC-derived DA neurons.

Although action potential firing in this previous study was described as spontaneous, the authors did not investigate whether the observed activity was being driven by synaptic activity rather than intrinsic properties (Hartfield et al., 20140. Here I show that firing is not intrinsic, instead being driven by synaptic activity. Action potential firing could be blocked by glutamate receptor and dopamine D2 receptor antagonists. Excitatory spontaneous postsynaptic currents (ESPSCs) developed from 2 weeks post-differentiation. These were blocked by the co-addition of NMDA and AMPA/Kainate receptor antagonists. The addition of extracellular glutamate resulted in increases in the

intracellular Ca^{2+} concentration, providing further evidence for influx through NMDA receptors. Another possibility is that glutamate-induced depolarisation is activating low-voltage activated VGCCs such as T-type channels. These lines of evidence, along with the observation that they developed simultaneously alongside action potential firing, points to their importance in generating the electrical activity seen in culture.

Although inhibitory postsynaptic currents were not identified, the presence of GABAergic input should not be excluded. Calculation of the equilibrium potential for Cl^- in the conditions used indicated that the Cl^- equilibrium was reversed at the -80 mV holding potential used. This indicates that under these conditions they would appear as depolarising currents rather than the hyperpolarising currents that are typical of GABA receptor activation. Indeed, small ESPSCs remained in the presence of glutamate receptor blockers. Given the information above, these could possibly correspond to excitatory GABAergic currents, though this would need to be determined experimentally to know for sure.

Although Hartfield et al describe the development of Ca^{2+} waves, it was not determined whether these waves were occurring below the threshold for action potential firing (as previously described in SNc neurons *in-vivo* (Puopolo et al., 2007)). Here I show that the addition of TTX blocked Ca^{2+} waves in the majority of cells. This indicates that they were action-potential dependent rather than subthreshold. TH-positive cells developed denser Ca^{2+} currents than TH-negative cells and the majority of TH-positive cells (>70%) immunostained against $Ca_V1.3$, a channel type that characterises SNc DA neurons *in-vivo* (Chan et al., 2007). The presence of this channel could explain the differences in excitability between TH-positive and TH-negative cells as $Ca_V1.3$ expression in SNc DA neurons *in-vivo* is suspected to underlie their pacemaker activity (Chan et al., 2007). However, the finding that $Ca_V1.3$ immunostaining was seen in the majority of cells in the cultures regardless of whether they were TH-positive along with the fact that a proportion of TH-negative cells are likely non-neuronal as seen by NeuN staining, it is possible that this result could also be confounded by the presence of non-neuronal cell types within the TH-negative population or by different channel localisation between these two groups.

It is possible, given the fact that the electrical properties of hiPSC-derived DA neurons in the previous study by Hartfield et al continued to mature up to 12 weeks post-differentiation and that the results here only investigated time points earlier in

development, that intrinsic pacemaking and subthreshold Ca^{2+} waves develop at later stages of maturity. Synaptic input and the entrainment of Ca^{2+} waves to action potential firing may be important steps that lead to the development of intrinsic pacemaking in these neurons in culture. The requirement of synaptic input for the development of intrinsic excitability has been seen in many other systems. Dopamine has been seen to induce synaptic plasticity in pyramidal neurons from the CA1 region of the hippocampus, resulting in long term changes in their intrinsic firing (Edelmann & Lessmann, 2013). Activation of NMDA receptors in cerebellar deep nuclear neurons results in changes in their response to current injection (Aizenman & Linden, 2000). Purkinje cells in the cerebellar cortex require GABAergic input to develop intrinsic excitability during their early development (Watt et al., 2009). "Intrinsic plasticity," whereby changes in ion channel expression in mature cells results in long-term changes in excitability, has been identified as an important requirement for the development of mature neuronal networks and has specifically been implicated in memory formation (Zhang & Linden, 2003).

hiPSC-derived DA neurons have previously been shown to be susceptible to cell death in response to incubation with the DA-specific toxin 6-hydroxydopamine (6-OHDA) (Nguyen et al., 2011) and show susceptibility to the mitochondrial toxin 1-methyl-4-phenyl-1,2,3,6-tetrahydropyridine (MPTP) in a similar fashion to SNc DA neurons (Hartfield et al., 2014). It was not known whether this susceptibility continued at higher concentrations of 6-OHDA or whether they are susceptible to glutamate-induced excitotoxicity. The results here confirm that TH-positive cells are selectively susceptible to 6-OHDA-induced cell death over TH-negative cells, though at very high concentrations general toxicity did occur.

Many neuronal cell types display excitotoxicity, where excessive activation of ionotropic glutamate receptors, such as NMDA receptors, results in excessive Ca^{2+} influx and cell death. Concentrations of extracellular glutamate that have previously been reported to induce cell death in neuronal cell types in culture range from 10 µM – 100 mM (Kritis et al., 2015). The results here show that all of the neurons in culture, from hNPCs to differentiated neurons, displayed a resistance to cell death in response to 24 hour incubation with extracellular glutamate concentrations up to 100 mM, at least up to 6 weeks post-differentiation. Reasons I suggest for this include a lack of synaptic maturity, the lack of formation of a tripartite synapse (see Rudy et al., 2015), the requirement of incubation times longer than 24 hours, the protective effects of

dopamine (Nicholls & Budd, 1998), the protective effects of AMPA receptors (Iihara et al., 2001), metabolic susceptibility preventing Ca^{2+} influx into mitochondria (Schapira et al., 1990) or the retention of stem cells or stem cell properties within the population having a neuroprotective effect (Lladó et al., 2004).

Whether $Ca_V1.3$ expression, which is suspected to be involved in the mechanism of selective cell death in mature SNc neurons *in-vivo* (Chan et al., 2007), increases the susceptibility of hiPSC-derived DA neurons to death in response to 6-OHDA or extracellular glutamate was not previously known. In Chapter 4 I show that TH-positive cells that immunostained against $Ca_V1.3$ are not more susceptible to death than TH-positive cells that are $Ca_V1.3$-negative. This was true for both glutamate and 6-OHDA up to 6 weeks post-differentiation from hNPCs. Although the results do not discount the possibility that $Ca_V1.3$-related susceptibility develops in these cells at later stages of maturity, or that susceptibility requires the co-addition of mitochondrial toxins as has been seen in primary SNc neurons from mice (Chan et al., 2007), the results do discount $Ca_V1.3$ as a primary factor in the susceptibility of hiPSC-derived DA neurons to cell death in response to extracellular glutamate and 6-OHDA at early stages in their development.

All in all, the data presented here fills in gaps in the literature surrounding the mechanisms and development of pacemaking in AtT20 anterior pituitary corticotrophs and hiPSC-derived DA neurons. This allows for an assessment of their suitability as model systems to study their respective diseases that is more informed than those previously in the literature.

Figure 5.2 summarises the ion channels that were investigated during the course of this thesis, highlighting those for which roles in pacemaking in hiPSC-derived DA neurons were identified.

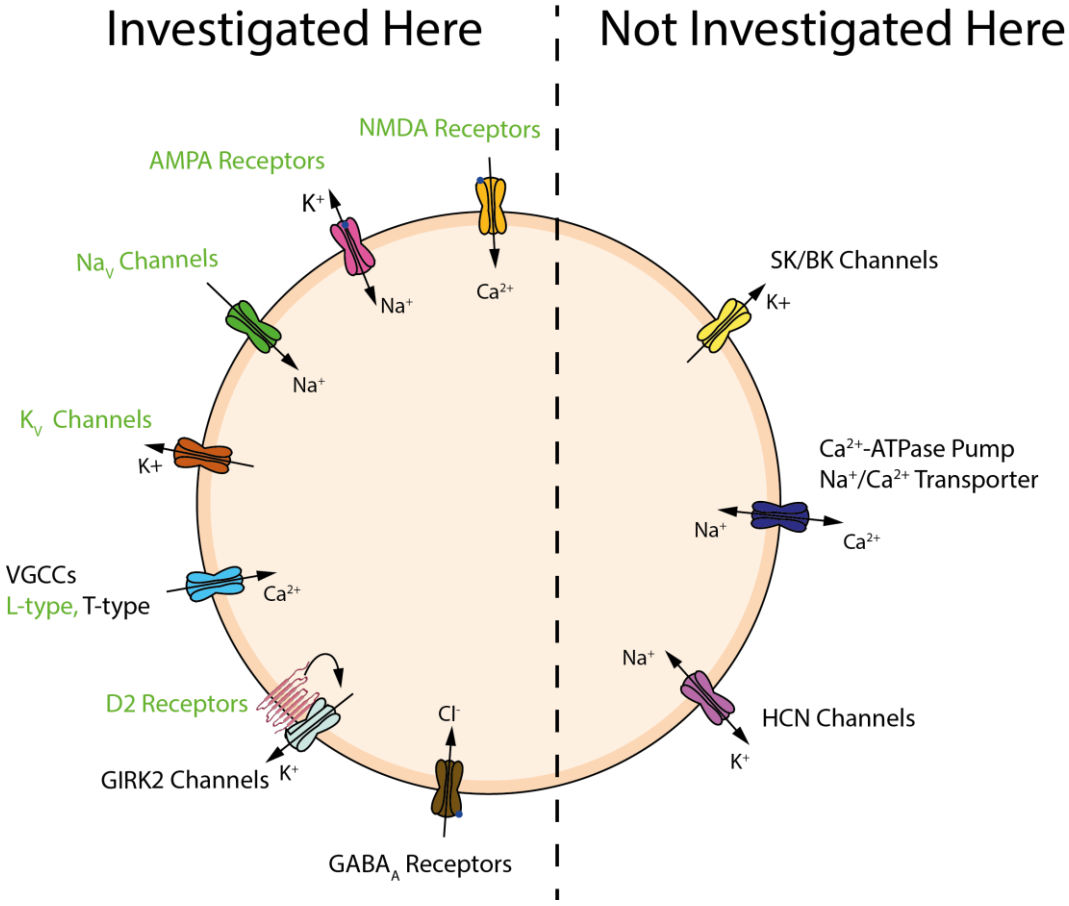

Figure 5.2 – The ion channels investigated in hiPSC-derived DA neurons. A graph showing the ion channels that were (left) and weren't (right) investigated during this research. Green highlights channels that were found to be involved in pacemaking. Red indicates channels that were found to not be involved.

5.2 Similarities & Differences Between AtT20s and Corticotrophs *In-Vivo*

5.2.1 Pacemaking and Control of ACTH Release

In-situ, pacemaking in corticotrophs is closely associated with the secretion of ACTH, controlling the timing of its release (Lee & Tse, 1997). Action potential firing patterns that have been observed include tonic firing, burst firing and quiescence all within the same population (Zemkova et al., 2016). The two main hormonal regulators of ACTH

secretion, CRH and arginine vasopressin (AVP), have been seen to induce firing in both active and quiescent cells *in-vivo* (Kuryshev et al., 1995; Lee et al., 2015). Similar activity patterns have been identified in AtT20s (Adler et al., 1983), which is confirmed by data here.

There is contradictory evidence over whether ACTH release is coupled to pacemaking in AtT20s. One study observed that membrane depolarisation and secretion occurred upon the addition of CRH (Guérineau et al., 1991). Another study found action potential firing did not induce secretion, with it instead being linked to increases in their cytosolic Ca^{2+} concentration (Surprenant, 1982). Here I provide evidence for the latter, as CRH had no effect on pacemaking. CRH is believed to act short term via activation of TREK-1 K^{+} channels and voltage-gated ion channels (Luini et al., 1985; Lee et al., 2015). It also acts long term via stimulation ACTH synthesis from its precursor, pro-opiomelanocortin, through the induction of cAMP pathways (Kageyama & Suda, 2009). It is possible that an effect would be seen over longer periods than the 10 minute recordings performed here, though the lack of any immediate effect indicates that CRH is likely disconnected from direct control of excitability. Data here therefore confirms that the outward patterns of intrinsic excitability appear similar between corticotrophs and AtT20s, though there is a difference in agonist-induced excitability.

Ca^{2+} waves have been seen to underlie pacemaking in corticotrophs, producing Ca^{2+}-dependent oscillations in membrane potential in the presence of TTX (Zemkova et al., 2016). Ca^{2+} waves have also been identified in AtT20s, acting completely independently of action potential firing (Fiekers & Konopka, 1996). Here I present data that disputes this independence, with action potentials being seen to entrain the amplitude and frequency of Ca^{2+} waves. This dependence acts both ways, with the Ca^{2+} waves then acting to maintain high frequency action potential firing. These waves continued in the presence of TTX though at an increased amplitude and a reduced frequency. This is backed by simultaneous patch clamp and Calcium Green-1 staining which showed Ca^{2+} influx primarily occurs after an action potential. No in-depth analysis of the effects of TTX on Ca^{2+} waves in corticotrophs has been performed so whether this constitutes a similarity or difference between AtT20s and corticotrophs *in-vivo* is yet to be seen. In both cell types, Ca^{2+} waves have been seen to be L-type VGCC dependent (Adler et al., 1983; Zemkova et al., 2016). Data here confirms this, with the L-type antagonist nifedipine blocking all pacemaking and Ca^{2+} waves. $Ca_V1.3$ staining partly confirms the previous finding that $Ca_V1.3$ and $Ca_V1.2$ are expressed in AtT20s

(Loechner et al., 2009). With more time, specific block of $Ca_V1.3$ channels with drugs such as Isradipine would have confirmed or discounted their involvement in pacemaking. It is not yet known which subtypes are involved in corticotrophs *in-vivo* so, as far as current evidence allows us to conclude, Ca^{2+} waves in AtT20s are produced via a similar mechanism to corticotrophs *in-vivo*.

5.2.2 Ion channels Involved in Intrinsic Pacemaking

Intrinsic pacemaking in corticotrophs requires the complex interplay of many different ion channels to function correctly. Firing appears to mainly be dependent upon Na_V channels and L-type VGCCs (Zemkova et al., 2016). This is also seen in AtT20s, with the removal of Na^+ from the extracellular medium preventing action potential firing while the antagonism of L-type VGCCs prevents both action potential firing and Ca^{2+} waves (Adler et al., 1983). These observations are backed by data here. I also provide evidence to suggest that L-type VGCCs are involved in a compensatory mechanism that retains intracellular Ca^{2+} concentrations at physiological levels despite changes in excitability. This is backed up by the finding that L-type VGCCs ($Ca_V1.2$ and $Ca_V1.3$) are critical for proliferation and survival in AtT20s (Loechner et al., 2009). This mechanism has not been studied *in-vivo* and may be worth investigating for its potential link to ACTH secretion.

Maintenance of the resting membrane potential in corticotrophs is performed by a variety of channels including K_V, BK, TREK-1, HCN and inward rectifying K^+ channels (Kuryshev et al., 1995; Liang et al., 2011; Liang, 2012; Kretschmannova et al., 2012). Quiescent cells have been noted to have a more depolarised membrane potential than firing cells, indicating the importance of the regulation of membrane potential in pacemaking (Zemkova et al., 2016). Computer modelling of BK channels has also indicated they are able to regulate activity patterns in firing cells but are unable to transition quiescent cells to a firing state (Fletcher et al., 2017). This effect has also been identified in BK channel knockouts (Liang, 2012). K^+ channels have also been identified in AtT20s, with BK channels suspected to drive membrane repolarisation following an action potential (Adler et al., 1983). K_V channels and inwardly rectifying K^+ channels have also been identified though their role in pacemaking has not been explored (Dousmanis & Pennefather, 1992). Various other channel types have been identified in AtT20s whose role in pacemaking *in-vivo* is unknown. These include two

types of Ca^{2+} dependent chloride channels, the Ca^{2+}-ATPase pump and the Na^{+}-Ca^{2+} transporter (Korn et al., 1991). TREK-1 channels in corticotrophs have also not yet been identified in AtT20s. All in all, there remain many gaps in our knowledge of the ion channels involved in corticotrophs *in-vivo* and in AtT20s. The mechanism of intrinsic pacemaking appears to be relatively well conserved between the two, meaning that the identification of a pacemaking-associated channel type in one cell type gives a strong grounding for investigating its possible role in the other.

Several VGCC subtypes have been identified in AtT20s and in rat corticotrophs. Although the role of L-type VGCCs has been relatively well characterised, many of these other subtypes had unknown roles in pacemaking. These subtypes are N-type, T-type and P/Q-type VGCCs (Mackie et al., 1995).

T-type VGCCs have been identified in both human and rat corticotrophs. They have been suggested to be involved in the generation of Ca^{2+} waves but not directly in firing (Guérineau et al., 1991). In support, computer-based modelling of corticotroph excitability suggests that conductances associated with T-type VGCCs can control firing patterns but have no role in action potential generation (LeBeau et al., 1997). Here I show that T-type channels are required for pacemaking in AtT20s. This could suggest either a difference in the mechanism of pacemaking between these two cell types or that refinement of these computer-based models is required in response to this updated information. The transient opening and closing of T-type channels at negative membrane potentials makes them ideal for activation close to the firing threshold, explaining their ability to drive Na_V-dependent action potentials (Perez-Reyes, 2003). It may be worth re-examining the roles of T-type channels in corticotrophs to determine whether they play a similar role *in-vivo*.

N-type VGCCs have been identified in AtT20s but whether they are expressed in corticotrophs *in-vivo* is unknown (Mackie et al., 1995). Data here suggests they play no major role in AtT20 pacemaking. Considering the lack of N-type associated pacemaking in the literature they likely play no role in corticotrophs *in-vivo*, though experimental evidence is needed to confirm this.

5.2.3 Suitability as a Model for Cushing's Disease

Corticotrophs *in-vivo* and the AtT20 pituitary tumour cell line show many similarities in their pacemaking properties. They display identical activity patterns with quiescent, burst firing and tonic firing cells seen within the same population. Similar complements of ion channels drive their excitability with L-type VGCCs playing critical roles. Several types and subtypes of ion channels that are involved in pacemaking in AtT20s have as of yet unidentified roles *in-vivo*. These include HCN channels, Ca^{2+} dependent Cl^- channels, Ca^{2+} pumps and, supported by data here, T-type VGCCs. This, coupled with the fully intrinsic nature of AtT20 electrical activity, means they serve as a useful model for the general mechanisms of pacemaking in corticotrophs.

Both corticotrophs in Cushing's disease and AtT20s show excessive secretion of ACTH. This is due to Cushing's disease being specifically caused by pituitary tumours (Nelson et al., 1960). *In-vivo*, ACTH release is coupled to pacemaking (Guérineau et al., 1991). Evidence for a loss of this coupling in AtT20s is contradictory. One study states that ACTH-releasing hormones cause membrane potential changes while another, supported by data here, provides evidence that no changes occur (Surprenant, 1982; Zemkova et al., 2016). This cell type may therefore not be suitable for studying the effects of abnormal excitability on ACTH release. They are, however, suitable for studying the mechanisms of secretion that are independent of electrical activity and for studying possible treatments for Cushing's disease. These include the suppression of growth of pituitary tumours and downregulation of ACTH production or secretion. These types of studies are already being performed in AtT20s, with the roles of the Brg1 and HDAC2 genes in ACTH production and the effects of Curcumin and Pasireotide on reducing secretion having been investigated (Bilodeau et al., 2006; Bangaru et al., 2010; Castillo et al., 2011).

5.3 Similarities and Differences Between hiPSC-Derived and SNc Dopaminergic Neurons

5.3.1 Properties of Pacemaking

Mature SNc DA neurons display two main activity patterns in rats: tonic firing at a frequency of 3-8 Hz that can occur in the absence of synaptic input and burst firing when in the presence of large quantities of synaptic input (Grace & Bunney, 1984; Tepper et al., 1998; Guzman et al., 2009). The same patterns of activity have been identified in hiPSC-derived DA neurons in a previous study (Hartfield et al., 2014) which is backed by data here. Hartfield et al described action potential firing as occurring at a similar frequency to SNc neurons in these animal studies, though data here found that firing occurred at far lower frequencies (>2 Hz). This is likely explained by the earlier developmental time points I investigated and by the fact that experiments here were performed at 21^{o}C rather than 37^{o}C as performed by Hartfield et al. Action potential firing began to develop from 2 weeks post-differentiation in this study and from 6-12 weeks post-differentiation in the study by Hartfield et al (bearing in mind a longer differentiation process in this previous study, equivalent to a 4-10 week period in the results here). This is roughly equivalent to the development of pacemaking in cultured SNc neurons from postnatal rats, which began to develop pacemaking from the second postnatal week and showed mature properties from week 4 (Tepper et al., 1990).

In-vivo recording from the primate SNc has shown that these neurons produce, slow rhythmic bursts of action potentials in response to current injection (Bayer et al., 2007). These "spike trains" have also been identified in hiPSC-derived DA neurons both here and by Hartfield et al. I carry this further, showing that DA neurons in culture are far more likely to produce spike trains than non-DA neurons. This finding, however, could be due to the presence of non-excitable cell types within the TH-negative population. Spike trains here appeared underdeveloped at 6-weeks post-differentiation compared to those by Hartfield et al at 12 weeks post-differentiation. This indicates that these neurons require extensive time in culture before they develop excitable properties similar to mature SNc neurons *in-vivo*.

5.3.2 Intrinsic vs Agonist Induced Excitability

Action potential firing in SNc DA neurons has been found to be TTX dependent, with subthreshold Ca^{2+}-dependent membrane potential oscillations still able to occur in the absence of firing (Puopolo et al., 2007). Immunohistochemical analysis of somatodendritic ion channel expression has identified a large range of channel types including voltage gated potassium channels ($K_V1.3$, $K_V2.1$, $K_V3.2$, $K_V3.3$, $K_V4.3$), Ca^{2+}-activated SK channels (SK1, SK2, SK3), HCN channels (HCN2, HCN4), L-type ($Ca_V1.2$, $Ca_V1.3$) and T-type VGCCs ($Ca_V3.1$, $Ca_V3.3$) (Dufour et al., 2014). Inside-out patch clamp recording has also identified Ca^{2+}-activated BK channels (Su et al., 2010). The study of postnatal rat SNc neurons revealed that the extent to which these channels are expressed in the dendrites increases as the cells mature, meaning that dendritic ion channel expression is likely important for the development of pacemaking (Dufour et al., 2014).

Here I show that hiPSC-derived DA neurons display voltage-gated Na^+ and K^+ currents which increase in density as they mature. They also selectively develop denser voltage-gated Ca^{2+} currents than non-DA neurons in culture, though this difference may be due to non-excitable cells within the cultures. No study has yet looked at whether other ion channels identified *in-vivo* are expressed in hiPSC-derived DA neurons. Doing so would provide valuable information on how similar the intrinsic mechanisms of pacemaking are between these two cell types.

Hartfield et al., supported by data here, identified Ca^{2+} waves in hiPSC-derived DA neurons that developed and matured between 6-12 weeks in culture. Here I show that these are TTX-dependent and are therefore not subthreshold as seen in mature SNc neurons in animal studies, at least up to 6 weeks post-differentiation from hNPCs. This does not discount the possibility that subthreshold waves are present in dendrites or that action potential dependence is required at early development stages to allow subthreshold waves to develop. Whether the observed increases in voltage-gated current density in hiPSC-derived DA neurons are due to an increase in dendritic expression has not been studied, though doing so would provide valuable information on whether ion channel expression in hiPSC-derived DA neurons matches those of SNc neurons *in-vivo*.

SNc DA neurons are characterised by the expression of the L-type VGCC subtype $Ca_V1.3$. This is thought to underlie both their pacemaking and their selective

vulnerability in PD (Chan et al., 2007). Expression of $Ca_V1.3$ has been identified in both the soma and dendrites of these neurons (Dufour et al., 2014). Data here confirms for the first time that hiPSC-derived DA neurons also express $Ca_V1.3$ in their soma and processes. Staining was identified in the majority of, but not all, TH-positive cells in culture. $Ca_V1.3$-positive cells are likely to be phenotypically similar to SNc DA neurons that project to the basal ganglia as part of the nigrostriatal pathway (Richards et al., 1997). $Ca_V1.3$-negative cells are perhaps phenotypically similar to DA neurons from other regions such as glutamatergic neurons within the SNc, locally projecting SNc GABAergic neurons or globus pallidus neurons which exhibit $Na_V1.6$ dependent pacemaking (Richards et al., 1997; Mercer et al., 2007; Root et al., 2016). Local release of dopamine has been identified within the SNc *in-vivo* (Vandecasteele et al., 2005). The TH-negative cells identified here could therefore represent a phenotype similar to the cells involved in this local release. Another possibility is that the $Ca_V1.3$ negative DA neurons represent immature SNc DA neurons. These have been seen to display HCN-dependent pacemaking in animal models before an increase in $Ca_V1.3$ current at later stages of maturity (Chan et al., 2007). Data here therefore shows that hiPSC-derived DA neurons in culture contain two or more phenotypically different populations that may correspond to different DA populations *in-vivo* or to SNc DA neurons at different stages of maturity.

Here I show that hNPCs stain for $Ca_V1.3$. This has been previously identified in the literature (Marschallinger et al., 2015) and brings about an interesting contradiction in the results. Voltage-gated Ca^{2+} currents in week 0 NPCs were small or non-existent yet they stained positive for $Ca_V1.3$. Expression of these channels may just be at a much lower density than could be identified in voltage clamp recordings. Another possibility is that space clamp issues could mean that Ca^{2+} currents in NPCs may not be identified if VGCCs are expressed in axons and dendrites rather than at the soma. VGCCs have been seen to be inactivated or inhibited in certain cell types due to regulation by PtdIns(4,5)P2 (Wu et al., 2002), activation in response to mechanical strain in bone cells (Walker et al., 2000) and synaptic activity in developing neurons (Magee & Johnston, 1995). Considering the suggested importance of $Ca_V1.3$ in NPC differentiation (Marschallinger et al., 2015) it could be that they require specific activation or disinhibition in response to e.g. transcription factors related to differentiation.

Pacemaking in SNc neurons has been shown to be Ca^{2+} dependent (Grace & Onn, 1989). Further experiments have narrowed this dependence to the action of L-type

VGCCs, in particular the $Ca_V1.3$ subtype (Chan et al., 2007; Guzman et al., 2009). Data here suggests that L-type VGCCs are also critical for firing in hiPSC-derived DA neurons, with action potential firing and spike trains being abolished by the addition of the L-type antagonist nifedipine in one TH-positive cell.

Intrinsic pacemaking has been seen to occur in dissociated rat SNc neurons that lack any synaptic input. In these instances, activity is often characterised by the tonic firing of action potentials in a rhythmic fashion (Grace & Bunney, 1984; Puopolo et al., 2007). SNc neurons *in-vivo* receive excitatory glutamatergic inputs from regions such as the STN, PPN and from within the SNc. Inhibitory inputs are also received from D2 receptor expressing GABAergic neurons in the neostriatum, globus pallidum and pars reticulata, and local dopamine inhibition through D2 autoreceptors (Cragg & Greenfield, 1997; Lee & Tepper, 2009; Pearlstein et al., 2015). Firing in hiPSC-derived DA neurons has previously been seen to be spontaneous without evidence to back the claim that it is intrinsic rather than synaptically driven (Hartfield et al., 2014). Here I show that firing during the first 6 weeks post-differentiation from hNPCs is dependent almost solely upon synaptic input, with no truly intrinsic pacemaking being identified. Action potential firing was dependent upon glutamatergic input and DA input through D2/D3 receptors.

ESPSCs have been seen to develop in hiPSC-derived DA neurons from 6-12 weeks post-differentiation by Hartfield et al and 2-6 weeks post-differentiation in this study. Data here suggests these currents are passed by NMDA and AMPA/Kainate receptors, which have been identified in SNc DA neurons both experimentally (Gotz et al., 1997; Jones & Gibb, 2005) and in computer-based models of their activity (Zakharov et al., 2016).

Inhibitory postsynaptic currents were not observed here nor were they observed by Hartfield et al (2014). Cultures of rat SNc neurons have been seen to develop inhibitory postsynaptic currents from postnatal week 2 (Tepper et al., 1990) and populations of GABAergic neurons have been identified within the rat SNc (Richards et al., 1997). Calculation of the equilibrium potential for Cl^- in the solutions used in both studies indicates that Cl^- flow through GABA receptors would be reversed at the holding potential of -80 mV used here for studying the postsynaptic currents. Low amplitude excitatory currents remained after the block of glutamate receptors in some cells. The possibility remains that these could correspond to excitatory GABA currents.

Experimental evidence is required to determine this, through further analysis of GABA currents and through identification of GABAergic neurons in the culture (which can be identified via expression of glutamate decarboxylase). This could also explain the lack of effect of picrotoxin on firing frequency and membrane potential. Since the reversal potential of Cl^- in these experiments (~ -40 mV) lies close to the resting potential of the neurons (-30 to -60 mV depending on the developmental week) it would mean that there would be little to no driving force for Cl^- flow through GABA receptors at these potentials.

Data here suggest at a major difference between SNc DA neurons and hiPSC-derived DA neurons in terms of the development of their synaptic networks. This fact is not surprising considering the difference in culture conditions. hiPSC-derived DA neurons in culture lack both the spatial conditions and the direct input from other brain regions seen *in-vivo*. Data here also suggests either that hiPSC-derived DA neurons are involved in the co-transmission of glutamate and dopamine as has been seen in an optogenetic study of midbrain DA neurons (Sulzer et al., 1998), or that there are separate populations of glutamatergic and DA neurons in these cultures. This is supported by a previous study of hiPSC-derived neuronal cultures (Root et al., 2016) and data here that shows that only up ~30% of the neurons in culture were TH-positive.

Although truly intrinsic activity was not seen in hiPSC-derived DA neurons within the first 6 weeks post-differentiation from hNPCs, they did, however, display a tendency towards excitable states. Here I show that action potential firing and spike trains were identified in statistically higher percentages of DA neurons than non-DA neurons in culture. Providing that these differences are not an artefact due to non-excitable cells within the TH-negative population, this could be an indicator that the capacity for intrinsic pacemaker activity may be developing. Neither this study nor the study by Hartfield et al discount the possibility that intrinsic pacemaking independent of synaptic activity develops at later stages of maturity.

5.3.3 Susceptibility to 6-OHDA

6-OHDA is a dopamine analogue that selectively induces cell death in DA neurons. It is often used to induce Parkinsonian-like symptoms in animal models (Tieu, 2011). Cell death *in-vivo* has been seen within several weeks in response to low doses (µg/ml) and *in-vitro* within hours or days at 10-100 µM concentrations (Michel & Hefti., 1990;

Perez-Rial et al., 2011). Selective death is suspected to be due to internal production of reactive oxygen species (ROS) after entry into the cell through dopamine uptake transporters (Glinka et al., 1997). Studies using cultured neurons have noted that the toxin is less selective *in-vitro*, causing cell death among non-DA neurons. This is suspected to be due to extracellular production of oxidative species such as hydrogen peroxide (Hanrott et al., 2006).

hiPSC-derived DA neurons have shown a similar susceptibility to 6-OHDA and other mitochondrial inhibitors to SNc neurons *in-vivo*. One study found that the mitochondrial membrane potential of hiPSC-derived DA neurons is reduced in the presence of the mitochondrial toxin MPTP (Hartfield et al., 2014). Another study identified the selective death of hiPSC-derived DA neurons over other cell types within the same culture at concentrations of 10 µM (Nguyen et al, 2016). Here I confirm these cultures are susceptible 6-OHDA induced cell death at concentrations of 10-200 µM, with an increase in general toxicity occurring at higher concentrations. It would appear then, given current evidence, that hiPSC-derived DA neurons and DA neurons *in-vivo* show a similar susceptibility to 6-OHDA, though a higher degree of non-selective cell death occurs *in-vitro* compared to *in-vivo*. This also provides further evidence for the DA phenotype of these cultures as this toxin is known to be specific to these neurons.

5.3.4 Susceptibility to Glutamate-Induced Excitotoxicity

Excitotoxicity is believed to play a role in SNc cell death in PD. Loss of DA neurons disinhibits the STN which in turn allows more glutamatergic input onto the SNc (Johnson et al., 2009). Mitochondrial dysfunction is believed to leave SNc neurons susceptible to excitotoxicity. This is believed to be due to the action of NMDA receptors, which have been identified in SNc neurons (Jones & Gibb, 2005; Meredith et al., 2009). Due to their compromised membrane potential in PD, mitochondria in these neurons are unable to adequately sequester the Ca^{2+} that passes into the cell through these channels, resulting in ROS production. This creates a feedback loop where further mitochondrial damage leads to an increased susceptibility to excitotoxicity leading to further mitochondrial damage. Backing this, cultured DA neurons become more susceptible to cell death in response to extracellular glutamate if they are first exposed to the mitochondrial toxin MPTP (Meredith et al., 2009). Antioxidants such as

resveratrol can protect against glutamate-induced cell death in murine DA neurons in culture (Moldzio et al., 2013).

Here I show that, from 0-6 weeks post-differentiation from hNPCs, hiPSC-derived DA neurons in culture show a resistance to glutamate-induced excitotoxicity. Cell death was only seen at high concentrations (100 mM+). Resistance to excitotoxicity has been seen in another PD model: The human neuroblastoma cell line SH-SY5Y, which displays phenotypic traits similar to DA neurons, has been shown to be sensitive only to high extracellular glutamate concentrations ranging from 8 to 80 mM (Xie et al., 2010).

Several reasons can be proposed for the resistance of hiPSC-derived DA neurons to excitotoxicity. *In-vivo*, glutamate is removed from the synaptic cleft and recycled by astrocytes. These are glial cells that are believed to interact directly with synapses in what is known as a "tripartite synapse." In situations involving high concentrations of glutamate, reversal of glutamate transporters on astrocytes can promote excitotoxity (see Rudy et al., 2015). It is not clear whether astrocytes were present in the cultures used here. Without the presence of astrocytes (at least in high numbers) the cycle of uptake and release of glutamate that promotes excitotoxicity *in-vivo* may not be occurring in these cultures.

The synaptic cleft *in-vivo* is relatively closed, with a width no larger than 10's of nanometres (Kandel et al., 1997). Due to the lower cell density and open nature of these cultures, it could be that glutamate is simply able to freely diffuse and is unable to accumulate to excitotoxic levels at synapses as occurs in the closed *in-vivo* environment.

Excitotoxicity is believed to be largely NMDA receptor dependent. Data here suggests that mature networks begin to form in hiPSC-derived DA neuron cultures at roughly 6 weeks post-differentiation. If low numbers of NMDA receptors are present before this time point then excitotoxicity may not be seen. Longer maturation periods may result in the formation of more mature, NMDA receptor dependent synaptic networks and the subsequent development of glutamate-induced excitotoxicity.Previous experiments on excitotoxicity in culture have used incubation periods up to 72 hours (Kritis et al., 2015). Incubating these neurons for longer than the 24 hours used here may result in an increase in excitotoxic cell death.

Dopamine has been seen to protect against excitotoxicity, reducing rises in intracellular Ca^{2+} that are associated with pathological levels of glutamate (Vaarmann et al., 2013). Dopamine release from DA neurons could therefore be providing neuroprotection to all the cells in culture.

AMPA receptors expressing the GluR2 subunit have been shown to protect against excitotoxicity due to their reduced permeability for Ca^{2+} (Iihara et al., 2001). This subunit, if expressed in hiPSC-derived DA neurons, could have a neuroprotective effect.

It has previously been shown that neurons with a compromised mitochondrial membrane potential are protected against the toxic effects of excessive glutamate receptor activation. This is due to their inability to accumulate Ca^{2+} into mitochondria as efficiently as other neurons (Nicholls & Budd, 1998). Since the mitochondrial membrane potential is known to be vulnerable in SNc DA neurons (Schapira et al., 1990) it could be that the vulnerable phenotype associated with these neurons is in itself providing a degree of neuroprotection against glutamate excitotoxicity. This theory does, however, contradict evidence that suggests SNc DA neurons are more susceptible to glutamate excitotoxicity in the presence of mitochondrial toxins (Meredith et al., 2009).

NPCs have also been shown to protect neurons against the toxic effects of glutamate through the release of neurotrophic factors (Lladó et al., 2004). The cells in these cultures have been differentiated from NPCs. If a proportion of the cells in culture have not gone through differentiation, or if they have retained certain phenotypic traits typical of NPCs due to their relative immaturity, they may provide neuroprotection to neurons in culture.

5.3.5 $Ca_V1.3$ Expression and Susceptibility

Expression of $Ca_V1.3$ in SNc DA neurons is associated with an increased susceptibility to 6-OHDA, with the $Ca_V1.3$ selective antagonist Isradipine able to protect against 6-OHDA induced cell death (Chan et al., 2007). Ca^{2+} influx during pacemaking has also been linked to increased susceptibility to excitotoxicity both *in-vivo* and *in-vitro* (Schapira et al., 1990; Shimizu et al., 2003). Here I show that hiPSC-derived DA neurons that stain for $Ca_V1.3$ are not more susceptible to death in response to 6-OHDA

or glutamate-induced excitotoxicity, at least during the first 6 weeks post-differentiation from hNPCs.

A likely explanation for this is the lack of mature intrinsic pacemaking in these cells at these early stages of development. Ca^{2+} influx through $Ca_V1.3$ channels is associated with mature pacemaking in SNc DA neurons *in-vivo*, with block of $Ca_V1.3$ channels showing neuroprotective effects. Early developmental pacemaking is seen in animal models which instead relies on HCN and Na_V channels. As these neurons matured, $Ca_V1.3$-dependent pacemaking began to dominate (Chan et al., 2007). Without mature $Ca_V1.3$-dependent pacemaking it is likely that mitochondrial stress due to Ca^{2+} accumulation in hiPSC-derived DA neurons is not occurring to the same extent, if at all. The possibility that $Ca_V1.3$ expression is associated with an increased susceptibility to 6-OHDA and glutamate induced excitotoxicity at later stages of maturity if or when intrinsic pacemaking develops should therefore not be discounted. It is also possible that the effects of $Ca_V1.3$ expression are subtle and require other stressors to be identified. One study, for example, has identified an increased susceptibility of cultured DA neurons to glutamate-induced excitotoxicity when in the presence of the mitochondrial toxin MPTP (Meredith et al., 2009). Data here therefore shows a difference in the effects of $Ca_V1.3$ expression on susceptibility to cell death between SNc DA neurons *in-vivo* and hiPSC-derived DA neurons *in-vitro* that is likely to be due to the relative immaturity of the cultures.

5.3.6 Suitability as a Model for Parkinson's Disease

Many similarities between hiPSC-derived DA neurons and SNc neurons exist. These include similarities in activity patterns, the ability to produce spike trains, the development of Ca^{2+} waves and the receiving of glutamatergic and DA inputs to modulate their activity. Both cell types develop a sensitivity to mitochondrial toxins such as MPTP and DA-specific toxins such as 6-OHDA (Michel & Hefti., 1990; Perez-Rial et al., 2011; Hartfield et al., 2014; Nguyen et al, 2016). Both cell types likely display L-type dependent pacemaking and express the L-type VGCC subtype $Ca_V1.3$ which is believed to underlie the selective death of SNc neurons in PD (Chan et al., 2007). This makes hiPSC-derived DA neurons suitable for studying the development of phenotypic traits associated with SNc DA neurons *in-vivo*. This includes the development of excitability, synaptic signalling, the role of D2 autoreceptor control of

excitability and the roles of $Ca_V1.3$ VGCCs. They can also be a useful tool for drug testing of new neuroprotective therapies that protect against PD due to their susceptibility to 6-OHDA and MPTP.

Many differences between these cell types also exist. Data here shows that electrical activity up to 6 weeks post-differentiation was found to not be intrinsic, unlike mature SNc DA neurons (Guzman et al., 2009). It is instead driven by synaptic activity. Inhibitory synaptic currents were not identified in this study nor by Hartfield et al though this may be due to the solutions used. hiPSC-derived DA neurons therefore do not truly mimic either the pacemaking or the synaptic networks of mature SNc neurons, lacking the intrinsic drive for pacemaking and perhaps the inhibitory input seen *in-vivo*.

hiPSC-derived DA neurons also display a resistance to excitotoxicity while SNc DA neurons *in-vivo* are suspected to display a selective vulnerability to its effects. hiPSC-derived DA neurons are therefore not suitable for modelling the role of excitotoxicity in PD unless, for example, they are cultured with other cell types such as astrocytes.

As evidence stands, caution should be taken when using hiPSCs-derived DA neurons to model PD as these cells, within the first 6-12 weeks of differentiation, appear to show a degree of immaturity in their electrical properties that does not fully mimic those of the mature SNc DA neurons that selectively die in PD. In both this study, which looks at the first 6 weeks post-differentiation from hiPSC-derived hNPCs, and a previous study by Hartfield et al, which looked at the first 12 weeks of differentiation from hiPSCs, the electrical properties of these neurons were observed to mature with time in culture, showing more and more properties typical of mature SNc DA neurons (Hartfield et al., 2014). Data here suggests that 6 weeks post-differentiation is a critical point in their development, with dramatic increases in synaptic activity, firing frequency and Ca^{2+} influx observed at this time point. Hartfield et al observed further maturation at later time points. The suitability of hiPSC-derived DA neurons as a model for PD may therefore be determined by the length of time these cells can be kept in culture. Extended maturation times past 12 weeks in culture could possibly result in the development of intrinsic pacemaking. In this study, time points past 6 weeks were associated with an increase in membrane leak and a decrease in cell viability. Hartfield et al's previous study, however, was able to maintain cultures for up to 12 weeks. Whether longer development periods are possible, along with the cost efficiency and

difficulty of maintaining lengthy cultures, may determine the viability of hiPSC-derived DA neurons as a model for PD.

5.4 Similarities and Differences Between AtT20s and hiPSC-Derived Dopaminergic Neurons

Comparing AtT20s and hiPSC-derived DA neurons reveals similarities in their pacemaking that are common across many cell types. Data here shows that tonic and phasic activity are seen in both models. These patterns are also identified in a variety of other pacemaker neurons such as in respiratory rhythm networks and mesencephalic DA neurons (Charlety et al., 1991; Smith et al., 2000).

Na_V channels, K_V channels and L-type VGCCs (in particular $Ca_V1.3$) are common to both cell types, with $Ca_V1.3$ likely responsible for the production of the observed Ca^{2+} waves in both models. This ion channel is found in other cell types with pacemaker properties such as cardiac cells of the sinoatrial node and adrenal chromaffin cells (Mangoni et al., 2003; Marcantoni et al., 2010). The expression of subthreshold-activated VGCCs likely constitutes a conserved feature between pacemaker cell types.

Ca^{2+} influx in both models occurs during action potentials, perhaps acting as a mechanism to control the timing of firing. Other conserved ion channel types that have been identified in their corresponding *in-vivo* cell types are HCN channels, Ca^{2+} activated K^+ channels such as SK and BK channels and inward rectifier K^+ channels, indicating that these cells have similar mechanisms that drive their intrinsic pacemaking *in-vivo* (Su et al., 2010; Dufour et al., 2014).

What is more interesting, however, are the differences in excitability between these two models. Despite their similarities in activity patterns and ion channel expression there are major differences over what is driving their pacemaking. AtT20 pacemaking is entirely intrinsic and appears to no longer be coupled to agonists such as CRH (Surprenant, 1982). Pacemaking is instead dependent upon increases in cytosolic Ca^{2+}. hiPSC-derived DA neurons, on the other hand, do not appear to show any intrinsic

pacemaking during their early development, though the results are confounded by the length of time that is required for their electrical properties to reach maturity. Activity is instead dependent upon synaptic input from glutamate and dopamine receptors, with intrinsic properties providing a mechanism that allows these neurons to be more likely to fire than other cell types within the same culture.

These models also display different responses to current injection. In data here, AtT20 cells produced single action potentials while hiPSC-derived DA neurons developed the ability to produce multiple action potentials in what is known as a "spike train." These differences are examples of how subtle changes in ion channel expression, either in terms of their density or localisation, can cause major differences in excitability. Computer-based modelling of various cell types has previously shown that subtly altering the conductances of several voltage-gated ion channel populations can result in activity patterns including quiescence, tonic firing and burst firing. This provides a basis for the differences in excitability seen between these cell types (Prinz et al., 2003). In rat SNc DA neurons, the expression of particular ion channels such as VGCCs and K_V channels becomes more prominent in dendrites as the cells mature in culture (Dufour et al., 2014). AtT20s represent a neuro-endocrine cell type *in-vivo* rather than a neuronal one. Corticotrophs *in-vivo* are therefore lacking the extensive axons and dendritic trees typical of neurons. Ion channel expression is therefore likely to be densely packed into the soma of these cells. Differences in the spatial distribution of ion channels likely regulates neuronal excitability as much as differences in ion channel expression do. This fact is highlighted clearly when comparing excitability in AtT20s and hiPSC-derived DA neurons.

Here I show that Ca^{2+} waves in AtT20s are still able to occur in the absence of action potential firing, acting to both maintain oscillatory changes in membrane potential and to maintain cytosolic Ca^{2+} at physiological concentrations whether a cell is firing or quiescent. Ca^{2+} waves in hiPSC-derived DA neurons were found to be action potential dependent, at least during the early development period investigated. This indicates a difference in the mechanism of pacemaking between the two. Subthreshold, L-type dependent Ca^{2+} waves are required for pacemaking in AtT20 cells, while hiPSC-derived DA neurons produce Ca^{2+} waves that are dependent upon action potentials and postsynaptic receptors. Data here therefore describe models displaying two distinct forms of excitability in culture: intrinsic excitability and agonist-induced excitability.

It has been previously found that AtT20s do not show robust pacemaking, with no ability to compensate for the loss of L-type VGCCs (Adler et al., 1983). In SNc neurons *in-vivo*, however, it has been shown that loss of L-type channels during development results in them reverting to a juvenile HCN-dependent form of pacemaking (Chan et al., 2007). The lack of subthreshold Ca^{2+} waves in hiPSC-derived DA neurons identified here could be explained by them still being dependent upon this HCN-dependent pacemaking during their early development in culture. This identifies a degree of robustness that is not present in AtT20s.

Data in chapter 3 shows that action potentials in hiPSC-derived DA neurons are blocked by the L-type antagonist nifedipine with no ability to compensate. This, however, may be explained by the relatively high concentration of nifedipine used that is likely to affect other channel types. This has previously been seen in dissociated rat SNc neurons, with the application of antagonists that are more selective for $Ca_V1.3$ showing that pacemaking continues after block of $Ca_V1.3$. With more time, Isradipine could have been applied to hiPSC-derived DA neurons here to confirm or refute the involvement of $Ca_V1.3$ in their pacemaking and to determine whether they are able to compensate for its block.

By highlighting the differences and similarities between pacemaking in these two cell types it allows for the identification of features that are both conserved and those that are different across pacemaker cells in the nervous system. By highlighting differences, such as intrinsic vs agonist-induced excitability in these two cell types, it allows studies that focus on the causes of these differences to be performed. This will in turn lead to more information on the general mechanisms of pacemaking in the nervous system and any associated diseases.

Supplementary

Supplementary 2.1 - Software-Based Calculation of Whole Cell Capacitance

The calculation of whole cell capacitance in chapter 2 was performed using the membrane test feature of Clampfit 10. This feature uses an exponential fitting algorithm in whole cell voltage clamp to determine passive membrane properties in response to square-wave voltage steps. In response to a step change in voltage (**Figure S2.1**, bottom panel), membrane currents display a transient increase in current that exponentially decays to a steady state (**Figure S2.1**, top panel).

Figure S2.1

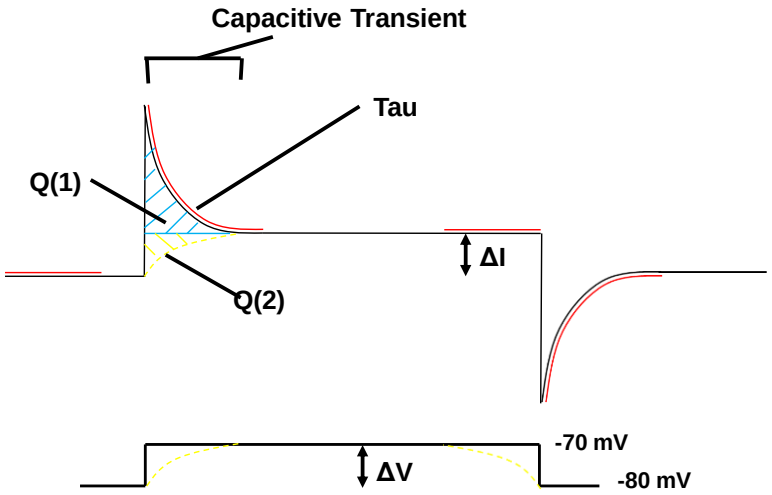

This transient is due to the charging of the membrane capacitance, an innate property of biological membranes that is dependent upon the surface area of the cell. Capacitance can therefore be used as a general indicator of changes in cell size/surface area. Capacitance introduces errors into voltage and current clamp recordings if not adequately compensated. By leaving it uncompensated, however, it is possible to calculate changes in capacitance over time by providing continuous voltage steps at a high frequency. Capacitance (C_m) is calculated according to the following equation, where Q(t) is the total charge under the capacitive transient and ΔV is the amplitude of the voltage pulse applied:

$$Cm = Q(t)/\Delta V$$

ΔV is decided by the user while Q(t) is calculated by integrating the area of the capacitive transient above the steady state level, as denoted in **Figure S2.1** as Q1. However, since capacitance causes errors in voltage during the observed transients (**Figure S2.1**, bottom panel, denoted by yellow lines), this means an error is introduced into the measurement of Q(t), denoted as Q2 (**Figure S2.1**, top panel denoted by yellow lines). This means that the actual Q(t) is calculated as:

$$Q(t) = Q1 + Q2$$

Q2 is calculated as:

$$Q2 = \Delta I * Tau$$

ΔI is the change in steady state current in response to the voltage step (and is measured before and after the capacitive transient at the straight line regions show in red (**Figure S2.1**). Tau is the time constant for the charging of a capacitor to ~63.2% of its capacitance and is calculated in-software using an exponential fitting algorithm during the capacitive transient, denoted by the curved lines in red (**Figure S2.1)**. All of these calculations are performed in-software to provide close to real time measurements of whole cell capacitance. Information here was obtained from the molecular devices website:

(http://mdc.custhelp.com/app/answers/detail/a_id/17006/~/membrane-test-algorithms). Diagram by M. Euston.

The membrane test parameters used during these experiments were:

- Holding potential: -80 mV
- Voltage step amplitude: +10 mV
- Step duration: 10 ms
- Step frequency: 50Hz
- Point averaging (to reduce noise): 5

Supplementary 2.2 - Control Experiments for $Ca_V1.3$ Antibody Staining of AtT20s

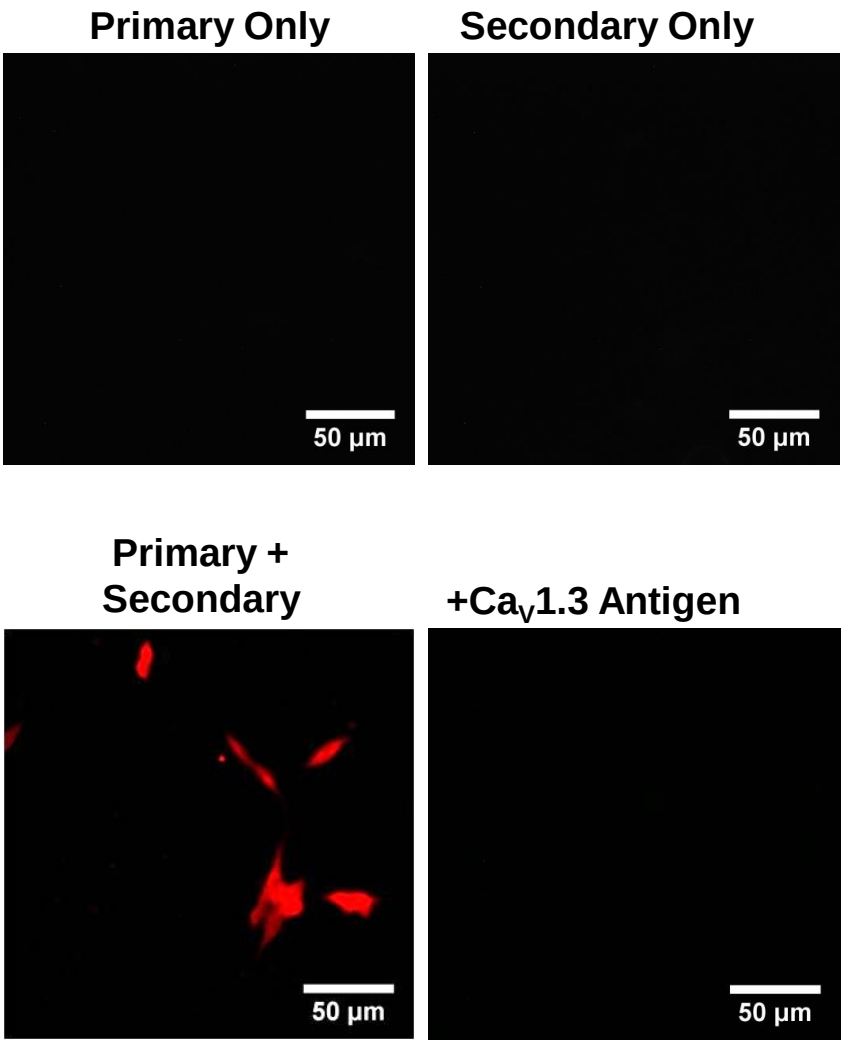

Figure S2.2 - $Ca_V1.3$ antibody controls for AtT20s. Representative fluorescence images from separate experiments showing AtT20 cells stained with the rabbit anti-$Ca_V1.3$ primary antibody only (top left), the goat anti-rabbit Alexa-647 secondary antibody only (top right), both antibodies (bottom left) and both antibodies after the primary antibody was incubated with a $Ca_V1.3$ antigen for 1 hour prior to staining. All antibodies were used at a dilution of 1:500.

Supplementary 3.1 - Secondary Control Experiments for TH and NeuN Antibody Staining

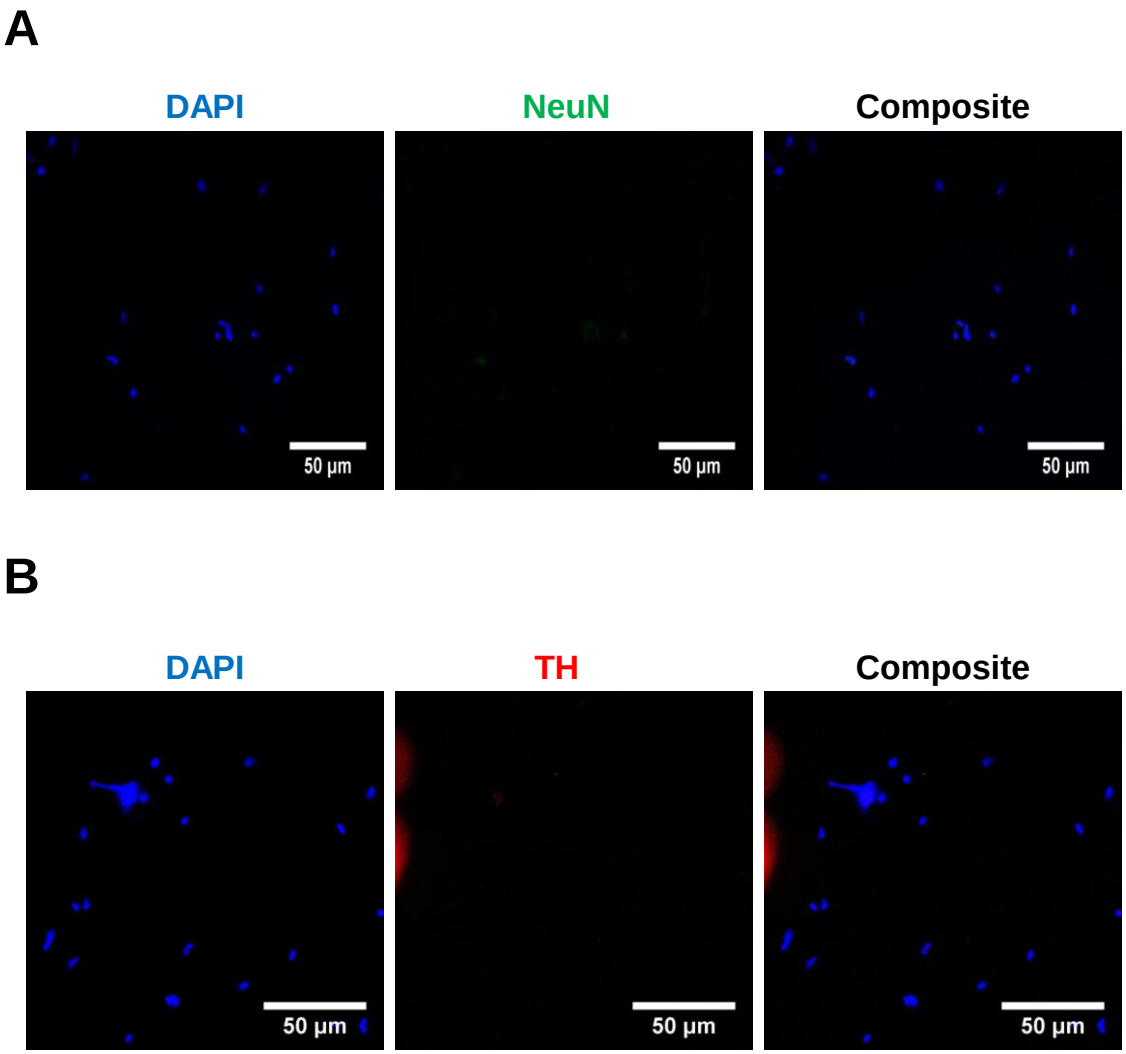

Figure S3.1 - Secondary antibody controls for TH and NeuN immunostaining. Antibody controls performed with the secondary antibody only for (A) the donkey anti mouse AlexaFluor-488 secondary antibody used during NeuN staining and (B) the goat anti rabbit AlexaFluor-647 secondary antibody used during TH staining. Experiments were performed at dilutions of 1:500.

Supplementary 4.1 - Ratiometric Determination of Percentage Cell Death Using Hoechst 33342

After the collection of Hoechst-stained fluorescence images (see Chapter 4 methods), the percentage of cell death in each image was calculated using ImageJ.

Using the threshold feature, nuclei in each image were converted to binary black and white, with nuclei above a defined threshold appearing as white particles within the image. By changing the threshold, one image could be separated into two separate images containing "all nuclei" or "bright nuclei." **Figure S4.1B** demonstrates the use of this threshold approach to produce two separate versions of the fluorescence image in Figure **S4.1A.** For experiments here, the threshold was set manually for each image.

As clusters of nuclei would introduce errors into the counting due to the difficulty of separating them into individual nuclei, the watershed function was performed. This is a feature of ImageJ that attempts to separate conjoined particles and, although not perfect, likely increases the accuracy of the results.

Particles were then counted using the analyse particle function. This is a feature that automatically counts and produces statistics on all of the particles within an image. A 10 pixel diameter particle exclusion filter was set, as it was decided that particles below this were likely too small to be nuclei, instead being artefacts within the image. An example of the output obtained from using this feature is shown in **Figure S4.1C**.

The number of total nuclei and the number of bright nuclei were summed from all of the images from 1 experimental repeat. The % cell death in this repeat was calculated as:

$$\%\ Cell\ Death\ = \frac{Number\ of\ bright\ nuclei}{Total\ number\ of\ nucei} * 100$$

Each experiment was repeated a minimum of 3 times, with the 3 or more values obtained used to calculate a mean and S.E.M for each condition.

A

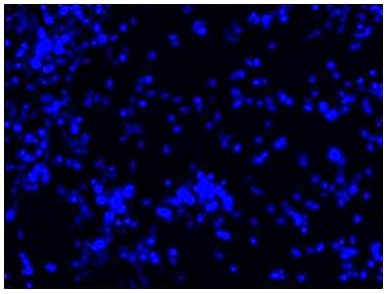

B

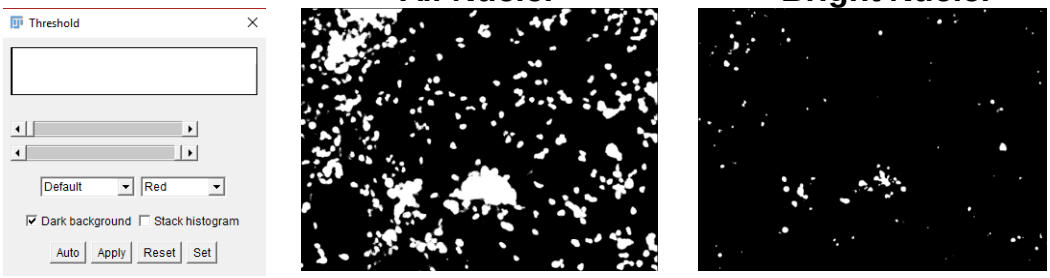

C

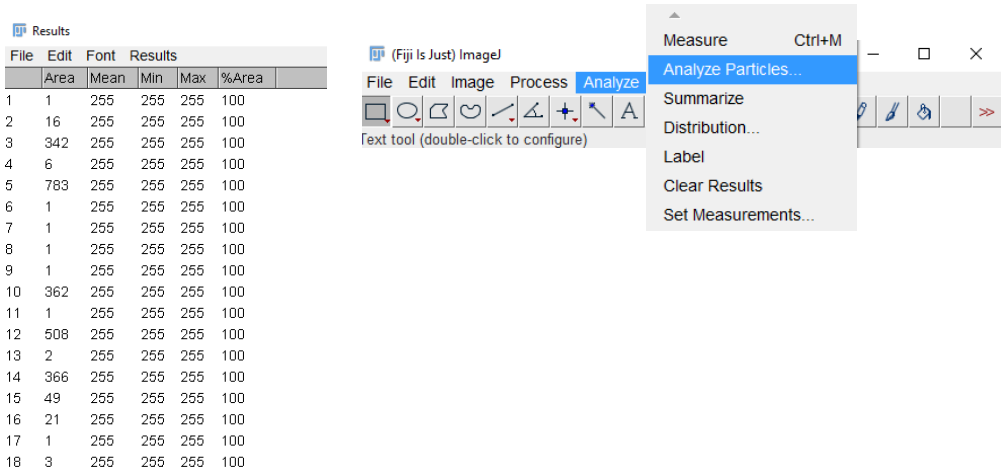

	Area	Mean	Min	Max	%Area
1	1	255	255	255	100
2	16	255	255	255	100
3	342	255	255	255	100
4	6	255	255	255	100
5	783	255	255	255	100
6	1	255	255	255	100
7	1	255	255	255	100
8	1	255	255	255	100
9	1	255	255	255	100
10	362	255	255	255	100
11	1	255	255	255	100
12	508	255	255	255	100
13	2	255	255	255	100
14	366	255	255	255	100
15	49	255	255	255	100
16	21	255	255	255	100
17	1	255	255	255	100
18	3	255	255	255	100

Figure S4.1 - Ratiometric determination of % cell death using Hoechst 33342. A Hoechst-stained image such as that in (A) was split into images containing "bright" or "all nuclei" using the threshold feature, shown in (B). These nuclei were then automatically counted using the analyse particle feature, shown in (C).

Supplementary 4.2 - Control Experiments for $Ca_V1.3$ Antibody Staining of hiPSC-Derived Dopaminergic Neurons

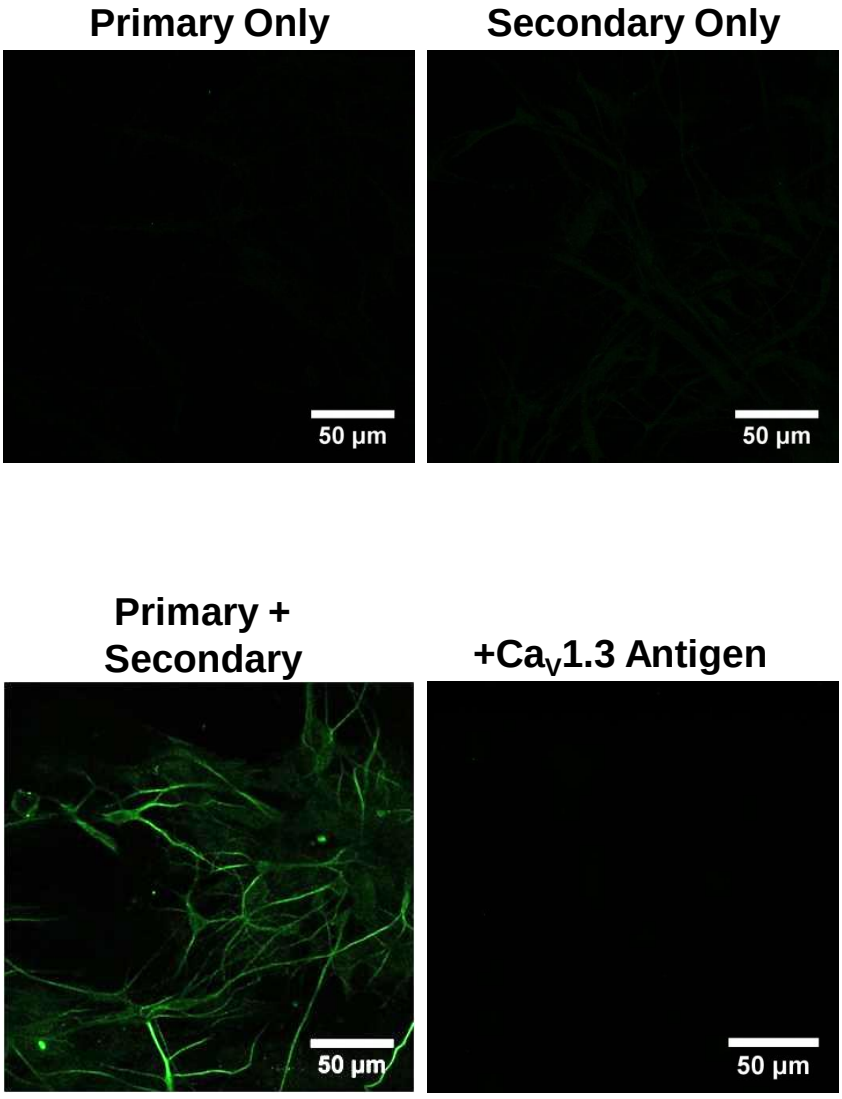

Figure S4.2 - $Ca_V1.3$ antibody controls for hiPSC-derived dopaminergic neurons. Representative fluorescence images from separate experiments showing cells 3 weeks post-differentiation that were stained with the rabbit anti-$Ca_V1.3$ primary antibody only (top left), the goat anti-rabbit Alexa-488 secondary antibody only (top right), both antibodies (bottom left) and both antibodies after the primary antibody was incubated with a $Ca_V1.3$ antigen for 1 hour prior to staining. All antibodies were used at a dilution of 1:500.

References

- Adler M, Wong B, Sabol S, Busis N, Jackson M, Weight F (1983) - Action potentials and membrane ion channels in clonal anterior pituitary cells, *PNAS* , 80(7), 2086-2090.
- Aghajanian G, Bunney B (1977) - Dopamine "Autoreceptors": Pharmacological characterization by microiontophoretic single cell recording studies, *Naunyn-Schmiedeberg's Archives of Pharmacology*, 297, 1.
- Aguado F, Gombau L, Majó G, Marsal J, Blanco J, Blasi J (1997) - Regulated secretion is impaired in AtT-20 endocrine cells stably transfected with botulinum neurotoxin type A light chain, *The Journal of Biological Chemistry*, 272(41), 26005-26008.
- Aguilera G, Rabadan-Diehl C (2000) - Vasopressinergic regulation of the hypothalamic-pituitary-adrenal axis: implications for stress adaptation, *Regulatory Peptides*, 96(1-2), 23-29.
- Aizenman L, Linden D (2003) - Rapid, synaptically driven increases in the intrinsic excitability of cerebellar deep nuclear neurons, *Nature*, 3(2), 109-111.
- Albert Von Kölliker (1817-1905) Würzburger Histologist (1968) - *JAMA*, 206(9), 2111-2112.
- Alvarez-Fischer D, Noelker C, Vulinović F, Grünewald A, Chevarin C (2013) - Bee Venom and Its Component Apamin as Neuroprotective Agents in a Parkinson Disease Mouse Model, *PLOS ONE* 8(4), e61700.
- Amaya F, Decosterd I, Samad T, Plumpton C, Tate S, Mannion R, Costigan M, Woolf C (2000) - Diversity of Expression of the Sensory Neuron-Specific TTX-Resistant Voltage-Gated Sodium Ion Channels SNS and SNS2, *Molecular and Cellular Neuroscience*, 15(4), 331-342.
- Anti-CaV1.3, http://www.alomone.com/p/anti-cav1.3/acc-005/1023, Alomone Labs.
- Armstrong C (2006) - Sodium channel inactivation from open and closed states, *PNAS*, 103(47), 17991-17996.
- Atwater I, Ribalet B, Rojas E (1978) - Cyclic changes in potential and resistance of the beta-cell membrane induced by glucose in islets of Langerhans from mouse, *The Journal of Physiology*, 278, 117-139.

- Avanzini G, de Curtis M, Panzica F, Spreafico R (1989) - Intrinsic properties of nucleus reticularis thalami neurones of the rat studied in vitro, *Journal of Physiology*, 416, 111-122.
- Ballard P, Tetrud J, Langston, J (1985) - Permanent human parkinsonism due to 1-methy 1–4-phenyl-1,2,3,6-tetrahydropyridine (MPTP), *Neurology*, 35(7), 949.
- Bando Y, Irie K, Shimomura T, Umeshima H, Kushida Y, Kengaku M, Fujiyoshi Y, Hirano T, Tagawa Y (2016) - Control of Spontaneous Ca^{2+} Transients Is Critical for Neuronal Maturation in the Developing Neocortex, *Cerebral Cortex*, 26 (1), 106-117.
- Bangaru M, Woodliff J, Raff H, Kansra S (2010) - Growth Suppression of Mouse Pituitary Corticotroph Tumor AtT20 Cells by Curcumin: A Model for Treating Cushing's Disease, *PLOS ONE*, 5(4), e9893.
- Bayer H, Lau B, Glimcher P (2007) - Statistics of Midbrain Dopamine Neuron Spike Trains in the Awake Primate, *Journal of Neurophysiology*, 98(3), 1428-1439.
- Beckstead M, Grandy D, Wickman K, Williams J (2004) - Vesicular dopamine release elicits an inhibitory postsynaptic current in midbrain dopamine neurons, *Neuron*, 42(6), 939-946.
- Benardete E, Kriegstein A (2002) - Increased excitability and decreased sensitivity to GABA in an animal model of dysplastic cortex, Benardete E, Kriegstein A - *Epilepsia*, 43(9), 970-982.
- Biglan K, Oakes D, Lang A, Hauser R, Hodgeman K, Greco B, Lowell J, Rockhill R, Shoulson I, Venuto C, Young D, Simuni T, Parkinson Study Group STEADY-PD III Investigators (2017) - A novel design of a Phase III trial of isradipine in early Parkinson disease (STEADY-PD III), *Annals of Clinical and Translational Neurology*, 2017, 4(6), 360-368.
- Bijlenga P, Liu J, Espinos E, Haenggeli C, Fischer-Lougheed J, Bader C, Bernheim L (2000) - T-type α1H Ca2+ channels are involved in Ca2+ signaling during terminal differentiation (fusion) of human myoblasts, *PNAS*, 97(13), 7627-7632.
- Bilodeau S, Vallette-Kasic S, Gauthier Y, Figarella-Branger D, Brue T, Berthelet F, Lacroix A, Batista D, Stratakis C, Hanson J, Meij B, Drouin J (2006) - Role of Brg1 and HDAC2 in GR trans-repression of the pituitary POMC gene and misexpression in Cushing disease, *Genes & Development*, 20, 2871-2886.

- Bischoff S, Barhanin J, Bettler B, Mulle C, Heinemann S (1997) - Spatial distribution of kainate receptor subunit mRNA in the mouse basal ganglia and ventral mesencephalon, *Journal of Comparative Neurology*, 379(4), 541-562.
- Blesa J, Przedborski S (2014) - Parkinson's disease: animal models and dopaminergic cell vulnerability, *Frontiers in Neuroanatomy*, 8, 155.
- Bliss T, Lømo T (1973) - Long-lasting potentiation of synaptic transmission in the dentate area of the anaesthetized rabbit following stimulation of the perforant path, *The Journal of Physiology*, 232(2), 331-356.
- Blythe S, Atherton J, Bevan M (2007) - Synaptic activation of dendritic AMPA and NMDA receptors generates transient high-frequency firing in substantia nigra dopamine neurons in vitro, *Journal of Neurophysiology*, 97(4), 2837-2850.
- Bornstein S, Engeland W, Ehrhart-Bornstein M, Herman J (2008) - Dissociation of ACTH and glucocorticoids, *Trends in Endocrinology & Metabolism*, 19(5), 175-180.
- Bresadola M (1998) - Medicine and science in the life of Luigi Galvani (1737–1798), *Brain Research Bulletin*, 46(5), 367-380.
- Brozoski T, Brown R, Rosvold H, Goldman P (1979) - Cognitive deficit caused by regional depletion of dopamine in prefrontal cortex of rhesus monkey, *Science*, 205(4409), 929-932.
- Burdyga T, Wray S (2005) - Action potential refractory period in ureter smooth muscle is set by Ca sparks and BK channels, *Nature Letters*, 436, 559-562.
- Burns R, Chiueh C, Markey S, Ebert M, Jacobowitz D, Kopin I (1983) - A primate model of parkinsonism: Selective destruction of dopaminergic neurons in the pars compacta of the substantia nigra by N-methyl-4-phenyl-1,2,3,6-tetrahydropyridine, *PNAS*, 80, 4546-4550.
- Burns R, Chiueh C, Markey s, Ebert M, Jacobowitz D, Kopin I (1983) - A primate model of parkinsonism: selective destruction of dopaminergic neurons in the pars compacta of the substantia nigra by N-methyl-4-phenyl-1,2,3,6-tetrahydropyridine, *PNAS*, 80(14), 4546-4550.
- Burrone J, O'Byrne M, Murthy V (2002) - Multiple forms of synaptic plasticity triggered by selective suppression of activity in individual neurons, *Nature*, 420, 414-418.
- Calabresi P, Picconi B, Tozzi A, Ghiglieri V, Di Filippo M (2014) - Direct and indirect pathways of basal ganglia: a critical reappraisal, *Nature Neuroscience*, 17, 1022-1030.

- Caldwell J, Schaller K, Lasher R, Peles E, Levinson S (2000) - Sodium channel Nav1.6 is localized at nodes of Ranvier, dendrites, and synapses, *PNAS*, 97(10), 5616-5620.
- Carter B, Giessel A, Sabatini B, & Bean B (2012) - Transient sodium current at subthreshold voltages: activation by EPSP waveforms, *Neuron*, 75(6), 1081–1093.
- Castillo V, Theodoropoulou M, Stalla J, Gallelli M, Cabrera-Blatter M, Haedo M, Labeur M, Schmid H, Stalla G, Arzt E (2011) - Effect of SOM230 (Pasireotide) on Corticotropic Cells: Action in Dogs with Cushing's Disease, *Neuroendocrinology*, 94, 124–136.
- Chan C, Guzman J, Ilijic E, Mercer J, Rick C, Tkatch T, Meredith G, Surmeier D (2007) - 'Rejuvenation' protects neurons in mouse models of Parkinson's disease, *Nature*, 447(7148):1081-1086.
- Charlety P, Grenhoff J, Chergui K, Chapelle B, Buda M, Svensson T, Chouvet G (1991) - Burst firing of mesencephalic dopamine neurons is inhibited by somatodendritic application of kynurenate, *Acta Physiologica Scandinavica*, 142, 105-112.
- Chatha B, Bernard V, Streit P, Bolam J (2000) - Synaptic localization of ionotropic glutamate receptors in the rat substantia nigra, *Neuroscience*, 101(4), 1037-1051.
- Cheli V, Santiago González D, Smith J, Spreuer V, Murphy G, Paez P (2016) - L-type voltage-operated calcium channels contribute to astrocyte activation in vitro, *Glia*, 64(8), 1396-1415.
- Chen C, Gettes L (1976) - Combined effects of rate membrane potential, and drugs on maximum rate of rise (Vmax) of action potential upstroke of guinea pig papillary muscle, *Circulation Research*, 38, 464-469.
- Chub N, O'Donovan M (1998) - Blockade and recovery of spontaneous rhythmic activity after application of neurotransmitter antagonists to spinal networks of the chick embryo, *Journal of Neuroscience*, 18, 294–306.
- Clark J, Clore E, Zheng K, Adame A, Masliah E, Simon D (2010) - Oral N-acetyl-cysteine attenuates loss of dopaminergic terminals in alpha-synuclein overexpressing mice, *PLoS One*, 5(8), e12333.
- Colombo M, Colombo A, Gross C (2002) - Bartolomeo Panizza's "Observations on the optic nerve*" (1855)*, *Brain Research Bulletin*, 30:58(6), 529-539.

- Condliffe S, Corradini I, Pozzi D, Verderio C, Matteoli M (2010) - Endogenous SNAP-25 Regulates Native Voltage-gated Calcium Channels in Glutamatergic Neurons, *The Journal of Biological Chemistry*, 285, 24968-24976.
- Cone R, Mountjoy K (1993) - Molecular genetics of the ACTH and melanocyte-stimulating hormone receptors, *Trends in Endocrinological Metabolism*, 4(7), 242-247.
- Conway A, Lee S, Rochet J, Ding T, Williamson R, Lansbury P (2000) - Acceleration of oligomerization, not fibrillization, is a shared property of both α-synuclein mutations linked to early-onset Parkinson's disease: Implications for pathogenesis and therapy, *PNAS*, 97(2), 571-576.
- Coulon P, Herr D, Kanyshkova T, Meuth P, Budde T, Pape H (2009) - Burst discharges in neurons of the thalamic reticular nucleus are shaped by calcium-induced calcium release, *Cell Calcium*, 46(5-6), 333-346.
- Cragg S, Greenfield S (1997) - Differential Autoreceptor Control of Somatodendritic and Axon Terminal Dopamine Release in Substantia Nigra, Ventral Tegmental Area, and Striatum, *Journal of Neuroscience*, 17(15) 5738-5746.
- Cullen D, Gilroy M, Irons H, LaPlaca M (2010) - Synapse-to-neuron ratio is inversely related to neuronal density in mature neuronal cultures, *Brain Research*, 1359, 44-55.
- Curtis H, Cole K (1942) - Membrane resting and action potentials from the squid giant axon, *Journal of Cellular Physiology*, 19(2), 135-144.
- Daubner S, Le T, Wang S (2011) - Tyrosine Hydroxylase and Regulation of Dopamine Synthesis, *Archives of Biochemistry and Biophysics*, 508(1), 1-12.
- Davila V, Yan Z, Craciun L, Logothetis D, Sulzer D (2003) - D3 dopamine autoreceptors do not activate G-protein-gated inwardly rectifying potassium channel currents in substantia nigra dopamine neurons, *Journal of Neuroscience*, 23(13), 5693-5697.
- Dawson T, Ko H, Dawson V (2010) - Genetic Animal Models of Parkinson's Disease, *Neuron*, 66(5), 646–661.
- de Lau L, Breteler M (2006) - Epidemiology of Parkinson's disease, *The Lancet Neurology* , 5(6), 525 - 535.
- De Marco R, Thiemann T, Groneberg A, Herget U, Ryu S (2016) - Optogenetically enhanced pituitary corticotroph cell activity post-stress onset causes rapid organizing effects on behaviour, *Nature Communications*, 7, 12620.

- de Vrind V, Scuvée-Moreau J, Drion G, Hmaied C, Philippart F, Engel D, Seutin V (2016) - Interactions between calcium channels and SK channels in midbrain dopamine neurons and their impact on pacemaker regularity: Contrasting roles of N- and L-type channels, *European Journal of Pharmacology*, 788, 274-279.
- Dennis, W (1948) - *Readings in the history of psychology*, 129-139.
- Do J, Kim J, Bakes J, Lee K Kaang B (2013) - Functional roles of neurotransmitters and neuromodulators in the dorsal striatum, *Learning & Memory*, 20, 21-28.
- Donovan M (1999) - The origin of spontaneous activity in developing networks of the vertebrate nervous system, *Current Opinion in Neurobiology*, 9(1), 94-104.
- Dousmanis A, Pennefather P (1992) - Inwardly rectifying potassium conductances in AtT-20 clonal pituitary cells, *Pflugers Archiv: European Journal of Physiology*, 422(2), 98-104.
- Dufour M, Woodhouse A, Goaillard J (2014) - Somatodendritic ion channel expression in substantia nigra pars compacta dopaminergic neurons across postnatal development, *Journal of Neuroscience Research*, 92(8), 981-999.
- Duncan P, Sengul S, Tabak J, Ruth P, Bertram R, Shipston M (2015) - Large conductance Ca^{2+}-activated K+ (BK) channels promote secretagogue-induced transition from spiking to bursting in murine anterior pituitary corticotrophs, *The Journal of Physiology*, 593, 1197-1211.
- Duncan P, Tabak J, Ruth P, Bertram R, Shipston M (2016) - Glucocorticoids Inhibit CRH/AVP-Evoked Bursting Activity of Male Murine Anterior Pituitary Corticotroph, *Endocrinology*, 157(8), 3108–3121
- Edelmann E, Lessmann V (2013) - Dopamine regulates intrinsic excitability thereby gating successful induction of spike timing-dependent plasticity in CA1 of the hippocampus, *Frontiers in Neuroscience*, 7, 25.
- Ekstrand I, Galter D (2009) - The MitoPark Mouse – An animal model of Parkinson's disease with impaired respiratory chain function in dopamine neurons, *Parkinsonism & Related Disorders*, 15, S185 - S188.
- Emmanouilidou E, Stefanis L, Vekrellis K (2010) - Cell-produced alpha-synuclein oligomers are targeted to, and impair, the 26S proteasome, *Neurobiology of Aging*, 31(6), 953-968.

- Eriksson P, Perfilieva E, Bjork-Eriksson T, Alborn A, Nordborg C, Peterson D, Gage F (1998) - Neurogenesis in the adult human hippocampus, *Nature Medicine*, 4(11), 1313-1317.
- Evans R, Zhu M, Khaliq Z (2017) - Dopamine inhibition differentially controls excitability of SNc dopamine neuron subpopulations through recruitment of T-type calcium channels, *Journal of Neuroscience*, 0117-17.
- Feigenspan A, Gustincich S, Bean B, Raviola E (1998) - Spontaneous Activity of Solitary Dopaminergic Cells of the Retina, *Journal of Neuroscience*, 18(17), 6776-6789.
- Feller M (1999) - Spontaneous Correlated Activity in Developing Neural Circuits, *Neuron*, 22(4), 653-656.
- Ferrari D, Mdzomba B, Dehorter N, Lopez C, Michel F, Libersat F, Hammond C (2012) - Midbrain dopaminergic neurons generate calcium and sodium currents and release dopamine in the striatum of pups, *Frontiers in Cellular Neuroscience*, 6(7).
- Fiekers J, Konopka L (1996) - Spontaneous transients of [Ca2+]i depend on external calcium and the activation of L-type voltage-gated calcium channels in a clonal pituitary cell line (AtT-20) of cultured mouse corticotropes, *Cell Calcium*, 19(4), 327-336.
- Findley L (2007) - The economic impact of Parkinson's disease, *Parkinsonism & Related Disorders*, 13, S8-S12.
- Fletcher P, Zemkova H, Stojilkovic S, Sherman A (2017) - Modeling the diversity of spontaneous and agonist-induced electrical activity in anterior pituitary corticotrophs, *The Journal of Neurophysiology*.
- Floor E, Wetzel, M (1998) - Increased Protein Oxidation in Human Substantia Nigra Pars Compacta in Comparison with Basal Ganglia and Prefrontal Cortex Measured with an Improved Dinitrophenylhydrazine Assay, *Journal of Neurochemistry*, 70, 268–275.
- Fortin D, Nemani V, Voglmaier S, Anthony M, Ryan T, Edwards R (2005) - Neural Activity Controls the Synaptic Accumulation of α-Synuclein, *Journal of Neuroscience*, 25(47) 10913-10921.
- Francis F, Middleton R, Garcia M (2012) - Pacemaking Neurons in the Study of Parkinson's Disease, Doctoral Thesis, Submitted by Maynooth University in 2012.

- Frère S, Lüthi A (2004) - Pacemaker channels in mouse thalamocortical neurones are regulated by distinct pathways of cAMP synthesis, *The Journal of Physiology*, 1(554), 111-125.
- Fu M, Li C, Lin H, Chen, P, Calkins M, Chang, Y, Yang, S (2015) - Stem cell transplantation therapy in Parkinson's disease, *SpringerPlus*, 4, 597.
- Fuchs J, Nilsson C, Kachergus J, Munz M, Larsson E, Schüle B, Langston J, Middleton F, Ross O, Hulihan M, Gasser T, Farrer M (2007) - Phenotypic variation in a large Swedish pedigree due to SNCA duplication and triplication, *Neurology*, 68(12), 916-922.
- Fulkerson W, Pamela J (1982) - Pattern of Cortisol Release in Sheep following Administration of Synthetic ACTH or Imposition of Various Stressor Agents, *Australian Journal of Biological Sciences*, 35, 215-222.
- Futami T, Takakusaki K, Kitai S (1995) - Glutamatergic and cholinergic inputs from the pedunculopontine tegmental nucleus to dopamine neurons in the substantia nigra pars compacta, *Neuroscience Research*, 21(4), 331-342.
- Fye, W (1995) - Julien Jean César Legallois, *Clinical Cardiology*, 18(10), 599-600.
- Gallo-Payet N, Payet M (2003) - Mechanism of action of ACTH: beyond cAMP, *Microscopy Research and Technique*, 15(61:3), 275-287.
- Gentet L, Stuart G, Clements J (2000) - Direct measurement of specific membrane capacitance in neurons, *Biophysical Journal*, 79(1), 314-320.
- Gerich J, Cryer P, Rizza R (1980) - Hormonal mechanisms in acute glucose counterregulation: The relative roles of glucagon, epinephrine, norepinephrine, growth hormone, and cortisol, *Metabolism*, 29(11), 1164-1175.
- Gilly W, Gillette R, McFarlane M (1997) - Fast and Slow Activation Kinetics of Voltage-Gated Sodium Channels in Molluscan Neurons, *Journal of Neurophysiology*, 77(5), 2373-2384.
- Glinka Y, Gassen M, Youdin M (1997) - Mechanism of 6-hydroxydopamine neurotoxicity, *Journal of Neural Transmission. Supplementum*, 50, 55-66.
- Golgi C (1873) - Sulla struttura della sostanza grigia del cervello, *Gazzetta Medica Italiana*, 33, 244-246.
- Götz T, Kraushaar U, Geiger J, Lübke J, Berger T, Jonas P (1997) - Functional properties of AMPA and NMDA receptors expressed in identified types of basal ganglia neurons, *Journal of Neuroscience*, 17(1), 204-215.

- Grace A, Bunney B (1984) - The control of firing pattern in nigral dopamine neurons: single spike firing, *The Journal of Neuroscience*, 4(11), 2866-2876.
- Grace A, Bunney B (1985) - Opposing effects of striatonigral feedback pathways on midbrain dopamine cell activity, *Brain Research*, 333(2), 271-284.
- Grace A, Onn S (1989) - Morphology and electrophysiological properties of immunocytochemically identified rat dopamine neurons recorded in vitro, *Journal of Neuroscience*, 9(10), 3463-3481.
- Greening J, Storr H, McKenzie S, Davies K, Martin L, Grossman A, Savage M (2006) - Linear growth and body mass index in pediatric patients with Cushing's disease or simple obesity, *Journal of Endocrinological Investigation*, 29(10),885-887.
- Gudala K, Kanukula R, Bansal D (2015) - Reduced Risk of Parkinson's Disease in Users of Calcium Channel Blockers: A Meta-Analysis, *International Journal of Chronic Diseases*, 2015, 697404.
- Guérineau N, Corcuff J, Tabarin A, Mollard P (1991) - Spontaneous and Corticotropin-Releasing Factor-Induced Cytosolic Calcium Transients in Corticotrophs, *Endocrinology*, 129(1), 409-420.
- Gumbiner B, Kelly R (1981) - Secretory granules of an anterior pituitary cell line, AtT-20, contain only mature forms of corticotropin and beta-lipotropin, *PNAS*, 78(1), 318-322.
- Gupta K, Hardingham G, Chandran S (2013) - NMDA receptor-dependent glutamate excitotoxicity in human embryonic stem cell-derived neurons, *Neuroscience Letters*, 543, 95-100.
- Gusel'nikova V, Korzhevskiy D (2015) - NeuN As a Neuronal Nuclear Antigen and Neuron Differentiation Marker, *Acta Naturae*, 2015, 7(2), 42-47.
- Guzman J, Sánchez-Padilla J, Chan C, Surmeier D (2009) - Robust Pacemaking in Substantia Nigra Dopaminergic Neurons, *The Journal of Neuroscience*, 29(35), 11011–11019.
- Hage T, Khaliq Z (2015) - Tonic Firing Rate Controls Dendritic Ca2+ Signaling and Synaptic Gain in Substantia Nigra Dopamine Neurons, *The Journal of Neuroscience*, 35(14), 5823-5836.
- Hanrott K, Gudmunsen L, O'Neill M, Wonnacott S (2006) - 6-Hydroxydopamine-induced Apoptosis Is Mediated via Extracellular Auto-oxidation and Caspase 3-dependent Activation of Protein Kinase Cδ, *The Journal of Biological Chemistry*, 281, 5373-5382.

- Hansson A, Cintra A, Belluardo N, Sommer W, Bhatnagar M, Bader M, Ganten D, Fuxe, K (2000) - Gluco- and mineralocorticoid receptor-mediated regulation of neurotrophic factor gene expression in the dorsal hippocampus and the neocortex of the rat, *European Journal of Neuroscience*, 12, 2918–2934.
- Hanukoglu I, Feuchtwanger R, Hanukoglu A (1990) - Mechanism of Corticotropin and cAMP Induction of Mitochondrial Cytochrome P450 System Enzymes in Adrenal Cortex Cells, *The Journal of Biological Chemistry*, 265(33), 20602-20608.
- Harris L, Almerigi J (2009) - Probing the human brain with stimulating electrodes: the story of Roberts Bartholow's (1874) experiment on Mary Rafferty, *Brain Cognition*, 70(1), 92-115.
- Hartfield E, Yamasaki-Mann M, Ribeiro Fernandes H, Vowles J, James W, Cowley S, Wade-Martins R (2014) - Physiological Characterisation of Human iPS-Derived Dopaminergic Neurons, *PLoS One*, 9(2), e87388.
- Hartshorne R, Catterall W (1981) - Purification of the saxitoxin receptor of the sodium channel from rat brain, *PNAS*, 78(7), 4620-4624.
- Hartshorne R, Keller B, Talvenheimo J, Catterall W, Montal M (1985) - Functional reconstitution of the purified brain sodium channel in planar lipid bilayers, *PNAS*, 82, 240–244.
- Häusser M, Clark B (1997) - Less Means More: Inhibition of Spontaneous Firing Triggers Persistent Increases in Excitability, *Neuron*, 19, 665–678.
- Häusser M, Clark B (1997) - Tonic synaptic inhibition modulates neuronal output pattern and spatiotemporal synaptic integration, *Neuron*, 19(3), 665-78.
- Healy D, Abou-Sleiman P, Lees A (2004) - Tau gene and Parkinson's disease: a case-control study and meta-analysis. *Journal of Neurology Neurosurgery and Psychiatry*, 75, 962-965.
- Heisler S (1985) - Stimulation of adrenocorticotropin secretion from AtT-20 cells by the calcium channel activator, BAY-K-8644, and its inhibition by somatostatin and carbachol, *The Journal of Pharmacology and Experimental Therapeutics*, 235(3), 741-748.
- Henn V, Baloh R, Hepp K (1984) – The sleep-wake transition in the oculo-motor system, *Experimental Brain Research*, 54(1), 166-176.
- Hettiarachchi N, Parker A, Dallas M, Pennington K, Hung C, Pearson H, Boyle J, Robinson P, Peers C (2009) - alpha-Synuclein modulation of Ca2+ signaling

in human neuroblastoma (SH-SY5Y) cells, *Journal of Neurochemistry*, 111(5), 1192-1201.

- Hille B (2001) - Ionic Channels of Excitable Membranes, Sinauer Associates, Sunderland, MA.
- Hirano Y, Moscucci A, January C (1992) - Direct measurement of L-type Ca2+ window current in heart cells, *Circulation Research*, 70, 445-455.
- Hodgkin A (1979) - Edgar Douglas Adrian, Baron Adrian of Cambridge, *30* November 1889 - 4 August 1977, *Biographical Memoirs of Fellows of the Royal Society*, 25(1), 73.
- Hodgkin A, Huxley A (1952) - A quantitative description of membrane current and its application to conduction and excitation in nerve, *The Journal of Physiology*, 117(4), 500-544.
- Hooper K, Banks D, Stordahl L, White I, Rebec G (1997) - Quinpirole inhibits striatal and excites pallidal neurons in freely moving rats, *Neuroscience Letters*, 237(2-3), 69-72.
- Huang X, Chen P, Poole C (2004) - APOE-epsilon2 allele associated with higher prevalence of sporadic Parkinson disease, *Neurology*, 62, 2198–2202.
- Huguenard J, Prince D (1992) - A novel T-type current underlies prolonged Ca(2+)-dependent burst firing in GABAergic neurons of rat thalamic reticular nucleus, *Journal of Neuroscience*, 12(10), 3804-3817.
- Hui A, Ellinor P, Krizanova O, Wang J, Diebold R, Schwartz A (1991) - Molecular cloning of multiple subtypes of a novel rat brain isoform of the alpha-1 subunit of the voltage-dependent calcium channel, *Neuron*, 7, 35-44.
- Hyun D, Lee M, Halliwell B, Jenner P (2002) - Proteasomal dysfunction induced by 4-hydroxy-2,3-trans-nonenal, an end-product of lipid peroxidation: a mechanism contributing to neurodegeneration, *Journal of Neurochemistry*, 83, 360–370.
- Iihara K, Joo D, Henderson J, Sattler R, Taverna F, Lourensen S, Orser B, Roder J, Tymianski M (2001) - The Influence of Glutamate Receptor 2 Expression on Excitotoxicity in GluR2 Null Mutant Mice, *The Journal of Neuroscience*, 21(7), 2224-2239.
- Isales C, Zaidi M, Blair H (2010) - *ACTH is a novel regulator of bone mass*, Annals of the New York Academy of Sciences, 1192, 110-116.

- Jablonka S, Beck M, Lechner B, Mayer C, Sendtner M (2007) - Defective Ca^{2+} channel clustering in axon terminals disturbs excitability in motoneurons in spinal muscular atrophy, *The Journal of Cell Biology*, 179(1), 139-149.
- Jackson-Lewis V, Jakowec M, Burke R, Przedborski S (1995) - Time course and morphology of dopaminergic neuronal death caused by the neurotoxin 1-methyl-4-phenyl-1,2,3,6-tetrahydropyridine, *Neurodegeneration*, 4(3), 257-269.
- Jeljeli M, Strazielle C, Caston J, Lalonde R (2003) - Effects of ventrolateral-ventromedial thalamic lesions on motor coordination and spatial orientation in rats, *Neuroscience Research*, 47(3), 309-316.
- Jenner P (2003) - Oxidative stress in Parkinson's Disease, *Annals of Neurology*, 53(S3), 26-38.
- Jensen P (1966) - Antimycin-insensitive oxidation of succinate and reduced nicotinamide-adenine dinucleotide in electron-transport particles. I. pH dependency and hydrogen peroxide formation, *Biochimica et Biophysica Acta*, 122, 157–166.
- Jeun S, Cho H, Kim K, Li Q, Sung K (2009) - Electrophysiological Characterization of AMPA and NMDA Receptors in Rat Dorsal Striatum, *The Korean Journal of Physiology & Pharmacology*, 13(3), 209-214.
- Johnson B, Kloppenburg P, Harris-Warrick R (2003) - Dopamine modulation of calcium currents in pyloric neurons of the lobster stomatogastric ganglion, *Journal of Neurophysiology*, 90(2), 631-643.
- Johnson K, Conn P, Nisswender C (2009) - Glutamate receptors as therapeutic targets for Parkinson's disease, *CNS Neurological Disorder Drug Targets*, 8(6), 475-491.
- Jones S, Gibb A (2005) - Functional NR2B- and NR2D-containing NMDA receptor channels in rat substantia nigra dopaminergic neurones, *Journal of Physiology*, 569(1), 209-221.
- Kageyama K, Suda T (2009) - Role and action in the pituitary corticotroph of corticotropin-releasing factor (CRF) in the hypothalamus, *Peptides*, 30(4), 810-816.
- Kandel E, Schwartz J, Jessell T (1997) - Principles of Neural Science, 3rd Edition, 2, 97.
- Keeler J, Pretsell D, Robbins T (2014) - Functional implications of dopamine D1 vs. D2 receptors: A 'prepare and select' model of the striatal direct vs. indirect pathways, *Neuroscience*, 282, 156-175.

- Khani S, Tayek J (2001) - Cortisol increases gluconeogenesis in humans: its role in the metabolic syndrome, *Clinical Science (London)*, 101(6), 739-47.
- Kim K, Adelstein R, Kawamoto S (2009) - Identification of neuronal nuclei (NeuN) as Fox-3, a new member of the Fox-1 gene family of splicing factors, *The Journal of Biological Chemistry*, 284(45), 31052-31061.
- Kim K, Doi A, Wen B, Ng K, Zhao R, Cahan P, Kim J, Aryee M, Ji H, Ehrlich L, Yabuuchi A, Takeuchi A, Cunniff K, Hongguang H, Mckinney-Freeman S, Naveiras O, Yoon T, Irizarry, R, Jung N, Seita J, Hanna J, Murakami P, Jaenisch R, Weissleder R, Orkin S, Weissman I, Feinberg A, Daley G (2010) - Epigenetic memory in induced pluripotent stem cells, *Nature* 467, 285–290.
- Kimm T, Khaliq Z, Bean B (2015) - Differential Regulation of Action Potential Shape and Burst-Frequency Firing by BK and K_V2 Channels in Substantia Nigra Dopaminergic Neurons, *Journal of Neuroscience*, 35(50), 16404–16417.
- Ko K, Arora P, Bhide V, Chen A, McCulloch C (2001) - Cell-cell adhesion in human fibroblasts requires calcium signaling, *Journal of Cell Science*, 114(6), 1155-1167.
- Kole M, Stuart G (2008) - Is action potential threshold lowest in the axon?, *Nature Neuroscience*, 11, 1253-1255.
- Kopin I (1992) - Features of the dopaminergic neurotoxin MPTP, *Annals of the New York Academy of Sciences*, 648, 96-104.
- Korn S, Bolden A, Horn R (1991) - Control of action potentials and Ca2+ influx by the Ca(2+)-dependent chloride current in mouse pituitary cells, *The Journal of Physiology*, 439, 423–437.
- Korn S, Horn R (1991) - A $[Na^+]_o$-independent, pH_o-dependent Mechanism for Reduction of Intracellular $[Ca^{2+}]$ after Influx through Ca^{2+} Channels in Mouse Pituitary Cells, *Journal of General Physiology*, 98, 893-907.
- Kretschmannova K, Kucka M, Gonzalez-Iglesias A, Stojilkovic S (2012) - The Expression and Role of Hyperpolarization-Activated and Cyclic Nucleotide-Gated Channels in Endocrine Anterior Pituitary Cells, *Molecular Endocrinology*, 26(1), 153-164.
- Kriks S, Shim J, Piao J, Ganat Y, Wakeman D, Xie Z, Carrillo-Reid L, Auyeung G, Antonacci C, Buch A, Yang L, Beal M, Surmeier J, Kordower J, Tabar V, Studer L (2012) - Floor plate-derived dopamine neurons from hESCs efficiently engraft in animal models of PD, *Nature*, 480(7387), 547-551.

- Kritis A, Stamoula E, Paniskaki K, Vavilis T (2015) - Researching glutamate – induced cytotoxicity in different cell lines: a comparative/collective analysis/study, *Frontiers in Cellular Neuroscience*, 9, 91.
- Kumar R, Lang A, Rodriguez-Oroz M, Lozano A, Limousin P, Pollak P, Benabid A, Guridi J, Ramos E, van der Linden C, Vandewalle A, Caemaert J, Lannoo E, van den Abbeele D, Vingerhoets G, Wolters M, Obeso J (2000) - Deep brain stimulation of the globus pallidus pars interna in advanced Parkinson's disease, *Neurology*, 55(12:S6), S34-39.
- Kurata K (2005) - Activity Properties and Location of Neurons in the Motor Thalamus That Project to the Cortical Motor Areas in Monkeys, *Journal of Neurophysiology*, 94(1), 550-566.
- Kurosumi K, Kobayashi Y (1966) - Corticotrophs in the Anterior Pituitary Glands of Normal and Adrenalectomized Rats as Revealed by Electron Microscopy, *Endocrinology*, 7(4), 745-758.
- Kuryshev Y, Childs G, Ritchie A (1995) - Corticotropin-Releasing Hormone Stimulation of Ca^{2+} Entry in Corticotropes Is Partially Dependent on Protein-Kinase-A, *Endocrinology*, 136, 3925-3935.
- Kuryshev Y, Haak L, Childs G, Ritchie A (1997) - Corticotropin releasing hormone inhibits an inwardly rectifying potassium current in rat corticotropes, *The Journal of Physiology*, 502(2), 265-279.
- Lau C, Zukin R (2007) - NMDA receptor trafficking in synaptic plasticity and neuropsychiatric disorders, *Nature Reviews Neuroscience*, 8, 413-426.
- LeBeau A, Robson A, McKinnon A, Donald R, Sneyd J (1997) - Generation of action potentials in a mathematical model of corticotrophs, *Biophysical Journal*, 73(3), 1263-1275.
- Lee A, Tse A (1997) - Mechanism underlying corticotropin-releasing hormone (CRH) triggered cytosolic Ca^{2+} rise in identified rat corticotrophs, *The Journal of Physiology*, 504(2), 367-378.
- Lee A, Tse F, Tse A (2015) - Arginine Vasopressin Potentiates the Stimulatory Action of CRH on Pituitary Corticotropes via a Protein Kinase C-Dependent Reduction of the Background TREK-1 Current, *Endocrinology*, 156, 3661-3672.
- Lee C, Tepper J (2009) - Basal ganglia control of substantia nigra dopaminergic neurons, *Journal of Neural Transmission Supplementation*, 73, 71-90.
- Lévêque C, el Far O, Martin-Moutot N, Sato K, Kato R, Takahashi M, Seagar M (1994) - Purification of the N-type calcium channel associated with syntaxin and

synaptotagmin. A complex implicated in synaptic vesicle exocytosis, *Journal of Biological Chemistry*, 269, 6306-6312.

- Li T, Li X, Hu X, Qiu X (2015) - The Inhibitory Effects of Ca2+ Channel Blocker Nifedipine on Rat Kv2.1 Potassium Channels, *PLOS ONE*, 10(4): e0124602.
- Liang Z (2012) - Ion channels and electrical excitability in native murine anterior pituitary corticotrophs, Thesis *Submission*, Awarded by the University of Edinburgh in March 2012.
- Liang Z, Chen L, McClafferty H, Lukowski R, MacGregor D, King J, Rizzi S, Sausbier M, McCobb D, Knaus H, Ruth P, Shipston M (2011) - Control of hypothalamic-pituitary-adrenal stress axis activity by the intermediate conductance calcium-activated potassium channel SK4, *The Journal of Physiology*, 589, 5965-5986.
- Lin D, Sugawara T, Strauss J, Clark B, Stocco D, Saenger P, Rogol A, Miller W (1995) - Role of steroidogenic acute regulatory protein in adrenal and gonadal steroidogenesis, *Science*, 267(5205), 1828-1831.
- Liu W, Kato M (2000) - 4-hydroxynonenol induces a cellular redox status-related activation of the caspase cascade for apoptotic cell death, *Journal of Cell Science*, 1(13), 635-641.
- Lladó J, Haenggeli C, Maragakis N, Snyder E, Rothstein J (2004) - Neural stem cells protect against glutamate-induced excitotoxicity and promote survival of injured motor neurons through the secretion of neurotrophic factors, *Molecular and Cellular Neuroscience*, 27(3), 322-331.
- Loane D, Lima P, Marrion N (2007) - Co-assembly of N-type Ca^{2+} and BK channels underlies functional coupling in rat brain, *Journal of Cell Science*, 120(6):985-995.
- Lobb C, Wilson C, Paladini C (2010) - A Dynamic Role for GABA Receptors on the Firing Pattern of Midbrain Dopaminergic Neurons, *Journal of Neurophysiology*, 104(1), 403-413.
- Lodish H, Berk A, Zipursky S (2000) - The Action Potential and Conduction of Electric Impulses, *Molecular Cell Biology, 4th edition*, Section 21.2.
- Loechner K, Salmon W, Fu J, Patel S, McLaughlin J (2009) - Cell Cycle-Dependent Localization of Voltage-Dependent Calcium Channels and the Mitotic Apparatus in a Neuroendocrine Cell Line(AtT-20), *International Journal of Cell Biology*, 487959.

- López-Muñoz F, Boya J, Alamo C (2006) - Neuron theory, the cornerstone of neuroscience, on the centenary of the Nobel Prize award to Santiago Ramón y Cajal, *Brain Research Bulletin*, 16:70(4-6), 391-405.
- Lorry, Anne-Charles (1760) - *Mémoires de l' Académie royale des sciences*.
- Ludwig A, Budde T, Stieber J, Moosmang S, Wahl C, Holthoff K, Langebartels A, Wotjak C, Munsch T, Zong X, Feil S, Feil R, Lancel M, Chien KR, Konnerth A, Pape H, Biel M, Hofmann F (2003) - Absence epilepsy and sinus dysrhythmia in mice lacking the pacemaker channel HCN2, *The EMBO Journal*, 22, 216-224.
- Luini A, Lewis D, Guild S, Corda D, Axelrod J (1985) - Hormone secretagogues increase cytosolic calcium by increasing cAMP in corticotropin-secreting cells, *PNAS*, 82(23), 8034-8038.
- Lv P, Kim H, Lee J, Sihn C, Gharaie S, Mousavi-Nik A, Wang W, Wang H, Gratton M, Doyle K, Zhang X, Chiamvimonvat N, Yamoah E (2014) - Genetic, Cellular, and Functional Evidence for Ca2+ Inflow through Cav1.2 and Cav1.3 Channels in Murine Spiral Ganglion Neurons, *The Journal of Neuroscience*, 34(21), 7383-7393.
- Mackie K, Lai Y, Westenbroek R, Mitchell R (1995) - Cannabinoids activate an inwardly rectifying potassium conductance and inhibit Q-type calcium currents in AtT20 cells transfected with rat brain cannabinoid receptor, *Journal of Neuroscience*, 15(10), 6552-6561.
- Magee J (2000) - Dendritic integration of excitatory synaptic input, *Nature Reviews Neuroscience*, 1, 181-190.
- Magee J, Johnston D (1995) - Synaptic activation of voltage-gated channels in the dendrites of hippocampal pyramidal neurons, *Science*, 268, 301.
- Malinow R, Malenka R (2002) - AMPA Receptor Trafficking and Synaptic Plasticity, *Annual Review of Neuroscience*, 25, 103-126.
- Mangoni M, Couette B, Bourinet E, Platzer J, Reimer D, Striessnig J, Nargeot J (2003) - Functional role of L-type Cav1.3 Ca2+ channels in cardiac pacemaker activity, *PNAS*, 100(9), 5543-5548.
- Mani B, Brueggemann L, Cribbs L, and Byron K (2009) - Opposite regulation of KCNQ5 and TRPC6 channels contributes to vasopressin-stimulated calcium spiking responses in A7r5 vascular smooth muscle cells, *Cell Calcium*, 45: 400-411.

- Maraganore D, de Andrade M, Elbaz A, Farrer M, Ioannidis J, Krüger R, Rocca W, Schneider N, Lesnick T, Lincoln S, Hulihan M, Aasly J, Ashizawa T, Chartier-Harlin M, Checkoway H, Ferrarese C, Hadjigeorgiou G, Hattori N, Kawakami H, Lambert J, Lynch T, Mellick G, Papapetropoulos S, Parsian A, Quattrone A, Riess O, Tan E, Van Broeckhoven C (2006) - Collaborative analysis of alpha-synuclein gene promoter variability and Parkinson disease, *JAMA*, 296(6), 661-670.
- Marcantoni A, Vandael D, Mahapatra S, Carabelli V, Sinnegger-Brauns M, Striessnig J, Carbone E (2010) - Loss of Cav1.3 Channels Reveals the Critical Role of L-Type and BK Channel Coupling in Pacemaking Mouse Adrenal Chromaffin Cells, *Journal of Neuroscience*, 30(2), 491-504.
- Marcantoni A, Vandael D, Mahapatra S, Carabelli V, Sinnegger-Brauns M, Striessnig J, Carbone E (2010) - Loss of Cav1.3 Channels Reveals the Critical Role of L-Type and BK Channel Coupling in Pacemaking Mouse Adrenal Chromaffin Cells, *Journal of Neuroscience*, 30(2), 491-504.
- Marcellino D, Kehr J, Agnati L, Fuxe K (2012) - Increased affinity of dopamine for D2-like versus D1-like receptors. Relevance for volume transmission in interpreting PET findings, *Synapse*, 66(3), 196–203.
- Marder E, Eisen J (1984) - Electrically coupled pacemaker neurons respond differently to same physiological inputs and neurotransmitters, *Journal of Neurophysiology*, 51(6), 1362-1374.
- Marschallinger J, Sah A, Schmuckermair C, Unger M, Rotheneichner P, Kharitonova M, Waclawiczek A, Gerner P, Jaksch-Bogensperger H, Berger S, Striessnig J, Singewald N, Couillard-Despres S, Aigner L (2015) - The L-type calcium channel Cav1.3 is required for proper hippocampal neurogenesis and cognitive functions, *Cell Calcium*, 58(6), 606-616.
- Marschang P, Brich J, Weeber E, David Sweatt J, Shelton J, Richardson J, Hammer R, Herz J (2004) - Normal Development and Fertility of Knockout Mice Lacking the Tumor Suppressor Gene LRP1b Suggest Functional Compensation by LRP1, *Molecular and Cellular Biology*, 24(9), 3782-3793.
- Martin A (1976) - The effect of membrane capacitance on non-linear summation of synaptic potentials, *Journal of Theoretical Biology*, 59(1), 179-187.
- Matschke L, Bertoune M, Roeper J, Snutch T, Oertel W, Rinné S, Decher N (2015) - A concerted action of L- and T-type Ca(2+) channels regulates locus coeruleus pacemaking, *Molecular and Cellular Neurosciences*, 68, 293-302.

- Matsuda W, Furuta T, Nakamura K, Hioki H, Fujiyama F, Arai R, Kaneko T (2009) - Single Nigrostriatal Dopaminergic Neurons Form Widely Spread and Highly Dense Axonal Arborizations in the Neostriatum, *Journal of Neuroscience*, 29(2), 444-453.
- Maturana A, Van Haasteren G, Piuz I, Castelbou C, Demaurex N, Schlegel W (2002) - Spontaneous Calcium Oscillations Control c-fos Transcription via the Serum Response Element in Neuroendocrine Cells, *The Journal of Biological Chemistry*, 277, 39713-39721.
- McCleskey E, Fox A, Feldman D, Cruz L, Olivera B, Tsien R, Yoshikami D (1987) - Omega-conotoxin: direct and persistent blockade of specific types of calcium channels in neurons but not muscle, *PNAS*, 84(12), 4327-4331.
- McCormack A, Mak S, Henderson J, Bumcrot D, Farrer M, Di Monte D (2010) - Alpha-synuclein suppression by targeted small interfering RNA in the primate substantia nigra, *PLoS One*, 5(8), e12122.
- McKeage K (2013) - Pasireotide: a review of its use in Cushing's disease, *Drugs*, 73(6). 563-574.
- Mejías-Aponte C, Drouin C, Aston-Jones G (2009) - Adrenergic and noradrenergic innervation of the midbrain ventral tegmental area and retrorubral field: Prominent inputs from medullary homeostatic centers, *The Journal of Neuroscience*, 29(11), 3613–3626.
- Mercer J, Chan C, Tkatch T, Held J, Surmeier D (2007) - *The Journal of Neuroscience*, 27(49), 13552-13566.
- Mercuri N, Bonci A, Calabresi P, Stratta F, Stefani A, Bernardi G (1994) - Effects of dihydropyridine calcium antagonists on rat midbrain dopaminergic neurones, *British Journal of Pharmacology*, 113(3): 831-838.
- Meredith G, Totterdell S, Beales M, Meshul C (2009) - Impaired glutamate homeostasis and programmed cell death in a chronic MPTP mouse model of Parkinson's disease, *Experimental Neurology*, 219(1), 334-340.
- Michel P, Hefti F (1990) - Toxicity of 6-hydroxydopamine and dopamine for dopaminergic neurons in culture, *Journal of Neuroscience Research*, 26(4), 428-435.
- Millán C1 Sánchez-Prieto J (2002) - Differential coupling of N- and P/Q-type calcium channels to glutamate exocytosis in the rat cerebral cortex, *Neuroscience Letters*, 330(1), 29-32.

- Mishizen-Eberz A, Guttmann R, Giasson B, Day G, Hodara R, Ischiropoulos H, Lee V, Trojanowski J, Lynch D (2003) - Distinct cleavage patterns of normal and pathologic forms of alpha-synuclein by calpain I in vitro, *Journal of Neurochemistry*, 84(4), 836-847.
- Missale C, Nash S, Robinson S, Jaber M, Caron M (1998) - Dopamine receptors: from structure to function, *Physiological Reviews*, 78(1), 189-225.
- Moldzio R, Radad K, Krewenka C, Kranner B, Duvigneau J, Rausch W (2013) - Protective effects of resveratrol on glutamate-induced damages in murine brain cultures, *Journal of Neural Transmission*, 120(9), 1271-1280.
- Moreno-Juan V, Filipchuk A, Antón-Bolaños N, Mezzera C, Gezelius H, Andrés B, Rodríguez-Malmierca L, Susín R, Schaad O, Iwasato T, Schüle R, Rutlin M, Nelson S, Ducret S, Valdeolmillos M, Rijli F, López-Bendito G (2017) - Prenatal thalamic waves regulate cortical area size prior to sensory processing, *Nature Communications*, 8, 14172.
- Morozova E, Zakharov D, Gutkin B, Lapish C, Kuznetsov A (2016) - Dopamine Neurons Change the Type of Excitability in Response to Stimuli, *PLOS Computational Biology*, 12(12), e1005233.
- Murphy M (2009) - How mitochondria produce reactive oxygen species, *Biochemical Journal*, 417, 1-13.
- Naundorf B, Wolf F, Volgushev M (2006) - Unique features of action potential initiation in cortical neurons, *Nature*, 440(7087), 1060-1063.
- Neher E, Sakmann B (1976) - Single-channel currents recorded from membrane of denervated frog muscle fibres, *Nature*, 260, 799-802.
- Nelson A, Gittis A, du Lac S (2005) - Decreases in CaMKII activity trigger persistent potentiation of intrinsic excitability in spontaneously firing vestibular nucleus neurons, *Neuron*, 46(4), 623-631.
- Nelson D, Meakin J, Thorn G (1960) - ACTH-Producing Pituitary Tumors Following Adrenalectomy for Cushing's Syndrome, Annals *of Internal Medicine*, 52, 560-569.
- Nguyen H, Byers B, Cord B, Shcheglovitov A, Byrne J, Gujar P, Kee K, Schüle B, Dolmetsch R, Langston W, Palmer T, Pera R (2016) - LRRK2 Mutant iPSC-Derived DA Neurons Demonstrate Increased Susceptibility to Oxidative Stress, *Cell Stem Cell*, 8(3), 267-280.

- Nicholls D, Budd S (1998) - Mitochondria and neuronal glutamate excitotoxicity, *Biochimica et Biophysica Acta - Bioenergetics*, 1366(1-2), 97-112.
- Nowycky M, Fox A, Tsien R (1985) - Three types of neuronal calcium channel with different calcium agonist sensitivity, *Letters to Nature*, 316, 440-443.
- Okada K, Wangpoengtrakul C, Osawa T (1999) - 4-Hydroxy-2-nonenal-mediated impairment of intracellular proteolysis during oxidative stress. Identification of proteasomes as target molecules, *The Journal of Biological Chemistry*, 274, 23787–23793.
- Pacelli C, Giguere N, Bourque M, Levesque M, Slack R, Trudeau L (2015) - Elevated Mitochondrial Bioenergetics and Axonal Arborization Size Are Key Contributors to the Vulnerability of Dopamine Neurons, *Current Biology*, 25, 2349-2360.
- Padiglia A, Medda R, Lorrai A, Biggio G, Sanna E, Floris G (1997) - Modulation of 6-hydroxydopamine oxidation by various proteins, *Biochemical Pharmacology*, 53(8), 1065-1068.
- Pan X, Liu J, Nguyen T, Liu C, Sun J, Teng Y, Fergusson M, Rovira I, Allen M, Springer D, Aponte A, Gucek M, Balaban R, Murphy E, Finkel T (2013) - The Physiological Role of Mitochondrial Calcium Revealed by Mice Lacking the Mitochondrial Calcium Uniporter, *Nature Cell Biology*, 15(12), 1464–1472.
- Pape H, Munsch T, Budde T (2004) - Novel vistas of calcium-mediated signalling in the thalamus, *Pflügers Archiv* , 448(2), 131–138.
- Park C, Kimler B, Smith T (1985) - Comparison of the supravital DNA dyes Hoechst 33342 and DAPI for flow cytometry and clonogenicity studies of human leukemic marrow cells, *Experimental Hematology*, 13(10), 1039-1043.
- Parkinson J (2002) - An Essay on the Shaking Palsy. 1817. - *The Journal of Neuropsychiatry and Clinical Neurosciences*, 14(2), 223-236.
- Pearce J (2001) - Emil Heinrich Du Bois-Reymond (1818-96), *Journal of Neurology, Neurosurgery, and Psychiatry*, 71(5), 620.
- Pearlstein E, Gouty-Colomer L, Michel F, Cloarec R, Hammond C (2015) - Glutamatergic synaptic currents of nigral dopaminergic neurons follow a postnatal developmental sequence, *Frontiers in Cellular Neuroscience*, 9, 210.
- Peña F, Parkis M, Tryba A, Ramirez J (2004) - Differential contribution of pacemaker properties to the generation of respiratory rhythms during normoxia and hypoxia, *Neuron*, 43(1), 105-117.

- Perez-Reyes E, Cribbs L, Daud A, Lacerda A, Barclay J, Williamson M, Fox M, Rees M, Lee J (1998) - Molecular characterization of a neuronal low-voltage-activated T-type calcium channel, *Nature*, 391, 896–900.
- Pérez-Rial S, García-Gutiérrez M, Molina J, Pérez-Nievas B, Ledent C, Leiva C, Leza J, Manzanares J (2011) - Increased vulnerability to 6-hydroxydopamine lesion and reduced development of dyskinesias in mice lacking CB1 cannabinoid receptors, *Neurobiology of Aging*, 32, 631–645.
- Perkel D, Schulman J, Bullock T, Moore G, Segundo J (1964) - Pacemaker Neurons: Effects of Regularly Spaced Synaptic Input, *Science*, 145(3627), 61-63.
- Peterson O, Maruyama Y (1984) - Calcium-activated potassium channels and their role in secretion, *Nature*, 307(5953), 693-696.
- Petri S, Krampfl K, Dengler R, Bufler J, Weindl A, Arzberger T (2002) - Human GABA A receptors on dopaminergic neurons in the pars compacta of the substantia nigra, *Journal of Comparative Neurology*, 452(4), 360-366.
- Petri S, Krampfl K, Dengler R, Bufler J, Weindl A, Arzberger T (2002) - Human GABAA receptors on dopaminergic neurons in the pars compacta of the substantia nigra, *Journal of Comparative Neurology*, 452, 360–366.
- Pike F, Meredith R, Olding A, Paulsen O (1999) - Rapid report: postsynaptic bursting is essential for 'Hebbian' induction of associative long-term potentiation at excitatory synapses in rat hippocampus, *The Journal of Physiology*, 15(518), 571-576.
- Pioli E, Meissner W, Sohr R, Gross C, Bezard E, Bioulac B (2008) - Differential behavioral effects of partial bilateral lesions of ventral tegmental area or substantia nigra pars compacta in rats, *Neuroscience*, 153(4):1213-1224.
- Pisarchik A, Slominski A (2001) - Alternative splicing of CRH-R1 receptors in human and mouse skin: identification of new variants and their differential expression, *The FASEB Journal*, 15, 2754-2756.
- Platkiewicz J, Brette R (2011) - Impact of Fast Sodium Channel Inactivation on Spike Threshold Dynamics and Synaptic Integration, *PLOS Computational Biology*, 7(5), e1001129.
- Poetschke C, Dragicevic E, Duda J, Benkert J, Dougalis A, DeZio R, Snutch T, Striessnig J, Liss B (2015) - Compensatory T-type Ca^{2+} channel activity alters D2-autoreceptor responses of Substantia nigra dopamine neurons from Cav1.3 L-type Ca2+ channel KO mice, *Scientific Reports*, 5, 13688.

- Potapenko E, Biancardi V, Florschutz R, Ryu P, Stern J (2011) - Inhibitory-excitatory synaptic balance is shifted toward increased excitation in magnocellular neurosecretory cells of heart failure rats, *Journal of Neurophysiology*, 106(3), 1545-1557.
- Prinz A, Billimoria C, Marder E (2003) - Alternative to Hand-Tuning Conductance-Based Models: Construction and Analysis of Databases of Model Neurons, *Journal of Neurophysiology*, 90, 3998-4015.
- Puopolo M, Raviola E, Bean B (2007) - Roles of subthreshold calcium current and sodium current in spontaneous firing of mouse midbrain dopamine neurons, *Journal of Neuroscience*, 27(3), 645-656.
- Qin Z, Hu D, Han S, Reaney S, Di Monte D, Fink A (2007) - Effect of 4-Hydroxy-2-nonenal Modification on α-Synuclein Aggregation, *Journal of Biological Chemistry*, 282, 5862-5870.
- Raff H, Sharma S, Nieman L (2014) - Physiological Basis for the Etiology, Diagnosis, and Treatment of Adrenal Disorders: Cushing's Syndrome, Adrenal Insufficiency, and Congenital Adrenal Hyperplasia, *Comprehensive Physiology*, 4(2), 739–769.
- Raikhinstein M, Hanukoglu I (1993) - Mitochondrial-genome-encoded RNAs: differential regulation by corticotropin in bovine adrenocortical cells, PNAS, 90(22), 10509–10513.
- Ramirez J, Tryba A, Pena F (2004) - Pacemaker neurons and neuronal networks: an integrative view, *Current Opinion in Neurobiology*, 14, 665–674.
- Rao B, Finkbeiner S (2007) – NMDA and AMPA receptors: old channels, new tricks, *Trends in Neurosciences*, 30(6), 284-291.
- Reid M, Herrera-Marschitz M, Hökfelt T (1990) - *Experimental Brain Research*, 82, 293.
- Rekling J, Champagnat J, Denavit-Saubie M (1996) - Electroresponsive properties and membrane potential trajectories of three types of inspiratory neurons in the newborn mouse brain stem in vitro, *Journal of Neurophysiology*, 75, 795-810.
- Richards C, Shiroyama T, Kitai S (1997) - Electrophysiological and immunocytochemical characterization of GABA and dopamine neurons in the substantia nigra of the rat, *Neuroscience*, 80(2), 545-557.

- Riven I, Iwanir S, Reuveny E (2006) - GIRK Channel Activation Involves a Local Rearrangement of a Preformed G Protein Channel Complex, *Neuron*, 51, 561–573.
- Robertson G, Damsma G, Fibiger H (1991) - Characterisation of dopamine release in the substantia nigra by in vivo microdialysis in freely moving rats, *The Journal of Neuroscience*, 11(7), 2209-2216.
- Root D, Wang H, Liu B, Barker D, Mód L, Szocsics P, Silva A, Maglóczky Z, Morales M (2016) - Glutamate neurons are intermixed with midbrain dopamine neurons in nonhuman primates and humans, *Scientific Reports*, 6, 30615.
- Rudy C, Hunsberger H, Weitzner D, Reed M (2015) - The Role of the Tripartite Glutamatergic Synapse in the Pathophysiology of Alzheimer's Disease, *Aging and Disease*, 6(2), 131-148.
- Sage D, Maurel D, Bosler O (2001) - Involvement of the suprachiasmatic nucleus in diurnal ACTH and corticosterone responsiveness to stress, *American Journal of Physiology - Endocrinology and Metabolism*, 280(2), 260-269.
- Sasaki M, Shibata E, Tohyama K, Takahashi J, Otsuka K, Tsuchiya K, Takahashi S, Ehara S, Terayama Y, Sakai A (2006) - Neuromelanin magnetic resonance imaging of locus ceruleus and substantia nigra in Parkinson's disease, *Neuroreport*, 17(11), 1215-1218.
- Schapira A, Cooper J, Dexter D (1990) Mitochondrial complex I deficiency in Parkinson's disease, *Journal of Neurochemistry*, 54:823–827.
- Schapira A, Olanow C, Greenamyre J, Bezard E (2014) - Slowing of neurodegeneration in Parkinson's disease and Huntington's disease: future therapeutic perspectives, *The Lancet*, 384(9942), 545-555.
- Schousboe A, Waagepetersen H (2005) - Role of astrocytes in glutamate homeostasis: implications for excitotoxicity, *Neurotoxicity Research*, 8(3-4), 221-225.
- Schwarting R, Huston J (1996) - The unilateral 6-hydroxydopamine lesion model in behavioral brain research. Analysis of functional deficits, recovery and treatments, *Progress in Neurobiology*, 50(2-3), 275-331.
- Schweitzer P, Madamba S, Siggins G (2003) - The sleep-modulating peptide cortistatin augments the h-current in hippocampal neurons, *Journal of Neuroscience*, 23, 10884-10891.
- Shampo M, Kyle R (1981) - Bartolomeo Eustachi, *JAMA*, 246(22) 2596.

- Shanks N, Greek R, Greek J (2009) - Are animal models predictive for humans?, Philosophy, *Ethics and Humanities in Medicine*, 4, 2.
- Shen R, Altar C, Chiodo L (1994) - Brain-derived neurotrophic factor increases the electrical activity of pars compacta dopamine neurons in vivo, *PNAS*, 91(19), 8920-8924.
- Sheng Z, Yokoyama C, Catterall W (1997) - Interaction of the synprint site of N-type Ca2+ channels with the C2B domain of synaptotagmin I, *PNAS*, 94(10), 5404-5410.
- Shi S, Hayashi Y, Petralia R, Zaman S, Wenthold R, Svoboda K, Malinow R (1999) - Rapid Spine Delivery and Redistribution of AMPA Receptors After Synaptic NMDA Receptor Activation, *Science*, 284(5421), 1811-1816.
- Shimizu K, Matsubara K, Ohtaki K, Fujimaru S, Saito O, Shiono H (2003) - Paraquat induces long-lasting dopamine overflow through the excitotoxic pathway in the striatum of freely moving rats, *Brain Research*, 976(2), 243-252.
- Siegel G, Agranoff B, Albers R (1999) - GABA Receptor Physiology and Pharmacology, *Basic Neurochemistry: Molecular, Cellular and Medical Aspects. 6th edition*.
- Smith J, Butera R, Koshiya N, Del Negro C, Wilson C, Johnson S (2000) - Respiratory rhythm generation in neonatal and adult mammals: the hybrid pacemaker–network model, *Respiratory Physiology*, 122(2-3), 131-147.
- Soldatov N (1994) - Genomic structure of human L-type Ca2+ channel, *Genomics*, 22, 77-87.
- Spencer B, Potkar R, Trejo M, Rockenstein E, Patrick C, Gindi R, Adame A, Wyss-Coray T, Masliah E (2009) - Beclin 1 gene transfer activates autophagy and ameliorates the neurodegenerative pathology in alpha-synuclein models of Parkinson's and Lewy body diseases, *The Journal of Neuroscience*, 29(43), 13578-13788.
- Spiga F, Harrison L, Wood S, Knight D, MacSweeney C, Thomson F, Craighead M, Lightman S (2009) - Blockade of the V1b receptor reduces ACTH, but not corticosterone secretion induced by stress without affecting basal hypothalamic–pituitary–adrenal axis activity, *Journal of Endocrinology*, 200, 273-283.
- Spillantini M, Crowther R, Jakes R, Hasegawa M, Goedert M (1998) - alpha-Synuclein in filamentous inclusions of Lewy bodies from Parkinson's disease and dementia with lewy bodies, *PNAS USA*, 95(11), 6469-6473.

- Spinedi E, Negro-Vilar A (1983) - Serotonin and Adrenocorticotropin (ACTH) Release:Direct Effects at the Anterior Pituitary Level and Potentiation of Arginine Vasopressin-Induced ACTH Release, *Endocrinology*, 112 (4), 1217-1223.
- Starkman M, Schteingart D (1981) - Neuropsychiatric Manifestations of Patients With Cushing's Syndrome: Relationship to Cortisol and Adrenocorticotropic Hormone Levels, *Archives of Internal Medicine*, 141(2), 215-219.
- Stellwagen D, Shatz C, Feller M (1999) - Dynamics of Retinal Waves Are Controlled by Cyclic AMP, *Neuron*, 24(3), 673-685.
- Steriade M, Domich L, Oakson G, Deschenes M (1987) - The deafferented reticular thalamic nucleus generates spindle rhythmicity, *Journal of Neurophysiology*, 57(1), 260-273.
- Strege P, Bernard C, Ou Y, Gibbons S, Farrugia G (2005) - Effect of mibefradil on sodium and calcium currents, *American Journal of Physiology - Gastrointestinal and Liver Physiology*, 289(2), G249-G253.
- Striessnig J, Pinggera A, Kaur G, Bock G, Tuluc P (2014) - L-type Ca2+ channels in heart and brain, *Wiley Interdisciplinary Reviews Membrane Transport and Signaling*, 3(2), 15-38.
- Su W, Song X, Ji J (2010) - Functional expression of a large-conductance Ca^{2+}-activated K^{+} channel in mouse substantia nigra pars compacta dopaminergic neurons, *Neuroscience Letters*, 471(1), 1-5.
- Sulzer D, Joyce M, Lin L, Geldwert D, Haber S, Hattori T, Rayport S (1998) - Dopamine neurons make glutamatergic synapses in vitro, *The Journal of General Physiology*, 18(12), 4588-4602.
- Sun Y, Zhang H, Selvaraj S, Sukumaran P, Lei S, Birnbaumer L, Singh B (2017) - Inhibition of L-Type Ca2+ Channels by TRPC1-STIM1 Complex Is Essential for the Protection of Dopaminergic Neurons, *The Journal of Neuroscience*, 37(12) 3364-3377.
- Surmeier D , Ding J, Day M, Wang Z, Shen W (2007) - D1 and D2 dopamine-receptor modulation of striatal glutamatergic signaling in striatal medium spiny neurons, *Trends in Neurosciences*, 30(5), 228-235.
- Surmeier D, Schumacker P, Guzman J, Ilijic E, Yang B, Zampese E (2017) - Calcium and Parkinson's Disease, *Biochemical and Biophysical Research Communications*, 483(4), 1013-1019.

- Surmeier J, Schumaker P (2013) - Calcium, Bioenergetics, and Neuronal Vulnerability in Parkinson's Disease, *The Journal of Biological Chemistry*, 288, 10736-10741,
- Surprenant A (1982) - Correlation between electrical activity and ACTH/beta-endorphin secretion in mouse pituitary tumor cells, *The Journal of Cell Biology*, 95(2), 559.
- Suzuki M, Nelson A, Eickstaedt J, Wallace K, Wright L, Svendsen C (2006) - Glutamate enhances proliferation and neurogenesis in human neural progenitor cell cultures derived from the fetal cortex, *European Journal of Neuroscience*, 24(3), 645-653.
- Sveinbjornsdottir S (2016) - The clinical symptoms of Parkinson's disease, *Journal of Neurochemistry*, 139(S1), 318-324.
- Swistowski A, Peng J, Liu Q, Mali P, Rao M, Cheng L, Zeng X (2010) - Efficient Generation of Functional Dopaminergic Neurons from Human Induced Pluripotent Stem Cells Under Defined Conditions, *STEM CELLS*, 28, 1893–1904.
- Takahashi K, Tanabe K, Ohnuki M, Narita M, Ichisaka T, Tomoda K, Yamanaka S (2007) - Induction of Pluripotent Stem Cells from Adult Human Fibroblasts by Defined Factors, *Cell*, 131(5), 861 - 872.
- Takahashi K, Yamanaka S (2006) - Induction of pluripotent stem cells from mouse embryonic and adult fibroblast cultures by defined factors, *Cell*, 126(4), 663-676.
- Tan E, Khajavi M, Thornby J, Nagamitsu S, Jankovic J, Ashizawa T (2000) - Variability and validity of polymorphism association studies in Parkinson’s disease, *Neurology*, 55, 533–538.
- Teitelman G, Alpert S, Polak J, Martinez A, Hanahan D (1993) - Precursor cells of mouse endocrine pancreas coexpress insulin, glucagon and the neuronal proteins tyrosine hydroxylase and neuropeptide Y, but not pancreatic polypeptide, *Development*, 118, 1031-1039.
- Tepper J, Paladini C, Celada P (1998) - GABAergic control of the firing pattern of substantia nigra dopaminergic neurons, *Advances in Pharmacology*, 42, 694-699.
- Tepper J, Trent F, Nakamura S (1990) - Postnatal development of the electrical activity of rat nigrostriatal dopaminergic neurons, *Developmental Brain Research*, 54(1), 21-33.

- Thaweerattanasinp T, Heckman C, Tysseling V (2016) - Firing characteristics of deep dorsal horn neurons after acute spinal transection during administration of agonists for 5-HT1B/1D and NMDA receptors, *Journal of Neurophysiology*, 116(4), 1644-1653.
- Thomas D, Tovey S, Collins T, Bootman M, Berridge M, Lipp P (2000) - A comparison of fluorescent Ca2+ indicator properties and their use in measuring elementary and global Ca2+ signals, *Cell Calcium*, 28(4), 213-233.
- Tian L, Shipston M (2000) - Characterization of hyperpolarization-activated cation currents in mouse anterior pituitary, AtT20 D16:16 corticotropes, *Endocrinology*, 141(8), 2930-2937.
- Tieu K (2011) - A Guide to Neurotoxic Animal Models of Parkinson's Disease. *Cold Spring Harbor Perspectives in Medicine, 1*(1), a009316.
- Tocris, Dopamine Receptors, https://www.tocris.com/pharmacology/dopamine-receptors.
- Tritsch N, Granger A, Sabatini B (2016) - Mechanisms and functions of GABA co-release, *Nature Reviews Neuroscience*, 17, 139-145.
- Turnbull A, Smith G, Lee S, Vale W, Lee K, Rivier C (1999) - CRF type I receptor-deficient mice exhibit a pronounced pituitary-adrenal response to local inflammation, *Endocrinology*, 140(2),1013-1017.
- Uchigashima M, Ohtsuka T, Kobayashi K, Watanabe M (2016) - Dopamine synapse is a neuroligin-2–mediated contact between dopaminergic presynaptic and GABAergic postsynaptic structures, *PNAS*, 113(15), 4206-4211.
- Vaarmann A, Kovac S, Holmstrom K, Ghandi S, Abramov A (2013) - Dopamine protects neurons against glutamate-induced excitotoxicity, *Cell Death & Disease*, 4(1), e455.
- Valenta L, Elias A, Eisenberg H (1986) - ACTH stimulation of adrenal epinephrine and norepinephrine release, *Hormone Research*, 23(1), 16-20.
- van den Berg G, Pincus S, Veldhuis J, Frölich M, Roelfsema F (1997) - Greater disorderliness of ACTH and cortisol release accompanies pituitary-dependent Cushing's disease, *European Journal of Endocrinology*, 136, 394-400.
- van den Top M, Lee K, Whyment A, Blanks A, Spanswick D (2004) - Orexigen-sensitive NPY/AgRP pacemaker neurons in the hypothalamic arcuate nucleus, *Nature Neuroscience*, 7, 493-493.
- van Wieringen J, Booij L, Shalgunov V, Elsinga P, Michel M (2013) - Agonist high- and low-affinity states of dopamine D2 receptors: methods of detection

and clinical implications, *Naunyn-Schmiedeberg's Archives of Pharmacology*, 386(2), 135-154.

- Vandecasteele M, Glowinski J, Venance L (2005) - Electrical Synapses between Dopaminergic Neurons of the Substantia Nigra Pars Compacta, *Journal of Neuroscience*, 25(2), 291-298.
- Volpicelli-Daley L, Luk K, Patel T, (2011) - Exogenous a-synuclein fibrils induce Lewy body pathology leading to synaptic dysfunction and neuron death, *Neuron*, 72, 57–71.
- Votyakova T, Reynolds I (2001) - DCm-Dependent and -independent production of reactive oxygenspecies by rat brain mitochondria, *Journal of Neurochemistry*, 79, 266-277.
- Walker L, Publicover S, Preston M, Said Ahmed, El Haj A (2000) - Calcium-channel activation and matrix protein upregulation in bone cells in response to mechanical strain, *Journal of Cellular Biochemistry*, 79, 648–661.
- Wang Q, Xu Y, Liu S, Ma Z (2017) - Isradipine attenuates MPTP-induced dopamine neuron degeneration by inhibiting up-regulation of L-type calcium channels and iron accumulation in the substantia nigra of mice, *Oncotarget*, 8(29), 47284-47295.
- Wang S, Zou C, Fu L, Wang B, An J, Song G, Wu J, Tang X, Li M, Zhang J, Yue F, Zheng C, Chan P, Zhang Y, Chen Z (2015) - Autologous IPSC-Derived Dopamine Neuron Transplantation in a Nonhuman Primate Parkinson's Disease Model, *Cell Discovery*, 1, 15012.
- Watabe-Uchida M, Zhu L, Ogawa S, Vamanrao A, Uchida N (2012) - Whole-Brain Mapping of Direct Inputs to Midbrain Dopamine Neurons, *Neuron*, 74(5), 858-873.
- Watt A, Cuntz H, Mori M, Nusser Z, Sjostrom P, Hausser M (2009) - Traveling waves in developing cerebellar cortex mediated by asymmetrical Purkinje cell connectivity, *Nature Neuroscience*, 12, 463–473.
- Wei Z, Linden D (2003) - The Other Side of the Engram: Experience-Driven Changes in Neuronal Intrinsic Excitability, *Nature Reviews Neuroscience*, 4(11), 885–900.
- Weik R, Spiess J (1992) - Isoproterenol enhances a calcium-independent potassium current in mouse anterior pituitary tumor cell, *Journal of Neurophysiology*, 68(1), 117-123.

- Weinstein R, Jilka R, Parfitt A, Manolagas S (1998) - Inhibition of osteoblastogenesis and promotion of apoptosis of osteoblasts and osteocytes by glucocorticoids. Potential mechanisms of their deleterious effects on bone, *The Journal of Clinical Investigation*, 102(2), 274-282.
- Woodard C, Campos B, Kuo S, Nirenberg M, Nestor M, Zimmer M, Mosharov E, Sulzer D, Zhou H, Paull D, Clark L, Schadt E, Sardi S, Rubin L, Eggan K, Brock M, Lipnick S, Rao M, Chang S, Li A, Noggle S (2014) - iPSC-Derived Dopamine Neurons Reveal Differences between Monozygotic Twins Discordant for Parkinson's Disease, *Cell Reports*, 9(4), 1173-1182.
- Woods M, Shipston M, Mullens E, Antoni F (1992) - Pituitary corticotrope tumor (AtT20) cells as a model system for the study of early inhibition by glucocorticoids, *Endocrinology*, 131(6), 2873-2880.
- Wu L, Bauer C, Xiao-guang Z, Xie C, Yang J (2002), Dual regulation of voltage-gated calcium channels by PtdIns(4,5)P2, *Nature*, 419, 947-952.
- Xie H, Hu L, Li G (2010) - SH-SY5Y human neuroblastoma cell line: in vitro cell model of dopaminergic neurons in Parkinson's disease, *Chinese Medical Journal*, 123(8), 1086-1092.
- Yamamori E, Iwasaki Y, Oki Y, Yoshida M, Asai M, Kambayashii M, Oiso Y, Nakashima N (2004) - Possible involvement of ryanodine receptor-mediated intracellular calcium release in the effect of corticotropin-releasing factor on adrenocorticotropin secretion, *Endocrinology*, 145(1), 36-38.
- Yashiro K, Philpot B (2008) - Regulation of NMDA Receptor Subunit Expression and Its Implications for LTD, LTP, and Metaplasticity, *Neuropharmacology*, 55(7), 1081-1094.
- Yokote R, Hisano S, Daikoku S (1991) - Immunohistochemical localization of glucocorticoid receptors in anterior pituitary cells of rats, *Archives Histology and Cytology*, 54(1), 103-12.
- Yuste R, Nelson D, Rubin W, Katz L (1995) - Neuronal domains in developing neocortex: mechanisms of coactivation, *Neuron*, 14(1), 7-17.
- Zakharov D, Kuznetsov A (2015) - Qualitatively different scenarios for co-activation of NMDA, AMPA and GABA receptor currents on dopaminergic neuron, *BMC Neuroscience*, 16(Supp 1), 138.
- Zakharov D, Lapish, Gutkin B, Kuznetsov A (2016) - Synergy of AMPA and NMDA Receptor Currents in Dopaminergic Neurons: A Modeling Study, *Frontiers in Computational Neuroscience*, 10, 48.

- Zakrzewska K, Cusin I, Stricker-Krongrad A, Boss O, Ricquier D, Jeanrenaud B, Rohner-Jeanrenaud F (1999) - Induction of obesity and hyperleptinemia by central glucocorticoid infusion in the rat, *Diabetes*, 48(2), 365-370.
- Zampini V, Johnson S, Franz C (2010) - Elementary properties of $Ca_V1.3$ Ca^{2+} channels expressed in mouse cochlear inner hair cells, *The Journal of Physiology*, 588(1), 187-199.
- Zemkova H, Tomic M, Kucka M, Aguilera G, Stojilkovic S (2016) - Spontaneous and CRH-Induced Excitability and Calcium Signaling in Mice Corticotrophs Involves Sodium, Calcium, and Cation-Conducting Channels, *Endocrinology*, 157, 1576-1589.
- Zhang L, Xue Y, Yang C, Yang W, Chen L, Zhang Q, Qu T, Huang S, Zhao L, Wang X, Duan W (2012) - Human Albumin Prevents 6-Hydroxydopamine-Induced Loss of Tyrosine Hydroxylase in In Vitro and In Vivo, *PLOS ONE*, 7(7), e41226.
- Zolles G, Klöcker N, Wenzel D, Weisser-Thomas J, Fleischmann B, Roeper J, Fakler B (2006) - Pacemaking by HCN Channels Requires Interaction with Phosphoinositides, *Neuron*, 52(6), 1027-1036.